Towards the Valorization of Humin By-products: Characterization, Solubilization and Catalysis

Bijdrage aan de Valorisatie van Humine-achtige Bijproducten: Karakterisatie, Oplossen en Katalytische Omzetting

(met een samenvatting in het Nederlands)

Proefschrift

ter verkrijging van de graad van doctor aan de Universiteit Utrecht op gezag van de rector magnificus, prof.dr. G. J. van der Zwaan, ingevolge het besluit van het college voor promoties in het openbaar te verdedigen op maandag 16 maart 2015 des ochtends te 10.30 uur

door

Ilona van Zandvoort

geboren op 3 augustus 1986 te Velsen

Promotor: Prof. dr. ir. B. M. Weckhuysen
Copromotor: Dr. P. C. A. Bruijnincx

This research has been performed within the framework of the CatchBio program. The authors gratefully acknowledge the support of the Smart Mix Program of the Netherlands Ministry of Economic Affairs and the Netherlands Ministry of Education, Culture and Science.

Voor mijn ouders

Life is what happens to you while you're busy making other plans
John Lennon

ISBN: 978-90-393-6291-4

TABLE OF CONTENTS

CHAPTER 1	*General Introduction*	7
CHAPTER 2	*Formation, Molecular Structure and Morphology of Humins in Biomass Conversion: Influence of Feedstock and Processing Conditions*	39
CHAPTER 3	*Full, Reactive Solubilization of Humin By-products by Alkaline Treatment and Characterization of the Alkali-treated Humins Formed*	61
CHAPTER 4	*Structural Characterization of ^{13}C-Enriched Humins and Alkali-treated ^{13}C Humins by 2D Solid-state NMR*	81
CHAPTER 5	*Aqueous Phase Reforming of Solubilized Glucose-derived Humins over Supported Pt Catalysts*	103
CHAPTER 6	*Unexpected Benefits of Using Real Feeds in Biomass Conversion: High Hydroxymethylfurfural Selectivity and Low Humin Formation in the Acid-catalyzed Dehydration of Sugar Beet-derived Thick Juice*	121
CHAPTER 7A	*Summary and Concluding Remarks*	145
CHAPTER 7B	*Samenvatting en Slotbeschouwing*	157
LIST OF ABBREVIATIONS		169
LIST OF PUBLICATIONS		170
DANKWOORD		172
CURRICULUM VITAE		176

CHAPTER 1

General Introduction

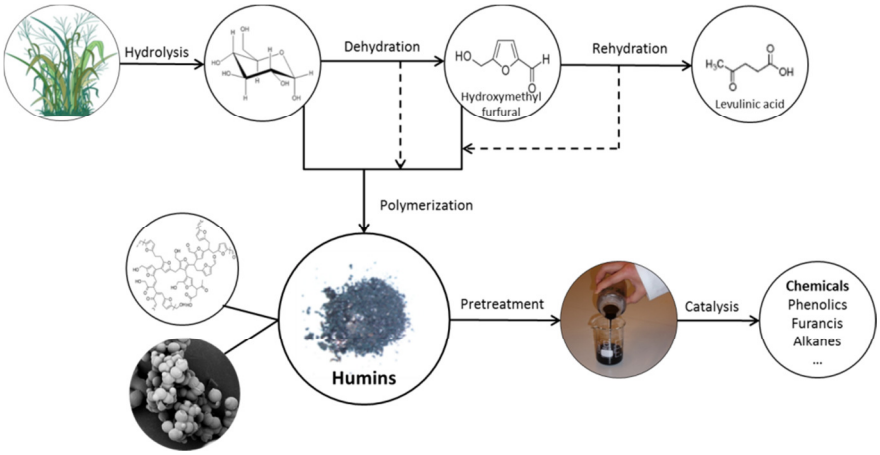

Abstract

During the acid-catalyzed dehydration of carbohydrates for the production of renewable bulk chemicals, such as furfural, hydroxymethylfurfural (HMF) and levulinic acid, large amounts of carbonaceous, insoluble by-products are typically formed by cross-polymerization reactions of HMF and several sugar-dehydration intermediates. The formation of these so-called humins leads to great efficiency losses in biorefinery operations. Indeed, a literature overview of conditions, kinetics and mechanisms of humin formation shows that hydrothermal treatment of sugars under acidic conditions unavoidably leads to the formation of humins. Although produced in abundance, the molecular structure of humins and their mechanism of formation are not yet unequivocally established. Detailed knowledge of both is required, however, to either prevent their formation or to find routes for the valorization of humins, which would both increase the economic feasibility of future biorefineries. This chapter summarizes the literature describing biorefinery concepts that involve humin formation, as well as those studies concerned with the (mechanism of) formation, characterization and valorization of humins.

1.1. Biomass as a Resource for the Production of Chemicals and Energy

For ages, mankind has been using renewable resources for heat and energy, *e.g*. burning of wood. However, since the industrial revolution the use of unrenewable fossil resources has increased, for instance by burning gas and oil-based fuels for transportation (Figure 1.1). This has led to global warming issues due to the emission of greenhouse gases, such as CO_2, and depletion of fossil reserves while energy demands keep increasing.[1,2] At the same time we also rely on oil for the production of bulk chemicals and materials.[3] To limit adverse greenhouse effects, several international agreements are in place that aim at reducing CO_2 emissions for instance, by replacing fossil fuels by biomass-derived alternatives. For example, the European Commission set as a goal that more than 20% of the liquid transportation fuels used should be derived from biomass by 2020.[4] In the same year, greenhouse gas emission levels should be reduced by 20% compared to 1990, as stated in the Kyoto protocol.[5] These pressing environmental issues and associated regulations have led to many research efforts aimed at the development of processes for renewable energy and chemicals.

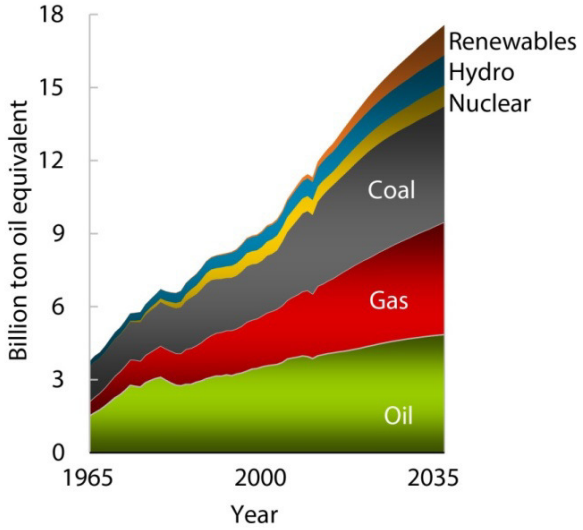

Figure 1.1. World energy consumption from 1965 till 2010 including the available energy sources, taken from the BP Energy Outlook.[6]

Biomass is currently the only sustainable resource for the large scale production of carbon-based chemicals and fuels. The first-generation biobased fuels that are being produced nowadays are derived from those plant fragments that are easily processed. Well-known examples are bioethanol from corn starch or sugar cane and biodiesels from fatty acids. To avoid competition with food production, second-generation biomass-based fuels and chemicals, for which the production facilities are gradually coming online at the moment, are derived from the non-edible parts of biomass instead. For such second-generation production processes, lignocellulosic biomass is obtained from agricultural

residues, forestry residues, waste streams or dedicated energy crops, such as switch grass.[7,8]

Lignocellulosic material is found in the plant cell wall, and consists of cellulose, hemicellulose and lignin (Figure 1.2).[7,9] Cellulose is a linear polymer consisting of glucose-monomers that form a chain of anhydroglucopyranose units that are connected by β-1,4-glycosidic bonds. A network of H-bonds is formed between parallel cellulose strands leading to the formation of microfibrils that give cellulose its high crystallinity and recalcitrance. Hemicellulose, on the other hand, is a branched polymer consisting of a mixture of C_5- and C_6-sugars and is found between the cellulose microfibrils and lignin. Its amorphous nature and readily accessible OH-groups make it the most reactive part of lignocellulosic biomass. Lignin, finally, is an amorphous phenolic polymer and responsible for the rigidity of the cell wall.[1,2] Valorization of the lignocellulosic biomass can either involve direct conversion of the whole biomass in one single process, or, alternatively, the biomass is pretreated and fractionated to its main components which are subsequently individually processed. These processes can be applied to produce low-value fuels or high-value chemicals from lignocellulosic biomass in a so-called biorefinery.

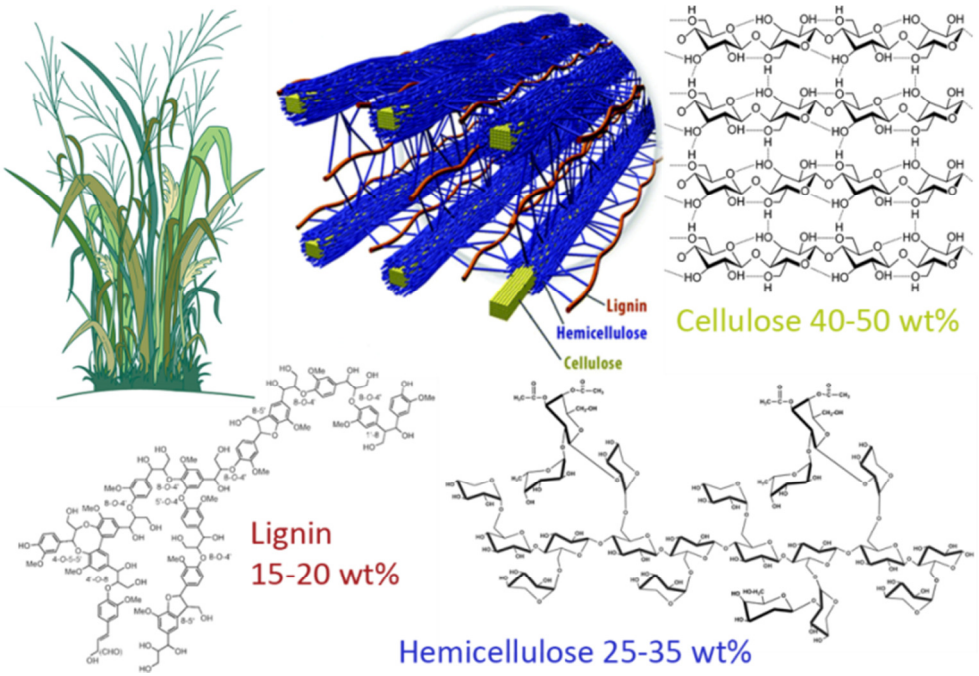

Figure 1.2. Composition of lignocellulosic biomass including its main components cellulose, hemicellulose and lignin and there relative abundances.[10] Adapted from [11–13] with permission.

1.2. Biorefinery Operations

The use of biomass as a resource for the production of chemicals and fuels requires the development of integrated conversion facilities called biorefineries where renewable materials are converted to low-value, high-volume fuels and high-value, low-volume chemicals, analogous to current oil refineries.[8] An important challenge for biorefinery operations is the production of bio-based fuels and chemicals in an economical, ethical and environmentally friendly way. This requires complete and efficient valorization of non-edible feedstock. Many different individual thermochemical, chemo- and biocatalytic conversion steps have been proposed to convert biomass into value-added products together with many different integrated conversion routes, of which some examples are given below. [1,7,9,14]

The first option is to convert the complete lignocellulosic biomass by thermochemical techniques. For instance by gasification to H_2 and CO, which can in turn be used for the production of alkanes by Fischer-Tropsch synthesis, among various other outlets. The gasification process can be applied for any kind of lignocellusic biomass; further processing of the syngas requires extensive purification, though, as impurities and water content of the feed can, for example, poison the Fischer-Tropsch catalyst.[10,15] Pyrolysis or liquefaction of complete biomass, on the other hand, is a cheap alternative to convert different types of biomass into a complex bio-oil. This product is, however, not suitable for combustion and requires extensive upgrading, *e.g.* by hydrodeoxygenation reactions, before it can be used as fuel.[10]

The second strategy for biomass conversion entails fractionation of the biomass into the three main components, which allows for the selective production of bulk chemicals or fuel. The lignocellucosic biomass can be fractionated by chemical or physical methods, such as milling, extraction or hydrolysis.[1,10] Complete valorization of the lignin fraction is still challenging, but this polymer could eventually be used for the production of aromatic compounds, such as benzene and phenols, or carbon fibers.[1,7,16] Valorization of the carbohydrate fractions is much further developed and typically consists of hydrolysis of the polymers to the individual sugar monomers, which are subsequently submitted to hydrogenolysis to produce polyols and alkanes,[17] fermentation to ethanol[1] or acid-catalyzed conversion for the production of renewable platform molecules such as hydroxymethylfurfural (FA), furfural (FF) and levulinic acid (LA).[7,10] The acid-catalyzed dehydration of (hemi)cellulose chemicals is favored over enzymatic treatment since higher (space time) yields can be obtained and a wider range of feedstocks and sugars can be applied.[18] The economic potential of carbohydrate-derived chemicals was assessed by the US Department of Energy (DOE) and LA, FF and 2,5-furandicarboxylic acid (which can be obtained by oxidation of HMF) were considered to have high potential as future platform molecules.[19]

1.2.1. Acid-catalyzed Dehydration of Components of Lignocellulosic Biomass

During the acid-catalyzed conversion processes a Brønsted acid catalyst is typically used for the depolymerization of cellulose to the individual glucose-units (C_6) while hemicellulose is hydrolyzed to a mixture of different C_6- and (mainly) C_5-sugars (xylose, for example). Acid-catalyzed dehydration of the C_6- and C_5-sugars in turn leads to the formation of HMF and FF, respectively. Under these acidic conditions, HMF is easily rehydrated to form LA and formic acid (FA) (Figure 1.3).[18] The applications of these compounds are numerous and some examples as well as the routes to their formation are discussed below.[8,10,16,18,20–24]

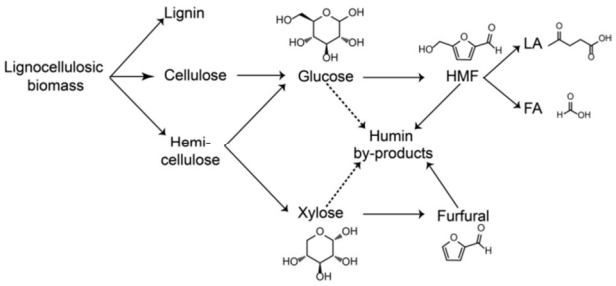

Figure 1.3. Production of levulinic acid (LA), hydroxymethylfurfural (HMF) and furfural (FF) from lignocellulose with humins formed as a by-product.

The acid-catalyzed dehydration of sugars in water to FA and a second acid, which was later identified as LA, was first reported by Mulder in 1840.[25] FA is already widely used in leather tanning, decalcification and as a platform for the production of chemicals, such as esters.[18] LA can also be used as a platform for the production of a broad range of chemicals. For example, the herbicide δ-aminolevulinic acid is easily produced from LA. The reaction of levulinic acid and two equivalents of phenol leads to the formation of diphenolic acid,[26] which is used in lubricants, adhesives and paints. Furthermore, LA can be converted to methyltetrahydrofuran, which is used as a fuel additive.[18,20] In addition, hydrogenation of LA to pentanoic acid and subsequent esterification yields alkyl (mono/di)valerate esters which are fuel and diesel-grade compounds.[22]

The formation of HMF from sugars was first reported in 1895.[23] HMF has recently been shown to be a promising platform chemical for, amongst others, the production of furandicarboxylic acid, which can be used as building block for the production of polyesters,[27] while ethers derived from HMF find application as fuel.[28] Another option to produce fuels from HMF or FF is by hydrogenation of the products obtained after aldol condensation with acetone.[21,23,29,30]

Several researchers have studied the formation of HMF and LA from a wide variety of feedstock, such as glucose, fructose, starch, cellulose and whole biomass.[23,31,32] In addition to these experimental studies the commercial interest in these carbohydrate-derived chemicals is exemplified by various industrial processes, which are at different stages of development. For example, the Biofine process is reported as the first commercial process for the production of LA. This process uses a double reactor approach

for continuous LA production and 40 wt% LA yields are claimed, based on the hexose content of the feedstock. In the first reactor lignocellulosic biomass is first hydrolyzed with 1.5-7 wt% H_2SO_4 at 210-250 °C for 7-30 s. Subsequently, HMF is rehydrated to form LA at 150-215 °C for 1-30 min. The efficiency of this process is limited due to the production of solid by-products, however.[18,33,34] Another important example of the commercialization of bio-based chemicals is provided by the Dutch company Avantium, which recently invested in the development of processes for the production of several furanics and levulinic acid esters and expects to run a commercial scale manufacturing plant by 2016.[35] The so-called YXY building blocks can be used for the production of, for example, polymers and fuel additives. The production of the furanic building blocks involves treatment of a glucose-containing feedstock with 1-20 mol% of acid catalyst at 175-225 °C for 1-60 min.[27,28,36]

As mentioned above, an important issue with processes that involve the hydrothermal treatment of aqueous carbohydrate solutions is the unavoidable and often extensive formation of solid by-products, in particular under the acidic conditions typically used in the HMF/FF/LA production chains. These carbonaceous solid by-products formed during the degradation of sugars are typically referred to as humins (Figure 1.3).[23,31,37–39] To our best knowledge, the term humin was first used for the solid materials formed during the acid-catalyzed dehydration of sucrose in 1840.[25] In literature, humin by-products are also referred to as humin-like substances,[40] humic solids,[41,42] or Biofine-char.[18] In the biofine process as much as 30 wt% of the carbohydrate source can end up in the humin by-product.[18] The amount of humin formed is often not reported in the open literature, but some authors report the formation of 8-20 mol% humin from HMF,[43] 16-34 mol% humin from fructose[43] and 32 wt% from glucose[44] using a homogeneous mineral acid in water. The commercial processes for the acid-catalyzed conversion are seriously hampered by the extensive formation of humin by-products that leads to great losses of the feed. Not only does this limit the efficiency of the process, the formation of solid by-products also leads to reactor fouling and considerable challenges in terms of engineering.

In order to improve the efficiency of acid-catalyzed conversions of sugars, humin formation should be avoided. This requires insight into the molecular structure and mechanism of formation of humins, both of which are not unequivocally established. Alternatively, humins could also be valorized if formed, for example, by conversion to chemicals *via* thermochemical or catalytic routes or by direct application in functional materials. Valorization again requires understanding of the humins molecular structure and chemical properties. An overview of literature describing the typical conditions, proposed mechanisms and kinetics of humin formation is given below. Furthermore, we reviewed the chemical properties and molecular structure of humins and related sugar-derived materials, such as hydrothermal carbon, caramels and degradation products of carbohydrates found in soil.

1.3. Formation of Humin By-products

Humins are formed during hydrothermal treatment of sugars under acidic conditions for the production of HMF, FF and LA. Several feedstocks can be applied for the production of HMF and LA, but most experimental studies are concerned with the conversion of pure fructose or glucose. It was shown that HMF formation from fructose is much faster, as isomerization of glucose to fructose precedes dehydration to HMF, a mechanism which was confirmed by ^{13}C NMR experiments.[46] Under acidic conditions HMF is easily rehydrated leading to the formation of LA and FA. The formation of humins is acid-catalyzed as well, leading to selectivity issues that require careful selection of the reaction conditions.[38,47,48] Numerous publications are concerned with the acid-catalyzed conversion of carbohydrates to HMF and LA and the reader is referred to extensive reviews describing the formation of HMF[23,30,32] and LA.[31] The discussion below is limited to some typical examples.

Homogeneous mineral acids, such as H_2SO_4 and HCl, are most used as catalyst for the conversion of C_6-sugars to HMF and LA. Some authors added a Lewis acid to increase the rate of isomerization from glucose to fructose and thus increase the yields.[23] Acid concentration is key to optimizing the yield of LA and to avoid the formation of humins. Most authors report an optimum acid concentration of 3.5-10 wt%. Another important factor is the reaction temperature which is typically ranges from 150 to 230 °C, with most authors reporting an optimum of 200-220 °C.[31] Selective production of HMF requires rehydration to LA to be prevented. This again emphasizes the need to carefully choose the conditions for the acid-catalyzed dehydration of sugars. Optimal residence times are key to efficient processing as well, since it was shown that at longer residence times HMF yield decreased due to rehydration to LA or condensation to humins.[43,49–51]

Some researchers applied heterogeneous catalysts for the production of LA from C_6-sugars. Yields from glucose and cellulose were relatively low, though.[31] This is probably caused by strong adsorption of LA on the catalyst surface.[52] However, successful conversion of cellulose to LA using a sulfonated chloromethyl polystyrene solid acid catalyst was recently reported.[53] For HMF formation over a heterogeneous solid acid catalyst more promising results were obtained, with several ion-exchange resins and water-stable oxides such as TiO_2 or ZrO_2 being reported as active catalysts.[23,31]

Next to the selection of the catalyst, solvents and co-solvents can be varied in order to optimize the HMF and LA yields. It was shown that addition of water-miscible organic solvents has a positive effect on the formation of HMF. For example, when the dehydration of fructose to HMF was performed in 70% ethylene glycol, the formation of HMF was much faster while its rehydration to LA was much slower leading to a higher maximum concentration of HMF compared to the reaction in pure water. In this case humins did not precipitate but stayed dissolved in ethylene glycol, which leads to new challenges in terms of the separation of the humins from the product.[54] Dehydration reactions in pure solvent require the use of very polar solvents, such as DMSO and DMF,

as dictated by the solubility of the sugars. Dehydration reactions performed in alcohols will lead to the formation HMF ethers or LA esters instead.[23,55]

The use of biphasic reaction media can further improve the yields by extraction of the products from the aqueous phase and thereby limiting humin formation. Dumesic *et al.* thus studied the formation of LA from cellulose in a biphasic system using γ-valerolactone as extraction solvent. The water phase contained HCl as catalyst and was saturated with NaCl to enhance phase separation and extraction. The humins formed during this reaction are solubilized in the organic layer and precipitated when water was added to the organic layer.[56] Dumesic *et al.*[57] also reported the use of phase modifiers for the production of HMF from fructose using homogeneous or heterogeneous catalysts. Biphasic systems were used and the organic phase methylisobutylketone was modified with different concentrations of 2-butanol, while the water layer was modified with DMSO and a hydrophilic polymer. It was shown that the addition of the phase modifiers increased the fructose conversion and HMF selectivity.[57]

1.3.1. Kinetics of Humin Formation

Several kinetic models for the dehydration of sugars to HMF and LA can be found in literature, but only few of these include the formation of humins. The available kinetic studies that do include humin formation, discussed in more detail below, in general indicate that high acid concentrations and lower reaction temperatures decrease the formation of humin by-products.[38,43–45,47,48,50,54,58–60]

An early example is the work of Kuster *et al.*[43,50,54] who studied the influence of substrate concentration and pH on formation of HMF and LA from fructose. It was shown that at 95 °C a high initial concentration of 1 M fructose or HMF decreased the LA yield and increased the amount of humin formed compared to low initial concentrations of 0.25 M. A kinetic model at constant initial substrate concentration was proposed, with reaction orders of humin formation of 1.3 and 1.7 being obtained for reactions starting from fructose and HMF, respectively.[43]

The Heeres group included humin formation in a kinetic model for the production of LA from HMF[47] and from more complex feedstock such as glucose,[38] cellulose[45] and water hyacinth.[58] The reaction conditions were varied with the aim to optimize the yield of LA, but the formation of humin by-products could not be avoided. Highest LA yields were obtained at low temperatures (140 °C) using high a concentration of sulfuric acid (1 M) as catalyst in a dilute sugar solution (0.1 M). Furthermore, the estimated activation energy for the formation of humins (164.7 kJ mol^{-1}) is much higher than all other activation energies during the acid-catalyzed dehydration of glucose, indicating that low reaction temperatures could limit humin formation.[38]

Huber *et al.*[44] proposed a kinetic model for the production of LA from glucose that fitted with their related experiments. It was shown that glucose dehydration, HMF rehydration and degradation of HMF to humins have an almost first order dependence of

acid concentration. While a near third order dependence was found for the degradation of glucose to humins and inversion products. Theoretical calculations furthermore showed that high temperatures (180-200 °C) and reaction times of < 1 min maximizes the HMF yield, while lower temperatures (140-160 °C) and reaction times longer than 100 min are needed to obtain a high LA yield.

The kinetics of LA production from cellulose was studied by Shen and Wyman,[60] who proposed a model with pseudo-first order reactions for all involved reactions. Furthermore, similar activation energies were found for the formation of humins and LA from HMF.[60]

Lund *et al.*[48] studied the kinetics of the acid-catalyzed dehydration of HMF to LA and FA. Their kinetic model showed that acid concentration affected the rate of LA formation more than the rate of humin formation. This higher order in acid concentration indicates that the use of high acid concentrations increases the selectivity to LA, which is in line with the findings of Heeres *et al.*[47,48] The above-mentioned studies describe the conditions leading to humin formation and how this might be avoided. The molecular details of the formation mechanism are, however, still largely unknown and insight in the molecular structure is required to better understand which intermediates are involved.

1.3.2. Chemical Properties and Molecular Structure of Humin By-products

The molecular structure of humin by-products formed during acid-catalyzed dehydration of sugars under the conditions typical for biorefinery operations has hardly been studied. Up to now, most knowledge about the structure of humin by-products is inferred from studies on related functional carbon material prepared under similar but not identical conditions, *i.e.* non-acid catalyzed hydrothermal treatment of carbohydrates and biomass or soil organic matter. An overview of the characterization data that has been reported for humins, soil organic matter, hydrothermal carbon (HTC) and other humin-like materials is given in Table 1.1 and will be discussed below.

In the first study on the formation of humins, by Mulder in 1840,[25] the elemental composition of humins prepared by the acid-catalyzed dehydration of sucrose with HCl was reported to be 64-65 wt% C, 5 wt% H, 31-32 wt% O.[25] Almost a century later, Schweitzer[39,61] reported on the elemental composition and chemical degradation of sucrose humins and proposed that sucrose humins are formed *via* dehydration reactions whereby the pyran ring of the sugar is not affected. A fragment of the humin structure, as proposed by the author, is depicted in Figure 1.4. [39,61]

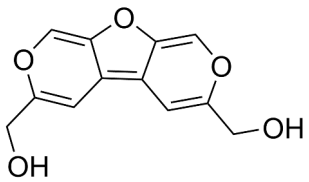

Figure 1.4. The first proposal for a fragment of the molecular structure of humins as proposed by Schweizer in 1937, based on elemental analysis and chemical degradation of humins.[39]

Further insight was obtained by Baugh *et al.*[41] who studied the decomposition of glucose and furfurals to optimize hydrothermal pretreatment of lignocellulose. The acid-catalyzed dehydration of several sugars, decomposition of furanics and formation of humins were studied. It was found that the composition of humins depended on feedstock as C contents of 58 and 62 wt% were reported for HMF-derived humins formed at pH 2.5 and glucose-derived humins formed at pH 2, respectively. The C content of the humins decreased to 56 wt% after treatment of glucose at a higher pH of 4. Furthermore, water-soluble humin precursors were found to have a molecular weight of 500-1000 as determined by ultrafiltration.[41] The group of Heeres *et al.* on the other hand, determined the elemental composition of the humins formed during the production of LA from HMF to be 61.2% C, 4.5% H and SEM images were acquired, which showed that agglomerated, spherical particles with a diameter of 5-10 µm were formed. However, further insight in the molecular structure of the humins was not obtained.[47] A more carbon-rich humin (65.5% C and 4.4% H) was found after treatment of fructose with phosphoric acid at 200 - 320 °C.[62]

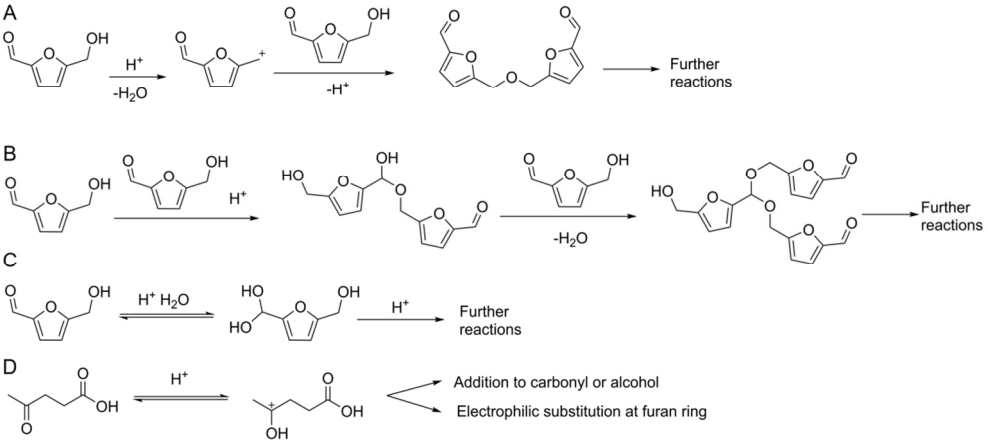

Figure 1.5. Formation of humins as proposed by Zarubin *et al*. based on IR, liquid-phase NMR and pyrolysis-GC-MS data. Adapted from Zarubin *et al.* with permission.[40]

The molecular structure of humin formed during acid treatment of different carbohydrates and HMF was investigated by Zarubin *et al.*.[40] The reaction was carried out with an aqueous solution of 5 wt% carbohydrate and 0.5% H_2SO_4 at 175-180 °C for 2 h. After isolation of the solids, the filtrate was neutralized in order to precipitate any acid-soluble polymers. About 20 wt% of the humins could be extracted with acetone. The IR spectra showed the soluble fraction to have a structure that is similar to the insoluble humins suggesting that this fraction can be regarded as shorter and less dense oligomers of the polymers present in the insoluble humin. The acetone-soluble fraction was further analyzed by ^{13}C NMR allowing the identification of several oxygen functionalities and furanic structures. IR spectra also confirmed the presence of oxygen-rich functional groups

and furanic rings. Furthermore, several furan derivatives were identified by pyrolysis-GC-MS. From this information it was concluded that the humin consists of 60% furan rings and 20% aliphatic linkers. A mechanism for the formation of humins was proposed, which involves the formation of ethers or acetal bonds, based on IR and NMR data, leading to a network of interconnected furan rings via the mechanisms A and B (Figure 1.5). HMF was also suggested to form hydrates (Figure 1.5C) that can enter the mechanisms A and B. It was furthermore proposed that protonation of LA can lead to a carbocation that reacts with HMF via addition to the carbonyl or alcohol or electrophilic substitution at the furan ring (Figure 1.5D).[40]

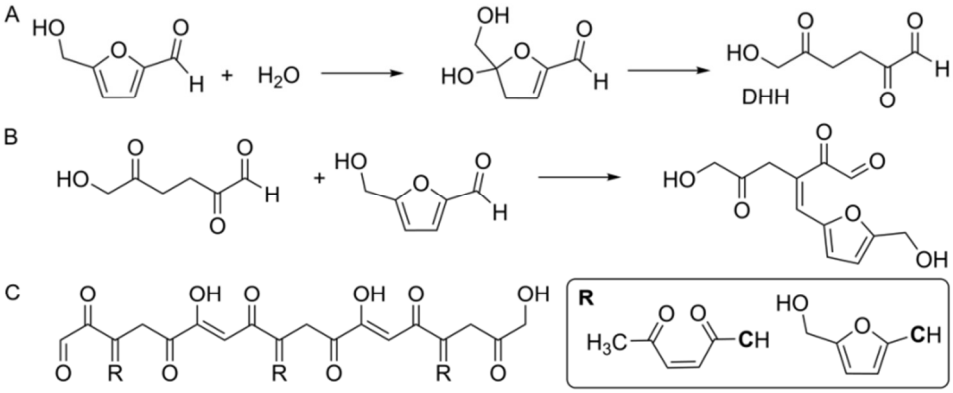

Figure 1.6 A. Formation of 2,5-dioxo-6-hydroxyhexanal (DHH) by rehydration of HMF. B. First condensation step of HMF with DHH. C. Idealized structure of humins formed via aldol condensation reactions of HMF with DHH according to Lund *et al.,* based on IR spectroscopy. Adapted from Lund *et al.* with permission.[48,63]

Lund *et al*. reported on the formation of humins and HTC from HMF. The IR spectra of acid-catalyzed and hydrothermal carbonization products indicated differences in the relative amount of functional groups. This, together with SEM images showing a different morphology of the HTC compared to the humins, indicates a difference in the formation mechanism. A mechanism for the formation of humins was proposed involving 2,5-dioxo-6-hydroxyhexanal (DHH), formed by rehydration of HMF (Figure 1.6A), as a key intermediate.[37] This intermediate was proposed to polymerize via subsequent aldol condensations with the carbonyl group of HMF to form humins (Figure 1.6B). The DHH intermediate was not detected in the reaction mixture, which was considered as an indication of the high reactivity of the compound.[48] Follow-up studies showed the differences between humins formed from HMF, glucose, fructose and cellobiose. While the particle size of the humins was found to increase with reaction time, the IR spectra indicated that this was not related to a change in the molecular structure in this case. Humins were proposed to be formed via aldol-condensations between DHH and HMF with the extent of incorporation of HMF in the humin structure depending on accumulation of

HMF during the acid-catalyzed conversion of the sugars. An idealized structure of humins as proposed by the authors is shown in Figure 1.6C. The accumulation of HMF is assumed to be higher during the acid-catalyzed dehydration of fructose, leading to the incorporation of more HMF in the structure, as compared to glucose- and cellobiose-derived humins.[63]

When complete biomass is used as a feedstock for the production HMF or LA, the humins become even more structurally complex due to the incorporation of unconverted biomass fragments. The structure is further complicated by possible cross-linking between the humins and unreacted fractions of biomass. For example, several features between 1000 and 1800 cm^{-1} seen in the FT-IR spectrum of Biofine chars indicated the incorporation of lignin fragments into the humins. Further analysis of these materials by TGA showed that the Biofine char contains limited amounts of cellulose and hemicellulose, in addition to the complete lignin fraction.[18] Indeed, solid-state NMR studies of the Biofine char from straw showed several features from the lignin residue, while Biofine char from paper showed features from cellulose around 100 ppm. Furthermore, a symmetric peak pattern was observed in the aromatic region that is, according to the authors, indicative for a fused polyaromatic structure.[64]

The group of Agrawal and Jones[65] studied the residues formed during the acid-catalyzed hydrolysis of loblolly pinewood with different acids at 120-200 °C using quantitative solid-state ^{13}C NMR. While the solid residues contained unconverted carbohydrates, lignin and humins, this study mainly focused on the quantification of the lignin in the isolated solids.[65] This research group furthermore studied the hydrolysis of sugars, including fructose, glucose, mannose and xylose,[66] and pine wood[67] in ionic liquids. It was shown that conversion of the sugars was faster at a high temperature, albeit with a concomitant increase in the formation of humins. These humins were thought to be formed by condensation reactions of soluble products and HMF was believed to play a key role in their formation.[65–67]

1.3.2.1. Soil Organic Matter

The name humin itself suggests a relation to the organic component found in soil called humus, a component which is formed by decay of plant or animal material. An important process during the formation of humus is the degradation of carbohydrates, from which the relation with our sugar-derived humins originates. Humus consists of three main components: fulvic acid, which is soluble in water at any pH, alkali-soluble humic acid and insoluble soil humin.[68] As discussed below, humin by-products from sugar dehydration processes might have a molecular structure that is similar to humic acid and to soil humin.[69,70] However, the humus fractions are expected to have a more complex structure as a result of the incorporation of fatty acids, amino acids, lignin, and inorganic materials.[68,71,72] The humus fractions have been extensively studied with several analytical techniques[73–75] and wet chemical techniques[71,76,77] revealing a complex

aromatic, mainly phenolic polymer with several oxygen and nitrogen functionalities, as illustrated by the structure for humic acid shown in Figure 1.7.[68,78,79]

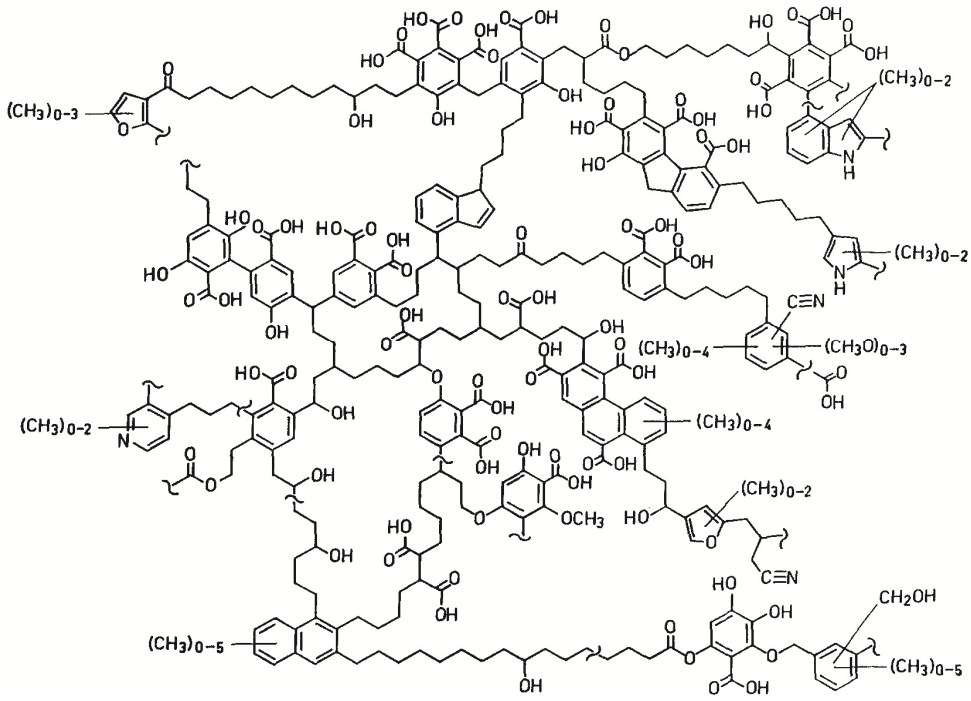

Figure 1.7. Schematic representation of the molecular structure of humic acid. Taken from Schnitzer *et al.* with permission.[82]

An indication for the structural relation between of sugar-derived humins[40,63] and fulvic and humic acid[80] can be found in their IR spectra, which show a strong resemblance, especially at wavenumbers below 2000 cm^{-1}. For example, strong peaks are observed at 1700 cm^{-1} and 1600 cm^{-1} in both spectra, indicating the presence of C=O and aromatic rings, respectively.[80] The acid-catalyzed dehydration of carbohydrates was actually studied as a model system for the formation of humic substances in soil chemistry. For example, Almendros *et al.* synthesized soil humin-like polymers from glucose. These were categorized in acid-soluble, alkaline-soluble and insoluble fractions and analyzed by ^{13}C NMR, elemental analysis, GPC and IR spectroscopy. Using this combination of techniques several furan-rich and polymeric structures were identified for the soil humin-like and humic acid-like fractions, while the fulvic acid-like fraction showed strong signals from the carbohydrate fraction.[69,81] Herzfeld *et al.*, on the other hand, used ^{13}C solid-state NMR to study the formation humin-like materials from sugars by solvent-free dehydration with oxalic acid. It was shown that under these conditions furan units act as a cross-linker between sugar molecules leading to the formation of complex

polymers.[70] These publications show that well-established techniques used to analyze or break down humus substances might be interesting for the characterization of humin by-products.

1.3.2.2. Hydrothermal Carbonization

More closely related to the humin by-products are the functional carbon materials that are prepared by hydrothermal treatment of carbohydrates or biomass, so-called hydrothermal carbon (HTC). This hydrothermal treatment differs from the above-mentioned processes that lead to humin formation in the fact that no acid is used in the formation of HTC and the process actually focusses on the production of a well-defined carbon material in high yield. The structural insights obtained for HTC are nonetheless very valuable, as similar feedstock and conditions are typically involved. The molecular structures and relevant mechanisms proposed in literature for HTC are reviewed below, while the processing conditions and HTC characterization data are summarized in Table 1.1. Two, somewhat conflicting proposals for the molecular structure of HTC have been postulated.[83,84,86]

Sevilla *et al.*[83,84] studied the influence of reaction temperature, time and feedstock on the structure of HTC. The amount of HTC formed during hydrothermal treatment increases with temperature, reaction time and (poly-)saccharide concentration. The size and chemical composition of the spherical HTC particles depended strongly on feed and processing parameters. XPS data showed the O/C ratio of the surface of the particles to be comparable to the bulk composition, as determined by elemental analysis, and indicated the presence of several reactive oxygen functional groups. With increasing temperature the O/C and H/C ratio decreased, suggesting further carbonization and aromatization of the sample, which was supported by a decrease of the IR signals from oxygen functionalities at the expense of signals from aromatic rings. Also, the Raman spectra of the carbon material show peaks at 1360 and 1587 cm^{-1} attributed to the D- and G-band of disordered graphite-like carbon. In addition, TEM images of HTC particles showed a slight difference in contrast between the core and the shell of the particle suggesting a difference in chemical composition. A mechanism for the formation of HTC was proposed involving condensation reactions between sugars and furanics formed during cellulose dehydration and subsequent aromatization of the polymers. The resulting spherical particles were proposed to consist of a polycyclic aromatic structure with hydrophilic groups on the surface and less reactive (hydrophobic) groups in the core (Figure 1.8).[83,84] It should be noted that the Raman data might overestimate the amount of polycyclic aromatic groups, as the D- and G-bands of graphite-like carbon have large Raman cross-sections leading to high intensities in the spectrum.[92]

Table 1.1 Overview of experimental conditions for HTC and humin production and techniques used for characterization of HTC and humin.

Ref	Processing conditions					Characterization					
	Feedstock	[sugar]	[acid]	*T* (°C)	*t* (h)	Elemental composition C%	H%	O%	Particle Size	IR Wavenumber (cm^{-1})	NMR δ (ppm)
[25]	sucrose	2:2:20 sugar:acid :water	HCl H_2SO_4	165	-	64-65	4.6-4.8	30.5-31.9	-	-	-
[61]	sucrose	-	5% HCl	100	24	61.5	4.4	34.1	-	-	-
[41]	D-glucose HMF	5.57 -333 mM	H_3PO_4 pH 4 pH 2 pH 2.5	 190 190 190	 0.25 1.25 2	 56 62 58	-	-	-	-	-
[47]	HMF	0.1-1.7	0-1 M H_2SO_4	98-181	≤10	61.2	4.5	-	5-10 µm	-	-
[62]	D-fructose	0.05 M	H_3PO_4	200-320	0.25	65.5	4.4	-	-	-	-
[40]	D-glucose HMF D-mannose D-galactose D- arabinose cellobiose methyl-α-D-glucoside	5 wt%	0.05 wt% H_2SO_4	175-180	2	66.4	4.7	28.9	-	3500-3200 CH polymeric, 2950-2800 CH aliphatic, 1710-1685 furanic aromatic or aliphatic ester, 1610-1650 furan, 1440-1415 CH OH COO^-, 1610-1360 furan ring, 1200-1000 C-O-C	220-186 C=O , 185-160 COOH, 164-140 furan-O 140-103 furan-H or –C, 103-96 acetal, 80-65 CH_2-O, 58-54 CH_3-O
[48]	HMF	0.1 M	0-0.1 M H_2SO_4	118 125 135	0.25-2 18	-	-	-	10 µm	1522, 1275, 1198, 1020, 962, 826, 777 furan ring	-

Ref	Processing conditions					Characterization					
	Feedstock	[sugar]	[acid]	*T* (°C)	*t* (h)	Elemental composition C%	Elemental composition H%	Elemental composition O%	Particle Size	IR Wavenumber (cm^{-1})	NMR δ (ppm)
[63]	HMF glucose fructose cellobiose	0.1 M	0.1 M H_2SO_4	118 125 135	0.5-24	-	-	-	-	1710 and 1625 C=O conjugated with C=C, 1525, 1030, 850 and 750 furan ring	-
[18,33,34,64]a	whole biomass straw paper	-	1.5-7 wt% H_2SO_4	210-220 190-200	12 s 20 min	-	-	-	-	~1700 carbonyl/carboxyl 1800-1000 lignin, ~1700 carbonyl/carboxyl ~1700 carbonyl/carboxyl	150-100 aryl , 150 O-aryl, 60 methoxyl lignin 150-100 aryl, ~110 di-O-alkyl cellulose
[65]	loblolly pinewood	1:9 solid:liquid	pH 1.65 H_2SO_4 HNO_3 TFA[b] HCl	120-200	1	-	-	-	-	-	221, 203, 173 acetyl hemicellulose, 153 O-aryl, 150 C=C-OH, 135 C=C substituted, 128 C=C,118 C=C unsubstituted, 105 carbohydrate, 89 carbohydrate, 82 hemicellulose, 73 carbohydrate, 63 carbohydrate, 56 methoxy lignin, 21 acetyl hemicellulose
[70]	D-ribose D-fructose D-glucose D-galactose D-mannose D-deoxyribose	1:1 molar ratio no solvent	oxalic acid	65	14-63 days	-	-	-	-	-	210 ketone, 175 acid or ester, 150 Cα furan substituted, 110 Cβ furan, 60-80 ether alcohol, 20-40 methylene

Ref	Processing conditions					Characterization					
	Feedstock	[sugar]	[acid]	*T*	*t*	Elemental composition			Particle Size	IR Wavenumber	NMR δ
				(°C)	(h)	C%	H%	O%		(cm^{-1})	(ppm)
[83]	D-glucose sucrose starch	0.5-1 M 0.5 M 0.1-0.5 M	-	170-240 190 180-200	0.5-15	64.9	4.2	30.9	0.4-6 µm	3000-3700 O-H, 2900 C-H, 1000-1450 C-O, 1620, 1513, 875-750 C=C, 1710 C=O	-
[84]	cellulose	40-320 g/L	-	200-250	2-4	71.4	4.3	24.3	2–10 µm	3000-3700 O-H ,2900 C-H, 1000-1450 C-O, 1620, 1513, 875-750 C=C , 1710 C=O	-
[85]	D-fructose	2.5 M	-	120-140	0.5-2	-	-	-	200-400 nm	3500 OH, 1704 COO^- , 1604 C=C	Solid-state: 100-230 aromatic functionality Liquid phase: fructose, formation of LA and HMF
[86]	^{13}C D-glucose	10 wt%	-	180	24	62	4	34	-	-	Solid-state: 13-74 sp^3 C, 110-156 sp^2 C, 175-179, 202-207, 218 C=O Liquid phase: HMF, LA, FA, glucose and dihydroxyacetone
[87]	D-glucose HMF maltose sucrose amylopectin starch D-xylose FF	10 wt%	-	180	24	64.5 68.6	4.7 4.1	30.9 27.3	500-1000 nm 100-1000 nm	-	208 C=O, 175 C=O, 150 C=C , 40 aliphatic, 20-40 methylene, 75 C-OH 40-50 sp^3C, 129 C=C

Ref	Processing conditions					Characterization					
	Feedstock	[sugar]	[acid]	*T* (°C)	*t* (h)	Elemental composition C%	H%	O%	Particle Size	IR Wavenumber (cm^{-1})	NMR δ (ppm)
[88]	D-glucose cellulose rye straw	10 wt%	-	120-280	24	-	-	-	glucose 160°C 474 nm 260°C 685 nm	1700 C=O Increases until 200-220°C, disappears when T increases further	150 O-C=CH, 110-118 O-C=CH , 208 C=O, 125-129 aromatic ring
[89]	D-xylose D-fructose sugar + phenolic compounds (1:1)	0.5 M total	-	130-170	12	61.2	4.1	34.7	-	3400 O-H, 1704 C=O, 1616 C=C aromatic ring/furan, 1290 1211 C-O-C 798 756 furan C-H out of plane def	-
[90]	HMF	0.02-0.15 M	-	350 450 250 bar	80 - 3000 s	-	-	-	0.05-0.2 µm	3300 O-H, 2950 C-H, 1670 C=O, 1620 C=C 1620-1490, 1515-1380, 1430-1330 2,5 substituted furan	-
[91]c	^{13}C D-glucose	No solvent	30% Fuming H_2SO_4	150 350	2 1	-	-	-	-	-	200 ketone, 180 acid, 155 Cα furan substituted or phenol, 120-130 fused aromatic rings, 115-125 Cβ furan or phenol, 30-60 alkyl

[a.] Biofine process involves a two reactor process. [b.] TFA = trifluoroacetic acid. [c.] Sugar is treated in fuming sulfuric acid or pyrolyzed at 350 °C

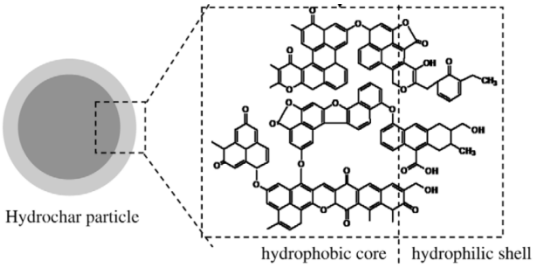

Figure 1.8. Molecular structure of HTC as proposed by Sevilla based on elemental analysis, XPS, Raman, IR. Adapted from Sevilla *et al.* with permission.[84]

Shin[85] and coworkers came to a similar proposal after a study of the dehydration of fructose with Raman spectroscopy. The spectroscopic data indicated the presence of aromatic groups with oxygen-rich functionalities. The presence of disordered carbon and graphite-like structures was confirmed by the D- and G-bands observed in the Raman spectra at 1385 cm^{-1} and 1585 cm^{-1}, respectively. TEM images again showed spheres thought to consist of a condensed, hydrophobic core and a less dense, hydrophilic shell, in line with the structure suggested by Sevilla *et al*.[85]

An alternative structure was suggested for various hexose- and pentose-derived HTC in a series of papers by the group of Titirici and Baccile.[86] Advanced solid-state ^{13}C NMR spectra of ^{13}C-labeled HTC led them to conclude that HTC consist of a furan-rich structure in which subunits are directly bound to or linked together by an aliphatic group on the C_α- or C_β-position, with levulinic acid being physically embedded in the polymer (Figure 1.9).[86] Data from carbonized sugars was compared to the characteristics of hydrothermally treated FF and HMF, which showed that HTC produced from C_5- and C_6-sugars resemble carbonized FF and HMF, respectively. SEM images showed that different carbohydrates lead to the formation of spheres with different particle sizes and elemental composition. For example, HTC from xylose was found to have a lower O/C and H/C ratio compared to the HTC from the other starting materials.[87] The ^{13}C NMR spectra of xylose-based HTC also indicated a lower amount of aliphatic groups, while the signals attributed to conjugated C=C systems were stronger when compared to glucose-derived HTC. This indicates that the molecular structure of HTC from C_5-sugars contains relatively more furanic moieties than HTC prepared from C_6-sugars.[88]

The same group used ^{13}C solid-state NMR to study the effect of heat treatment on the molecular structure HTC compared to the structures formed during heat treatment of sugars. Hydrothermal treatment (180 °C) of sugars gave a furanic polymer with aliphatic linkers, as discussed before.[86] On the other hand, after calcination at 350 °C of HTC or sugars a more conjugated aromatic structure is observed, which was ascribed to the formation of small polycyclic aromatic structures *via* fusion of the furanic rings. Treatments above 400 °C finally led to the formation of graphene-like polyaromatic sheets (Figure 1.10). These results show that the molecular structure of HTC strongly depends on the reaction temperature.[93]

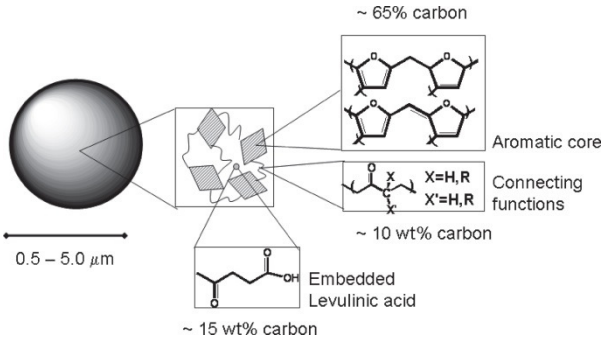

Figure 1.9. Molecular structure of HTC as proposed by Baccile *et al.* based on solid-state NMR. Taken with permission from [86].

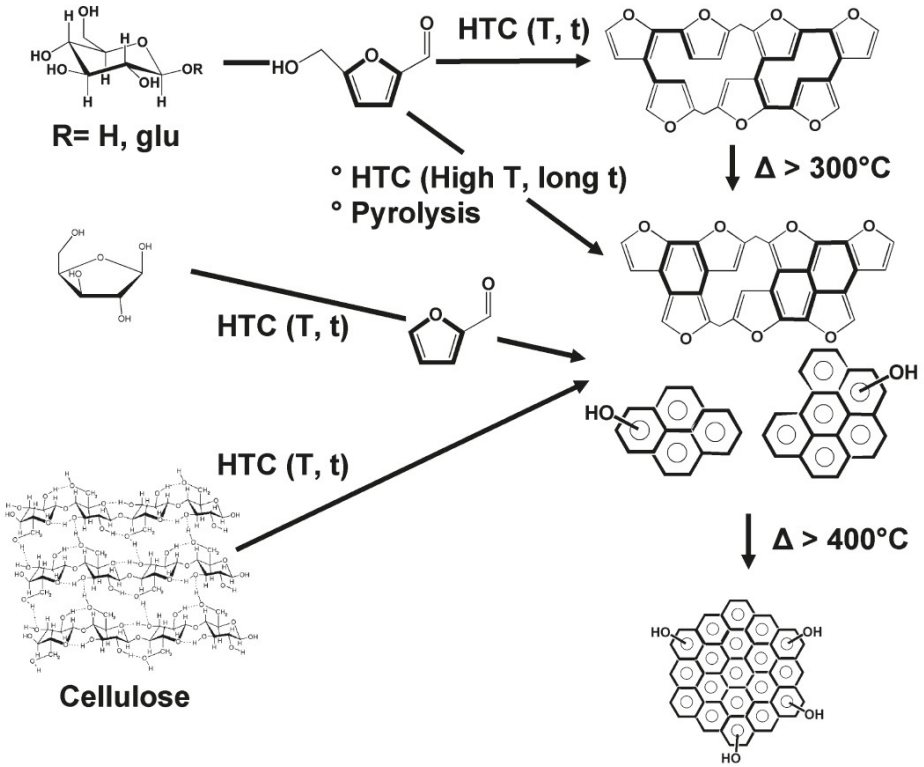

Figure 1.10. Molecular structure of HTC, pyrolyzed HTC and pyrolyzed cellulose based on solid-state NMR. Taken from Baccile *et al.* with permission.[93]

Suh *et al*.[89] studied the effect of such phenolic compounds on the formation of HTC from sugars, demonstrating indeed a substantial increase in carbon yield. A twentyfold increase in carbon material formed was observed upon addition of 1,3,5-trihydroxybenzene, for instance. In addition, the spheres were larger than the particles prepared without aromatics in the feedstock. Addition of 1,3,5-trihydroxybenzene also increased the oxygen content of the HTC formed.[89] The isomer, 1,2,4-trihydroxybenzene

(TB) is a minor product during sugar dehydration formed from HMF during carbohydrate dehydration and might also be involved in humin formation.[94]

HTC and comparable materials can be formed under varying conditions and from many different feedstocks including, but not limited to, saccharides, polysaccharides, complete biomass. In addition, subjecting HMF to harsh, aqueous conditions also results in the formation of carbonaceous materials. For example, tarry material and char were obtained after treatment of HMF in subcritical (350 °C, 250 bar) and supercritical (450 °C, 250 bar) water. SEM images of the char particles revealed a spherical morphology. The IR spectra of the char showed peaks strong peaks from OH and C=O, while peaks at 1620-1460, 1515-1380 and 1330 cm^{-1} indicated the presence of furanic rings in the polymer. The peak at 1620 cm^{-1} could also point at the presence of benzene rings. The D- and G-bands detected by Raman spectroscopy in turn pointed at the presence of crystalline and amorphous aromatic carbon. The char was thought to be formed via 2,5-polymerization, ring fusion and substitution reactions of HMF and reactions with HMF degradation products such as TB. Further dehydration to arene sheets was suggested as well, leading to the molecular structure shown in Figure 1.11.[90]

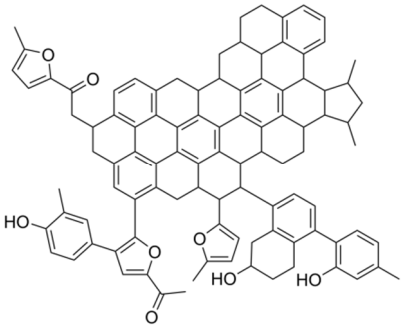

Figure 1.11. Molecular structure of char after treatment of HMF in supercritical water based on IR and Raman spectroscopy. Reproduced from Matsumura *et al.* with permission.[90]

An important class of functional carbon materials are solid acid catalyst, which are prepared by pyrolysis of sugar and/or treatment with sulfuric acid.[95] In order to get insight in these materials, Schmidt-Rohr *et al.*[91] studied the effect of treatment with fuming sulfuric acid on the molecular structure of $^{13}C_6$-glucose and pyrolyzed $^{13}C_6$-glucose using 2D solid-state NMR techniques, which were supported by DFT calculations. Dipolar-dephased Double-Quantum Single Quantum (DQSQ) measurements allowed them to selectively study cross peaks between non-protonated carbon atoms. In addition, the fully complementary method of Exchange with Protonated and Non-protonated Spectral Editing (EXPANSE)[91] provided information on the interactions between protonated and non-pronated carbon atoms, which allowed the authors to distinguish, for example, between signals from substituted furans from phenols. An advantage of both techniques is the absence of a diagonal ridge, which often obscures various expected cross peaks in carbonaceous samples. It was shown that the acid-treated glucose sample had a furan-rich

structure while the pyrolyzed and subsequently acid-treated glucose sample had a more highly carbonized, structure with small polycyclic aromatic units (Figure 1.12).[91]

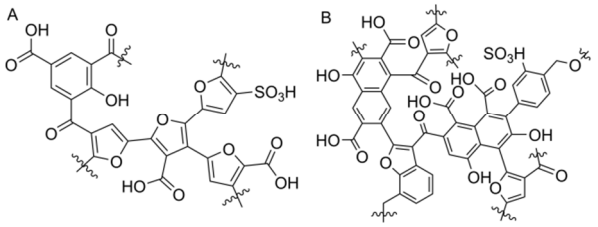

Figure 1.12. Molecular structure of acid-treated glucose (A) and acid-treated pyrolyzed glucose (B), based on solid-state NMR. Reproduced from Schmidt-Rohr *et al*. with permission.[91]

1.3.2.3. Food Chemistry: Caramel and Browning Reactions

The topic of non-enzymatic browning reactions of sugar-containing products is well-studied in food science and also bears relevance to humin formation and structure. This process is often caused by Maillard reactions between carbohydrates and amino acids, *e.g*. browning of meat, but could also be caused by formation of furanic molecules from sugars, *e.g.* caramelization.[96] Interestingly, for the unwanted browning of dehydrated orange juice during storage a relation between the formation of HMF and the browning reaction was found.[97] Other authors also studied the acid-catalyzed dehydration of sugars to understand the role of HMF in browning reactions.[98,99]

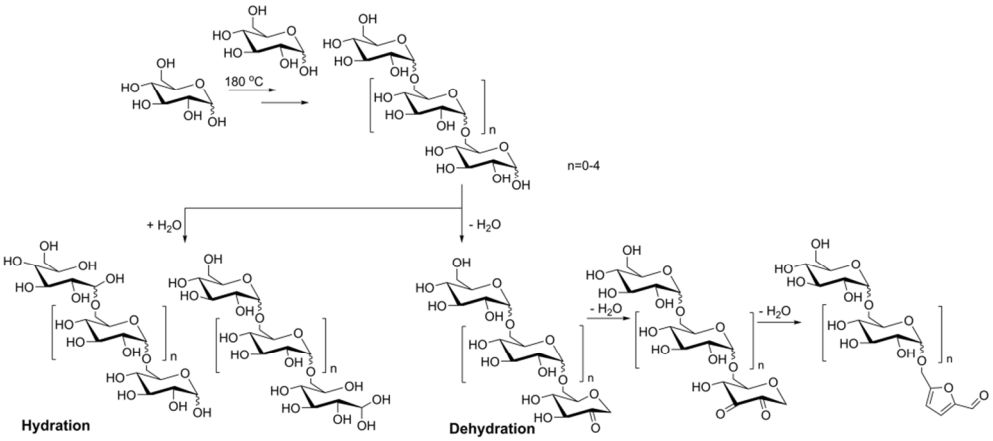

Figure 1.13. Proposed formation mechanism and molecular structures for caramel fragments as determined using a combination of mass spectrometry and NMR techniques. Reproduced from Kuhnert *et al.* with permission.[100]

In the formation of caramel, the candy that can be obtained by heating a variety of sugars, the browning reaction gives the typical aroma that is obtained by heating sugars or sugar syrup.[96] Older studies on the chemical composition of caramel and humins have shown that a structural relation between humin and caramel exists.[39,61] Furthermore,

several furanic compounds were detected by GC-MS in the volatile fraction of caramel. The solid fraction was studied by mass spectrometry and NMR revealing a polysaccharide structure that was formed via condensation reactions between the sugar monomers leading to the formation of oligomers, which are further dehydrated to furanic molecules (Figure 1.13).[100–102]

1.3.3. Mechanism of Humin Formation

The molecular structure of humins has not yet been unequivocally established, nor has the mechanism of formation. Several researchers postulated mechanisms of humin formation, however, implicating various intermediates whereby the role of HMF leads to discussion. Self-condensation of HMF (or FF) to give humins has been suggested.[103] This route was also proposed for the formation of tar or char during the treatment of sugars in (sub)-critical water.[59,62,90,104] Polymerization of FF via the free 5-position is well-known in the formation of resins,[105] while the polymerization of HMF is much less studied. Others have discarded this self-condensation route, based on the argument that FF and HMF do not have an α H-atom and therefore cannot undergo this type of reaction.[106] Therefore, it is often assumed that humins from C_6-sugars are formed via cross-polymerization reactions between sugars and HMF or reactive molecules formed from HMF.[23] The formation of humins from C_5-sugars is studied even less. The various pathways proposed for humin formation from C_6-sugars are reviewed below.

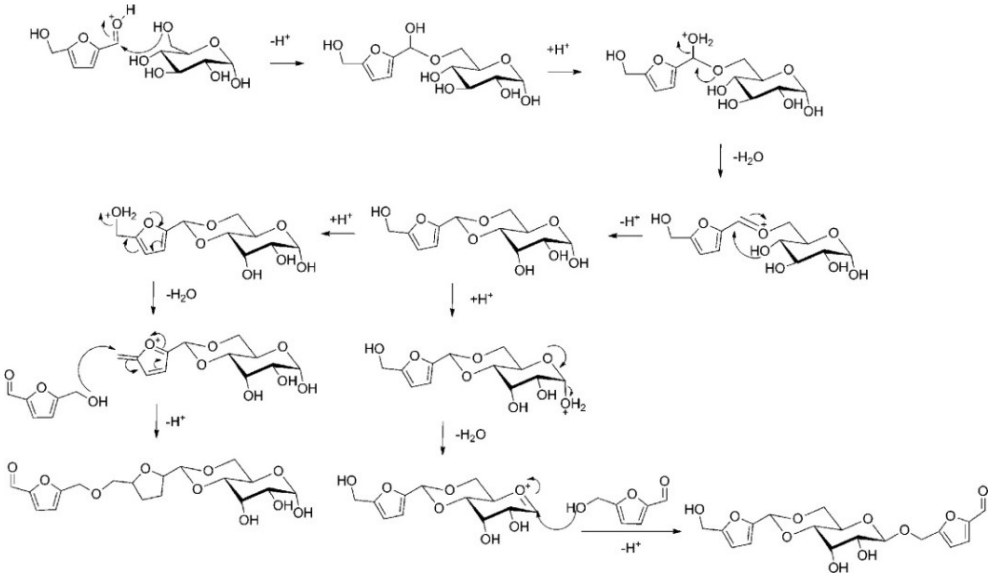

Figure 1.14. Formation of humins via polymerization reactions of HMF with glucose as proposed by Bell *et al*. and taken with permission.[107]

Bell *et al.*[107] studied the hydrolysis of cellulose to glucose and formation of by-products in ionic liquids catalyzed by sulfuric acid. In this study HMF, glucose and

cellobiose and cellulose were used as starting material. Depending on acid concentration, up to 30 mol% humin was formed from cellulose. The role of HMF in the formation of humins was indicated by the increase of humin yield at high HMF concentrations. No characterization data on the humins was reported, but the authors did suggest that humins are formed by condensation polymerization of HMF with glucose as shown in Figure 1.14. This process is initiated by protonation of the aldehyde function of HMF followed by reaction with a monosaccharide.[107] Other researchers suggested that humins from xylose are similarly formed via reactions between xylose and FF.[108–110]

Pidko *et al.*[111] studied the mechanism of Brønsted acid-catalyzed conversion of glucose and fructose to LA and HMF using DFT calculations and also pointed at the role of HMF in the formation of humins. An intermediate denoted as H-1 (Figure 1.15) that is formed by dehydration of HMF can react with several other intermediates leading to the formation of oligomeric products. A similar pathway for humin formation was reported before by Zarubin *et al.*,[40] as discussed above (Figure 1.5). These polymerization steps are actually energetically preferred over the rehydration step that would ultimately lead to LA (Figure 1.15).[111] These results were in contrast with the kinetic model presented by Heeres *et al.*. [38] Notably, Pidko *et al.*[111] also proposed an alternative route for the direct formation of LA from glucose, without fructose or HMF being involved as intermediate. The proposed direct route entails protonation at the glucose O-2 or O-3 atom (Figure 1.16). It was found that the overall outcome of the reaction was dictated by the site of initial protonation, with O-5 protonation giving isomerization to fructose, while protonation of the O-1 or O-4 atom leads to humins and reversion products (Figure 1.16). The calculated Gibbs free energies show that protonation on the O-1 and O-4 atoms is actually favored, which suggests that a selectivity challenge in an early stage of the reaction ultimately leads to low LA yields.[111]

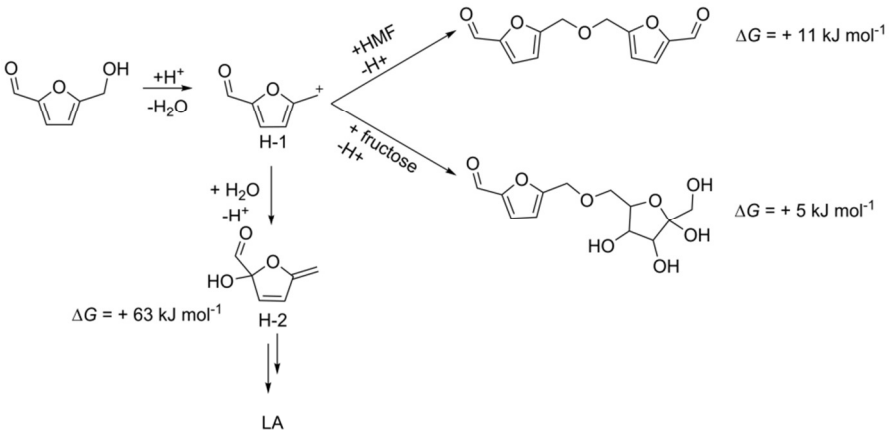

Figure 1.15. Formation intermediation H-1 from HMF leading to the formation of LA and humins as proposed by Pidko *et al.* including the calculated Gibbs free energy for the model reactions. Adapted with permission.[111]

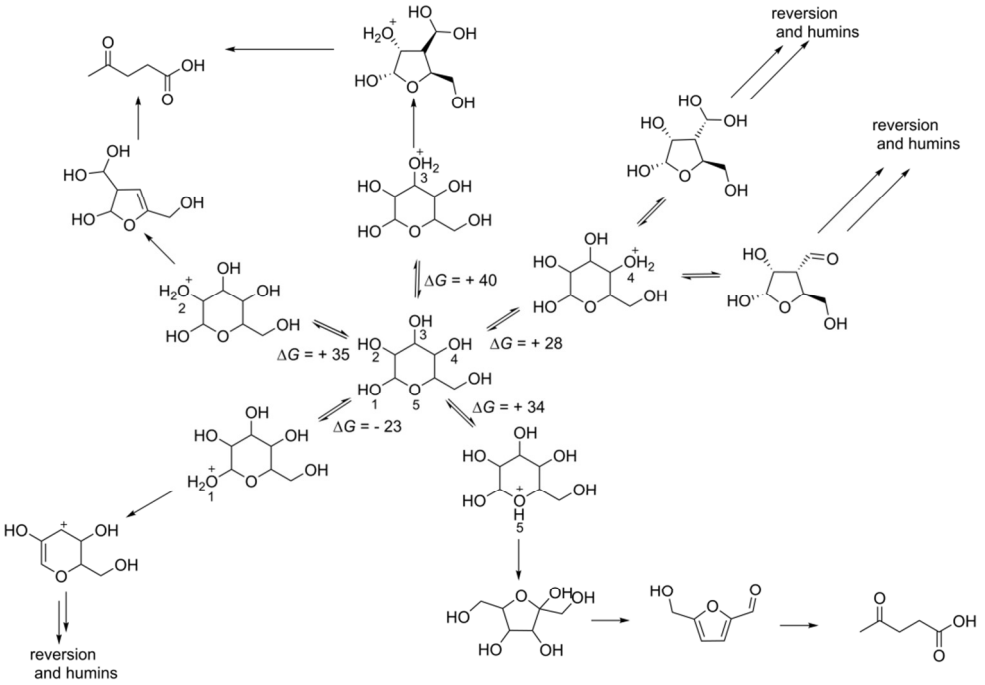

Figure 1.16. Protonation of glucose on different O atoms and subsequent formation of LA, HMF and humins including the calculated Gibbs free energy (in kcal/mol) of the protonation reaction showing that humin formation from glucose is favored over the reaction path leading to LA. Adapted with permission.[111]

Another intermediate held responsible for humin formation was suggested by Šunjić *et al.*[37] who detected several intermediates in the formation of LA from HMF in ^{13}C NMR studies. A mechanism for the formation of LA and humins from HMF was proposed as shown in Figure 1.17. It was postulated that LA formation is initiated by 4,5-addition of water to HMF, while humin formation was thought to start with 2,3-addition of water, leading to the formation of 2,5-dioxo-6-hydroxy-hexanal (DHH). This intermediate was not observed in the NMR spectra but is believed to polymerize readily leading to the formation of humins.[37] Lund *et al.,*[48,63] further built on this theory and suggested that humins are formed by aldol condensation reactions between DHH and HMF. The proposed molecular structure and characterization of these humins are discussed above (Figure 1.6).

Horvath *et al.* monitored the acid-catalyzed dehydration of fructose to HMF in DMSO using *in situ* NMR studies and ^{13}C labeling studies. Four intermediates were identified and reversible formation of **3** (Figure 1.18) was observed, which could be a mechanistic limitation for selective formation of HMF. Furthermore, the formation of **7** (Figure 1.18) was observed, which was dehydrated to **8** (Figure 1.18) and is believed to polymerize to form humins. Based on the NMR data a reaction network for the dehydration of fructose was proposed where the furanose form (Figure 1.18, 1b and 1c)

leads to the formation of HMF, while its pyranose form (Figure 1.18, 1d and 1e) leads to humin formation.[112]

In conclusion, the intermediates, growth mechanisms, reactions and functional groups involved in humin formation are largely unknown. This is further complicated by the fact that the intermediates involved in the formation of FF, HMF and LA are not completely understood yet.[23,24,31] This reflects the complexity of the reactions involved in humin formation and the necessity to obtain more insight in the involved intermediates and mechanisms. This can be achieved by detailed characterization of the humins.

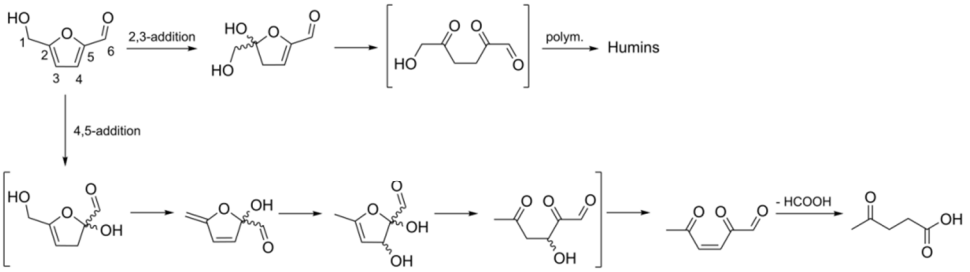

Figure 1.17. Mechanism for the formation of LA via 4,5-addition of water, and humins by 2,3-addition of water as proposed by Šunjić *et al*. by liquid-phase NMR: structures between brackets are postulated intermediates and were not identified. Reproduced with permission.[37]

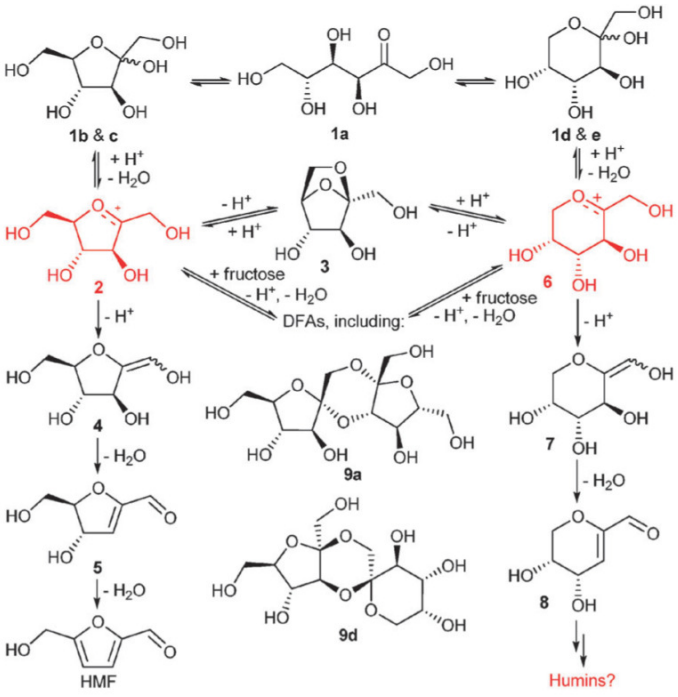

Figure 1.18. Mechanism for the formation of HMF and humins as proposed by Horvath *et al*. based on liquid-phase NMR: intermediates in red were not detected. Taken with permission.[112]

1.3.4. Utilization of Humin By-products

As stated before, humin formation limits the efficiency of the production of bulk chemicals from carbohydrates. In order to improve the economic feasibility of the acid-catalyzed conversion of sugars the formation of humins should be avoided or routes for the valorization of humins should be developed. Complete exclusion of humin formation is very unlikely as sugar dehydration, HMF rehydration and humin formation are all acid-catalyzed processes. In addition, DFT calculations even suggest that humin formation is thermodynamically favored.[111] Therefore, a certain amount of humins will always be formed and should be valorized to accomplish a low-waste and efficient biorefinery process. The valorization of humins has so far been hardly explored, most probably due to the limited insight in its molecular structure and chemical properties. In commercial processes, such as the Biofine process, humins are currently burnt for their heating value as coal-like fuel.[18] Better understanding of the humins structure might, however, contribute to the development of higher-value applications of humins.

As the molecular structure of humins is expected to be similar to HTC, application as functional carbon material, for example in soil improvement or CO_2 sequestration, can be expected.[18,113,114] HTC and chars obtained by pyrolysis of biomass also find application as active carbon for the adsorption of metal ions[115–118] or phenol.[118] After functionalization, humins could be used as solid acid catalysts. Indeed, sulfonated, pyrolyzed sugars are reported to give stable solid acid catalysts for the esterification of fatty acids to produce biofuel or hydrolysis of polysaccharides.[95,119,120]

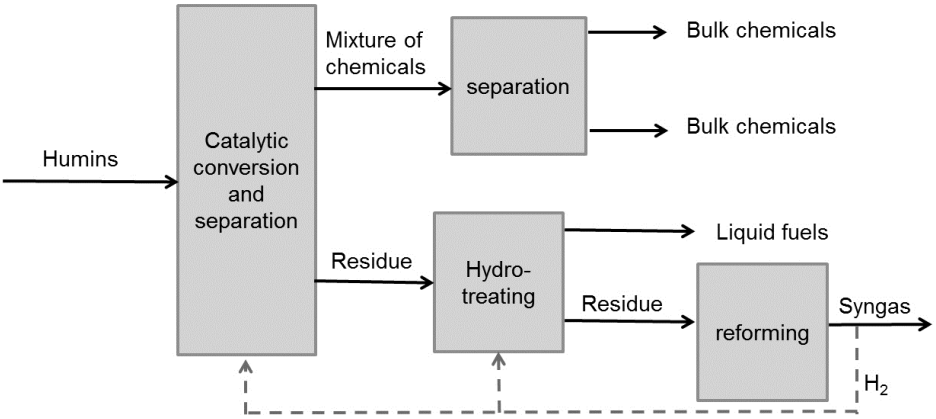

Figure 1.19. Proposed scheme for humin valorization showed within the CatchBio consortium.

Alternatively, routes could be sought for the valorization of humins to chemicals, for instance by thermochemical conversion of the humins to syngas by gasification[18,121,122] or steam reforming.[121,122] The produced syngas can, for example, be used for the production of alkanes by Fischer-Tropsch synthesis. On the other hand,

humin-oils could be obtained by pyrolysis of the humins, with a first example of such a process already reporting about 30 wt% of the humin intake to be converted to volatiles such as 2,5-dimethylfuran.[123] Chemocatalytic routes that aim for a more selective formation of chemicals from the humins have, to our best knowledge, not yet been reported in literature. Such more selective valorization strategies could consists of the catalytic valorization of humins via an integrated approach where the humins are converted to several bulk chemicals, with residual material being further processed by hydrotreatment for the formation of liquid fuel. The hydrogen that might be needed for such processes could be produced by reforming of the remaining residue (Figure 1.19). Chemical valorization of the humin by-product over a (heterogeneous) catalyst is, however, hampered by its complex molecular structure and general insolubility.

1.4. Scope and Outline of this Thesis

The work described in this PhD thesis aims for a better understanding of the mechanism of formation and molecular structure of humin by-products and explores possible routes for the catalytic valorization of humins. To achieve this, the formation of both humins and platform chemicals from different sugars and a raw feed was monitored. The humins formed were extensively characterized using several analytical and spectroscopic techniques. The solubility of humins was subsequently improved, as the valorization of humins is also hampered by their typical insolubility, which limits substrate-catalyst interactions. Finally, an attempt to the valorization of humins to chemicals was made by aqueous phase reforming over a heterogeneous catalyst.

In **Chapter 2** a multi-parameter and multi-technique approach is described with the aim to get insight in the formation, morphology and chemical properties of the humin by-products from different sugars. Process parameter variation by Design of Experiment (DoE) gave insight in the reaction parameters leading to humin formation. Based on the characterization data (including elemental analysis, IR, ^{13}C solid-state NMR and pyrolysis-GC-MS) a representative model for the molecular structure of humins is proposed.

Chapter 3 addresses the general insolubility of the humins studied and describes an alkaline pretreatment method for the reactive solubilization of humins from different sugar feeds. Temperature, base concentration and reaction time were optimized to achieve complete solubilization of humins from glucose, fructose and xylose. The alkali-treated humins were recovered from solution and characterized in order to identify changes in their molecular properties upon alkaline pretreatment, *i.e.* the treatment leads to further aromatization.

In **Chapter 4** the molecular structure of ^{13}C-labeled humins is studied in further detail by complementary 1D and 2D solid-state NMR studies. A combination of 1D ^{13}C NMR, 2D ^{1}H-

^{13}C and 2D ^{13}C-^{13}C NMR was applied using direct excitation and cross polarization techniques. This allows one to distinguish between furanic and phenolic rings and the data led to a refinement of the molecular structure described in Chapter 2. Alkali-treated ^{13}C-labeled humins were also analyzed by 1D ^{13}C NMR and 2D ^{13}C-^{13}C NMR after direct excitation and cross polarization, giving additional information on the chemical changes in the humins after alkaline treatment.

Chapter 5 describes the Aqueous Phase Reforming (APR) of alkali-treated humins and untreated, solid humins over supported platinum catalysts for the production of aromatic monomers and hydrogen. Pt/Al_2O_3 was included for benchmarking and the effect of a more water-stable support was tested using Pt/TiO_2. The influence of alloying was investigated using a $Pt\text{-}Re/ZrO_2$ catalyst. The obtained gases were analyzed and the composition of the limited amounts of humin-oil formed was determined by GCxGC-MS.

In **Chapter 6** thick juice, a sucrose-rich syrup from a sugar beet refinery, was studied to assess the effect of using a raw, unpurified feedstock in hydrothermal, acid-catalyzed biorefining. Reaction parameters were screened to optimize the HMF and LA yields and the humins formed were characterized using elemental analysis, IR, ^{13}C solid-state NMR and pyrolysis-GC-MS. The raw sucrose-containing feed behaved remarkably different from purified sucrose, both in terms of HMF/LA production as well as with regards to the amount and nature of the humins formed.

In **Chapter 7** a summary of the research described in this PhD thesis is given, together with some concluding remarks.

1.5. References

[1] Y. H. P. Zhang, *J. Ind. Microbiol. Biotechnol.* **2008**, *35*, 367–375.

[2] C. A. S. Hill, in *Wood Modification: Chemical, Thermal and Other Processes* (Ed.: C. V. Stevens), John Wiley & Sons, Ltd, Chichester, UK, **2006**.

[3] C. E. Morrell, *Ind. Eng. Chem.* **1959**, *51*, 247–247.

[4] "Motor vehicles: use of biofuels," can be found under http://europa.eu/legislation_summaries/energy/renewable_energy/l21061_en.htm, **2003**.

[5] "EU greenhouse gas emissions and targets," can be found under http://ec.europa.eu/clima/policies/g-gas/index_en.htm, **2013**.

[6] "World energy consumption," can be found under http://www.bp.com/en/global/corporate/about-bp/energy-economics/energy-outlook.html, **2014**.

[7] A. J. Ragauskas, C. K. Williams, B. H. Davison, G. Britovsek, J. Cairney, C. A. Eckert, W. J. Frederick Jr, J. P. Hallett, D. J. Leak, C. L. Liotta, J. R. Mielenz, R. Murphy, R. Templer, T. Tschaplinski, *Science* **2006**, *311*, 484–489.

[8] J. J. Bozell, G. R. Petersen, *Green Chem.* **2010**, *12*, 539–728.

[9] P. Gallezot, *ChemSusChem* **2008**, *1*, 734–737.

[10] D. M. Alonso, J. Q. Bond, J. A. Dumesic, *Green Chem.* **2010**, *12*, 1493–1513.

[11] "U.S. Department of Energy's Office of Biological and Environmental Research," can be found under https://public.ornl.gov/site/gallery/default.cfm

[12] M. Ochoa-Villarreal, E. Aispuro-Hernández, I. Vargas-Arispuro, M. Ángel Martínez-Téllez, in *Polymerization* (Ed.: A. De Souza Gomes), InTech, **2012**.

[13] A. Brandt, J. Gräsvik, J. P. Hallett, T. Welton, *Green Chem.* **2013**, *15*, 537–848.
[14] J. J. Bozell, *Clean* **2008**, *36*, 641–647.
[15] J. Hu, F. Yu, Y. Lu, *Catalysts* **2012**, *2*, 303–326.
[16] F. Cherubini, A. H. Strømman, *Biofuels, Bioproducts and Biorefining* **2011**, *5*, 548–561.
[17] P. Gallezot, *Green Chem.* **2007**, *9*, 295–302.
[18] D. J. Hayes, J. Ross, M. H. B. Hayes, S. W. Fitzpatrick, in *Biorefineries - Industrial Processes and Products* (Eds.: B. Kamm, P.R. Gruber, M. Kamm), Wiley, **2006**, 139–164.
[19] "Top Value Added Chemicals from Biomass Volume I - Results of Screening for Potential Candidates from Sugars and Synthesis Gas Top Value Added Chemicals From Biomass," can be found under http://www1.eere.energy.gov/bioenergy/pdfs/35523.pdf, **2004**.
[20] J. J. Bozell, L. Moens, D. C. Elliott, Y. Wang, G. G. Neuenscwander, S. W. Fitzpatrick, R. J. Bilski, J. L. Jarnefeld, *Resour. Conserv. Recycl.* **2000**, *28*, 227–239.
[21] J. P. Lange, E. van der Heide, J. van Buijtenen, R. Price, *ChemSusChem* **2012**, *5*, 150–166.
[22] J. P. Lange, R. Price, P. M. Ayoub, J. Louis, L. Petrus, L. Clarke, H. Gosselink, *Angew. Chem. Int. Ed.* **2010**, *49*, 4479–4483.
[23] R. J. van Putten, J. C. van der Waal, E. de Jong, C. B. Rasrendra, H. J. Heeres, J. G. De Vries, *Chem. Rev.* **2013**, *113*, 1499–1597.
[24] J. Lewkowski, *Arkivoc* **2001**, *i*, 17–54.
[25] Mulder, *J. Pract. Chemie* **1840**, *21*, 203–240.
[26] A. R. Bader, A. D. Kontowicz, *J. Am. Chem. Soc.* **1954**, *76*, 4465–4466.
[27] E. De Jong, M. A. Dam, L. Sipos, G. J. M. Gruter, in *Biobased Monomers, Polymers, and Materials* (Eds.: P.B. Smith, R.A. Gross), American Chemical Society, **2012**, 1–13.
[28] E. De Jong, T. Vijlbrief, R. Hijkoop, G. J. M. Gruter, J. C. Van Der Waal, *Biomass and Bioenergy* **2012**, *36*, 151–159.
[29] R. M. West, Z. Y. Liu, M. Peter, J. A. Dumesic, *ChemSusChem* **2008**, *1*, 417–24.
[30] A. A. Rosatella, S. P. Simeonov, R. F. M. Frade, C. A. M. Afonso, *Green Chem.* **2011**, *13*, 754–793.
[31] D. W. Rackemann, W. O. S. Doherty, *Biofuels, Bioproducts and Biorefining* **2011**, *5*, 198–214.
[32] T. Wang, M. W. Nolte, B. H. Shanks, *Green Chem.* **2014**, 548–572.
[33] S. W. Fitzpatrick, *US Patent 4,897,497*, **1990**.
[34] S. W. Fitzpatrick, *US Patent 5,608,105*, **1997**.
[35] "XYX technology," can be found under http://www.avantium.com/yxy/YXY-technology/YXY-process-technology/manufacturing.html
[36] G. J. M. Gruter, F. Dautzenberg, *EP 1,834,951 A1*, **2007**.
[37] J. Horvat, B. Klaić, B. Metelko, V. Šunjić, *Tetrahedron Lett.* **1985**, *26*, 2111–2114.
[38] B. Girisuta, L. P. B. M. Janssen, H. J. Heeres, *Chem. Eng. Res. Des.* **2006**, *84*, 339–349.
[39] A. Schweizer, Caramel En Humine, PhD Thesis, Delft University, **1937**.
[40] I. V. Sumerskii, S. M. Krutov, M. Y. Zarubin, *Russ. J. Appl. Chem.* **2010**, *83*, 320–327.
[41] K. D. Baugh, P. L. McCarty, J. A. Levy, *Biotechnol. Bioeng.* **1988**, *31*, 50–61.
[42] C. Chang, X. Ma, P. Cen, *Chin. J. Chem. Eng.* **2006**, *14*, 708–712.
[43] B. B. F. M. Kuster, H. S. van der Baan, H. van der Baan, *Carbohydr. Res.* **1977**, *54*, 165–176.
[44] R. Weingarten, J. Cho, R. Xing, W. C. Conner, G. W. Huber, *ChemSusChem* **2012**, *5*, 1280–1290.
[45] B. Girisuta, L. P. B. M. Janssen, H. J. Heeres, *Ind. Eng. Chem. Res.* **2007**, *46*, 1696–1708.
[46] H. Kimura, M. Nakahara, N. Matubayasi, *J. Phys. Chem. A* **2011**, *115*, 14013–14021.
[47] B. Girisuta, L. P. B. M. Janssen, H. J. Heeres, *Green Chem.* **2006**, *8*, 701–709.
[48] S. K. R. Patil, C. R. F. Lund, *Energy Fuels* **2011**, *25*, 4745–4755.
[49] C. Moreau, R. Durand, S. Razigade, J. Duhamet, P. Faugeras, P. Rivalier, P. Ros, G. Avignon, *Appl. Catal. A Gen.* **1996**, *145*, 211–224.
[50] B. F. M. Kuster, H. M. G. Temmink, *Carbohydr. Res.* **1977**, *54*, 185–191.
[51] A. S. Amarasekara, A. Razzaq, *Carbohydr. Res.* **2014**, *386*, 86–91.
[52] B. Girisuta, Levulinic Acid from Lignocellulosic Biomass, PhD Thesis, Rijksuniversiteit Groningen, **2007**.
[53] Y. Zuo, Y. Zhang, Y. Fu, *ChemCatChem* **2014**, *6*, 753–757.
[54] B. F. M. M. Kuster, *Carbohydr. Res.* **1977**, *54*, 177–183.
[55] D. W. Brown, A. J. Floyd, R. G. Kinsman, Y. Roshan-Ali, *J. Chem. Technol. Biotechnol.* **2007**, *32*, 920–924.
[56] S. G. Wettstein, D. M. Alonso, Y. Chong, J. A. Dumesic, *Energy Environ. Sci.* **2012**, *5*, 8199–8203.
[57] Y. Román-Leshkov, J. N. Chheda, J. A. Dumesic, *Science* **2006**, *312*, 1933–1937.
[58] B. Girisuta, B. Danon, R. Manurung, L. P. B. M. Janssen, H. J. Heeres, *Bioresour. Technol.* **2008**, *99*, 8367–8375.
[59] F. S. Asghari, H. Yoshida, *Ind. Eng. Chem. Res.* **2007**, *46*, 7703–7710.

[60] J. Shen, C. E. Wyman, *AIChE J.* **2012**, *58*, 236–246.
[61] A. Schweizer, *Recl. des Trav. Chim. des Pays-Bas* **1938**, *57*, 345–382.
[62] F. S. Asghari, H. Yoshida, *Ind. Eng. Chem. Res.* **2006**, *45*, 2163–2173.
[63] S. K. R. Patil, J. Heltzel, C. R. F. Lund, *Energy Fuels* **2012**, *26*, 5281–5293.
[64] E. H. Novotny, M. H. B. Hayes, E. R. de Azevedo, T. J. Bonagamba, S. W. Fitzpatrick, in *International Biochar Initiative Conference*, Terrigal, Australia, **2007**.
[65] C. Sievers, T. Marzialetti, T. J. C. Hoskins, M. B. Valenzuela Olarte, P. K. Agrawal, C. W. Jones, M. B. V. Olarte, *Bioresour. Technol.* **2009**, *100*, 4758–4765.
[66] C. Sievers, I. Musin, T. Marzialetti, M. B. Valenzuela Olarte, P. K. Agrawal, C. W. Jones, *ChemSusChem* **2009**, *2*, 665–671.
[67] C. Sievers, M. Valenzuela-Olarte, T. Marzialetti, I. Musin, P. K. Agrawal, C. W. Jones, *Ind. Eng. Chem. Res.* **2009**, *48*, 1277–1286.
[68] R. Sutton, G. Sposito, *Environ. Sci. Technol.* **2005**, *39*, 9009–9015.
[69] G. Almendros, J. Sanz, I. Sobrados, *Sci. Total Environ.* **1989**, *81/82*, 91–98.
[70] J. Herzfeld, D. Rand, Y. Matsuki, E. Daviso, M. Mak-Jurkauskas, I. Mamajanov, *J. Phys. Chem. B* **2011**, *115*, 5741–5745.
[71] C. Deport, A. Kribii, L. Lemee, A. Ambles, *Org. Geochem.* **2008**, *39*, 178–187.
[72] F. J. Stevenson, Humus Chemistry: Genesis, Reactions and Composition, Wiley, New York, **1994**.
[73] M. Tatzber, M. Stemmer, H. Splegel, C. Katziberger, G. Haberhauer, A. Mentler, M. H. Gerzabek, *J. Plant Nutr. Soil Sci. Fur Pflanzenernahrung Und Bodenkd.* **2007**, *170*, 522–529.
[74] A. J. Simpson, G. X. Song, E. Smith, B. Lam, E. H. Novotny, M. H. B. Hayes, *Environ. Sci. Technol.* **2007**, *41*, 876–883.
[75] A. Naidja, D. W. Anderson, P. M. Huang, C. Van Kessel, *Appl. Spectrosc.* **2002**, *56*, 318–324.
[76] J. A. Neyroud, M. Schnitzer, *Geoderma* **1975**, *13*, 171–188.
[77] O. B. Maximov, T. V Shvets, Y. N. Elkin, *Geoderma* **1977**, *19*, 63–78.
[78] A. Piccolo, *Soil Sci.* **2001**, *166*, 810–832.
[79] J. A. Rice, *Soil Sci.* **2001**, *166*, 848–857.
[80] R. Baigorri, M. Fuentes, G. González-Gaitano, J. M. García-Mina, G. Almendros, F. J. González-Vila, *J. Agric. Food Chem.* **2009**, *57*, 3266–3272.
[81] G. Almendros, J. A. Leal, *J. Soil Sci.* **1990**, *41*, 51–59.
[82] H.-R. Schulten, M. Schnitzer, *Naturwissenschaften* **1993**, *80*, 29–30.
[83] M. Sevilla, A. B. Fuertes, *Chem. Eur. J.* **2009**, *15*, 4195–4203.
[84] M. Sevilla, A. B. Fuertes, *Carbon* **2009**, *47*, 2281–2289.
[85] C. Yao, Y. Shin, L. Q. Wang, C. F. Windisch Jr., W. D. Samuels, B. W. Arey, C. Wang, W. M. Risen Jr., G. J. Exarhos, *J. Phys. Chem. C* **2007**, *111*, 15141–15145.
[86] N. Baccile, G. Laurent, F. Babonneau, F. Fayon, M. M. Titirici, M. Antonietti, *J. Phys. Chem. C* **2009**, *113*, 9644–9654.
[87] M. M. Titirici, M. Antonietti, N. Baccile, *Green Chem.* **2008**, *10*, 1204–1212.
[88] C. Falco, N. Baccile, M. M. Titirici, *Green Chem.* **2011**, *13*, 3273–3281.
[89] J. Ryu, Y.-W. Suh, D. J. Suh, D. J. Ahn, *Carbon* **2010**, *48*, 1990–1998.
[90] A. Chuntanapum, Y. Matsumura, *Ind. Eng. Chem. Res.* **2009**, *48*, 9837–9846.
[91] R. L. Johnson, J. M. Anderson, B. H. Shanks, X. Fang, M. Hong, K. Schmidt-Rohr, *J. Magn. Reson.* **2013**, *234*, 112–124.
[92] A. C. Ferrari, J. Robertson, *Phys. Rev. B - Condens. Matter Mater. Phys.* **2000**, *61*, 14095–14107.
[93] C. Falco, F. Perez Caballero, F. Babonneau, C. Gervais, G. Laurent, M. M. Titirici, N. Baccile, *Langmuir* **2011**, *27*, 14460–14471.
[94] G. C. A. Luijkx, F. Van Rantwijk, H. Van Bekkum, C. A. Luijkx, V. Bekkum, *Carbohydr. Res.* **1993**, *242*, 131–139.
[95] K. Nakajima, M. Hara, *ACS Catal.* **2012**, *2*, 1296–1304.
[96] H. D. Belitz, W. Grosch, P. Schieberle, *Food Chemistry*, Springer-Verlag, Berlin Heidelberg, **2009**.
[97] R. E. Berry, J. H. Tatum, *J. Agric. Food Chem.* **1965**, *13*, 588–590.
[98] S. S. Bharate, S. B. Bharate, *J. Food Sci. Technol.* **2014**, *51*, 2271–2288.
[99] R. L. Handwerk, R. L. Coleman, *J. Agric. Food Chem.* **1988**, *36*, 231–236.
[100] A. Golon, N. Kuhnert, *J. Agric. Food Chem.* **2012**, *60*, 3266–3274.
[101] E. Suárez-Pereira, E. M. Rubio, S. Pilard, C. Ortiz Mellet, J. M. García Fernández, *J. Agric. Food Chem.* **2010**, *58*, 1777–1787.
[102] J. Defaye, M. G. Fernandez, *Carbohydr. Res.* **1994**, *256*, C1–C4.
[103] F. Ilgen, D. Ott, D. Kralisch, C. Reil, A. Palmberger, B. König, *Green Chem.* **2009**, *11*, 1948–1954.

[104] R. Hashaikeh, I. S. Butler, J. A. Kozinski, *Energy Fuels* **2006**, *20*, 2743–2747.
[105] A. Gandini, M. N. Belgacem, *Prog. Polym. Sci.* **1997**, *22*, 1203–1379.
[106] G. W. Huber, J. A. Dumesic, *Catal. Today* **2006**, *111*, 119–132.
[107] S. J. Dee, A. T. Bell, *ChemSusChem* **2011**, *4*, 1166–1173.
[108] S. P. Daniel, K. J. Zeitsch, *WO 0047569 A1*, **2000**.
[109] R. Weingarten, J. Cho, W. C. Conner, Jr., G. W. Huber, *Green Chem.* **2010**, *12*, 1423–1429.
[110] H. Rasmussen, H. R. Sørensen, A. S. Meyer, *Carbohydr. Res.* **2013**, *385C*, 45–57.
[111] G. Yang, E. A. Pidko, E. J. M. Hensen, *J. Catal.* **2012**, *295*, 122–132.
[112] G. R. Akien, L. Qi, I. T. Horváth, *Chem. Commun.* **2012**, *48*, 5850–5852.
[113] M. M. Titirici, A. Thomas, M. Antonietti, *New J. Chem.* **2007**, *31*, 787–789.
[114] A. B. Fuertes, M. Sevilla, J. A. Macia, J. A. Maciá-Agulló, *Biomass and Bioenergy* **2011**, *35*, 3152–3159.
[115] Z. G. Liu, F. S. Zhang, *J. Hazard. Mater.* **2009**, *167*, 933–939.
[116] P. Regmi, J. L. Garcia Moscoso, S. Kumar, X. Cao, J. Mao, G. Schafran, *J. Environ. Manag.* **2012**, *109*, 61–69.
[117] S. Kumar, V. a Loganathan, R. B. Gupta, M. O. Barnett, *J. Environ. Manag.* **2011**, *92*, 2504–2512.
[118] Z. Liu, F.-S. Zhang, *Desalination* **2011**, *267*, 101–106.
[119] S. Suganuma, K. Nakajima, M. Kitano, S. Hayashi, M. Hara, *ChemSusChem* **2012**, *5*, 1841–1846.
[120] J. A. Maciá-Agulló, M. Sevilla, M. A. Diez, A. B. Fuertes, *ChemSusChem* **2010**, *3*, 1352–1354.
[121] T. M. C. Hoang, L. Lefferts, K. Seshan, *ChemSusChem* **2013**, *6*, 1651–1658.
[122] T. M. C. Hoang, E. R. H. van Eck, W. P. Bula, J. G. E. Gardeniers, L. Lefferts, K. Seshan, *Green Chem.* **2014**, DOI 10.1039/C4GC01324G.
[123] C. B. Rasrendra, M. Windt, Y. Wang, S. Adisasmito, I. G. B. N. Makertihartha, E. R. H. van Eck, D. Meier, H. J. Heeres, *J. Anal. Appl. Pyrolysis* **2013**, *104*, 299–307.

CHAPTER 2

Formation, Molecular Structure and Morphology of Humins in Biomass Conversion: Influence of Feedstock and Processing Conditions

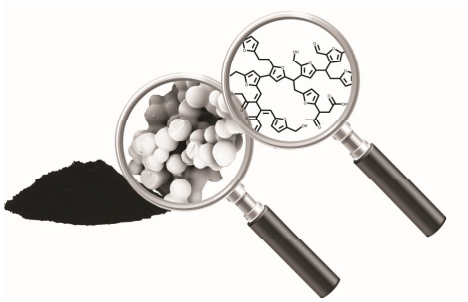

Abstract

Neither the routes via which humin by-products are formed, nor their molecular structure are yet unequivocally established. A better understanding of the formation and physicochemical properties of humins would aid in making biomass conversion processes more efficient. Here, an extensive multiple technique-based study of the formation, molecular structure and morphology of humins is presented as a function of sugar feed, the presence of additives (*e.g*. ,1,2,4-trihydroxybenzene), and the applied processing conditions. Elemental analyses indicate that humins are formed via a dehydration pathway, with humin formation and levulinic acid yields strongly depending on the processing parameters. The addition of implied intermediates to the feed showed that furanics and phenolics formed during the acid-catalyzed dehydration of sugars are indeed included in the humin structure. IR spectra, sheared sum projections of 2D PASS ^{13}C solid-state NMR spectra, and pyrolysis GC-MS data indicated that humins consist of a furan-rich polymer network containing different oxygen functional groups. The structure is furthermore found to strongly depend on the type of feedstock. A model for the molecular structure of humins is proposed based on the presented data.

Based on: I. van Zandvoort, Y. Wang, C. B. Rasrendra, E. R. H. van Eck, P. C. A. Bruijnincx, H. J. Heeres, B. M. Weckhuysen, "Formation, Molecular Structure, and Morphology of Humins in Biomass Conversion: Influence of Feedstock and Processing Conditions" *ChemSusChem* **2013**, 6, 1745-1758.

Ilona van Zandvoort and Yuehu Wang contributed equally to this chapter; it is therefore part of both PhD theses.

2.1. Introduction

In a lignocellulosic biorefinery operation, the cellulose and hemicellulose fractions generally need to be depolymerized first to the individual glucose (C_6) and pentose units (C_5, *e.g.* xylose) before the constituent monosaccharides can be further converted to a whole slate of sustainable chemicals and fuels. A prominent example of such a subsequent conversion step is the acid-catalyzed dehydration of glucose or xylose to form the key platform molecules 5-hydroxymethylfurfural (HMF) and furfural (FF), respectively.[1–6] Rehydration of HMF finally yields the valuable building blocks levulinic acid (LA) and formic acid (FA).[3,7,8] The strong current interest from industry in the production of HMF and LA-based chemicals is exemplified, for instance, by the efforts of the Dutch company Avantium, which has recently announced the construction of a pilot plant that converts carbohydrates into various furanics. The so-called YXY furanic building blocks can subsequently be used for the production of tailored polymers and biofuels.[9] The commercial scale production of levulinic acid *via* the Biofine process is another well-known example.[10] Such acid-catalyzed conversions of the (hemi) cellulose fraction of lignocellulosic biomass to these platform chemicals are, however, unavoidably accompanied by the formation of so-called artificial humin by-products, in short referred to as humins.[8,11,12] Humins are carbonaceous, heterogeneous, poly-disperse materials of which the molecular structure is largely unknown. For the Biofine process it is known that humin formation decreases LA yield and poses considerable challenges in terms of reactor engineering.[10]

Humin by-products have so far received very little attention with respect to the mechanism of the formation and the elucidation of their molecular structure.[13–15] Knowledge about both is nonetheless required if further optimization of the HMF or LA production processes, or, alternatively, the valorization of the humins themselves is targeted. Indeed, here, we aim to better understand the formation mechanism and to obtain insight in the molecular structure and morphology of the humin by-product. This information can then subsequently be used to limit the formation or to devise catalytic routes that valorize the humins that are formed during biomass conversion processes.

Up to now, most knowledge about the structure of humin or humin-like components is based on the characterization of functional carbon materials that are prepared by hydrothermal treatment of carbohydrates or biomass, so-called hydrothermal carbon (HTC).[16–18] This hydrothermal treatment differs from the above-mentioned processes that lead to humin formation in the fact that no acid is used in the formation of HTC. The structural insights obtained for HTC are nonetheless valuable, as similar feedstock and conditions are involved. Two, somewhat conflicting proposals for the molecular structure of HTC have been postulated. Based on IR, Raman, XPS and elemental analysis a polyaromatic, condensed structure was proposed,[16,17] while other researchers suggested a polyfuranic structure based on solid-state NMR spectra.[18] The molecular structures and relevant mechanisms proposed in literature for HTC and humin

are reviewed in Chapter 1 and the processing conditions and characterization data are summarized in Table 1.1.

A systematic study on the acid-catalyzed formation of humins and the influence of both feed and process parameters on their molecular structure and morphology is not yet available. Indeed, most research is focused on either the conversion of C_6-sugars to LA and HMF or on the production of functional carbon materials from carbohydrates. Here, we report on the conversion of (mixtures of) carbohydrates to the platform chemicals HMF, LA or FF under various process conditions as well as the extent of humin formation and their structural characteristics. The process conditions were chosen to fall within the operating window in which formation of humin by-products is typically expected in a biorefinery operation.[10] In addition to a study of the influence of these processing conditions and feedstock, the effect of addition of invoked intermediates, namely HMF and TB, on the extent of formation and chemical structure of humins is reported.

The reaction products and humin samples were analyzed using several analytical techniques. The analytical tools utilized for the characterization of humins are based on techniques for the analysis of HTC, soil samples, coal and complex biomass samples. The bulk chemical composition of the humins is determined using elemental analysis. Chemical structure and functional group information is based on FTIR, pyrolysis-GC-MS and solid-state NMR spectroscopy, while the morphology of the samples has been analyzed by SEM. This multiple parameter and multiple technique approach provides increased insight into the formation and chemical structure of humin by-products as a function of feedstock and processing conditions and how this affects the production of furanics and LA from sugars.

2.2. Results and Discussion

2.2.1. Preparation and Purification of Humin Samples

Humin samples were prepared by acid-catalyzed dehydration of carbohydrates and purified according to the procedure depicted in Figure 2.1. The solids were isolated by filtration and washed with a large excess of water in order to remove the remaining sugars, HMF, LA, and FA and soluble humin precursors. This was found not to be sufficient to remove all water-soluble compounds from the solid material, however. To allow for a fair comparison between the various humin samples an extra purification step was necessary. A 24 h Soxhlet extraction with water (Figure 2.1) did finally remove all water-soluble compounds from the humin samples.

Reaction conditions were chosen to fall within the window of a typical biorefinery operation. Longer reaction times were used, however, in order to obtain sufficient amounts of humin from the batch reactions for further characterization. The influence of feedstock was studied by preparation of humin samples from glucose, fructose, and xylose and mixtures of these carbohydrates at standard reaction conditions of 180 °C, 1 M [sugar] and 0.01 M [H_2SO_4]. The influence of proposed intermediates HMF and TB on humin

formation was assessed by addition of these compounds to the initial sugar feed (Table 2.1).

An additional study was performed for D-glucose to assess the effect of process conditions on humin yields. This involved 17 experiments with temperature (113-247 °C), glucose concentration (0.66-2.34 M) and sulfuric acid concentration (0-0.13M) as the independent variables at a fixed reaction time of 6 h (Table 2.2).

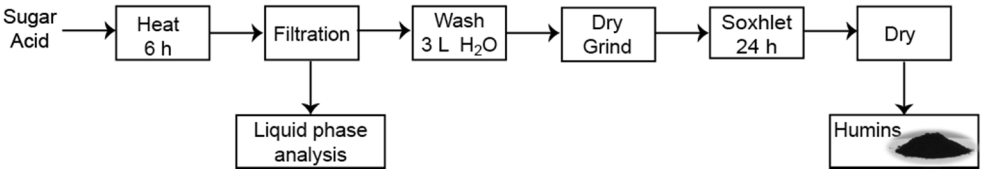

Figure 2.1. Preparation and purification of humin samples.

2.2.2. Formation of Humin By-products

The yield of humin by-products was calculated as gram humin formed per 100 gram of feedstock (Table 2. 1). The humin yield for the various sugars reacted under the standard conditions of 180 ^{o}C, 1 M sugar and 0.01 M of acid ranges from 30-39 wt%. The acid-catalyzed dehydration of fructose yielded more humins than glucose or xylose. The difference in humin yields between glucose and fructose can be attributed to the (on average) higher concentrations of HMF in solutions of the latter sugar. That higher HMF concentrations lead to higher humin yields is in line with the route proposed by Lund *et al*., who have reported humin formation to be first order in HMF.[14] Comparison of the humin yields of glucose and xylose is less straightforward, but the results indicate that HMF is more reactive and prone to polymerization than FF is. Addition of HMF (1:0.2 glucose:HMF ratio, humin6) to the glucose feed does not affect the solid yield significantly. On the contrary, addition of TB to the glucose feed (humin7 and 8) clearly increases the extent of humin formation during acid-catalyzed dehydration of glucose, as previously observed by Ryu *et al.*[19] The increase in humin formation indicates that TB functions as a cross-linker. It should be noted that the incorporation of TB in the humin cannot be accounted for with the mechanism proposed by Lund *et al*. for the formation of humins from HMF, in which aldol (condensation) reactions are proposed as the primary route for humin growth.[13,14]

To quantify the formation of humins from glucose as a function of processing parameters, a systematic study was performed where the range of conditions was selected by Design of Experiment (DoE) (Table 2.2). The design contained 5 replicates (*i.e*. 180 °C, 1.50 M glucose and 0.05 M H_2SO_4) and humin yields of these experiments were 33 +/-2 wt%, indicative for a good reproducibility of the experiments. The results indicate that, at the chosen experimental window, humin formation mainly depends on temperature and to a lesser extent to the acid concentration. The glucose concentration is

statistically not significant. Comparison to literature shows that these conditions are opposite to those that lead to high LA yields.[24] The dependence of humin yield on temperature and acid concentration was statistically modeled and the result is depicted as a surface response plot in Figure 2.2. Agreement between experiment and model is satisfactorily, as expressed by the R^2-value of 0.935.

The humin yield (in wt%) may be quantified by Equation 2.1:

$$\textit{Humin yield} = -120 + 1.507\ T - 63.58\ [H_2SO_4] - 3.56 \cdot 10^{-3}\ T^2 \qquad (2.1)$$

Table 2.1. Carbohydrate conversion, yields, elemental composition of humins and particle sizes formed during acid-catalyzed conversion of different feedstock at 180 °C.

Sample	Feed	Conversion[a]	Yield[b]				Oligomers	Elemental composition		Particle size
		(mol %)	humins (wt%)	HMF (mol%)	FF (mol%)	LA (mol%)	M_w[c] (g/mol)	O/C	H/C	(µm)
Humin1	D-glucose	82	30	1	-	27	480	0.36	0.79	3-5
Humin2	D-fructose	100	39	< 1	-	31	400	0.36	0.76	5-7
Humin3	D-xylose	99	32	-	26	< 1	650	0.33	0.68	4-7
Humin4	D-glucose D-fructose 1:1[d]	95 100	36	< 1	-	31	270	0.35	0.77	4-7
Humin5	D-glucose D-fructose D-xylose 1:1:1[d]	98 99[e]	30	< 1	2	20	440	0.34	0.74	4-7
Humin6	D-glucose HMF 1:0.2[d]	95 98	30	< 1	-	29	420	0.34	0.76	4-7
Humin7	D-glucose TB 1:0.2[d]	88 100	39	< 1	-	17	380	0.39	0.70	3-5 1-2
Humin8	D-glucose TB 1:0.01[d]	98 100	34	< 1	-	23	460	0.39	0.78	6-8

[a] Conversion of sugars, HMF and TB in mol%. [b] Humin yield determined as mass of humin formed from 100 g of starting material. [c] Average molecular weight determined by GPC with maltose as a standard. [d] Molar ratio. [e] Conversion of both fructose and xylose: these carbohydrates cannot not separated by our HPLC protocol.

Table 2.2. Overview of humin yields versus process conditions (6 h reaction time).

Run	Temperature (°C)	[glucose] (M)	[acid] (M)	Conversion glucose (mol%)	Humin yield (wt%)
1	220	2.00	0.1	100	33
2	180	1.50	0.055	100	36
3	247	1.50	0.055	100	32
4	180	2.34	0.055	100	32
5	180	1.50	-	90	33
6	180	1.50	0.055	100	31
7	180	1.50	0.055	100	34
8	180	1.50	0.055	100	31
9	140	2.00	0.1	66	14
10	180	1.50	0.055	100	33
11	220	1.00	0.1	100	29
12	180	1.50	0.131	100	28
13	113	1.50	0.055	45	3
14	140	1.00	0.1	52	8
15	220	2.00	0.01	100	35
16	180	0.66	0.055	100	31
17	220	1.00	0.01	100	36

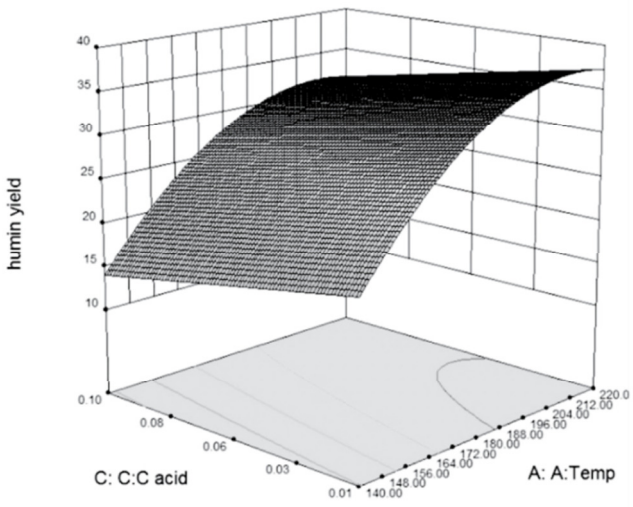

Figure 2.2. Surface response plot for the humin yield as a function of temperature and acid concentration (glucose concentration at 1.5 mol/L).

2.2.3. Elemental Composition of Humin By-products

The elemental compositions of the humins prepared from different feedstocks are given in Table 2.1. The observed changes in atomic ratios during acid-catalyzed dehydration of sugars are summarized in a van Krevelen diagram (Figure 2.3). The van Krevelen diagram allows one to determine what kind of chemical transformations are taking place during product formation, as elemental reactions, *e.g.* dehydration, are represented by straight lines. The plot clearly shows that the elemental composition of the humin samples is the result of consecutive dehydration steps from the sugars via HMF. This implies that humins are formed via condensation reactions between sugars, HMF and intermediates formed during the dehydration of carbohydrates. This plot also implies that the rehydration product LA is not to a large extent incorporated in the humin structure and that any occluded LA can be washed away by Soxhlet extraction.

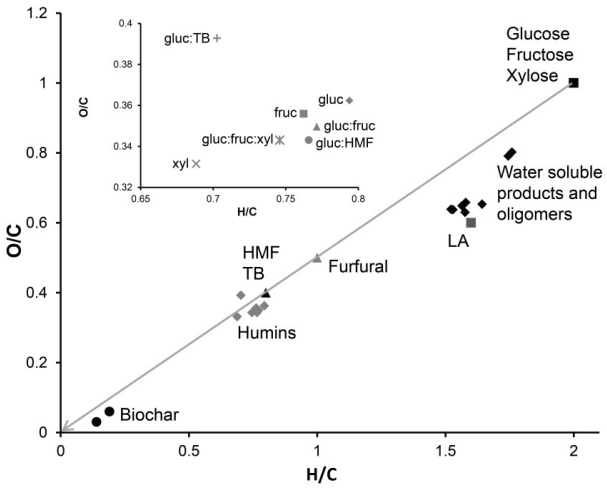

Figure 2.3. Van Krevelen plot depicting the changes in H/C and O/C ratio during acid-catalyzed dehydration of sugars: (black square) carbohydrates, (grey square) LA, (grey triangle) HMF and TB, (black triangle) FF, (black diamonds) water-soluble products. The insert shows the elemental composition of the different humin samples.

The elemental composition of humin1 is slightly different from the elemental composition of glucose-derived HTC samples and humins found in literature (Table 1.1). This can be attributed to differences in the processing parameters or washing procedure. Xylose-derived humin3 has a lower H/C and O/C ratio than the humins prepared from C_6-sugars, indicating that less aliphatic linkers and less oxygen functional groups are present in the structure compared to the C_6-sugar-derived humins. The addition of HMF to the glucose feed hardly changed the elemental composition of the humin. This, together with the spectroscopic evidence given below, is another indication that humins are mainly derived from HMF.

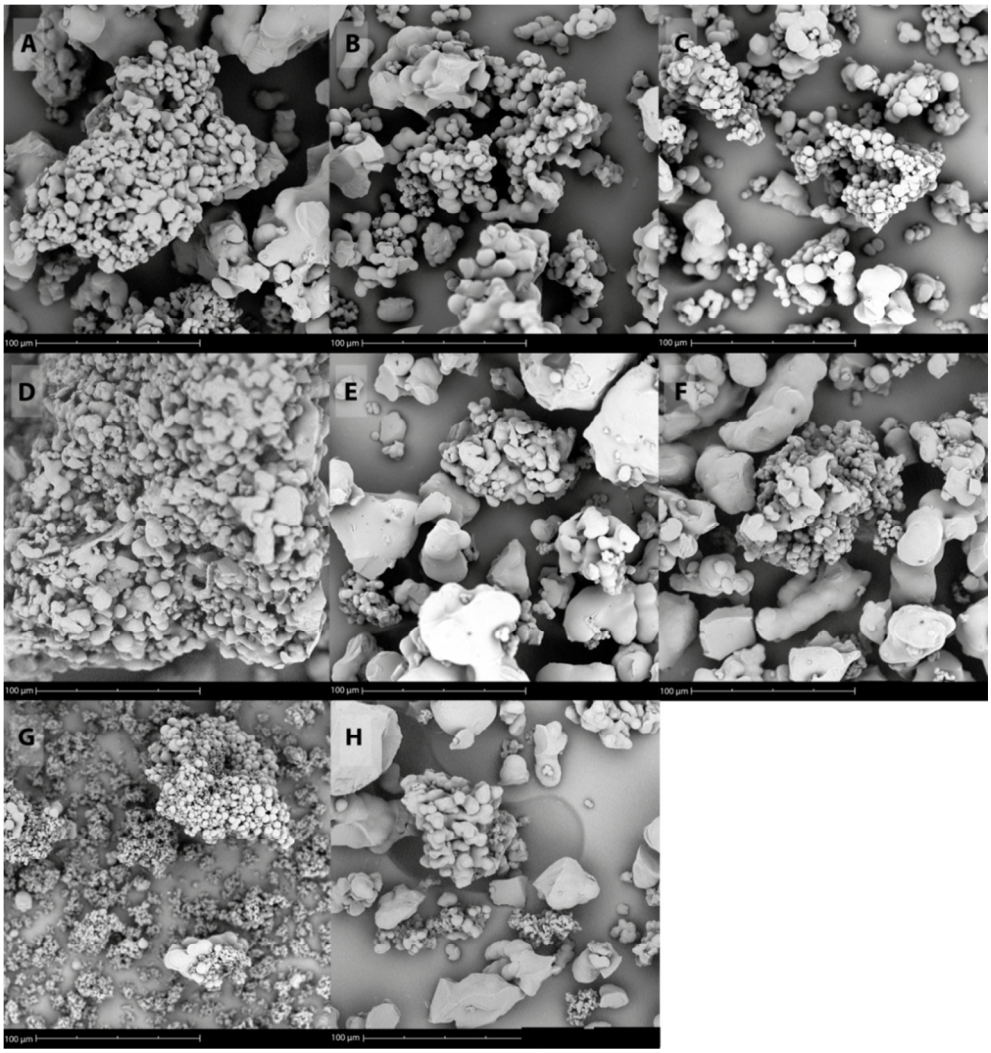

Figure 2.4. SEM of the samples humin1-8 (A-H), which were prepared under the standard processing conditions, but with varying feedstock.

2.2.4. Morphology of Humin By-products

Figure 2.4 shows the scanning electron micrographs of the samples humin1-8, which were prepared under the standard processing conditions but with varying feed; the particles sizes are reported in Table 2.1. The humins formed from C_6-sugars appear as spherical, interconnected particles of 3-5 µm. Humin2, formed from fructose, consists of slightly bigger particles than humin1, which is formed from glucose. The samples show some flattened particles and big lumps, which are believed to be formed as a result of collisions with the reactor wall and stirrer. Humin3 consists of spherical, isolated particles formed from xylose. Mixtures of carbohydrates lead to agglomeration of particles, as can be clearly seen in the morphology of humin5 (Figure 2.4). Compared to humin1, the addition

of HMF to the reaction mixture leads to further agglomeration of the particles. Addition of 1 mol% TB (humin8) to the feedstock slightly increased the particle size of the humin (Figure 2.4). On the other hand, the addition of 20 mol% TB (humin7) to the feedstock resulted in the formation of isolated, spherical particles. In this case, the majority of the particles are 2 or 3 times smaller than the particles formed from pure glucose (Figure 2.4). This indicates that TB affects the crystallization/precipitation behavior of the humins, for instance, by changing the rates of nucleation and agglomeration.

These results show that the morphology of humin by-products strongly depends on the composition of the feedstock. Comparable results, i.e. formation of interconnected and isolated particles from C_6- and C_5-sugars, respectively, were found for HTC.[20] The reported HTC particle sizes are much smaller, however, than the humin particles formed during acid-catalyzed dehydration (Table 1.1 and 2.1). It should be noted in this respect that the protocols for the production of HTC are optimized to obtain small and monodisperse particles. Interestingly, phenolic additives were reported to have an opposite effect on HTC particle size, as HTC particle size increased upon addition of phenolics.[19]

2.2.5. Characterization of Liquid Phase Products

The liquid phase was sampled after reaction and analyzed by HPLC, GPC, NMR and elemental analysis. Sugar conversion and yield of soluble dehydration products were determined by HPLC (Table 2.1). Carbohydrate conversion was found to be lowest for glucose at 82 %, while fructose and xylose showed almost full conversion of the carbohydrate. HMF yields were low for all C_6-sugar reactions, while LA yields were over 25 %. FA yield was assumed to be equal to the yield of LA since LA and FA are formed in a 1 to 1 ratio. Expectedly, the LA yield from fructose is higher as HMF can be formed directly from fructose without the isomerization step that is required for glucose. Addition of TB to the feedstock led to a considerable decrease in the LA yield due to increased humin formation. The acid-catalyzed dehydration of xylose yields FF, formed in about 26 % yield, rather than HMF. Though FF can in principle be converted to organic acids, these were not observed in the liquid phase. FF therefore accumulates in the liquid phase. Humin formation, however, hardly increased compared to dehydration of glucose, which indicates that FF is less reactive than HMF.

The sum of humin yield and products detected by HPLC analysis did not close the mass balance, which points at the presence of water-soluble oligomers. Further analysis of the liquid phase was performed in order to detect the presence of any such water-soluble oligomers. For this purpose, the liquid-phase samples were dried and the recovered solids were redissolved in d_6-DMSO for NMR analysis. The ^{1}H and ^{13}C spectra confirmed only the presence of LA as a main product. Elemental analysis of the dried aqueous phase shows slightly higher H/C and O/C ratios than expected for pure LA, however (Table 2.1). This points at the presence of LA, FA, soluble oligomers and residual sugar. Furthermore, it is

an indication that initial dehydration reactions lead to water-soluble oligomers, which upon further water loss precipitate from solution to give an insoluble product. GPC analysis of the liquid phase confirmed the presence of such water-soluble oligomers and indicated that the relative average molecular weights of the water-soluble products and oligomers are between 300 and 500 g/mol for C_6-sugar-derived products (Table 2.1). This indicates that soluble humin precursors are relatively small oligomers, since *e.g*. HMF already has a molecular weight of 126.11 g/mol. In addition, it suggests that the solubility of the oligomers is already reduced considerably when the degree of oligomerization is still relatively low, leading to water-insoluble products. The differences in average molecular weight indicate that the oligomer intermediates of humin formation differ in solubility depending on the original sugar feed. The average molecular weight of xylose-derived products is higher, for instance, than for glucose, pointing at increased solubility. Fructose-derived liquid phase products, on the other hand, have a lower average molecular weight than glucose-derived products, which points at a lower solubility in water of the fructose-derived oligomers. This is in line with the higher humin yield and faster humin formation from fructose. Addition of TB to the feed also leads to faster humin formation and thus a lower average molecular weight of the water-soluble compounds.

2.2.6. Molecular Structure: ATR-IR, ^{13}C Solid-state NMR and Pyrolysis-GC-MS

The ATR-IR spectra of humins derived from several carbohydrates are shown in Figure 2.5. The spectra of glucose- and fructose-derived humins, humin1 and humin2 respectively, are very similar and several peaks could be assigned. A broad peak from C-O stretch of alcohols is observed around 3400 cm^{-1}, weak contributions from an aliphatic C-H stretch were observed around 2900 cm^{-1}, at 1700 cm^{-1} the C=O stretch from acids, aldehydes and ketones was observed. Various contributions in the spectra could be ascribed to substituted furan rings, *e.g.* at 1600 cm^{-1} a C=C stretch and at 1020 cm^{-1} a C-O stretch or furan ring deformation. The signals from C-H out of plane deformation around 800 and 765 cm^{-1} can be ascribed to substituted furans. The IR spectra of the glucose-derived humins are very similar to the spectra of HTC and humins reported in literature.[13–17,21] The furan-rich structure is further supported by strong similarities with the IR spectrum of furanic resins.[22–25] The IR spectra of humins reported by Lund *et al.* indicate differences between the IR spectra of humins derived from glucose and fructose around 1500 and 1020 cm^{-1}, which is explained by the authors as differences in the amount of HMF that is included in the humin structure.[13] These differences were not observed between the spectra of humin1 and humin2. This can probably be explained by the difference in reaction conditions. The humins studied in this work were produced at higher reaction temperature leading to faster glucose conversion and on average lower HMF concentrations during the reaction. Other experimental differences are related to the

reaction times. Both humin1 and humin2 are formed during a reaction of 6 h rather than until a certain sugar conversion was obtained.

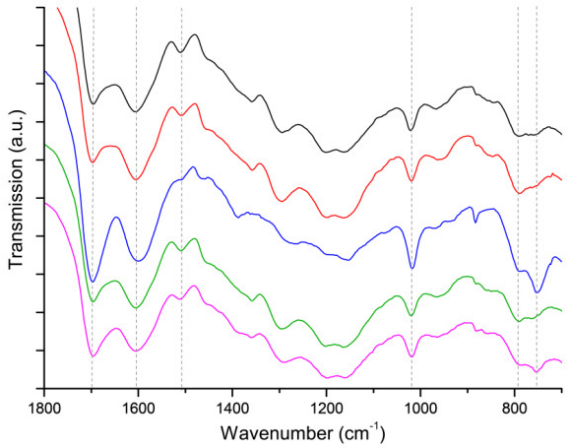

Figure 2.5. ATR-IR spectra of humins prepared from different carbohydrates and mixtures of carbohydrates: humin1 (black), humin2 (red), humin3 (blue), humin4 (green), humin5 (pink).

In the IR spectrum of xylose-derived humins, the furanic C=C stretch vibration appears at 1595 cm^{-1} and is weaker than the one observed for C_6-sugar-derived humins. The peaks around 791 and 751 cm^{-1}, assigned to the C-H out of plane deformation of furan, are relatively stronger and sharper than those observed in the spectra of humin1 and humin2. This indicates a different substitution pattern of the furan rings. When fructose, glucose and xylose are used as a mixed feedstock both characteristic features from glucose- and xylose-derived humins can be observed in IR spectrum of humin5. The addition of C_5-sugars to the feedstock thus leads to changes in the furanic structure (Figure 2.5).

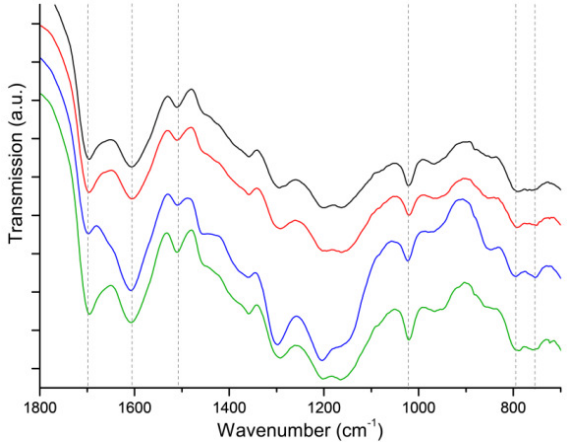

Figure 2.6. ATR-IR spectra of glucose-derived humin and glucose-derived humins with added intermediates: humin1 (black), humin6 (red), humin7 (blue), humin8 (green).

The addition of HMF to the feed hardly led to any discernible changes in the IR spectrum of humin6 compared to glucose-derived humin1. This implies that the molecular structure of the two humins is very similar and that the humin structure in turn is mainly derived from HMF. On the contrary, the addition of TB led to significant differences in the IR spectrum (humin7). Compared to humin1, the broad signal in the C-O stretch region is narrower and shows a clear peak at 1200 cm^{-1}, which indicates the presence of phenolic OH groups. The signals from C-H out of plane deformation show an increase around 856 cm^{-1} and a sharper peak 798 cm^{-1}. These changes are ascribed to the contribution of C-H out of plane deformations of 1,2,4-trisubstituted aromatic rings. It can therefore be concluded that TB is indeed included in the molecular structure, where it probably functions as a cross-linker and therefore causes increased formation of humin by-products (Figure 2.6).

The molecular structure of the humins was further studied by ^{13}C solid-state NMR. A common problem in solid-state NMR is that sidebands arise from functional groups with a high anisotropy, such as carbonyl groups and aromatic rings. These sidebands can overlap with main resonances and lead to erroneous interpretation. This can be addressed by using a high MAS speed, but this severely limits the amount of sample that can be used and consequently the signal to noise ratio suffers accordingly. Alternatively, a large sample volume can be used when spinning sidebands are suppressed using a TOSS sequence,[26–28] but this method has the drawback that the signal intensity is lost from the anisotropic carbons. In order to circumvent this, a 2D PASS sequence[29–31]] was employed here, in which the spinning sidebands are separated in a second dimension (Figure 2.7). The CP-MAS spectrum can then be reconstructed by adding up the projections of the 2D spectrum. After shearing of the data a sideband-free spectrum is obtained at low MAS speeds. This way, a sideband-free spectrum with high resolution can be obtained. This technique turned out to be particularly useful here, as several spinning sidebands are located in important regions of the spectrum. The projections of the sidebands only give insight in their position and in the presence of anisotropic groups such as ketones and aromatic rings.

The sheared sum projections of the 2D PASS NMR spectra of humins1-7 are shown in Figure 2.8. The NMR spectra can be divided in several areas: δ = 0-60 ppm aliphatic C, δ = 60-90 ppm C-O from ethers and alcohols (both regions representing sp^3 hybridized carbons), δ = 90-160 ppm aromatic C (sp^2), and δ = 160-220 ppm C=O from carbonyl groups (sp^2). Integration of the different areas in the NMR spectra of glucose- and xylose-derived humins did not reveal significant differences in the relative amounts of the chemical species: for glucose-derived humins about 17% of the carbon intensity is from alkanes, 53% from aromatics and 13% from carbonyl groups. It is well-known that the cross polarization used to obtain the spectra, results in the amount of non-protonated carbon and methyl group to be underestimated.[32,33]

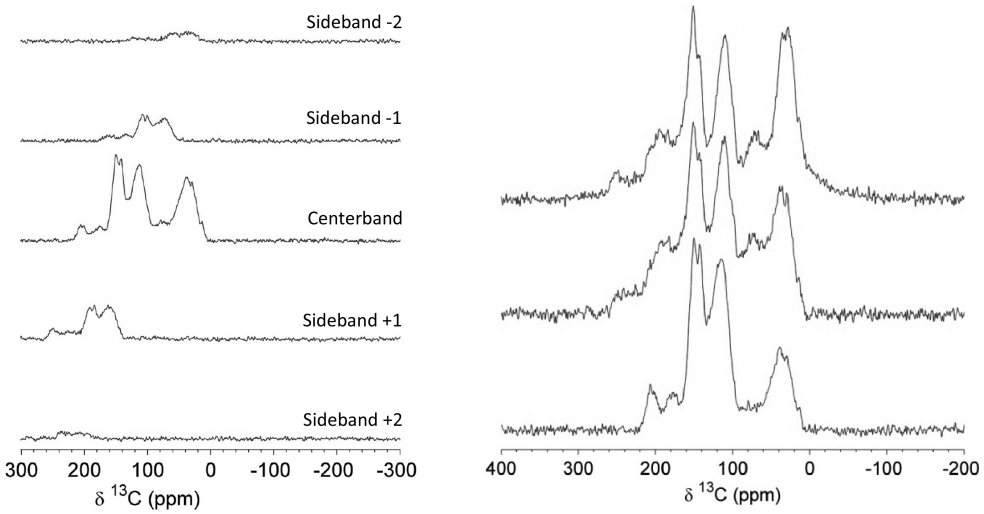

Figure 2.7. Left: Separation of the sidebands and centerbands from the 2D PASS NMR spectrum (humin1). Right (top to bottom): CP MAS spectrum, reconstruction of the MAS spectrum by adding up the projections of the 2D PASS spectra, and the sheared sum projection giving a sideband free spectrum (humin7).

Peak assignments for the humins are listed in Table 2.3. The region from δ = 0-60 ppm shows that saturated aliphatic groups are present in the structure of all humins. The spectra show a limited presence of methyl groups (δ = 15 ppm) and CH_2 linkers (around δ = 30 ppm). This is in line with the IR spectrum, which shows a low intensity for C-H stretch from CH_2 and CH_3 groups. In comparison, the higher signal intensity observed between δ = 30-60 ppm is evident for a stronger presence of tertiary or quaternary aliphatic carbon atoms. Some intensity is also observed between δ = 70 and 90 ppm, a region typical for signals from alcohols and ethers. The intensity in this region is broad, as a result of multiple small contributions rather than large contributions from carbohydrates or HMF.[34] The aromatic region of the spectrum clearly shows that the humins do not consist of a graphite-like structure, as an intense peak around δ = 130 ppm should then be observed.[22,35] The signals at δ = 112, 120 and 128 ppm are ascribed to the C_β of furan, linked C_β and conjugated structures, respectively. At δ = 142 ppm, signals from terminal furan C_α and linked C_α are detected at δ = 150 ppm, respectively (Figure 2.8).[14,34] Weak, yet distinct signals are seen in the region between δ = 165 and 185 ppm. These signals could be from esters and acids, functional groups that can be formed by ester formation or aldol condensations of LA or by acid formation due to ring opening of the furanic units. A comparison with the IR spectra indicates that the amount of ester groups must be very low, though, making an assignment to acid groups more likely. Finally, aldehydes and ketones are observed between δ = 195 and 220 ppm, which can for instance result from

the aldehyde function in HMF, ketones formed as an intermediate in the rehydration of HMF (*e.g.*, furan ring opening), or aldol condensation with ring opening products such as 2,5-dioxo-6-hydroxyhexanal (DHH). The 2D PASS spectrum of glucose-derived humins is quite similar to the CP-MAS NMR spectrum of unlabeled HTC, as reported by Baccile *et al.* The HTC sample does contain unreacted glucose, however, as indicated by a signal around δ = 75 ppm, which seems hardly present in our humin samples. Further differences can be found in the region ascribed the peak from free CH_2 groups, which seem relatively more intense in the spectrum of HTC. In the aromatic region the intensity around δ = 130 ppm is slightly higher for humin1, which indicates a higher degree of conjugation in the humin sample.[18,35]

Table 2.3. Assignment of peaks in the ^{13}C NMR spectra of humins.

δ (ppm)	Functional group	Chemical formula
205	Ketone, aldehyde	C=O, HC=O
175	Acid, ester	COOH, COOR
150	C_α furan linked	C=C-O
142	C_α furan terminal	C=HC-O
128	Furan conjugated	C-C=C-C
120	C_β furan linked	C-C=C-O
112	C_β furan	C-HC=C-O
78	Alcohol, ether	C-OH, C-O-C
48	Aliphatic	C-H, C
39	Aliphatic	C-H, C
28	Aliphatic	$-CH_2-$
15	Aliphatic	$-CH_3$

The NMR spectra of glucose- and fructose-derived humins show that the humin structures must be similar. The relative peak intensities in aromatic region nevertheless differ, indicating differences in substitution pattern of the furanic network. This is even more clearly seen in the NMR spectrum of the xylose-derived humin. Differences are indeed expected between the C_6- and C_5-sugars, as the latter allow direct linking of the furanic rings via the free 5-position of the FF intermediate. This results in more extended conjugated network, which is indeed indicated by an increase in intensity around δ = 130 ppm. An increase in signal intensity around δ = 130 ppm is also found when mixtures of C_6-sugars and xylose are used as feedstock. Comparison to literature shows that the same structures can be found in HTC derived from xylose.[20] Addition of HMF to the glucose feed led only to very minor changes in the NMR spectrum, again confirming that humin formation pathway predominantly goes through HMF. Addition of TB leads to changes in the signals from arene/phenolic groups. It should be noted that signals from substituted

furan α-carbons and substituted carbons in a phenolic ring, or furan C_β and unsubstituted carbons in a phenolic ring are difficult to distinguish. Indeed, this is clearly illustrated by a comparison of the NMR spectrum of humin7 with the CP MAS NMR spectrum of a furanic-aromatic polyester.[36]

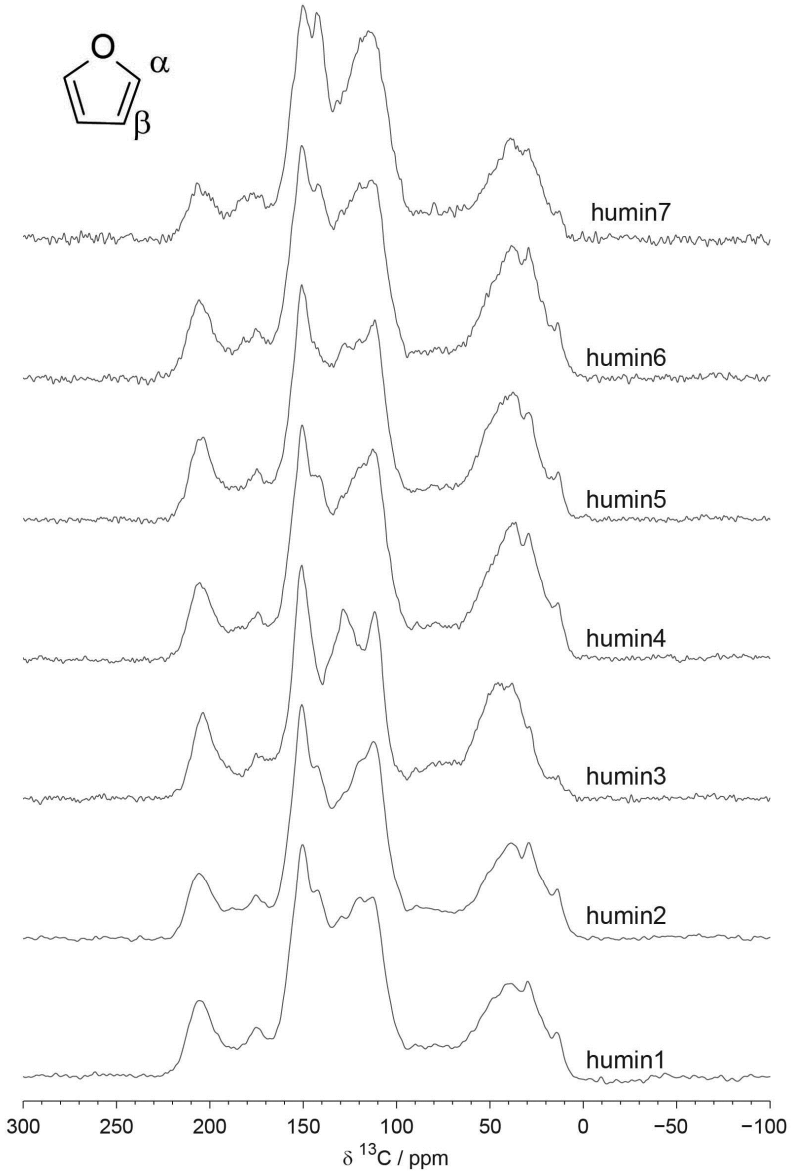

Figure 2.8. Sheared sum projections of the 2D PASS ^{13}C NMR spectra of humins prepared from different feedstocks. Insert: C_α- and C_β-position of furan.

Finally, pyrolysis-GC-MS was performed on representative humine samples. A typical example for a glucose-derived humin is given in Figure 2.9. It shows the presence of various furanics (*e.g.* 2-methyl-furan, 2,5-dimethylfuran, furfural), which is a strong indication for the presence of several furanic groups in the humin samples. Comparable products were observed during the pyrolysis of furfuryl alcohol resins, further supporting the furanic nature of humins.[25]

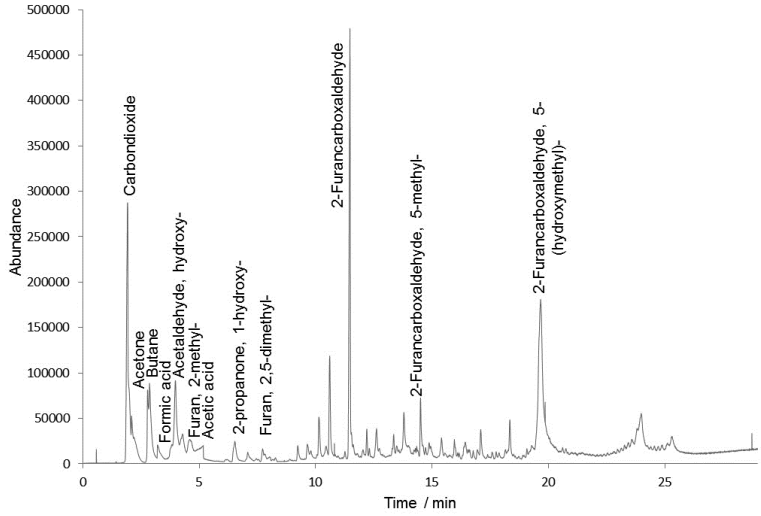

Figure 2.9. Pyrolysis-GC-MS chromatogram (600 °C) of glucose-derived humins.

Based on the data presented above and taking into account the structures previously reported for HTC, a polyfuranic molecular structure is proposed for C_6-sugar-derived humins (Figure 2.10A). The molecular structure of humin is very heterogeneous therefore a representative fragment including the most imported linkages was drawn. The proposed structure includes some features of previously proposed HTC or humin structures, but also differs from them in important ways.[13,14,18] Substitution at the β-position is thought to result from nucleophilic attack of the furan ring on the carbonyl group of HMF. Linking via the α-position occurs via condensation reactions between the HMF molecules. Inclusion of rehydration products such as DHH and, to a very limited extent, LA occurs via aldol condensations with the aldehyde functions of HMF or DHH itself.

The IR and NMR spectra also show that xylose-derived humins differ in molecular structure from glucose-derived humins. The free 5-position of FF offers the possibility for self-condensation reactions leading to a structure in which furanic units are linked by aliphatic CH_2 and CH groups, an option not available for humins that are formed from HMF as intermediate. Further dehydration of this structure will lead to a polymer with more highly conjugated moieties, as indicated by our NMR spectra. As a result, the structure of

a xylose-derived humin is expected to be more similar to the structure of FF resins, for which a structure was proposed by Gandini *et al*.[37]; a model for xylose-derived humins structure is proposed in Figure 2.10B. Linking via the β-position of furfural is possible, however, less likely compared to HMF because the free 5-position of furfural is more reactive than its β-position.

The NMR spectra of our humins (derived from an acid-catalyzed process) are very similar to those of HTC (derived from a non-acid-catalyzed process), for which a structure was proposed by Baccile *et al.* with furanic units linked by CH_2 groups.[18] However, the elemental composition of this HTC model conflicts with the van Krevelen plot (Figure 2.3), because the formation of this structure requires loss of C atoms, involving a reaction other than dehydration. Our IR and NMR data furthermore show that the signals from CH_2 groups are weak. Also, no spectroscopic evidence is found to indicate any significant presence of acetal bonds,[49] which were suggested by Zarubin *et al*., as linkages between the furanics. The elemental analyses also indicate that our humin samples are further dehydrated than Zarubin's model suggests.[15] According to the model proposed by Lund *et al.* humins are formed via aldol condensations between HMF and DHH, with high HMF concentrations leading to a furan-rich humin. Our NMR data do not fully support this model, which does not contain any tertiary or quaternary carbons. Furthermore, this model does not consider the presence of linked C_β leading to the more cross-linked structures that are identified in our NMR data. Lund *et al.* also suggest that reactions with LA do not occur. However, aldol condensation of HMF with the ketone group of LA is a plausible way to include a small amount of acids in the humin structure. Indeed, extracts of humin1 did not contain any LA, demonstrating that the observed signals from acid groups are not caused by physically embedded LA. Finally the possibility to include TB in the humin structure also indicates that humins are not formed purely by aldol condensation reactions.[13,14] The models presented in Figure 2.10 fit with the elemental composition as well as the spectoscopic charcteristics of glucose- and xylose-derived humins.

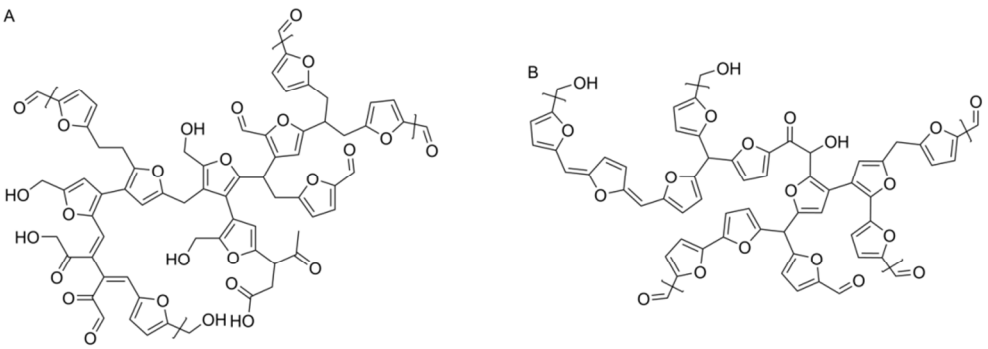

Figure 2.10. Model representing the molecular structure of a humin fragment, including the most important linkages for: A. Glucose-derived humin B. Xylose-derived humin.

2.3. Conclusions

The formation, morphology and molecular structure of humin by-products were studied as a function of feedstock and processing parameters. For the pure sugars, the acid-catalyzed dehydration of fructose yielded the highest amount of humin since HMF is directly formed from fructose. Humin yields from xylose were slightly higher than from glucose. During this reaction furfural accumulates in solution, indicating a lower propensity of furfural to form organic acids and humin as compared to HMF. Addition of 1,2,4-trihydroxybenzene to the feed led to an increase in humin formation indicating that this molecule is included in the humin structure as a cross-linker. Furthermore, it shows that humin formation also involves reactions other than aldol condensations. The influence of acid concentration, sugar intake and temperature on the formation of humins from glucose was studied using a DoE-based approach. The data show that humin formation is strongly influenced by reaction temperature and acid concentration, but statistically hardly depends on sugar concentration. It was found that conditions for high humin production are opposite to those that will lead to high yields in LA. Analysis of the liquid phase by HPLC showed that LA is the main product formed from C_6-sugars while C_5-sugars yield furfural. Furthermore, GPC analysis showed that water-soluble humin precursors are present in the liquid phase.

Humin samples prepared from different feedstock were characterized by several analytical techniques. SEM indicates that the humin by-products have a spherical morphology, which strongly depends on feedstock and processing conditions. A study on the molecular structure of humin by-products using elemental analysis, IR, ^{13}C solid-state NMR spectra and pyrolysis-GC-MS revealed a furanic structure with alcohol, acid, ketone and aldehyde functional groups, which is formed via a dehydration pathway. Based on this information a model for the molecular structure for glucose-derived humins was proposed. It was also found that xylose-derived humins have a more conjugated molecular structure. This can be explained by the free 5-position of furfural which leads to direct linking of the furan leading to less aliphatic groups and a more condensed network of furans moieties.

The models for the molecular structure of the humins derived from C_5- and C_6-sugars that are presented here will aid the development of catalytic routes for the valorization of these by-products. Indeed, humins can be seen as another recalcitrant feedstock that needs to be valorized in order to realize low-waste, competitive biorefinery processes. In this sense, the analogy can be made with the development of valorization strategies for lignin, another example of a recalcitrant, highly heterogeneous, aromatic biopolymer of limited solubility. The considerable advances in the structural characterization of lignin, in particular the type and occurrence of specific linkages and the influence of pretreatment on the lignin structure, have clearly guided the development of catalytic lignin conversion strategies.[38] Similar advances are to be expected for the valorization of humins. Pyrolysis, a process that has been quite extensively studied for lignin, of humins is a promising example of this.[39] Alternatively, the insights gained in

humin formation and structure can aid in managing the extent of humin formation, or can improve our understanding and application of related materials such as biochars.

2.4. Experimental Section

2.4.1. Preparation of Humins

Master batches of humin1-8 were prepared by heating 500 mL of an aqueous solution containing 1 M carbohydrate (D-glucose, D-fructose, D-xylose) and 0.01 M H_2SO_4 to 180˚C in a glass-lined 1 L batch reactor (Parr) for 6 h. The reactor was flushed with N_2 before heating. Humins were isolated by filtration, washed with 3 L water, dried under vacuum (0.3 mbar) for 12 h at 80 ˚C and ground. After Soxhlet extraction with water for 24 h, the samples were dried for 24 h at 80 °C under vacuum. The yield of humin was calculated as mass solids formed per 100 g starting material. For the samples humin4 and humin5 prepared from mixtures of carbohydrates, *i.e*. glucose:fructose 1:1 and glucose:fructose:xylose 1:1:1, the total concentration was kept at 1 M. HMF and 1,2,4-trihydroxybenzene were added to the reaction mixture in a molar ratio 1:0.2 sugar:aromatic with a total concentration of 1 M for samples humin6 and humin7. Humin8 was formed with TB added to the glucose feedstock in a 1:0.01 ratio.

2.4.2. Design of Experiment

The 17 humin samples for the DoE study were prepared in a 100 mL autoclave (Parr) using glucose as the feed. Reaction conditions, *i.e.* temperature (113-247 °C), glucose concentration (0.66-2.34 M) and H_2SO_4 concentration (0-0.13 M) were varied. A reaction time of 6 h was applied. The experimental humin yields were analyzed statistically by means of the Design Expert 8 software package (Stat-Ease Inc.). The response was modeled with a quadratic model using the following standard expression (Equation 2.2):

$$y_k = b_0 + \sum_{i=1}^{3} b_i x_i + \sum_{i=1}^{3} b_{ii} x_i^2 + \sum_{\substack{i=1 \\ i \neq j}}^{3} \sum_{j=2}^{3} b_{ij} x_i x_j \qquad (2.2)$$

Here, *i* represents the independent variables (temperature, acid concentration and glucose concentration), while b_i, b_{ii}, b_{ij} are the regression coefficients which were obtained by statistical analyses of the data. The significant factors were selected based on their *p*-value in the analysis of variance (ANOVA). Factors with a *p*-value below 0.05 were regarded as significant and included in the response model. Step-wise elimination was applied to eliminate all statistically insignificant terms. After each elimination step a new ANOVA table was generated until all insignificant factors were removed.

2.4.3. Characterization of Humins

Humins and dried water-soluble products were analyzed using an automated Euro EA3000 CHNS. Oxygen content was calculated by difference. SEM images were taken using a

Phenom G2 (Fei company). Samples were coated with 4 nm Pt with 10 wt% Pd. The liquid phase was analyzed by an Agilent HPLC system equipped with a Bio-Rad Aminex HPX-87H column, and a differential refractometer. The eluent was 5 mM H_2SO_4 and a flow rate of 0.55 mL/min was maintained at 60 ˚C with the detector temperature set to 40 °C. Further liquid phase analysis was performed with an Agilent Technologies 1200 GPC system equipped with a ZORBAX Eclipse CDB-C18 Analytical (4.6×150 mm 5 µm) column. The system was operated at 23 ˚C with 5 mM $NaNO_3$ as a mobile phase and maltose was used as a standard. ^{1}H NMR and ^{13}C NMR spectra were taken in d_6-DMSO with a Varian AS200 spectrometer.

ATR-IR spectra were recorded on a Bruker Tensor 37 IR spectrometer using a diamond ATR crystal. For each spectrum 32 scans with a resolution of 4 cm^{-1} were averaged. Two IR spectra were taken of each humin sample and averaged.

The ^{13}C solid-state NMR spectra were recorded at Radboud University Nijmegen. All spectra were measured on a 300 MHz solid-state NMR spectrometer using a 7.5 mm double resonant chemagnetics APEX probe, tuned at 75.45 MHz for carbon. All spectra were obtained using ramped CPMAS at an rf-field of 55 kHz for carbon and 51 kHz for protons. Proton decoupling during acquisition was accomplished with a Spinal-64 sequence at an rf-field of 55 kHz, optimized to a pulse width and phase of 9 µs and 7°, respectively. MAS speeds were 4 kHZ except for sample humin7 where the speed was 3.2 kHz. After cross polarization a 2D PASS sequence was used to separate the spinning sidebands, employing cogwheel phase cycling.[40]

Analytical PTV-GC-MS of humins was conducted with a HP 5890 GC Series II system equipped with a 5972 MS detector, and the PTV was controlled by an Optic 2 device. Typically 1 mg of sample was used. The pyrolysis temperature program was: 40 °C for 2 min, then heating to 600 °C at a rate of 16 °C/s, and finally at 600 °C for 1 min. After pyrolysis, the products were transferred into a capillary column (Agilent Technologies VF-5ms, 30 x 0.25 x 1.0) via a GC-injector (split 50:1). Helium was used as the carrier gas at a flow rate of 1 ml/min. The following GC temperature program was applied: starting temperature of 40 °C for 5 min, heating up at a rate of 10 °C/min to a final temperature of 250 °C. The MS detector was operated in the electron ionization mode (70 eV) with an interface temperature 280 °C. A scan range of 35-400 m/z was applied. Pyrolysis products were identified by comparison with mass spectra of authentic compounds and masses.

2.5. Acknowledgements

Yuehu Wang, dr. C.B. Rasrendra and prof. dr. ir. Erik Heeres from University of Groningen are acknowledged for humin preparation, DoE, liquid phase analysis, elemental analysis, Pyrolysis-GC-MS and their contributions to the chapter. We would like to acknowledge dr. Ernst van Eck from Radboud University Nijmegen for recording the solid-state NMR spectra and the Netherlands Organization for Scientific Research (NWO) for their support of the solid-state NMR facility for advanced materials research.

2.6. References

[1] R. J. van Putten, J. C. van der Waal, E. de Jong, C. B. Rasrendra, H. J. Heeres, J. G. De Vries, *Chem. Rev.* **2013**, *113*, 1499–1597.

[2] J. P. Lange, E. van der Heide, J. van Buijtenen, R. Price, *ChemSusChem* **2012**, *5*, 150–166.

[3] G. W. Huber, S. Iborra, A. Corma, *Chem. Rev.* **2006**, *106*, 4044–4098.

[4] S. G. Wettstein, D. M. Alonso, E. I. Gürbüz, J. A. Dumesic, *Curr. Opin. Chem. Eng.* **2012**, *1*, 218–224.

[5] J. P. Lange, R. Price, P. M. Ayoub, J. Louis, L. Petrus, L. Clarke, H. Gosselink, *Angew. Chem. Int. Ed.* **2010**, *49*, 4479–4483.

[6] A. Corma, S. Iborra, A. Velty, *Chem. Rev.* **2007**, *107*, 2411–2502.

[7] S. G. Wettstein, D. M. Alonso, Y. Chong, J. A. Dumesic, *Energy Environ. Sci.* **2012**, *5*, 8199–8203.

[8] J. Horvat, B. Klaić, B. Metelko, V. Šunjić, *Tetrahedron Lett.* **1985**, *26*, 2111–2114.

[9] E. De Jong, M. A. Dam, L. Sipos, G. J. M. Gruter, in *Biobased Monomers, Polymers, and Materials* (Eds.: P.B. Smith, R.A. Gross), American Chemical Society, **2012**, 1–13.

[10] D. J. Hayes, J. Ross, M. H. B. Hayes, S. W. Fitzpatrick, in *Biorefineries - Industrial Processes and Products* (Eds.: B. Kamm, P.R. Gruber, M. Kamm), Wiley, **2006**,. 139–164.

[11] B. Girisuta, L. P. B. M. Janssen, H. J. Heeres, *Green Chem.* **2006**, *8*, 701–709.

[12] B. Girisuta, L. P. B. M. Janssen, H. J. Heeres, *Chem. Eng. Res. Des.* **2006**, *84*, 339–349.

[13] S. K. R. Patil, J. Heltzel, C. R. F. Lund, *Energy Fuels* **2012**, *26*, 5281–5293.

[14] S. K. R. Patil, C. R. F. Lund, *Energy Fuels* **2011**, *25*, 4745–4755.

[15] I. V. Sumerskii, S. M. Krutov, M. Y. Zarubin, *Russ. J. Appl. Chem.* **2010**, *83*, 320–327.

[16] M. Sevilla, A. B. Fuertes, *Carbon* **2009**, *47*, 2281–2289.

[17] M. Sevilla, A. B. Fuertes, *Chem. Eur. J.* **2009**, *15*, 4195–4203.

[18] N. Baccile, G. Laurent, F. Babonneau, F. Fayon, M. M. Titirici, M. Antonietti, *J. Phys. Chem. C* **2009**, *113*, 9644–9654.

[19] J. Ryu, Y.-W. Suh, D. J. Suh, D. J. Ahn, *Carbon* **2010**, *48*, 1990–1998.

[20] M. M. Titirici, M. Antonietti, N. Baccile, *Green Chem.* **2008**, *10*, 1204–1212.

[21] M. M. Titirici, A. Thomas, S. H. Yu, J. O. Muller, M. Antonietti, *Chem. Mater.* **2007**, *19*, 4205–4212.

[22] C. Burket, R. Rajagopalan, A. Marencic, K. Dronvajjala, H. Foley, *Carbon* **2006**, *44*, 2957–2963.

[23] S. Şen, B. Bardakçı, A. G. Yavuz, A. U. Gök, *Eur. Polym. J.* **2008**, *44*, 2708–2717.

[24] V. Hernandez, F. J. Ramirez, G. Zotti, J. T. López Navarrete, *Chem. Phys. Lett.* **1992**, *191*, 419–422.

[25] R. Sánchez, C. Hernández, G. Keresztury, *Eur. Polym. J.* **1994**, *30*, 43–50.

[26] W. T. Dixon, J. Schaefer, M. D. Sefcik, E. O. Stejskal, R. A. McKay, *J. Magn. Reson.* **1982**, *49*, 341–345.

[27] W. T. Dixon, *J. Chem. Phys.* **1982**, *77*, 1800–1809.

[28] E. T. Olejniczak, S. Vega, R. G. Griffin, *J. Chem. Phys.* **1984**, *81*, 4804–8417.

[29] O. N. Antzutkin, S. C. Shekar, M. H. Levitt, *J. Magn. Reson.* **1995**, *115*, 7–19.

[30] Z. Song, O. N. Antzutkin, X. Feng, M. H. Levitt, *Solid State Nucl. Magn. Reson.* **1993**, *2*, 143–146.

[31] F. G. Vogt, J. M. Gibson, D. J. Aurentz, K. T. Mueller, A. J. Benesi, *J. Magn. Reson.* **2000**, *143*, 153–160.

[32] R. Fründ, H. Lüdemann, *Sci. Total Environ.* **1989**, *81/82*, 157–168.

[33] P. Kinchesh, D. S. Powlson, E. W. Randall, *Eur. J. Soil Sci.* **1995**, *46*, 125–138.

[34] P. E. Pfeffer, K. B. Hicks, M. H. Frey, S. J. Opella, W. L. Earl, *J. Carbohydr. Chem.* **1984**, *3*, 197–217.

[35] C. Falco, F. Perez Caballero, F. Babonneau, C. Gervais, G. Laurent, M. M. Titirici, N. Baccile, *Langmuir* **2011**, *27*, 14460–14471.

[36] M. Gomes, A. Gandini, *J. Polym. Sci. A Polym. Chem.* **2011**, *49*, 3759–3768.

[37] A. Gandini, M. N. Belgacem, *Prog. Polym. Sci.* **1997**, *22*, 1203–1379.

[38] J. Zakzeski, P. C. A. Bruijnincx, A. L. Jongerius, B. M. Weckhuysen, *Chem. Rev.* **2010**, *110*, 3552–3599.

[39] C. B. Rasrendra, M. Windt, Y. Wang, S. Adisasmito, I. G. B. N. Makertihartha, E. R. H. van Eck, D. Meier, H. J. Heeres, *J. Anal. Appl. Pyrolysis* **2013**, *104*, 299–307.

[40] N. Ivchenko, C. E. Hughes, M. H. Levitt, *J. Magn. Reson.* **2003**, *164*, 286–293.

CHAPTER 3

Full, Reactive Solubilization of Humin By-products by Alkaline Treatment and Characterization of the Alkali-treated Humins Formed

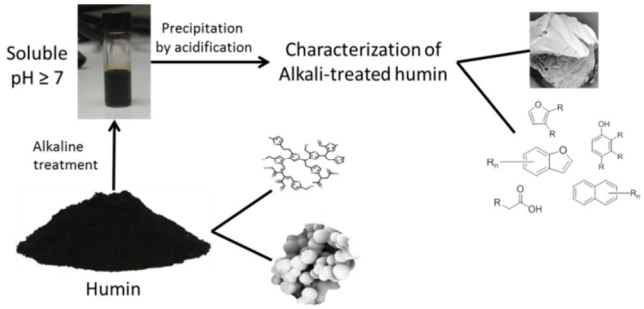

Abstract

The valorization of the humin by-products that are formed during hydrothermal, acid-catalyzed dehydration of carbohydrates is hampered by their insolubility. Here, we report on an alkaline pretreatment method that allows for the insolubility of this highly recalcitrant and structurally complex feed to be overcome. The reactive solubilization of glucose-derived humin was found to require a treatment at 200 °C in 0.5 M NaOH for 3.5 h. Fructose- and xylose-derived humins were found to be more recalcitrant and complete dissolution required raising the temperature to 240 °C. Gel permeation chromatographic analyses show the relative average molecular weight of the now soluble humins to decrease with increasing temperature and reaction time. The alkali-treated humins are soluble in water of pH ≥ 7. Elemental analysis, IR, 2D PASS ^{13}C solid state NMR, and pyrolysis-GC-MS data indicate that the alkaline pretreatment leads to considerable changes in the molecular structure of the humins. Cleavage of C-O-C bonds and further aromatization of the originally highly furanic humins result in the formation of polycyclic aromatic structures decorated with carboxylic acids. The combination of the reduction in Mw and the formation of polar functional groups is thought to be the reason behind the improved solubility.

Based on: I. van Zandvoort, E. R. H van Eck, P. de Peinder, H. J. Heeres, P. C. A. Bruijnincx, B. M. Weckhuysen, "Full, Reactive Solubilization of Humin By-products by Alkaline Treatment and Characterization of the Alkali-treated Humins Formed". *ACS Sustainable Chem. Eng., accepted.*

3.1. Introduction

Hydroxymethylfurfural (HMF), furfural (FF) and levulinic acid (LA) are bio-based platform chemicals with immense potential.[1,2] The production of these platform molecules in a biorefinery operation typically entails the hydrolysis of polysaccharides such as cellulose (C_6-sugars) or hemicellulose (C_6- and C_5-sugars) to individual sugar monomers, followed by subsequent acid-catalyzed dehydration of the C_6- and C_5-sugar monomers to form HMF and FF, respectively. Under these acidic conditions HMF is in turn easily rehydrated to form LA and formic acid.[3,4] A major problem during such hydrothermal, acid-catalyzed treatments of sugars is the formation of insoluble,[5] carbonaceous by-products, called humins.[3] The formation of humins can lead to a considerable loss of the sugar feed, thereby strongly decreasing the efficiency of the process and the economic viability of biorefineries.[6] This can be ameliorated by developing (catalytic) routes for the further valorization of these humin by-products to value-added chemicals by, for example, gasification,[6,7] pyrolysis[8] or catalytic depolymerization. For such (catalytic) conversion to proceed efficiently both insight in the molecular structure as well as solubilization of the material is desired.

Still relatively little is known about the complex structure of humins, however.[9–12] The challenges faced with regards to humin structure elucidation are actually quite similar to those previously addressed in lignin and soil chemistry and the analytical techniques developed for those complex matrices could in principle also be applied to humins to get more insight in their molecular structure and chemical properties. So far, most knowledge about the molecular structure of humins is based on the molecular structures proposed for hydrothermal carbons, a functional material prepared by the hydrothermal treatment of carbohydrates. In literature two prominent, but conflicting proposals can be found. Baccile *et al.*[13] suggested that HTC has a furanic structure with methylene linkages and several oxygen functionalities, mainly based on 2D solid-state NMR spectra.[13] On the other hand, a more condensed polycyclic aromatic structure was proposed based on elemental analysis, XPS, IR and Raman data by Sevilla *et al.*.[14,15]

As for humins, Zarubin *et al.*[9] characterized humins obtained from different sugars and HMF by elemental analysis, IR and NMR of acetone extracts and proposed a furan-rich structure with ether and (hemi)acetal as the main linkages.[9] On the other hand, Lund *et al.*[10,11] suggested that rehydration of HMF could lead to the formation of 2,5-dioxo-6-hydroxy hexanal (DHH). This compound is then thought to react with HMF and several sugar dehydration intermediates via aldol condensations leading to the formation of humins, with the inclusion of furanic rings depending on the accumulation of HMF during the dehydration reaction.[10,11] In Chapter 2 we reported on the formation and molecular structure of humin by-products as a function of feedstock and processing conditions. A combination of elemental analysis, IR, solid-state NMR and pyrolysis-GC-MS data revealed an HMF-derived, furan-rich polymeric network in which the furan units are linked by short aliphatic chains and several oxygen functionalities could be identified.

The next step towards valorization of the humins is to improve the solubility of the material. As reported before,[5] we also noted that the humins prepared under our standard conditions have a very low solubility in common organic solvents. For example, Soxhlet extraction for 24 h with acetone and ethanol resulted in weight losses of only 3% and 5%, respectively. This in contrast to the results reported for the humin fraction of soil organic matter (SOM), which was found to be almost completely soluble in DMSO with 6% H_2SO_4 (v/v);[16] our humins were hardly soluble under these conditions, however. The availability of dissolved humins would bring many advantages, as it would, for instance, greatly enhance the interaction between the substrate and a (heterogeneous) catalyst. Alkaline treatment, *i.e*. hydrothermal treatment of a solid in the presence of base, is a well-known method to improve the solubility of recalcitrant materials, such as SOM and lignin.[17–20] For example, the solubility of humic acid and fulvic acid fractions from SOM is improved by hydrolysis of C-O bonds at 170-250 °C in 2-5 M NaOH, thereby increasing the amount of extractable components.[17–19] Another example of alkaline treatment is found in lignin depolymerization, in which base is used to fragment the lignin to obtain aromatic monomers. During the alkaline treatment of lignins, rather extensive recondensation occurs leading to the formation of unwanted condensation products and limited monomer yields.[21–23] Such possible complications aside, a similar base treatment could also prove to be very beneficial for the solubilization of humins.

Here, we show that reactive dissolution of the humins is indeed possible in aqueous media using an alkaline pretreatment method. Reaction conditions have been optimized for glucose-derived humins and were tested and adjusted for fructose- and xylose-derived humins. The influence of temperature, reaction time and base concentration on the average molecular weight of the dissolved humins was monitored by gel permeation chromatography (GPC). The alkali-treated humins can be easily recovered by acidification of the liquid phase and changes in elemental composition are reported as well as the changes in molecular structure of the regenerated humins based on IR, 2D PASS ^{13}C solid state NMR and pyrolysis-GC-MS analyses.

3.2. Results and Discussion

3.2.1. Reactive Solubilization of Humins

Humin samples were prepared by our standardized method for the acid-catalyzed dehydration of sugars as described in Chapter 2. The humin samples were subsequently subjected to an alkaline pretreatment based on a method used in soil chemistry using an unstirred Teflon-lined autoclave.[17,18] Reaction temperature (150-240 °C), reaction time (2-24 h) and base concentration (0-2 M) were varied in order to find the mildest conditions for complete reactive solubilization of the humins (Table 3.1). Any residual solids were isolated by filtration, washed and dried before characterization.

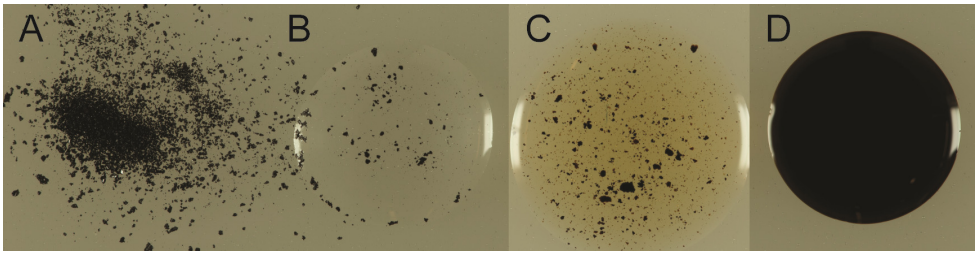

Figure 3.1. A. Glucose-derived humins. B. Droplet of a glucose-derived humins suspended in water at RT. C. Droplet of glucose-derived humins suspended in 0.5 M NaOH at RT. D. Droplet of a solution of glucose-derived humins after reactive solubilization by alkaline pretreatment at 240 °C.

In a typical reaction, glucose-derived humins were suspended in 0.5 M NaOH at 240 °C for 3 h. After reaction and cooling to RT the humins were completely dissolved and a dark brown solution was obtained (Figure 3.1, Table 3.1 Run 4). Lowering the temperature to 200 °C and slightly extending the reaction time to 3.5 h also led to complete solubilization of the humins (Run 3). The reaction time was varied from 2-24 h at 200 °C and from 1-16 h at 240 °C. At 240 °C a reaction time of 2 h was found to be sufficient to dissolve the humins completely (Run 17), while at 200 °C a reaction time of 3.5 h is required. A further decrease in temperature to 175 °C and 150 °C led to the solubilization of only 50 wt% and 6 wt% of the humins, respectively, after 3 h (Run 1 and 2).

A blank experiment showed that base is indeed required for solubilization of the humins, as after treatment of the humin in pH neutral water only 7 wt% and 14 wt% of the humin was dissolved at 200 °C and 240 °C, respectively (Run 5 and 6). Variation of the base concentration from 0.1 to 2 M showed that a minimal base concentration of 0.25 M is needed to solubilize the humins completely (Run 7-10).

Only for those experiments in which complete solubilization was achieved, the liquid phase was analyzed by alkaline GPC to assess the influence of reaction parameters on the extent of depolymerization and the distribution of molecular weights and sizes (Table 3.1). This is, to our best knowledge, the first report of liquid-phase analysis of solubilized humins obtained by the acid-catalyzed dehydration of mono-saccharides. Note that the weight-average molecular weight (Mw) and polydispersity (PD) values obtained should be used to assess relative rather than absolute changes in molecular weight and PD, as the parent humin is insoluble and its molecular weight thus unknown; a proper standard for humins is furthermore not available.

The GPC data showed that depolymerization is more efficient at higher temperatures, with the average molecular weight of the humins treated at 200 °C for 3.5 h being almost three times higher than the Mw of humins treated at 240 °C for 3 h. Further analysis of the effect of reaction time at 200 °C and 240 °C showed that the Mw and PD gradually decrease with increasing reaction time and reach a plateau. This indicates that

no significant repolymerization, as often reported for lignins in alkaline depolymerization processes,[21–23] occurs at high temperatures or long reaction times (Figure 3.2). Increased base concentration, on the other hand, seemed to have little effect on the decrease of Mw and PD.

Table 3.1. Optimization of reaction conditions for the solubilization of glucose-derived humins.

Run #	Time (h)	Temp (°C)	NaOH (M)	Mw[a] (g/mol)	PD[a]	Residue (wt%)
Influence of temperature						
1	3	150	0.5	-	-	94
2	3	175	0.5	-	-	50
3	3.5	200	0.5	17400	12.2	0
4	3	240	0.5	6100	7.4	0
Influence of [NaOH]						
5	3	240	0	-	-	86
6	3.5	200	0	-	-	93
7	3.5	200	0.1	-	-	65
8	3.5	200	0.25	24100	15.4	0
9	3.5	200	1	19000	13.9	0
10	3.5	200	2	13400	10.5	0
Influence of time						
11	2	200	0.5	-	-	
12	3	200	0.5	23000	14.9	2
13	6	200	0.5	11900	10.2	0
14	16	200	0.5	7800	7.9	0
15	24	200	0.5	7500	8.8	0
16	1	240	0.5	-	6.6	86
17	2	240	0.5	8600	9.1	0
18	3	240	0.5	6100	7.4	0
19	4	240	0.5	4800	6.8	0
20	6	240	0.5	4300	6.7	0
21	16	240	0.5	3300	6.5	0

[a] Sodium polystyrene sulfonates were used for calibration of the molar mass distribution.

The mildest conditions required for complete solubilization of glucose-derived humins were next tested for dissolving fructose- and xylose-derived humins. These humins proved to be considerably more recalcitrant to alkaline treatment, however, as such a treatment at 200 °C for 3.5 h in 0.5 M NaOH only dissolved 40-50 wt%. Increasing the reaction temperature to 240 °C did nonetheless result in complete solubilization also of these humins (Table 3.2). The recalcitrance of, in particular, the fructose-derived humins is remarkable, since various techniques including ^{13}C solid-state NMR, ATR-IR and elemental

analysis showed their molecular structure to actually be very similar to glucose-derived humins (Chapter 2). The recalcitrance of xylose-derived humins to dissolve is less surprising since the same study indicated that these humins have a more conjugated structure with more direct linkages between the furan rings, which may explain the higher recalcitrance to the alkaline treatment. Another explanation would be that the original humin samples derived from the various monomeric sugars already show large differences in molecular weight, something which unfortunately cannot be checked due to their insolubility. In Chapter 2, higher humin yields were reported for fructose-derived humins, though, which might indicate that these humins are indeed more cross-linked or less soluble than the glucose-derived humins. Furthermore, the average molecular weight of the oligomers that were still found in solution after acid-catalyzed dehydration of fructose was lower than for the other sugars, again pointing at a low solubility of the fructose-derived humins.

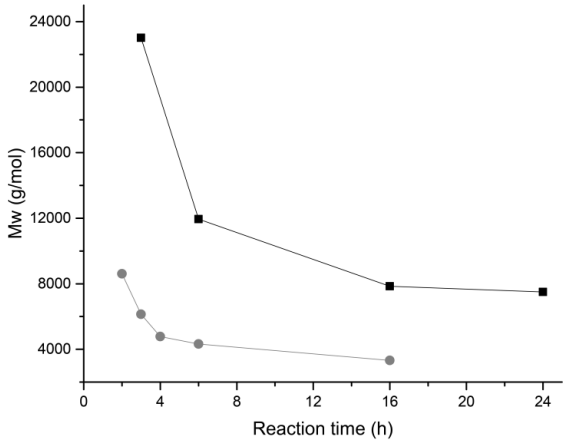

Figure 3.2. Changes in average molecular weight of glucose-derived humins as a function of reaction time at 200 °C (black squares) and 240 °C (grey dots) in 0.5 M NaOH (Mw determined by GPC relative to polystyrene standards).

Table 3.2. Alkaline pretreatment of glucose-, fructose- and xylose-derived humins.

Humin source	Time (h)	Temperature (°C)	NaOH (M)	Mw[a] (g/mol)	PD [a]	Residue (wt%)
Glucose	3.5	200	0.5	17400	12.2	0
Fructose	3.5	200	0.5	-	-	56
Xylose	3.5	200	0.5	-	-	41
Glucose	3	240	0.5	6100	7.4	0
Fructose	3	240	0.5	6700	8.8	0
Xylose	3	240	0.5	6900	9.1	0

[a] Sodium polystyrene sulfonates were used for calibration of the molar mass distribution.

3.2.2. Characterization of Residual Humins

For those reactions for which solubilization of the glucose-derived humins was incomplete (Run 1, 2, 5-7 Table 3.1), the solid residue was isolated by filtration, washed, dried and analyzed by ATR-IR spectroscopy (Figure 3.3). We and others have previously reported on the assignment of the ATR-IR spectra of humins.[11,12] The ATR-IR spectrum of the residue obtained after reaction without base showed only minor changes in the molecular structure. The ratio between the peaks assigned to the carbonyl stretch vibration of a carboxylic acid at 1700 cm^{-1} and the ring stretch of aromatics and furans at 1600 cm^{-1} is slightly changed after treatment in water, though; pointing at either a loss of C=O groups or an increase of C=C bonds. The peak at 1510 cm^{-1}, assigned to a furanic in-phase ring stretch, is slightly weaker which might indicate changes in the furanic network. Some signals in the C-O stretch area (1300-1000 cm^{-1}) are weakened, which points at changes in the oxygen functionalities. The blank reaction shows that the increase in C=C bonds from aromatic rings, which points at the formation of arene ring at the expense of furanic rings, and C-O functional groups is partially caused by hydrothermal reactions. A similar effect was observed for HTC at extended reaction times, with dehydration and aromatization of the sample being observed.[15] However, aromatization was not as strong as observed for the humins that were completely solubilized by alkaline pretreatment (see below), showing that aromatization is not a purely thermal effect.

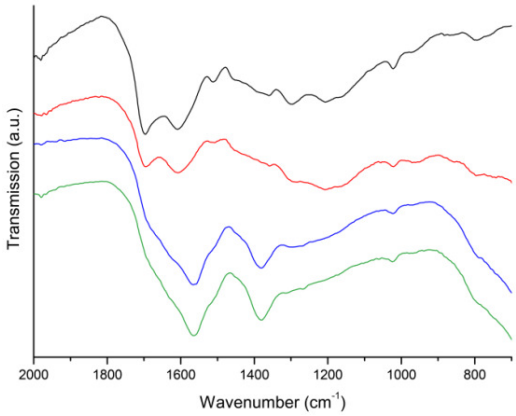

Figure 3.3. ATR-IR spectra of residual humins after alkaline pretreatment at 150 °C (green), in 0.1 M NaOH (blue) and a blank reaction (red) compared with the parent glucose-derived humine (black).

The residues found after alkaline pretreatment at 200 °C in 0.1 M NaOH and treatment in 0.5 M NaOH at 150 °C have almost identical ATR-IR spectra. These spectra are very different from the spectra of the parent humin and are dominated by the strong peaks at 1565 and 1385 cm^{-1}, assigned to the anti-symmetric and symmetric stretch of carboxylate anions (COO^-), respectively. A shoulder around 1700 cm^{-1} is also seen in the ATR-IR spectrum of the residue, indicating that some other carbonyl groups, most likely ketones, are present as well. Other parts of the spectrum were difficult to assign since the peaks from COO^- dominate the signals. Such carboxylic acid groups were already detected

in the parent humins but only in minor amounts; the new carboxylic acid groups might be the result of a reaction with the hydroxide in a Cannizzaro-like reaction where aromatic aldehydes react with hydroxide to form a carboxylic acid.

3.2.3. Characterization of Recovered Alkali-treated Humins

Soluble humin obtained from solubilization reactions run at 240 °C in 0.5 M NaOH for 3 h were taken for the characterization studies, as these conditions are sufficient to solubilize all three humin samples completely. After alkaline treatment, the solubilized humins stay in solution down to a pH of about 7. Indeed the humins can be precipitated by further acidification of the liquid phase with H_2SO_4 to pH 1 (redissolution requires the pH to be ≥ 7). The recovered humins were subsequently washed, dried at 70 °C under vacuum and characterized by several analytical techniques. This way, about 75 wt% of the original humin intake could be recovered.

3.2.3.1. SEM

Figure 3.4 shows the SEM images of the parent humin and humin recovered after alkaline pretreatment. It is clear that the typical spherical morphology of the parent humin is completely lost after alkaline pretreatment, showing that the humins indeed were completely solubilized by treatment with base.

Table 3.3. Elemental analysis of glucose-, fructose- and xylose-derived humins before and after alkaline treatment.[a]

	wt% C	wt% H	wt% S	wt% O[b]	H/C	O/C
Original humin						
Glucose humin	64.55	4.27	<0.01	31.19	0.79	0.36
Fructose humin	65.02	4.13	<0.01	30.86	0.76	0.36
Xylose humin	66.70	3.83	<0.01	29.48	0.69	0.33
Recovered alkali-treated humin						
Glucose humin	71.96	4.75	<0.01	23.29	0.82	0.26
Fructose humin	71.51	4.66	<0.01	23.83	0.78	0.25
Xylose humin	72.23	4.72	<0.01	23.04	0.79	0.24

[a] N <0.01 wt% [b] Calculated by difference

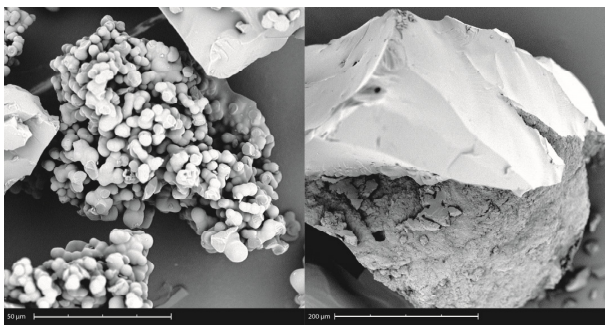

Figure 3.4. SEM images of the parent humin (left) and recovered glucose-derived humin after alkaline pretreatment and precipitation by acidification.

3.2.3.2. Elemental Analysis

The elemental compositions of the parent and recovered, alkali-treated humins are given in Table 3.3. The data, visualized by a Van Krevelen plot in Figure 3.5, clearly shows loss of oxygen content with a concomitant slight increase in H/C, indicating net loss of oxygen functionalities in the structure. These changes in the elemental composition are similar to the differences observed in elemental composition of cellulose samples after thermal treatment in neutral and alkaline media (pH 11).[24] The decrease in the O/C ratio and increase in the H/C ratio indicate that elimination of CO or CO_2 occurs during alkaline treatment of the humins.[25] Such a decarboxylation pathway (red line in Figure 3.5) is close to the observed changes in elemental composition, however, it does not fit with the increase in carboxylic acid content that was observed and discussed below. The van Krevelen plot shows that exclusive loss of CO does not fit with the observed elemental composition neither (blue line in Figure 3.5). Instead, the data suggests a combination of dehydration and loss of CO during the alkaline treatment of humins (green line in Figure 3.5).

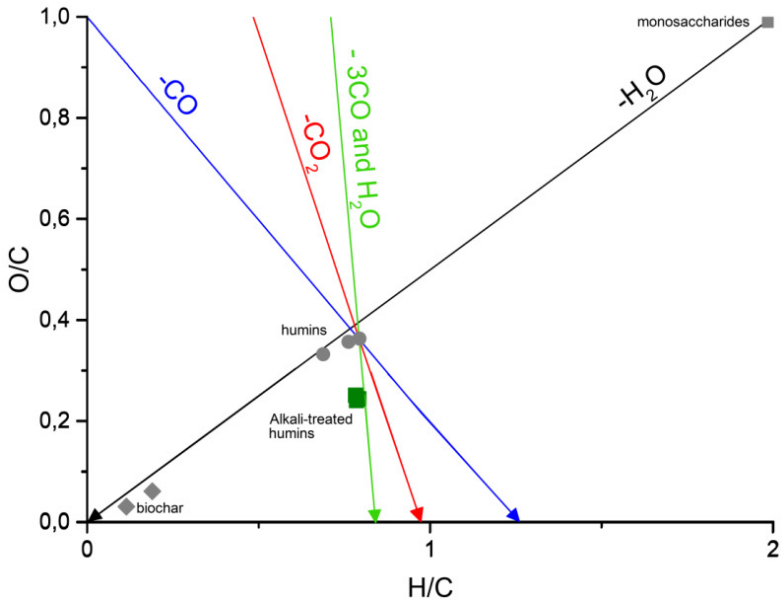

Figure 3.5. Van Krevelen plot showing changes in the elemental composition of humins (grey circle) formed during the acid-catalyzed dehydration of monosaccharides (grey square). Complete dehydration of sugars, indicated by the black arrow, yields biochar (grey diamonds). Alkaline treatment of humins (green squares) changes the elemental composition; possible pathways are decarboxylation (red arrow), loss of CO (blue arrow) and a combination of dehydration and CO loss (green line).

3.2.3.3. Molecular Structure of Alkali-treated Humins: ATR-IR, ^{13}C Solid-state NMR and Pyrolysis-GC-MS

The ATR-IR spectra of three alkali-treated humin samples (Figure 3.6) proved to be very similar. After acidification of the liquid phase, sulfates arising from sulfuric acid could be present in the sample, but comparison to the ATR-IR spectrum of Na_2SO_4 and H_2SO_4 showed that major contributions from sulfates in the ATR-IR spectra of alkali-treated humins can be excluded; this is further confirmed by the low sulfur content of the humins (< 0.01 wt%, Table 3.3).

Compared to the ATR-IR spectra of the parent humins, major changes in the molecular structure are observed, though (Figure 3.6). The O-H stretch band is shifted slightly to lower wavenumbers and has become very broad, which again could point at the formation of carboxylic acids. At 3000-2800 cm^{-1} clear C-H stretch vibrations can be seen which are much more pronounced than in the ATR-IR spectra of the parent humins. The signal at 1700 cm^{-1}, assigned to C=O bonds, is slightly broader in the alkali-treated sample. The peak at 1610 cm^{-1}, attributed to a C=C ring stretch vibration, is shifted slightly to lower wavenumbers after alkaline pretreatment. For the glucose- and fructose-derived humins, the signals from C=C and C=O stretch vibrations are much stronger in the alkali-treated humins, indicating an increase in the amount of these functional groups or the formation of a more uniform structure. A distinct difference is the disappearance of the peak at 1510 cm^{-1} in glucose- and fructose-derived humin and of the signal at 1465 cm^{-1} in xylose-derived humin after alkaline pretreatment. This, together with a decrease of the peak at 1020 cm^{-1} ascribed to furan ring deformation, and a shift of the peaks around 800 cm^{-1} from C-H out of plane vibrations of aromatic rings points at a decrease in furanic content after alkaline pretreatment. The strongest changes are observed in the C-O stretch region, however, as several details between 1300 and 1000 cm^{-1} (C-O stretch from alcohols and ethers) have disappeared. In the same region, a broad peak centered around 1150 cm^{-1} appeared, which can be ascribed to a hydroxyl group bonded to C=C or to an aromatic ring, *i.e.* a phenolic OH.

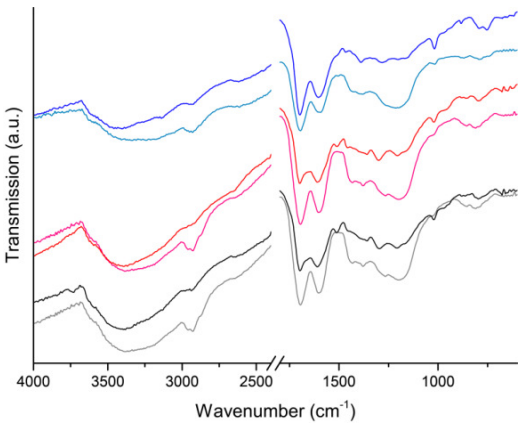

Figure 3.6. ATR-corrected IR spectra of original humins (dark colors) and alkali-treated (light colors) humins derived from glucose (black), fructose (red) and xylose (blue).

^{13}C solid-state NMR studies provided further insight into the changes in the molecular structure of the humins upon alkaline treatment. The NMR spectra of the alkali-treated humins were recorded using a Two Dimensional Phase Adjusted Spinning Sidebands (2D PASS) pulse sequence that separates the spinning sidebands from the centerband into a 2nd dimension. The sidebands arise from the anisotropy in the chemical shifts , which is large for groups such as aromatic and carbonyl functional groups.[12,26,27] The 2D PASS solid-state NMR spectra of the original humins and their interpretation have been reported in Chapter 2. A pattern characteristic of oxygen-containing aromatic rings was observed which is ascribed to furanic rings based on the typical signals for C_α and C_β observed at δ = 140 - 150 ppm and δ = 110 - 120 ppm, respectively, which were observed in a 1:1 ratio.[28]

The solid-state NMR spectra of glucose-derived humins before and after alkaline treatment (Figure 3.7) again confirm the significant chemical changes in the molecular structure of the humin. Major changes can be seen in the C=C region (δ = 90-160 ppm), especially the peaks from furanic C_α and C_β were less intense than observed in the parent humins. A strong, new signal centered around δ = 130 ppm appeared, which can be ascribed to a conjugated aromatic network.[28,29] The increase in intensity of the signal at δ = 176 ppm furthermore points at the formation of (additional) carboxylic acid groups; note that the assignment of this peak to ester functional groups is considered unlikely in strong alkali. The formation of these ionizable carboxylic acid groups, together with the considerable reduction in molecular weight, can explain the increased solubility of the humins at higher pH. The peak assigned to ketones and aldehydes at δ = 209 ppm has become much less intense for the alkali-treated humin. Finally, the changes in the aliphatic region are remarkably small and the ratio between saturated and unsaturated (aromatic) carbons is very similar for the humins before and after alkaline treatment. The low, undefined intensity in the alcohol/ether region seen for the parent humins, has almost disappeared after alkaline pretreatment, showing that any such bonds were hydrolyzed during the treatment.

Although the solid-state NMR spectra of the parent humins from different sugar feeds showed clear differences, the spectra of the three alkali-treated humins are overall very similar (Figure 3.8). Small differences can still be seen though for the alkali-treated humins from C_6- and C_5-sugars.[12] An additional shoulder appeared in the alkali-treated xylose humin spectrum at δ = 110 ppm, while the shoulder at δ = 141 ppm on the main aromatic peak is weaker. These shoulders originate from non-substituted C_β and C_α in furan, respectively.[13,28]

To further support the assignments made for the 2D PASS ^{13}C NMR spectra of the alkali-treated humins, spectra were recorded with two different cross polarization (CP) mixing times as well as with an interrupted decoupling (ID) pulse sequence. The spectra with a short CP mixing time (5 μs) mainly show protonated carbons, while longer CP mixing times (1 ms) will show all carbons and give the complete NMR spectrum. It should

be noted in this respect that the amount of methyl groups is always underestimated with CP methods due their fast rotation.[30] In addition, further elongation of the CP time (2 ms) combined with an interrupted decoupling pulse sequence[31,32] should, in principle, selectively show only the non-protonated carbons; note that some methyl or methoxy groups can also appear in an ID spectrum as their fast rotation which reduces the CH dipolar couplings.

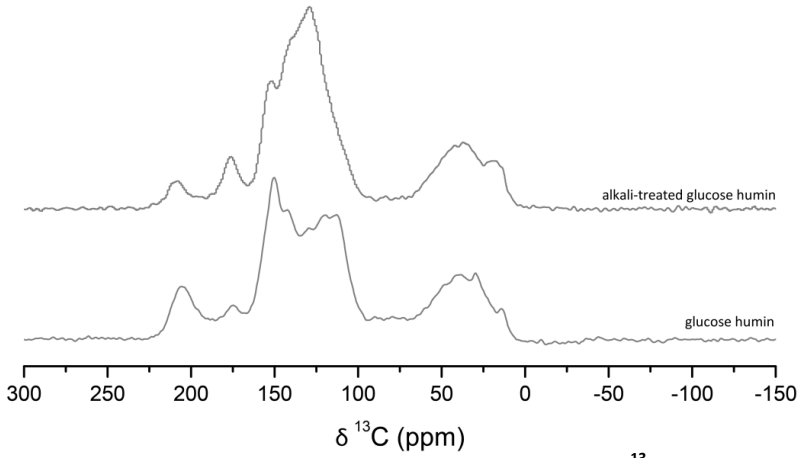

Figure 3.7. Sheared-sum projections of the 2D PASS solid-state ^{13}C NMR spectra of glucose-derived humin before and after alkaline treatment.

The CP (ID) spectra of alkali-treated xylose-derived humins are shown in Figure 3.9 to illustrate what information can be gained as function of mixing time and decoupling. In addition to the strong signal expected for the aliphatic carbons at around δ = 37 ppm that is seen with a short CP mixing time, protonated carbons from furan are observed at δ = 111 ppm and δ = 142 ppm in the aromatic region, from unsubstituted C_β and C_α, respectively.[28] These signals are similar to the chemical shifts expected for C_α and C_β in benzofuran,[33] whose presence would be in agreement with the more aromatic character of the treated humins; the presence of nonfused furanic rings cannot be excluded, though. The peak at δ = 127 ppm can be assigned to protonated carbon atoms in polyaromatic structures,[34] and the signal at 153 ppm might be caused by pyrone-like structures.[35] Furthermore, a weak signal around δ = 176 ppm was observed as well, which might indicate the presence of some aldehyde functional groups probably connected to a furan ring.[36]

The ID spectrum shows a signal for the methyl groups at around δ = 17 ppm, but no quaternary sp^3 carbons. The broad signal centered around δ = 141 ppm suggests the presence of non-protonated carbons in polyaromatic structures,[34] while the peak at δ= 151 ppm can be ascribed to substituted C_α's in furan[28,33] or a C_α in phenol,[37] two options which are actually difficult to distinguish in 1D ^{13}C solid-state NMR (see Chapter 4 for a

detailed discussion).[38] The C=O at δ = 176 ppm in the interrupted decoupling spectrum is again assigned to carboxylic acid groups, while the fact that the signal at δ = 209 ppm, not seen in the short CP spectrum, is actually seen with the ID signal proves that the C=O carbon is non-protonated and should be ascribed to ketones. In conclusion, the ^{13}C solid-state NMR spectra of alkali-treated humins further confirm the formation of an arene-rich structure with an increase in carboxylic acid functionalities.

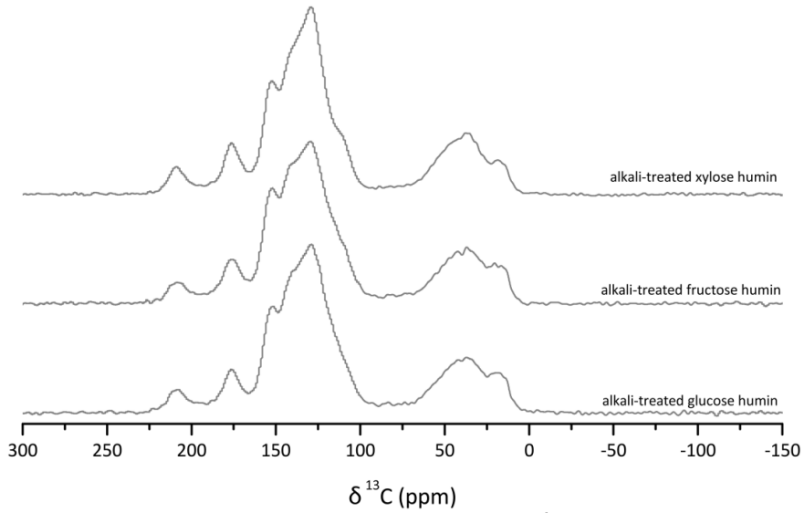

Figure 3.8. Sheared-sum projections of the 2D PASS ^{13}C solid-state NMR spectra of alkali-treated glucose-, fructose- and xylose-derived humin.

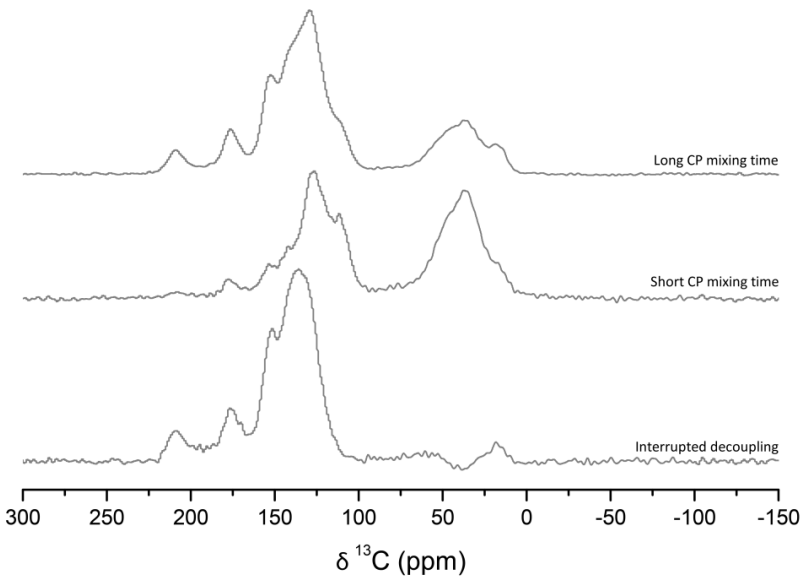

Figure 3.9. 2D PASS ^{13}C solid-state NMR spectra of alkali-treated xylose humin recorded using long CP time, short CP mixing time and interrupted decoupling.

Pyrolysis-GC-MS data was previously reported for the parent humins and showed several low molecular weight furanic compounds to be released upon pyrolysis, supporting our proposal of a furan-rich molecular structure.[8,12] Pyrolysis of the alkali-treated humins yielded more substituted benzenes and less furanics, further supporting the more arene-like structure indicated by ^{13}C solid-state NMR (Figure 3.10).[8,12] As expected from the ^{13}C solid-state NMR and ATR-IR data, the pyrolysis-GC-MS chromatograms of the three different alkali-treated humins proved to be very similar (not shown).

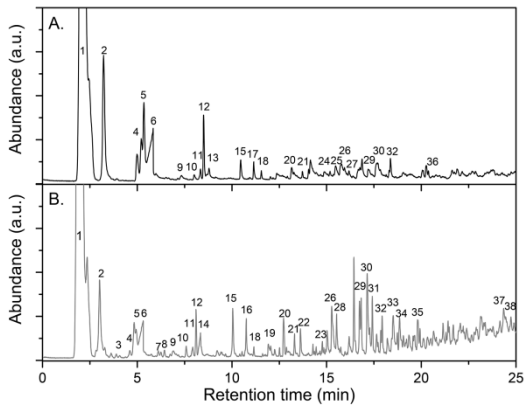

1. CO_2
2. acetone
3. cyclopentene
4. butanone
5. 2-methylfuran
6. acetic acid
7. 1,3-cyclohexadiene
8. 3-methylcyclopentene
9. benzene
10. 2-pentanone
11. 2-ethylfuran
12. 2,5-dimethylfuran
13. 2,4-dimethylfuran
14. propanoic acid
15. toluene
16. 2-ethyl-5-methylfuran
17. acetylfuran
18. 2,3,5-trimethylfuran
19. 2-cyclopen-1-one
20. 1,3-dimethylbenzene
21. 1,2-dimethylbenzene
22. 2-methyl-cyclopen-1-one
23. 1-ethyl-4-methylbenzene
24. 5-methylfuranone
25. 3-methyl-2-cyclopen-1-one
26. phenol
27. benzofuran
28. 1,2,3-trimethylbenzene
29. 2-methylphenol
30. 3-methylphenol
31. 4-methylphenol
32. 2-methylbenzofuran
33. 2,4-dimethylphenol
34. 2-ethylphenol
35. cinnamaldehyde
36. 4,7-dimethylbenzofuran
37. 6,7-dimethylbenzofuran
38. 2-naphthalenol

Figure 3.10. Pyrolysis-GC MS chromatograms and peak assignments of glucose-derived humins (A) and alkali-treated humins (B).

The combination of different analytical tools and spectroscopic techniques now allows us to identify the chemical changes that occur in the humin samples during alkaline pretreatment. Elemental analysis indicated an increase in H/C ratio while the O/C decreased for all humin samples after alkaline treatment, which indicates the loss of CO or CO_2 and probably water, also leading to a slight decrease in molecular weight. Loss of C and O without a net decrease of H could also indicate net decarboxylation, which is unlikely, however, as the ATR-IR and ^{13}C solid-state NMR spectra of alkali-treated humins point at carboxylic acid formation instead. The formation of these acids could be explained by a Cannizzaro-like reaction where the hydroxide ion reacts with an aromatic aldehyde leading to the formation of acids.

Both the ATR-IR and ^{13}C solid-state NMR spectra indicate changes in the furanic nature of the humin's molecular structure upon alkaline pretreatment. A clear signal from conjugated aromatic systems was observed in the ^{13}C solid-state NMR spectra of alkali-treated, however, typical signals for oxygen-containing aromatic rings are still observed. These could be substituted furanic groups, which is not unexpected given the structure of

the parent humins. The formation of a network containing benzofuran and furan rings fused with larger (polycyclic) aromatic structures is more plausible, however, given the overall aromatization of the sample. An overview of the functional groups and structural motifs likely to be present in alkali-treated humins is given in Table 3.4 together with an estimation of their abundance. The formation of aromatic, conjugated systems was observed before for the gasification of humins,[7] upon pyrolysis of carbohydrate-derived functional materials[29,39] and in furanic resins.[28] The aromatization of the sample and conversion of the furanic structures to more arenic/phenolic ones is furthermore confirmed by pyrolysis-GC-MS measurements. At the same time, both the IR and ^{13}C NMR spectra of the alkali-treated humins still show strong signals from aliphatic carbon. Both IR and NMR spectra point at changes in the aliphatic linkers originally present in the humins, showing that these groups are not left unchanged during the formation of the (polycyclic) aromatic structures. Alternatively, new aliphatic groups could be formed by Diels-Alder reactions between furanic rings or furans and dienophiles. Further dehydration of the Diels-Alder product could in turn lead to the formation of benzofuran or arene rings.[40,41] Another possible pathway is based-catalyzed ring-opening, which leads to the formation of aldehydes in the base-catalyzed furan ring-opening as was demonstrated for furan-3,4-dicarbaldehyde in methanol.[42]

The increased solubility of the humins seems a bit counterintuitive, given the more extensive aromatization of the humins upon alkaline treatment; this hydrophobization can nonetheless be offset by the formation of carboxylic acids and the gradual decrease in molecular weight. The latter can be caused by the cleavage of C-C, *e.g.* by retro aldol reactions,[43] and C-O bonds, *e.g.* by hydrolysis of ethers and acetals. The first reaction cannot be verified by our experimental data. C-O cleavage, however, is supported by the disappearance of signals from aliphatic C-O bonds in IR and solid-state NMR spectra after alkaline pretreatment, which indicates that the relatively few ether-like bonds that are present in the humins are hydrolyzed during alkaline pretreatment. The presence of acetals and ethers in the humin's structure has been suggested before by Zarubin *et al.,*[9] but were not incorporated in our model of humin molecular structure presented in Chapter 2 as such bonds could not be clearly observed in our data. Based on the results presented here, the molecular structure of humins can now be refined somewhat by including a small amount of ether or acetal bonds.

Table 3.4. Functional groups and molecular structures present in alkali-treated humins including assignment of the signals in the solid state NMR spectra (in ppm).

Functional group	Chemical structure	Relative abundance	Functional group	Chemical structure	Relative abundance
Carboxylic acids[44]	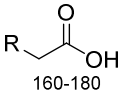	High	Furans Benzofurans [13,28,33]	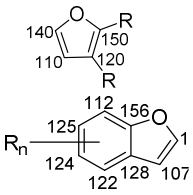	Low
Alkanes[44]	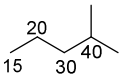	High	Furan ring-opening products[45,46]	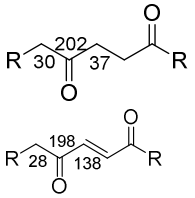	Low
Polycyclic aromatic sheets[34]	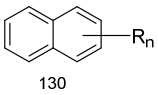	High	Ketones[44]		Low
Aldehydes[36,44]	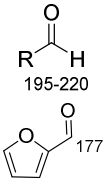	Low	Phenols[37]	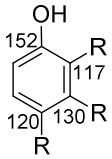	Low
Alkenes[44]	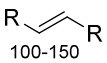	Low	4*H*-pyrones [35,47]	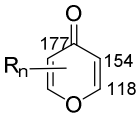	Low
Benzene[48]	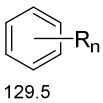	Low	Alcohols Ethers Acetals [44,49]	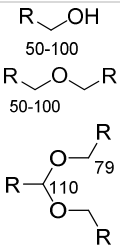	Very low

3.3. Conclusions

Alkaline pretreatment proved to be an effective method for the reactive solubilization of humin by-products. Higher temperatures and prolonged reaction times led to a decrease in the weight-average molecular weight of the dissolved humins as determined by GPC. A hydroxide concentration of 0.5 M was sufficient for the complete solubilization of the humins, while further increase of the base concentration hardly lowered the average molecular weight any further. Fructose- and xylose-derived humins proved to be more recalcitrant to the alkaline pretreatment and required higher treatment temperatures for full solubilization. While this was rather unexpected for the fructose-derived humin given its structural similarity to the glucose-derived humin, it was not for the more highly cross-linked structure of the xylose-derived humins.

Characterization of the alkali-treated humins using elemental analysis, ATR-IR, solid-state NMR and pyrolysis-GC-MS revealed considerable changes in the humin structure. The more (polycyclic) aromatic structure that is formed is possibly the result of Diels-Alder reactions combined with dehydration reactions; the formation of new aliphatic groups might be the result of ring-opening of the furan, with other furanic rings now most probably being part of benzofurans. Oxygen-containing functional groups change upon alkaline treatment as the amount of ketone groups decreased, while the acid content increased; the latter is linked to the increased solubility of the alkali-treated humins. The reduction in molecular weight can be explained by cleavage of the C-O-C bonds of which small amounts are present in the parent humin; C-C cleavage might occur as well, but cannot be evidenced from our data.

Although alkaline pretreatment changes the molecular structure of the humins, the increased solubility in water pH ≥ 7 could assist the catalytic valorization of the humin by-products allowing better catalyst-substrate interaction, especially when a heterogeneous catalyst is used. Examples of possible valorization routes for the water-soluble humins include, for example, aqueous phase reforming for the production of hydrogen and chemicals or catalytic hydrotreatment using a supported catalyst and molecular hydrogen. The former is well-known for bio-based oxygenates[50,51] and was tested for the production of aromatic monomers from lignin,[52] which indicates that recalcitrant fractions of biomass can be converted by aqueous phase processing. The aqueous phase reforming of alkali-treated humins is the subject of Chapter 5.

3.4. Experimental Section

Humin samples were prepared from an aqueous solution containing 1 M sugar (D-glucose, D-fructose or D-xylose) and 0.01 M H_2SO_4; the solution was heated to 180 °C for 6 h in a 1 L batch autoclave (Buchi). The solid humins formed were isolated by filtration, washed with excess water and dried at RT. To remove all water-soluble components occluded in the solid, the humins were subjected to a Soxhlet extraction with water for 24 h and

subsequently dried at 70 °C under vacuum. A detailed description of the preparation of the humin samples can be found in Chapter 2.

Solubilization reactions were run in a Teflon-lined unstirred autoclave vessel filled with 0.5 g glucose-derived humin and 50 mL NaOH solution and heated in an oven. Reaction parameters were varied: time 3-24 h, NaOH concentration 0-2 M, temperature 150-240 °C. Relevant reactions were repeated with fructose- and xylose-derived humins and conditions were independently optimized. The reaction mixture was cooled to RT, filtered and any remaining residues were washed with water and dried at RT. The amount of residue was weighed and expressed as wt% of the amount of starting material.

For further characterization of the solubilized humins from the different feedstocks, 5 g (glucose-, fructose-, or xylose-derived) humin was treated with 80 mL 2 M NaOH at 240 °C for 3 h. The humins were precipitated from the solution by acidification to pH 1 with 6 M H_2SO_4, isolated by filtration, washed with 6 L water and dried under vacuum for 24 h at 70 °C.

The aqueous phase was analyzed by GPC on an alkaline SEC by Waters Alliance system equipped with a manually packed column (4.6 x 30 cm) with ethylene glycolmethacrylate copolymer TSK gel Toyopearl HW-55F according to the work of Gosselink *et al*.[53] The system was operated at 40 °C with 0.5 M NaOH eluent at a flow rate of 1 mL min^{-1} and UV detection at 280 nm. Sodium polystyrene sulfonates (Mw range 891 to 976 000 Da) were used for calibration of the molar mass distribution. Humin samples were diluted to a concentration of 1 g mL^{-1} using 0.5 M NaOH.

ATR-IR spectra were recorded on a Bruker Tensor 37 IR spectrometer using a PIKE MIRacle ATR accessory with a diamond crystal. For each spectrum 32 scans with a resolution of 4 cm^{-1} were averaged. Elemental analyses (CHNS) were performed at the University of Groningen. The oxygen content was calculated by difference. The ^{13}C solid-state NMR spectra were recorded at the Radboud University Nijmegen. All spectra were measured on a 300 MHz solid state NMR spectrometer using a 7.5 mm double resonant chemagnetics APEX probe, tuned at 75.45 MHz for carbon. All spectra were obtained using ramped CPMAS at a radio frequency (rf) field of 55 kHz for carbon and 51 kHz for protons. Proton decoupling during acquisition was accomplished with a Spinal-64 sequence at an rf field of 55 kHz, optimized to a pulse width and phase of 9 μs and 7°, respectively and Magic Angle Spinning speeds were 4 kHz. After cross polarization a 2D PASS sequence was used to separate the spinning sidebands, employing cogwheel phase cycling.[54] The NMR spectra were normalized to a total area of 1.

Analytical programmed temperature vaporization (PTV) GC-MS of humins was conducted with a HP 5890 GC Series II system equipped with a 5972 MS detector, and the PTV was controlled by an Optic 2 device. Typically 1 mg of sample was used. The pyrolysis temperature program started at 40 °C followed by heating to 600 °C at a rate of 16 °C min^{-1}, and finally held at 600 °C for 0.5 min. After pyrolysis, the products were transferred into a capillary column (Agilent Technologies VF-5ms, 30 x 0.25 x 1.0) by a GC injector

(split 50:1). Helium was used as the carrier gas at a flow rate of 1 mL min^{-1}. The following GC temperature program was applied: starting temperature of 40 °C for 5 min followed by heating at a rate of 10 °C min^{-1} to a final temperature of 250 °C. The MS detector was operated in the electron ionization mode (70 eV) with an interface temperature 280 °C. A scan range of m/z 35-400 was applied. Pyrolysis products were identified by comparison with mass spectra of authentic compounds and masses.

3.5. Acknowledgements

We would like to thank Prof. dr. ir. Erik Heeres, Yuehu Wang, Henk van de Bovenkamp, Léon Rohrbach from the University of Groningen for humin preparation, elemental analysis, pyrolysis-GC-MS measurements and contributing to the chapter. Jacinta van der Putten and Dr. Richard Gosselink from Wageningen University are thanked for performing the GPC analyses. Dr. Ernst van Eck from Radboud University Nijmegen is thanked for solid-state NMR analysis. Support of NWO for the "Solid state NMR facility for advanced materials science" in Nijmegen is gratefully acknowledged. Dr. Peter de Peinder from VibSpec is thanked for helping with the interpretation of the IR spectra. Dr. Marleen Kerssens from Utrecht University is thanked for taking the photographs shown in Figure 3.1.

3.6. References

[1] J. P. Lange, E. van der Heide, J. van Buijtenen, R. Price, *ChemSusChem* **2012**, *5*, 150–166.
[2] J. P. Lange, R. Price, P. M. Ayoub, J. Louis, L. Petrus, L. Clarke, H. Gosselink, *Angew. Chem. Int. Ed.* **2010**, *49*, 4479–4483.
[3] J. Horvat, B. Klaić, B. Metelko, V. Šunjić, Tetrahedron Lett. 1985, 26, 2111–2114.
[4] D. M. Alonso, J. Q. Bond, J. A. Dumesic, *Green Chem.* **2010**, *12*, 1493–1513.
[5] E. Bartels, Über Die Bildung von Huminstoffen Aus Ketosen Durch Einwirkung Konzentrierter Halogenwasserstoffsäuren, PhD Thesis Hamburg University, **1966**.
[6] D. J. Hayes, J. Ross, M. H. B. Hayes, S. W. Fitzpatrick, in *Biorefineries - Industrial Processes and Products* (Eds.: B. Kamm, P.R. Gruber, M. Kamm), Wiley, **2006**, 139–164.
[7] T. M. C. Hoang, L. Lefferts, K. Seshan, *ChemSusChem* **2013**, *6*, 1651–1658.
[8] C. B. Rasrendra, M. Windt, Y. Wang, S. Adisasmito, I. G. B. N. Makertihartha, E. R. H. van Eck, D. Meier, H. J. Heeres, *J. Anal. Appl. Pyrolysis* **2013**, *104*, 299–307.
[9] I. V. Sumerskii, S. M. Krutov, M. Y. Zarubin, *Russ. J. Appl. Chem.* **2010**, *83*, 320–327.
[10] S. K. R. Patil, C. R. F. Lund, *Energy Fuels* **2011**, *25*, 4745–4755.
[11] S. K. R. Patil, J. Heltzel, C. R. F. Lund, *Energy Fuels* **2012**, *26*, 5281–5293.
[12] I. van Zandvoort, Y. Wang, C. B. Rasrendra, E. R. H. van Eck, P. C. A. Bruijnincx, H. J. Heeres, B. M. Weckhuysen, *ChemSusChem* **2013**, *6*, 1745–1758.
[13] N. Baccile, G. Laurent, F. Babonneau, F. Fayon, M. M. Titirici, M. Antonietti, *J. Phys. Chem. C* **2009**, *113*, 9644–9654.
[14] M. Sevilla, A. B. Fuertes, *Carbon* **2009**, *47*, 2281–2289.
[15] M. Sevilla, A. B. Fuertes, *Chem. Eur. J.* **2009**, *15*, 4195–4203.
[16] G. Song, E. H. Novotny, A. J. Simpson, C. E. Clapp, M. H. B. Hayes, E. Solos, R. J. Bota, R. De Janeiro, S. Paul, *Eur. J. Soil Sci.* **2008**, *59*, 505–516.
[17] J. A. Neyroud, M. Schnitzer, *Geoderma* **1975**, *13*, 171–188.
[18] T. Jakab, P. Dubach, N. C. Metha, H. Deuel, *Zeitschrift für Pflanzenernährung, Düngung, Bodenkd.* **1963**, *102*, 8–17.
[19] R. Bourbonniere, *Org. Geochem.* **1983**, *5*, 131–142.

[20] D. Dimmel, G. Gellerstedt, in (Eds.: C. Heitner, D.R. Dimmel, J.A. Schmidt), Taylor And Francis Group, Boca Raton, **2010**, 349–391.
[21] R. W. Thring, *Biomass and Bioenergy* **1994**, *7*, 125–130.
[22] A. Toledano, L. Serrano, J. Labidi, *Fuel* **2014**, *116*, 617–624.
[23] A. Toledano, L. Serrano, J. Labidi, *J. Chem. Technol. Biotechnol.* **2012**, *87*, 1593–1599.
[24] J. P. Schuhmacher, F. J. Huntjes, D. W. Van Krevelen, *Fuel* **1960**, *39*, 223–234.
[25] D. W. Van Krevelen, D. Van Krevelen, *Fuel* **1950**, *29*, 269–284.
[26] O. N. Antzutkin, S. C. Shekar, M. H. Levitt, *J. Magn. Reson.* **1995**, *115*, 7–19.
[27] F. G. Vogt, J. M. Gibson, D. J. Aurentz, K. T. Mueller, a J. Benesi, *J. Magn.* Reson. 2000, 143, 153–160.
[28] C. Burket, R. Rajagopalan, A. Marencic, K. Dronvajjala, H. Foley, Carbon 2006, 44, 2957–2963.
[29] C. Falco, F. Perez Caballero, F. Babonneau, C. Gervais, G. Laurent, M. M. Titirici, N. Baccile, Langmuir 2011, 27, 14460–14471.
[30] W. Kolodziejski, J. Klinowski, *Chem. Rev.* **2002**, *102*, 613–28.
[31] S. J. Opella, M. H. Frey, *J. Am. Chem. Soc.* **1979**, *101*, 5854–5856.
[32] L. B. Alemany, D. M. Grant, T. D. Alger, R. J. Pugmire, *J. Am. Chem. Soc.* **1983**, *105*, 6697–6704.
[33] T. Okuyama, T. Fueno, *Bull. Chem. Soc. Jpn.* **1974**, *47*, 1263–1266.
[34] P. E. Hansen, *Org. Magn. Reson.* **1979**, *12*, 109–142.
[35] D. Hobuß, S. Laschat, A. Baro, *Synlett* **2005**, 123–124.
[36] F. Fringuelli, S. Gronowitz, A.-B. Hörnfeldt, I. Johnson, A. Taticchi, B. Mannervik, *Acta Chem. Scand. B* **1974**, *28*, 175–184.
[37] B. R. Sinha, D. O'Connor, F. D. Blum, *J. Appl. Polym. Sci.* **1989**, *38*, 163–171.
[38] M. Gomes, A. Gandini, *J. Polym. Sci. A Polym. Chem.* **2011**, *49*, 3759–3768.
[39] R. L. Johnson, J. M. Anderson, B. H. Shanks, X. Fang, M. Hong, K. Schmidt-Rohr, *J. Magn. Reson.* **2013**, *234*, 112–124.
[40] M. Shiramizu, F. D. Toste, *Chem. Eur. J.* **2011**, *17*, 12452–12457.
[41] Y.-T. Cheng, G. W. Huber, *ACS Catal.* **2011**, *1*, 611–628.
[42] S. Trofimenko, *J. Am. Chem. Soc.* **1963**, *85*, 1357.
[43] J. Gierer, *Wood Sci. Technol*. **1985**, *19*, 289–312.
[44] M. Balci, Basic ^{1}H-and ^{13}C-NMR Spectroscopy, **2005**.
[45] C. Asta, J. Conrad, S. Mika, U. Beifuss, *Green Chem.* **2011**, *13*, 3066–3069.
[46] J. H. Clark, D. G. Cork, H. W. Gibbs, *J. Chem. Soc. Perkin Trans. 1* **1983**, 2253–2258.
[47] M. J. Loots, L. R. Weingarten, R. H. Levin, *J. Am. Chem. Soc.* **1976**, *98*, 4571–4577.
[48] S. A. Richards, J. C. Hollerton, *Essential Practical NMR for Organic Chemistry*, John Wiley & Sons, Ltd, Chichester, UK, **2010**.
[49] E. Taskinen, M. L. Pentikäinen, *Tetrahedron* **1978**, *34*, 2365–2370.
[50] R. R. Davda, J. W. Shabaker, G. W. Huber, R. D. Cortright, J. A. Dumesic, *Appl. Catal. B Environ.* **2005**, *56*, 171–186.
[51] R. Cortright, R. Davda, J. Dumesic, *Nature* **2002**, *418*, 964–967.
[52] J. Zakzeski, B. M. Weckhuysen, *ChemSusChem* **2011**, *4*, 369–378.
[53] R. J. A. Gosselink, J. E. G. van Dam, E. L. Scott, E. de Jong, J. P. M. Sanders, J. Li, G. Gellerstedt, *Holzforschung* **2010**, *64*, 193–200.
[54] N. Ivchenko, C. E. Hughes, M. H. Levitt, *J. Magn. Reson.* **2003**, *164*, 286–293.

CHAPTER 4

Structural Characterization of ^{13}C-Enriched Humins and Alkali-treated ^{13}C Humins by 2D Solid-state NMR

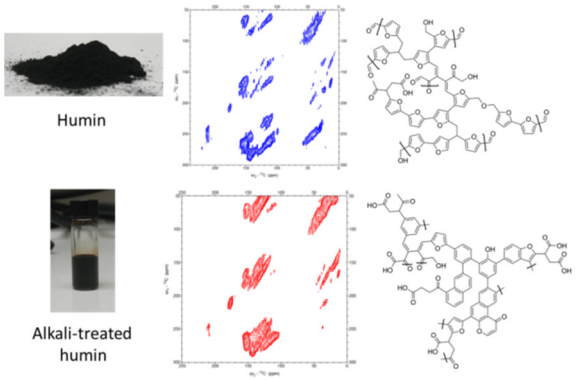

Abstract

Humin by-products are formed during the acid-catalyzed dehydration of carbohydrates to bio-based platform molecules, such as hydroxymethylfurfural and levulinic acid. The molecular structure of these humins has not yet been unequivocally established. 1D ^{13}C solid-state NMR data reported have, for example, provide considerable insight, but do not allow for the unambiguous assignment of key structural motifs. Therefore, complementary (2D) techniques are needed to gain additional insight into the molecular structure of humins. In this chapter, the preparation of ^{13}C-enriched humins is reported, together with the reactive solubilization of these labeled humins and their characterization with complementary 1D and 2D solid-state ^{13}C NMR techniques. 1D cross polarization (CP) and direct excitation (DE) ^{13}C solid-state NMR spectra, heteronuclear correlation (HETCOR) spectra recorded with different contact times and double-quantum single-quantum (DQSQ) experiments with CP and DE unambiguously established that the original humins have a furan-rich structure with aliphatic linkers and allowed for a refinement of the molecular structure proposed in Chapter 2. Solid-state NMR data of alkali-treated ^{13}C-labeled humins showed that an arene-rich structure is formed at the expense of the furanic network during alkaline pretreatment.

Based on: I. van Zandvoort,* E. J. Koers,* P. C. A. Bruijnincx, M. Baldus, B. M. Weckhuysen, "Structural Characterization of ^{13}C-Enriched Humins and Alkali-treated ^{13}C Humins by 2D Solid-state NMR" *submitted for publication. *Both authors contributed equally to this work.*

4.1. Introduction

Humins are carbonaceous, polymeric by-products that are almost inevitably formed during acid-catalyzed, hydrothermal processing of sugars to bio-based platform molecules, such as hydroxymethylfurfural (HMF) and levulinic acid (LA).[1–3] Under such conditions, C_6-sugars, such as glucose and fructose, are first dehydrated to form HMF, which in turn can be readily rehydrated to form LA and formic acid. The humins form as a result of uncontrolled cross-polymerization reactions of HMF and other reaction intermediates. Up to 30 wt% of the carbohydrate feedstock can end up in these humin by-products, which severely limits the efficiency and, as a result, economic viability of the biorefinery operation.[3] To increase the economic potential of such biorefineries, the formation of humins should either be limited and/or value-added outlets should be found for any humins that are formed. In addition to serving as a source for heat and power or to direct application in functional materials,[4] such valorization can be achieved by further conversion by gasification,[3,5] pyrolysis,[6] or chemo-catalytic routes to value-add chemicals or fuel components. Any attempt at humin valorization is hampered, however, by fact that still little is known about the chemical structure and properties of these humins, as well as by the general insolubility of these materials.[7] Indeed, more insight is needed in the molecular structure and their mechanism of formation. The various suggestions made for the molecular structure of humins are discussed below.[5,6,8–10]

Much of the current knowledge about the humin molecular structure is derived from studies of the molecular structure of hydrothermal carbon (HTC). The chemical and physical properties of HTC are much better studied, but conflicting structures are still found in literature.[11,12] HTC is also formed by hydrothermal treatment of sugars, but under non-acidic conditions, and are thought to be structurally somewhat similar to humins. For example, ^{13}C solid-state NMR studies by Baccile *et al.*[11] of HTC obtained from combinations of unlabeled glucose, $^{13}C_1$- and $^{13}C_6$-labeled glucose provided much insight in their molecular structure. A single-pulse ^{13}C spectrum showed the HTC molecular structure to be complex with 13% of the carbon being part of C=O groups, 64% found in sp^2 C=C (of which 29% furan C_α, 29% furan C_β and 6% arene sheets) and 23% in aliphatic groups, as determined by integration of the spectrum. The 1:1 ratio observed for the signals assigned to the C_α and C_β atoms of an oxygenated or oxygen-containing aromatic ring was a first indication that the aromatic rings are furan-based rather than arene-based in nature. A refocused, Insensitive Nuclei Enhanced by Polarization Transfer (INEPT) experiment was used to study through-bond ^1H-^{13}C interactions, while Cross Polarization (CP) and Inversion Recovery Cross Polarization (IRCP) measurements provided information on ^1H-^{13}C through-space interactions of the aromatic and aliphatic carbons in the HTC, respectively. Insight in the ^{13}C-^{13}C connectivity of the various HTC constituents was obtained from a Double-Quantum Single-Quantum (DQSQ) experiment. Taken together, these NMR techniques revealed a furanic network in HTC, in which the furan rings are mainly linked through the α-position by a methylene group. Minor linkages included direct

bonds between furan rings via the C_α or C_β carbons. The DQSQ spectrum furthermore suggested LA molecules to be physically embedded in the polymer, which was confirmed by a ^{13}C-^{13}C proton-driven magnetization exchange experiment without CP.[11]

In another example of the detailed information that advanced solid-state NMR studies can bring on complex organic structures, Schmidt-Rohr *et al.*[13] reported on spectrally-edited 2D ^{13}C solid-state NMR data for the characterization of glucose-derived and ^{13}C-enriched carbon materials, obtained by pyrolysis and by carbonization with fuming sulfuric acid. Dipolar-dephased DQSQ measurements allowed them to selectively study cross peaks between non-protonated carbon atoms. In addition, Exchange with Protonated and Non-protonated Spectral Editing (EXPANSE)[13] data provided information on the interactions between protonated and non-pronated carbon atoms, which allowed the authors to distinguish, for example, between signals from substituted furans and phenols. An advantage of both techniques is the absence of a diagonal ridge, which often obscures various expected cross peaks in carbonaceous samples. It should be noted, that even though the materials reported by Baccile and Schmidt-Rohr are probably much more condensed than the humins studied here, the characteristic signals detected and identified for substituted furans, phenols, arenes, and polycyclic aromatic structures could be very relevant for humin structure elucidation.[11,13,14]

Only a few reports describe the structural characterization of actual humins rather than HTC materials. Zarubin *et al.,* for instance, investigated humins formed during acid-catalyzed dehydration of different carbohydrates and HMF. Based on IR and pyrolysis-GC-MS analysis of the solids, it was concluded that the humins consist of about 60% furan rings and 20% aliphatic linkers. The authors suggested that humins are formed via a poly-condensation pathway leading to a network of furan rings linked by ether or acetal bonds.[10] Lund *et al.* studied the molecular structure of HMF-derived humins by IR spectroscopy and proposed that the humins were formed by aldol condensations of HMF with 2,5-dioxo-6-hydroxy-hexanal (DHH), which is formed by rehydration of HMF. This leads to a conjugated network of C=C and furanic rings with several aldehydes, ketones and aromatic alcohols as functional groups.[8] A comparison of the IR spectra of HMF-glucose-, fructose- and cellobiose-derived humins suggested that the humins could not be formed directly from the sugars.[9] Recently, Seshan *et al.*[15] presented a molecular structure of humins where furanic rings are connected via ethylene and methyl linkers with ketone functionalities. This structure was based on 1D ^{13}C solid-state NMR, IR and pyrolysis data.[15]

In Chapter 2, a multi-technique, multi-process parameter approach was reported that provided new insights into the formation and molecular properties of humin by-products formed from various carbohydrate feeds. A combination of IR, 1D ^{13}C solid-state NMR and pyrolysis-GC-MS measurements revealed a furan-rich structure containing several oxygen functionalities, in which the furan rings are connected directly or via aliphatic linkages. Based on this data a model for the molecular structure of glucose- and

xylose-derived humins was proposed. Direct, conclusive evidence for the nature and connectivity of, in particular, the aromatic constituents of the humins was, however, difficult to obtain. Indeed, the 1D ^{13}C solid-state NMR spectra did not allow unambiguous identification of the moieties giving rise to the broad signal intensity in the aromatic region. Furanic and phenolic aromatic groups could, for instance, both be formed under the conditions that lead to humin formation[16] and would give very similar signal patterns around the same chemical shifts.[13,17] In contrast, 2D solid-state NMR studies could provide the resolution and information needed to distinguish between such a furanic or phenolic motifs and thus help to improve and strengthen the proposed model for the molecular structure of humins.[11,13]

Similar insight is needed into any changes that occur in the structure of humins upon further valorization. Such changes were previously noted in thermochemical conversion processes, such as gasification or pyrolysis. Seshan *et al.*, for instance, showed with CP MAS ^{13}C solid-state NMR studies that aromatic rings are formed in the humin when gasified at 700 °C. A more detailed description of the remaining char could not be given, however.[5] The hydrothermal, alkaline solubilization method for reactive solubilization of humins, that is described in Chapter 3, also changes the molecular structure of the humins considerably. IR, elemental analysis, 1D solid-state NMR and pyrolysis-GC-MS data indicate further aromatization of the structure, among other changes. More information was needed, nonetheless, to propose a model for the molecular structure of the alkali-treated humin. Also here, advanced 2D solid-state NMR studies could further our understanding of the reactions and structural changes during the alkaline pretreatment.

This chapter describes the structural characterization of humin by-products obtained from $^{13}C_6$-D-glucose by employing various 1D and 2D solid-state NMR methods. A combination of DE and CP 1D ^{13}C NMR, ^{1}H-^{13}C heteronuclear correlation (HETCOR) and CP and DE DQSQ ^{13}C solid-state NMR experiments allowed us to refine the molecular structure of the humin by-products. The results provided new insight into the type and connectivity of the aromatic structures and improved our understanding of the chemical changes that occur during the alkaline pretreatment.

4.2. Results and Discussion

4.2.1. ^{13}C-labeled Humin Synthesis and IR Characterization

A ^{13}C-labeled glucose-derived humin sample was prepared by heating 25 mL of an aqueous solution of 1 M $^{13}C_6$-D-glucose and 0.01 M H_2SO_4 to 180 °C for 7 h. The humins were subjected to a Soxhlet extraction with water to remove any starting material, HMF or LA. The ATR-IR spectra of the labeled humins were found to be in good agreement with the humin samples reported in Chapter 2 (Figure 4.1), with vibrations being shifted to lower wavenumber as a result of the change in reduced mass caused by the ^{13}C labels.

These shifts actually help to improve the peak assignments made in literature and Chapter 2.[8,9] The vibration at 1700 cm^{-1} was originally assigned to the C=O stretch from acids, aldehydes, and/or ketones. In the spectrum of ^{13}C-labeled humin this band has shifted to 1640 cm^{-1}. This shift of 60 cm^{-1} indicates that this vibration is strongly influenced by coupling with a labeled carbon-carbon bond and that the C=O bond is part of an enone functional group, *i.e.* conjugated with a C=C double bond. Broadening of this band also confirms that multiple C=O functional groups are present in different chemical environments. The peak ascribed to the C=C stretch from a furanic ring shifted from 1605 cm^{-1} to 1546 cm^{-1}, confirming its assignment. The peaks at 1292 and 1202 cm^{-1} shift to 1265 and 1179 cm^{-1}, respectively. These smaller shifts of ~20 cm^{-1} show that these peaks are, as expected, caused by C-O stretch vibrations. The C-H bending modes at 1020 cm^{-1} show only a shift to 1010 cm^{-1}, which indicates only a small contribution of the carbon atom to this vibration. The peaks below 1000 cm^{-1} have hardly shifted at all, suggesting they belong to C-H out of plane deformations of aromatic rings. [18]

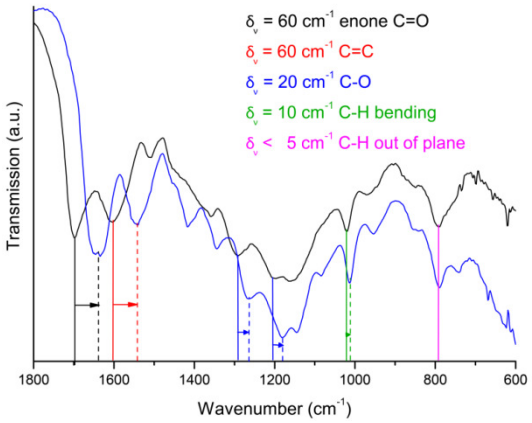

Figure 4.1. ATR-IR spectra of unlabeled humins (black) and ^{13}C-labeled humins (blue).

4.2.2. NMR Analysis of ^{13}C-labeled Humins

1D ^{13}C solid-state NMR spectra of the ^{13}C-labeled humin sample were recorded by DE and by CP via ^{1}H. The spectra are shown in Figure 4.2 and peak assignments can be found in Table 4.1.[11,13,19] The spectrum can be divided into three main regions, covering the aliphatic carbons between δ = 0-90 ppm, C=C bonds and aromatic compounds from δ = 90 ppm to δ =160 ppm, and C=O signals between δ = 160 ppm and δ = 220 ppm. Due to the large chemical shift anisotropy of aromatic rings and carbonyl groups, spinning sidebands are observed that overlap with the spectrum at δ = 70 and 177 ppm.

In the DE spectrum, the highest signal intensity for the aliphatic carbons is observed at δ = 38 ppm, indicating that most aliphatic carbons are tertiary or quaternary, or could be located next to a C=O group. From the limited signal intensity in the region δ = 60-90 ppm, it can also be seen that the humin structure contains only limited amounts of

alcohols and ethers and that the amount of residual sugar is negligible. A typical pattern for oxygen-containing aromatics, such as (substituted) furanics and phenolics, is observed in the aromatic region. Protonated C_α and C_β atoms of furanic rings are typically observed at δ = 140 ppm and δ = 110 ppm (see Figure 4.3 for the labeling scheme), respectively, while (C-)substituted C_α and C_β signals should give rise to signals around δ = 150 ppm and δ = 120 ppm, respectively. For phenol rings, C_α appears around δ = 150 ppm, while C_β is observed at δ = 100-120 ppm depending on the substitution pattern. The similarity in signal position complicates distinguishing furanic from phenolic components in the humins based on 1D ^{13}C NMR spectra alone. A first indication is nonetheless offered by the intensity ratio of the signals from C_α and C_β being roughly 1:1, which points at the presence of furan rings rather than phenolics, for which a 1:2 ratio would be expected.[13,17] The peak at 177 ppm could be assigned to acids and esters, but a spinning sideband is also found at around this position. Finally, the signal at δ = 207 ppm can be ascribed to aldehydes and/or ketones, two functional groups that again cannot be readily distinguished in these DE 1D spectra.

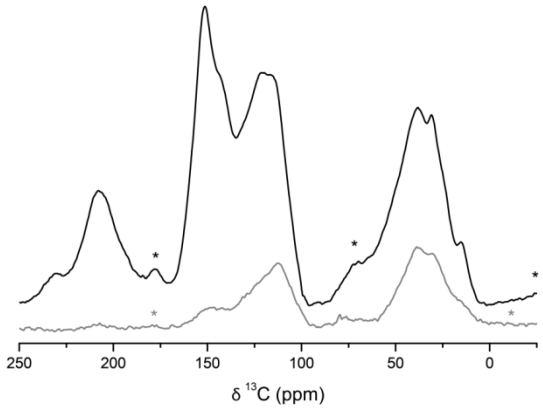

Figure 4.2. 1D ^{13}C solid-state NMR spectra of ^{13}C-labeled humins obtained by DE (black) and CP via ^{1}H (grey). Spinning sidebands are indicated by *.

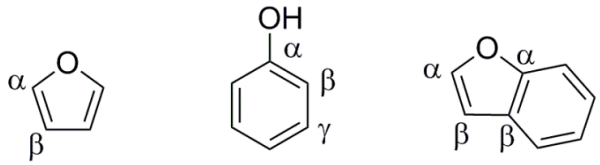

Figure 4.3. Labeling schemes for furan, phenol and benzofuran moieties.

The 1D DE spectrum of the ^{13}C-labeled humin is similar to the solid-state NMR spectra reported for HTC[11] and the 2D PASS NMR spectra of unlabeled, glucose-derived humins shown in Chapter 2. Small differences can, nonetheless, be observed between the DE and 2D PASS spectra of labeled and unlabeled humins, respectively. The first shows a higher signal intensity in the aliphatic region and for the C=O signal (δ = 207 ppm), while the peak from acids and esters is obscured by a spinning sideband (note that the 2D PASS

spectrum is free of spinning sidebands). Furthermore, a lower intensity in the C-O region was observed as well as a small downfield shift of the peaks at δ = 112 and 142 ppm in aromatic region compared to the 2D PASS NMR spectrum. Another clear difference is the absence of conjugated aromatic carbon around δ = 130 ppm in the DE spectra. These differences could be caused the 2D PASS spectrum being recorded after CP excitation, which is known to underestimate the amount of non-protonated carbons and methyl groups.[20] Differences in sample preparation scale of the labeled and unlabeled humins, might also influence the structures somewhat. The heating and cooling rates of the small autoclave used to prepare the ^{13}C-enriched humins, are faster than those of the 1 L autoclave that was used for the larger scale preparation of the. This leads to longer residence times for the latter, which can result in further dehydration of the humin structure and a relatively more arene-rich structure.

Table 4.1. Peak assignments for the 1D ^{13}C NMR spectra of ^{13}C-labeled humins.

δ (ppm)	Functional group	Chemical formula	Protonated [a]
207	Ketone	C=O	no
151	C_α phenol or linked furan	C=C-OH or C=C-O	no
142	C_α free furan	C=CH-O	yes
129	Conjugated C=C	C-C=C-C	no
121	C_β phenol or furan linked	C=C-OH or C-C=C-O	no
116	C_β phenol or furan protonated	HC=C-OH or C-HC=C-O	yes
78	Alcohol, ether, aliphatic	C-OH, C-O-C	yes
39	Aliphatic	tert. C-H, quart. C	yes
31	Aliphatic	sec. -CH_2-	yes
15	Aliphatic	prim. -CH_3	yes

[a] Based on comparison between DE and CP MAS NMR spectra shown in Figure 4.2.

The 1D CP MAS NMR spectrum was recorded with a contact time of 400 µs. This way, magnetization of the carbon atoms by polarization transfer is only efficient for protonated carbons, which therefore dominate the spectrum (Figure 4.2). As expected, the CP MAS ^{13}C solid-state NMR spectrum had a much lower intensity than the one obtained by DE and showed strong peaks at δ = 30 and 38 ppm from aliphatic carbons. In the aromatic region, a pronounced peak at δ = 112 ppm from protonated C_β is observed together with a much weaker signal at δ = 145 ppm, which is ascribed to C_α atoms. The fact that the signal at δ = 145 ppm is much weaker, indicates that a very limited, yet distinct amount of the C_α atoms are actually protonated, as was previously observed for HTC.[11] As such unsubstituted, *i.e.* protonated, C_α atoms cannot be present in phenolic structures but can occur in furanic rings, these results already point at the furanic nature of the humins (Figure 4.3). Notable absences of intensity in the CP spectrum also provide

additional information. The absence of a signal at δ = 207 ppm, for instance, shows that the carbonyl carbon is non-protonated and thus belongs to a ketone group.

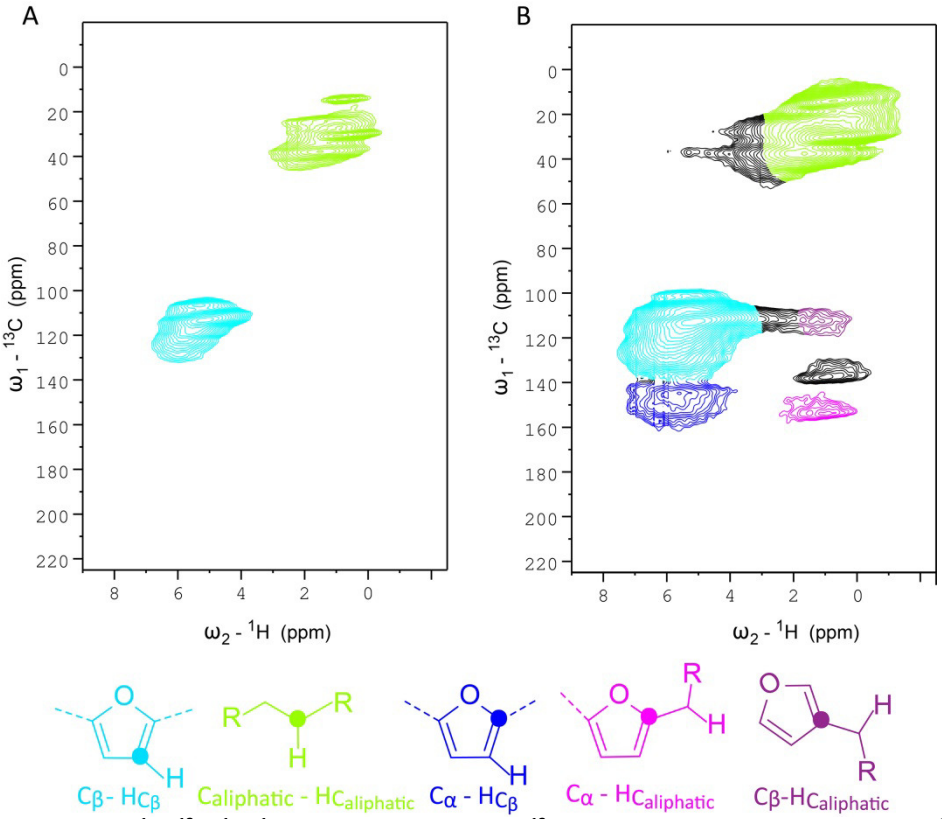

Figure 4.4.A. (^{1}H)-^{13}C-(^{1}H)-^{1}H correlation spectrum of ^{13}C-labeled humins recorded with 900 (1st CP) and 50 µs (2nd CP) contact time and 5 ms ^{1}H-^{1}H mixing time (MIRROR) showing short range correlations. B (^{1}H)-^{13}C-^{1}H correlation spectrum of ^{13}C-labeled humins with a contact time of 2500 µs (both CPs) showing long-range correlations.

A HETCOR (^{1}H)-^{13}C-(^{1}H)-^{1}H spectrum of ^{13}C-labeled humins was recorded with a short contact time of 50 µs to study short-range ^{13}C-^{1}H correlations (Figure 4.4A). Very few interactions between ^{13}C and ^{1}H nuclei were observed, again indicating that most carbon atoms are not protonated. The correlations seen between δ ^{1}H = 0-4 ppm/δ ^{13}C = 0-50 ppm and δ ^{1}H = 5-7.5 ppm/ δ ^{13}C = 110-140 confirm that mainly the aliphatic carbons and furanic C_{β}'s are protonated. Furthermore, the absence of a C-H correlation peak for the carbonyl groups (at δ ^{13}C = 207 ppm) corroborates the assignment of this signal to ketones. The humins differ in this sense from the HTC samples studied by Baccile *et al.*, who could identify aldehydes based by a HETCOR experiment with a longer contact time of 500 µs.[11]

Long-range ^{1}H-^{13}C correlations were studied with a longer contact time of 2500 µs (Figure 4.4B). In addition to the strong signals from directly connected ^{1}H-^{13}C groups in the aliphatic and aromatic region, long-range interactions between C_α (δ ^{13}C = 150 ppm) and aliphatic protons were also detected. These interactions are also observed for C_β, which shows that the aliphatic groups located close to the aromatic rings. A cross peak between C_α and protons connected to C_β was observed as well. At lower contour levels a weak cross peak indicates that the acids and ketone groups are located closer to the aliphatic groups than to the aromatic rings (not shown in this spectrum).

A CP-DQSQ of the ^{13}C humins was recorded to get insight in the connectivity between carbon atoms in the different structural motifs (Figure 4.5). A CP time of 600 µs was chosen to find a balance between the spectrum being dominated by signals from protonated carbons, and allowing sufficient sensitivity. It should be thus kept in mind that the spectrum does not exclusively consists of protonated carbon signals; indeed, the CP mixing time used was longer than for the 1D CP MAS spectrum.

In the aromatic region of the CP-DQSQ spectrum, a typical pattern of interaction between C_α and C_β carbons was observed; such a pattern can, in principle, be assigned both to furanic and phenolic rings, as noted before for HTC[11] and acid-treated glucose.[13] Nonetheless, the clear correlation seen between the C_β atoms (see Figure 4.5 for the structures), is most probably the result of interactions in a furanic ring and is very unlikely in phenolic structures.[13] Furthermore, a weak, yet distinct signal can be seen for an interaction between C_α carbons and aliphatic carbons, which is again not possible in phenolic rings in which the C_α is by definition substituted with the OH-group. In addition, the C_β-C_γ cross peaks expected for phenolic rings, expected at C_β δ =110-120 ppm and Cγ δ = 130-140 ppm, are not observed. These observations provide further evidence for the furanic nature of the humins.

The broad peak from the aliphatic carbons at δ = 0-60 ppm shows several ^{13}C-^{13}C correlations between the aliphatic carbon atoms. These peaks also show some correlation with the aliphatic carbons that are connected to C_α. Furthermore, the (weak) signals around δ = 175 ppm indicate the presence of aliphatic carboxylic acids. Baccile *et al.*[11] also observed these signals and ascribed them to physically embedded LA. Given that our samples are purified by extensive Soxhlet extraction, any residual, physically occluded LA should have been removed during purification, suggesting that the detected, probably LA-derived, carboxylic acids are actually chemically bound to the humin structure. The CP-DQSQ also shows a correlation between aliphatic carbons and a C-O group, which might be caused by alcohols but could also be from ether or acetal bonds. These two possibilities cannot be distinguished, however, based on the current data. The presence of ether or acetal bonds would partially explain the reactive solubilization and reduction in molecular weight of the humins after alkaline pretreatment, though, as discussed in Chapter 3. Be it alcohols, ethers or acetals, these bonds are only present in small amounts given the (very weak) signal intensity in the δ = 60-90 ppm region in the DE 1D ^{13}C solid-state NMR

spectrum. A very weak correlation between C_β (δ = 115 ppm) and aliphatic C (δ = 30 ppm) was finally observed indicating that linking via C_β occurs to a very limited extent (not highlighted in Figure 4.5). The correlations seen by Baccile *et al.*[11] between C=O and the furan rings, indicating aldehyde and acid functional groups on the furanic ring, were not observed in our spectrum.

It should be kept in mind that the mixing time chosen for the CP DQSQ measurement strongly influences to which extent protonated and non-protonated carbons are probed; indeed, the relatively short mixing time used for the spectrum depicted in Figure 4.5 ensured that mainly protonated carbons were observed. Certain linkages that might be present in the molecular structure of the humins involving non-protonated carbons, such as C_β-C_β linkages between furanic rings, other structural motifs, such as benzofuran and polycyclic aromatic sheets, and oxygen functionalities on aromatic rings are not expected to appear in the spectrum depicted in Figure 4.5 or are at least underestimated. To study if such features are actually present, a second DQSQ was recorded with DE of the ^{13}C atoms (Figure 4.6). This DQSQ spectrum after DE of ^{13}C is similar to the CP one, with the distinction that several interactions between non-protonated carbons are now indeed much more pronounced. In addition, signals from protonated carbons are weaker or not observed at all, indicating that these are present only to a minor extent in the molecular structure. Correlations between $C_{C\text{-}O}$-$C_{aliphatic}$ and C_β-$C_{aliphatic}$ were not observed, for example. Clear signals from C_α-C_β and C_β-C_β correlations were seen. Taken together with the observed links between C_α and $C_{aliphatic}$ discussed previously, this proves that humins are indeed mainly composed of furanic rings and that aliphatic groups are the main linkers. Comparison with the 1D spectra shows that several C_β's are substituted and therefore probably cross-linked as suggested by Baccile *et al.*.[11] To further confirm this, future efforts should include dipolar-dephased DQSQ measurements of the humins.[13] In addition, C_α-C_α interactions are observed around δ = 140-145 ppm,[13] indicating that direct, inter-furanic linkage between C_α's does occur, a possibility that furans offer but phenolics not. Finally, stronger signals from the functional groups acid and ketone functional groups are observed and both show a clear correlation with the aliphatic carbons. However, these aliphatic chains show little correlation with the aliphatic linkers that connect the furanic rings. This indicates that the acids and ketones are not located on these aliphatic linkers and could be caused by chemical incorporation of LA or intermediates from sugar dehydration and HMF rehydration.

The model for the molecular structure of humins proposed in Chapter 2, which was based on elemental analysis, IR, 1D (2D PASS) ^{13}C solid-state NMR and pyrolysis-GC-MS data did already include short aliphatic linkers between the furanic rings. The C_α-C_α and C-O-C linkages that have now been identified in the 2D NMR spectra were not included, however, as the 1D NMR spectra did not offer this insight. The CP-DQSQ spectrum furthermore suggests some linkages to involve C_β as well, as does the peak at δ = 120 ppm in the 1D DE NMR spectrum, which indicates that some of the C_β is not

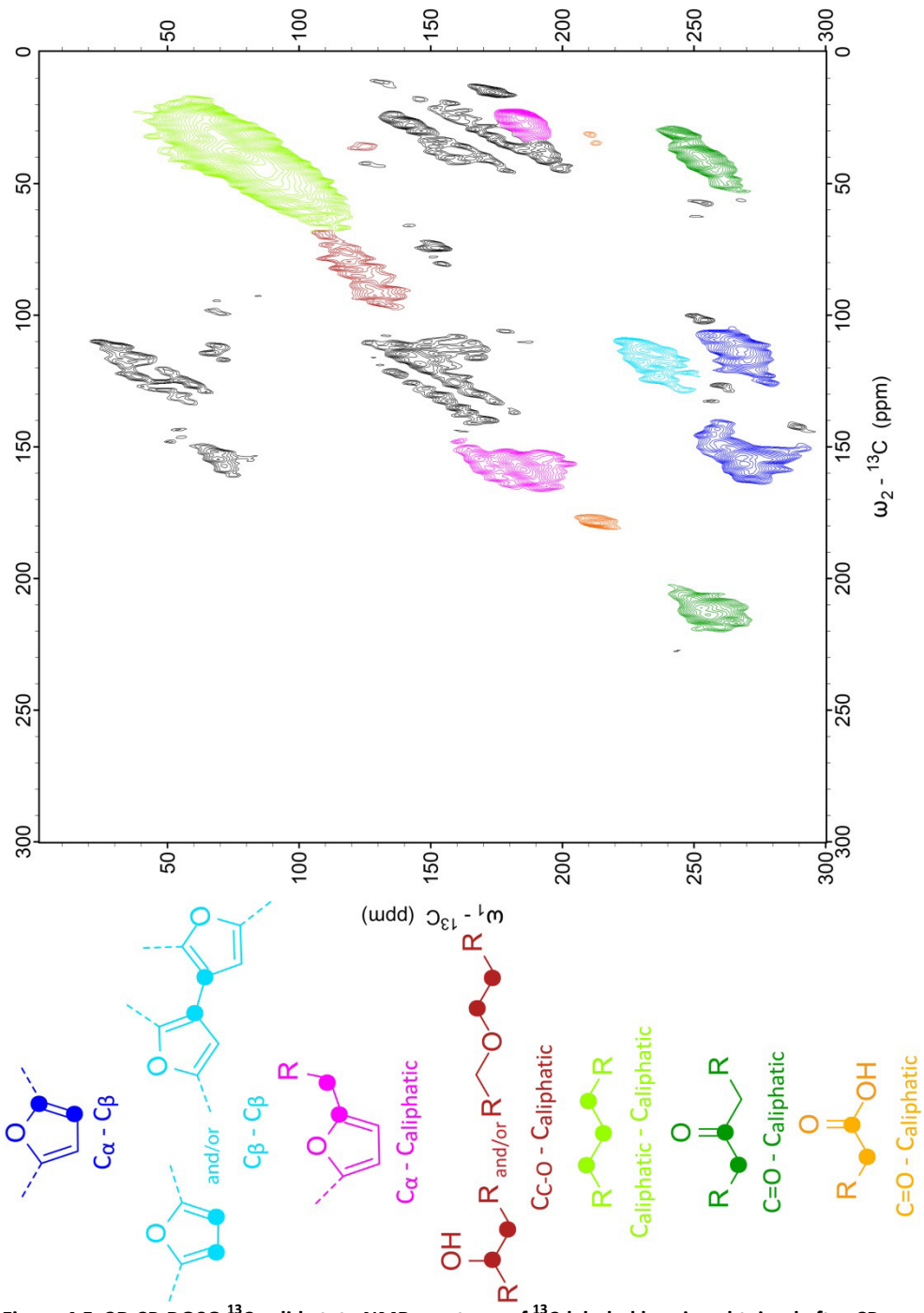

Figure 4.5. 2D CP-DQSQ ^{13}C solid-state NMR spectrum of ^{13}C-labeled humins obtained after CP.

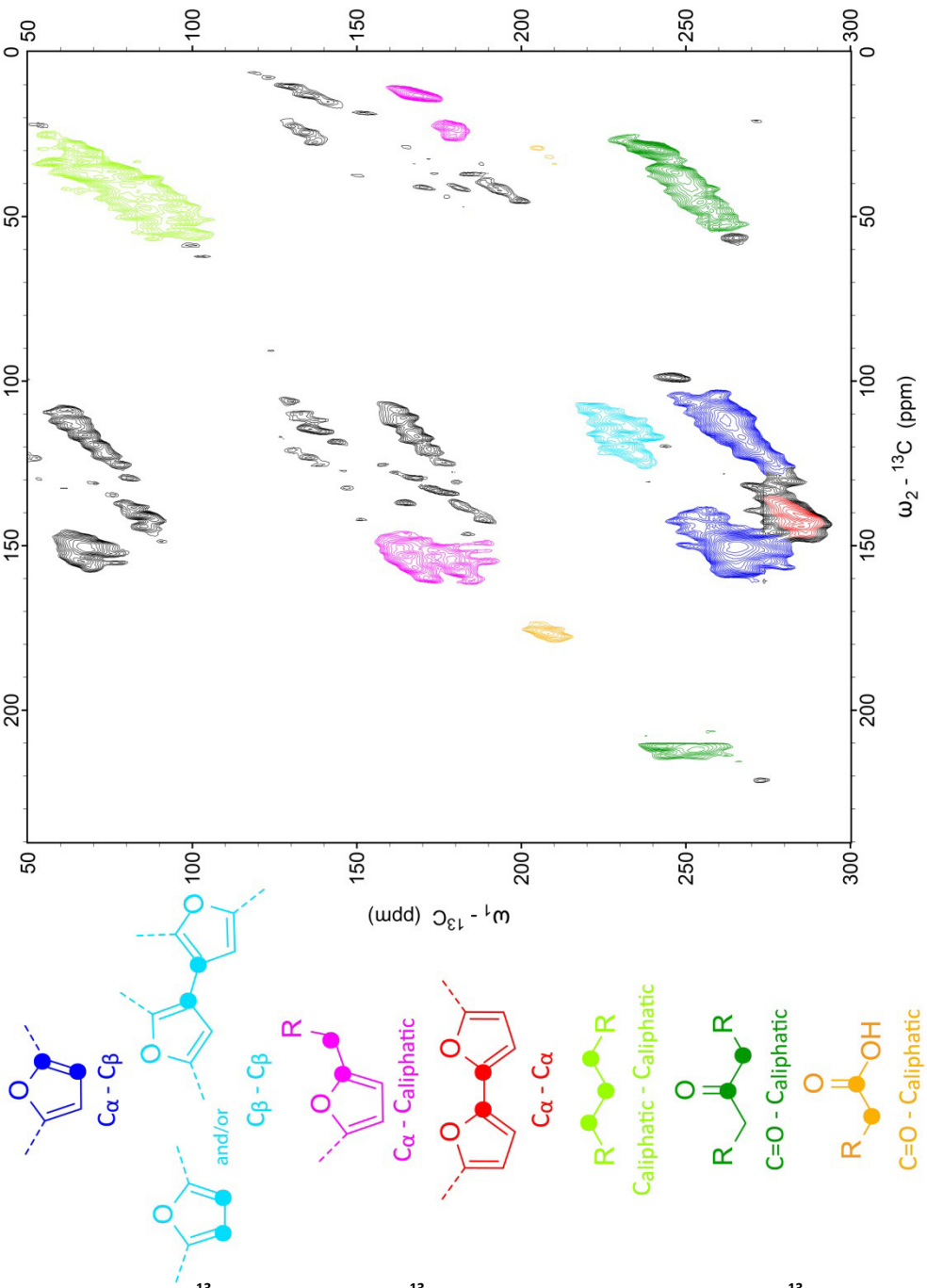

Figure 4.6. 2D DQSQ ^{13}C solid-state NMR of ^{13}C-labeled humins obtained after DE of ^{13}C.

protonated. While clear signals from C_β-C_β correlations are also observed in the 2D spectra, it is still difficult to distinguish between correlations within one furan ring and between furan rings; direct linkages between the C_β's of two furan rings could not be excluded nor proven therefore. Based on this information, a refined model of the molecular structure of glucose-derived humins is proposed (Figure 4.7), taking into account the overall elemental composition as reported in Chapter 2.

Some observations can be made with regards to previous proposals for the molecular structure of humins. Zarubin *et al.* proposed a furanic network where the furan rings were connected by C-O-C bonds.[10] The CP-DQSQ spectrum suggests that some acetal or, alternatively, ether linkages are present in very limited amounts in our humins. Instead, the main linkages observed in our 2D ^{13}C spectra are C_α-C_α and $C_{aliphatic}$-C_α.

Lund *et al.*,[8,9] proposed an aldol condensation mechanism for humin formation where HMF reacts with its rehydration product 2,5-dioxo-6-hydroxyhexanal, but the correlations expected for the C=C bonds of the conjugated enones formed are not observed in our DQSQ NMR spectra. Finally, both the Zarubin and Lund models do not account for the aliphatic C-C correlations that were observed in our DQSQ NMR spectra. It should be noted though, that experimental conditions for the formation of these humins differ somewhat from our procedure.

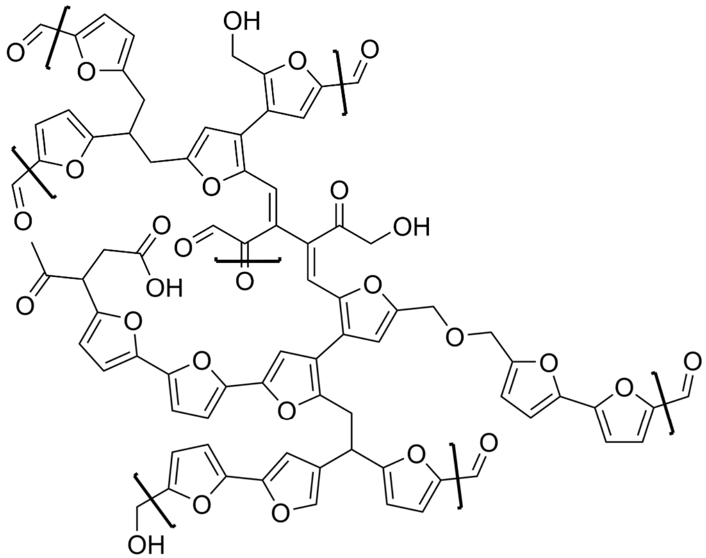

Figure 4.7. Revised model for the molecular structure of glucose-derived humins.

The model proposed by Seshan *et al.*[15] was based on humins that were prepared under the same conditions as described in this work. Their model, which was mainly based on 1D solid-state NMR, shows some important differences compared to the structure shown in Figure 4.7. Our 2D NMR spectra, for instance, show that the ketone groups are

not directly connected to the furanic rings and that most linkages are direct C_α-C_α linkages or are longer than a single methylene group.[15] This demonstrates that 2D NMR spectra give valuable information about the specific linkages in the molecular structure of humins.

The NMR data can also be compared to the two conflicting molecular structures that are found in literature for HTC. On the one hand, an arene-rich, polycyclic aromatic structure has been proposed for HTC from glucose and starch prepared at temperatures of 170-240 °C. This structure proposal was based on XPS, elemental analysis, IR and Raman data.[12] No indications for the presence of polyaromatic sheets in the molecular structure of humins could be seen in our spectra, however. The other structure proposed for HTC from glucose involves a furan-rich network, in which the furan moieties are connected by methylene groups.[11] While our spectra also strongly suggest a furanic motif, the proposed HTC structure would not give rise to the correlations seen between the aliphatic carbons that are present in our DQSQ spectra. Other sugar-derived materials, such as the acid-treated glucose-derived carbon reported by Schmidt-Rohr *et al.,* is also furan-rich, yet much more acidic than our humins. In this case, the acid functional groups are directly connected to the aromatic rings instead of on the aliphatic chains as observed for our humins.[13] This comparison shows that humins formed during the acid-catalyzed dehydration of glucose are similar to, yet distinct from HTC and acid-treated glucose, as different linkages and functional groups are observed.

4.2.3. NMR Analysis of Alkali-treated ^{13}C-labeled Humin

The ^{13}C-labeled humins were treated in 2 M NaOH at 240 °C for 3 h, after which the humins were completely dissolved and a dark brown solution was obtained (Chapter 3). The pH of the solution was decreased to 1 with 6 M sulfuric acid to precipitate the humins from solution. Humins were isolated by filtration, washed extensively with water and dried under vacuum. The obtained alkali-treated, ^{13}C-labeled humins were analyzed by 1D and 2D ^{13}C solid-state NMR.

A comparison of the DE 1D ^{13}C NMR spectra of alkali-treated humins (Figure 4.8, Table 4.2) and the parent humin clearly shows that the molecular structure of humins significantly changed upon alkaline pretreatment. The largest differences are observed in the aromatic region where strong signals from conjugated systems can now be seen around δ = 130 ppm, indicating further aromatization by transformation of the furanic rings into arenes or polyaromatic structures. Less pronounced differences were observed in the aliphatic region (δ = 0-50 ppm) where the overall intensity decreased while the signal from methyl groups at δ = 19 ppm increased. All intensity between δ = 60-90 ppm is lost, indicating that all C-O bonds were hydrolyzed during alkaline treatment, as discussed in Chapter 3. A signal from substituted C_α was still observed at δ = 151 ppm, but no signals for C_β could be distinguished in the 1D spectrum. The latter might due to be overlap with the broad peak at δ = 130 ppm. The decrease in oxygen content of the material, as noted by the elemental analysis data reported in Chapter 3, is reflected in the decrease of the

signal from ketone groups, together with a slight shift downfield to δ = 210 ppm, with suggests that the carbonyls are on average less conjugated.[13] The aromatic region of the 1D spectrum of alkali-treated humins are most similar to the Total suppression Of Spinning Sidebands (CP TOSS) spectra reported by Schmidt-Rohr *et al.* of the sulfuric-acid treated carbon material that was formed by pyrolysis at 350 °C,[13,14] with the exception that these carbons show a much higher signal for carboxylic acid groups.

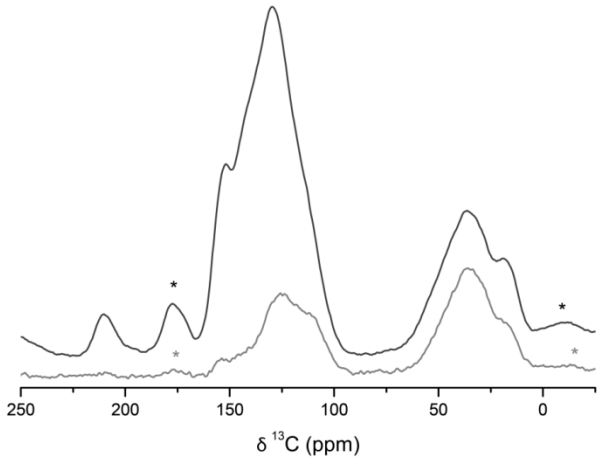

Figure 4.8. 1D ^{13}C NMR spectra of ^{13}C-labeled alkali-treated humins obtained by DE (black) and CP via ^{1}H (grey). Spinning sidebands are indicated by *.

Table 4.2. Assignment of peaks in the 1D ^{13}C NMR spectra of ^{13}C-labeled alkali-treated humins.

δ (ppm)	Functional group	Chemical formula	Protonated[a]
210	Ketone	C=O	no
177	Acid	COOH	no
153	α carbon phenol or linked furan	C=C-OH or C=C-O	no
130	Conjugated C=C	C-C=C-C	no
125	Conjugated C=C	C=HC=C	yes
112	β carbon phenol or furan protonated	HC=C-OH or C-HC=C-O	yes
36	Aliphatic	quart. C, tert. C-H, sec. -CH_2-,	yes
18	Aliphatic	prim. -CH_3	yes

[a] Based on comparison between DE and CP MAS NMR spectra in Figure 4.8.

The CP spectrum (400 µs contact time) again showed a much lower intensity, in particular in the aromatic region, than the DE spectrum. This shows that that the aliphatic carbons are mainly protonated while the aromatic carbons are not. The shoulder peak at δ = 111 ppm suggests the presence of protonated C_β, while the signals at δ = 125 and 153 ppm point at two more protonated aromatic carbons. The former can be attributed to

protonated carbons in polycyclic aromatic systems, but assignment of the latter is more difficult. Furanic groups seem unlikely, as the chemical shift is too high for a protonated C_α; pyrone-like structures might give rise to such a signal, as suggested in Chapter 3.[21]

The CP-DQSQ (600 µs contact time, Figure 4.9) spectrum of the alkali-treated humins also shows clear changes in the aromatic region compared to the parent humin. Some C_α-C_β correlations were still present, but cross peaks from C_β-C_β correlations were not observed any more. While this could mean that phenolic structures have been formed, C_β-C_γ correlations expected for phenol were nonetheless not found due to overlap with a new feature in the 2D spectrum, which is observed around δ = 125-145 ppm and can be attributed to the formation of aromatic conjugated structures.

As the 1D CP ^{13}C solid-state NMR showed that the alkali-treated humin does not contain many protonated carbon atoms, a DE DQSQ spectrum was recorded to study the structure in more detail (Figure 4.10). Again, a correlation between C_α and C_β was observed, but neither aliphatic linkages on the C_α nor C_β-C_β interactions, which would indicate the presence of furans, were present. If benzofuran would have formed upon alkaline treatment, as suggested in Chapter 3, a C_β-C_β cross peak would be expected around δ = 110 ppm and δ = 130 ppm.[22] This signal and C_β-C_γ cross peak from phenol, which is expected around the same chemical shift, were not observed in the DQSQ spectra. Formation of such species cannot be excluded, however, as such signals could be overlapped with the strong signals from arenes and fused rings. A strong peak at the diagonal around 130 ppm, reported to indicate the presence of graphene-like polycyclic aromatic sheets, was absent.[13,14] The spectrum thus suggests that the changes in molecular structure upon alkaline treatment involve further condensation of the humins to an arene-rich structure with some (benzo)furan or phenol rings.

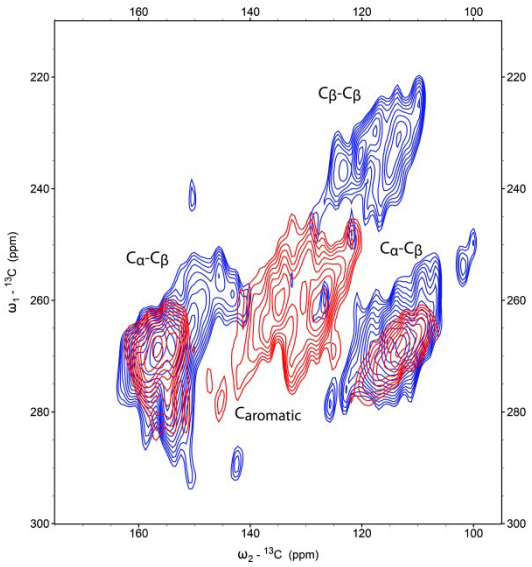

Figure 4.9. Aromatic region of the 2D CP-DQSQ spectra of 13C-labeled humins (blue) and alkali-treated humins (red).

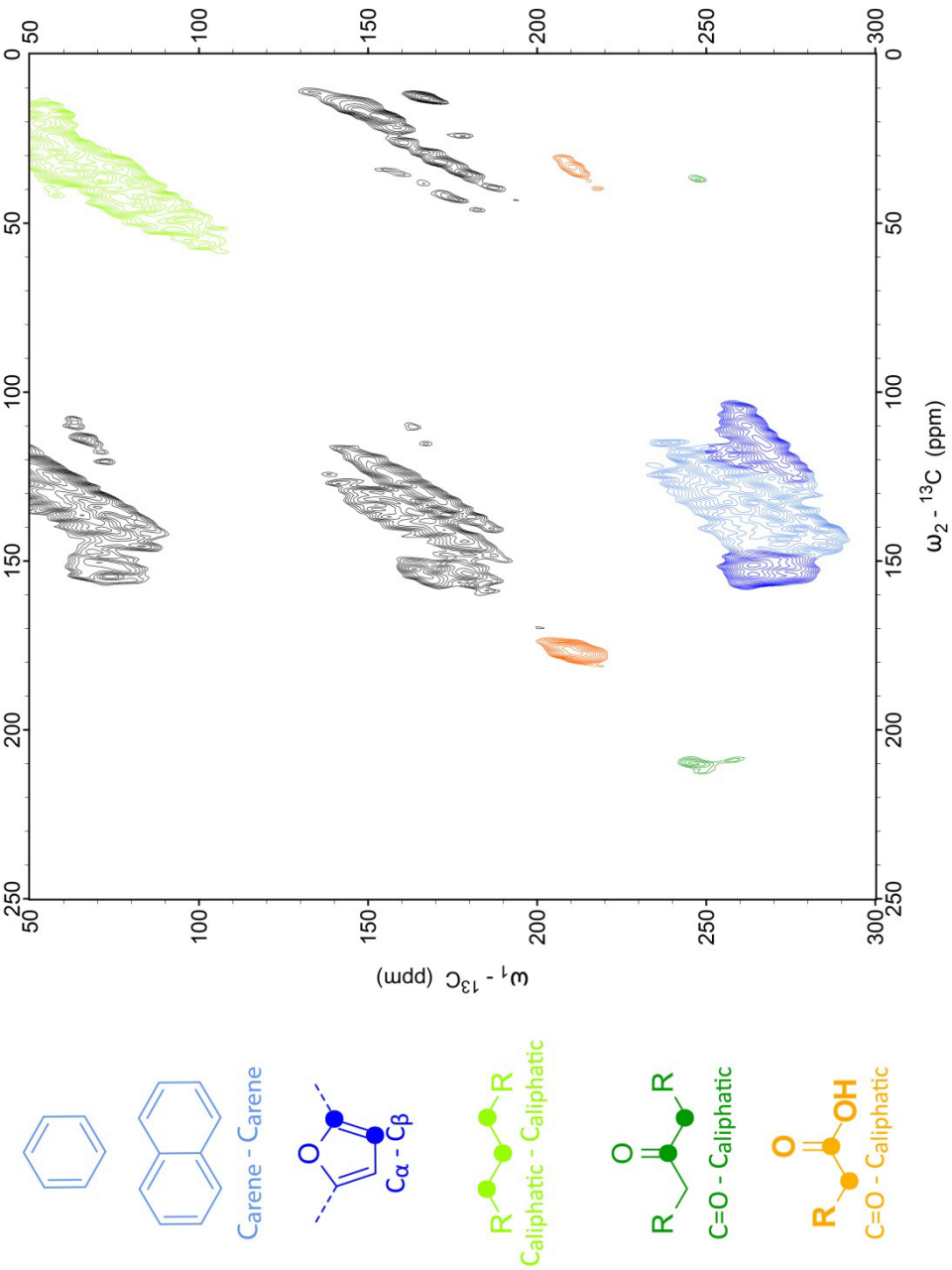

Figure 4.10. 2D DQSQ ^{13}C solid-state NMR of alkali-treated, ^{13}C-labeled humins obtained after DE of ^{13}C.

Correlations between aromatic and aliphatic groups are not observed, indicating that the aliphatic groups are located further from the aromatic ring rather than forming the linkages between the rings as in the untreated humins. Furthermore, in comparison with the parent humin more acidic groups are detected and less ketones. Correlations between the signals from the aliphatic groups and acid and ketones shows that the oxygen functional groups are located on the aliphatic groups, this in contrast to the acid-treated carbon materials reported by Schmidt-Rohr *et al*.[13,14] Even though these signals are very similar to the pattern ascribed to physically embedded LA by Baccile *et al.,*[11] occluded LA cannot be present after alkaline treatment, providing further evidence that LA is in fact chemically bonded or that other short aliphatic branches with ketone and acid functionalities are present. Based on the NMR spectra and the elemental composition presented in Chapter 3, a model for the molecular structure of alkali-treated humin is presented in Figure 4.11.

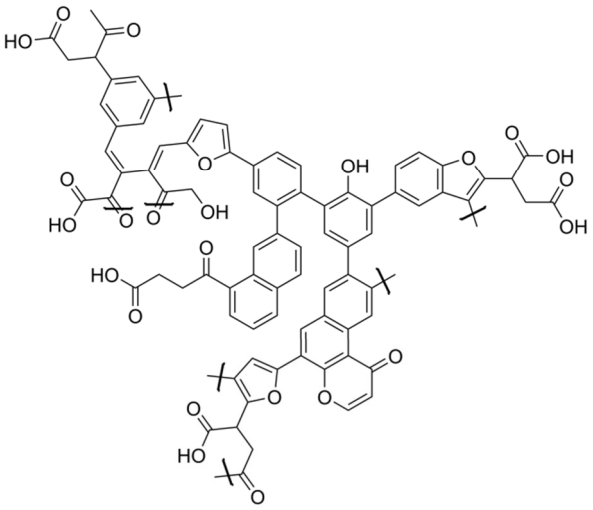

Figure 4.11. Model proposed for the molecular structure of alkali-treated, glucose-derived humins.

4.3. Conclusions

The 1D and 2D solid-state NMR spectra of ^{13}C-labeled humins provided further insight into the molecular structure of these highly complex and structurally heterogeneous materials and, most importantly, confirmed the furanic nature of these biorefinery by-products. Various different linkages could be identified in the 2D NMR spectra, ranging from the most abundant C_α-$C_{aliphatic}$ and C_α-C_α linkages to minor ones such as C_β-C_β and C_β-$C_{aliphatic}$ cross-links. C-C correlations between the aliphatic carbons indicated that the linkers are not simply methylene groups, but rather are short aliphatic chains. The spectrum furthermore indicated that some LA, which is formed during acid-catalyzed conversion of

sugars, is included in the molecular structure through covalent bonds. These results allowed us to refine the molecular structure previously proposed for humins in Chapter 2.

Upon alkaline treatment of the humins, an arene-rich structure is formed at the expense of the furan content. A large increase in carboxylic acids was furthermore observed, which could in part explain the increased solubility of humins at alkaline conditions. It was also shown that the aliphatic and aromatic carbons are located far from each other, while C=O functional groups are located on the aliphatic carbon atoms. Taken together, these observations allowed a molecular structure to be proposed also for the alkali-treated humins.

Insight in the molecular structure of humins, with or without reactive solubilization, can contribute to the development of routes for their chemical valorization. Indeed, an analogy can be made here with the advanced NMR studies that have contributed much to the progress made in the structure elucidation of lignin, which is also a recalcitrant material from biomass with a complex, aromatic structure. These extensive characterization efforts have led to increased understanding of the molecular structure including the linkages within lignin, structural differences between lignins and changes in the structure upon (catalytic) conversion. For humins, comparable analytical strategies can be developed to further elucidate the molecular structure and its changes upon chemical treatment, which will aid the development of humin valorization processes.

4.4. Experimental Section

4.4.1. Preparation of Humins

Humins were prepared by heating 25 mL of an aqueous solution of 1 M D-glucose or $^{13}C_6$ D-glucose (99%, Buchem) and 0.01 M H_2SO_4 in an unstirred Teflon-lined autoclave vessel at 180 °C for 7 h in an oven. Humins were isolated by filtration, wash with water and dried at RT. The humins were submitted to a 24 h Soxhlet extraction with water and dried at 70 °C under vacuum (Chapter 2). For alkaline pretreatment 0.5 g humin was treated with 80 mL 0.5 M NaOH for 3 h in an unstirred Teflon-lined autoclave vessel in an oven at 240 °C. The humins were precipitated by decreasing the pH to 1 using 6 M H_2SO_4, isolated by filtration, washed with excess water and dried at 70 °C under vacuum (Chapter 3). IR spectra were recorded on a Tensor 37 IR spectrometer using a diamond ATR crystal. For each spectrum 32 scans with a resolution of 4 cm^{-1} were averaged. The elemental composition of the humins was 59.6 %C, 3.8%H and 36.6 %O as determined with an automated Euro EA3000 CHNS. Oxygen content was calculated by difference.

4.4.2. NMR Analysis

DE spectra were recorded with a 5 µs 90 ° pulse and 14 kHz MAS (alkali-treated humin) or 8 KHz (humin) (3.2 mm rotor) using a Bruker 9.4 T spectrometer. Processing: window function EM with 100 Hz line broadening. The ^{13}C CP MAS was recorded with a 50 kHz field

on ^{13}C and a CP contact time of 400 µs and 14 kHz MAS (3.2 mm rotor) using a 9.4 T spectrometer. Processing: window function EM with 100 Hz line broadening. The ^{1}H spectrum was recorded with a 3 µs 90 ° pulse and 60 kHz MAS (1.3 mm rotor) using a 18.8 T spectrometer.

(^{1}H)-^{13}C-(^{1}H)-^{1}H heteronuclear correlation spectrum (HETCOR with ^{1}H-^{1}H mixing step) was recorded with 60 kHz spinning (1.3 mm rotor) using a 18.8 T spectrometer. CP contact times were 0.9 ms and 0.05 ms for the 1st and 2nd CP. After these CP's a 5 ms dipolar recoupling element (MIRROR[23]) was used enabling 1H-1H magnetization transfer. PISSARRO[24]decoupling: 165 kHz during t1 and 16 kHz during t2. Number of TD points (acquisition time) are: 356 (9.0 ms), 400 (4 ms) for direct and indirect dimension, respectively. For signal averaging, 32 scans were used. For both dimensions, 1k zero filling has been used. A sine-squared window function with a sine bell shift of 3 was applied to the spectrum.

(^{1}H)-^{13}C-^{1}H heteronuclear correlation (HETCOR) spectrum was recorded with 60 kHz spinning (1.3 mm rotor) using an 18.8 T Bruker spectrometer. CP contact times were 2.5 ms and 2.5 ms for the 1st and 2nd C, respectively. PISSARRO decoupling: 165 kHz during t_1 and 16 kHz during t_2. Number of TD points (acquisition time) are: 268 (9.0 ms), 250 (2.5 ms) for direct and indirect dimension, respectively. For signal averaging, 16 scans were used. For both dimensions, 1k zero filling has been used. A sine-squared window function with a sine bell shift of 3 was applied to the spectrum.

Double quantum-single quantum experiments were done at 10 kHz MAS (3.2 mm rotor) with a 9.4 T spectrometer. CP contact time: 600 µs, excitation-reconversion (2 ms) was done with the SPC5 sequence[25]. Heteronuclear decoupling during t_1 (CW),t_2 (SPINAL64[26]): 83 kHz and during excitation-reconversion: 120 kHz. Number of TD points (acquisition time) are: 768 (7.7 ms), 120 (1.5 ms) for direct and indirect dimension, respectively. For signal averaging, 128 scans were used. For both dimensions, 1k zero filling has been used. A sine-squared window function with a sine bell shift of 3 was applied to the spectrum.

Experimental conditions for the DE DQSQ were similar to the DQSQ (with CP). Recycle delay: 15 s, excitation-reconversion time: 2 ms. Number of TD points (acquisition time) are: 768 (7.7 ms), 120 (1.5 ms) for direct and indirect dimension, respectively. For signal averaging, 128 scans were used. For both dimensions, 1k zero filling has been used. A sine-squared window function with a sine bell shift of 3 was applied to the spectrum.

4.5. Acknowledgements

Dr. Eline Koers and Prof. dr. Marc Baldus from Utrecht University are thanked for performing the solid-state NMR measurements and their contributions to the chapter. Dr. Peter de Peinder from VibSpec is thanked for help with the interpretation of the ATR-IR spectra.

4.6. References

[1] J. Horvat, B. Klaić, B. Metelko, V. Šunjić, *Tetrahedron Lett.* **1985**, *26*, 2111–2114.
[2] D. M. Alonso, J. Q. Bond, J. A. Dumesic, *Green Chem.* **2010**, *12*, 1493–1513.
[3] D. J. Hayes, J. Ross, M. H. B. Hayes, S. W. Fitzpatrick, in *Biorefineries - Industrial Processes and Products* (Eds.: B. Kamm, P.R. Gruber, M. Kamm), Wiley, **2006**, 139–164.
[4] J. M. Pin, N. Guigo, A. Mija, L. Vincent, N. Sbirrazzuoli, J. C. van der Waal, E. de Jong, *ACS Sustainable Chem. Eng.* **2014**, *2*, 2182–2190.
[5] T. M. C. Hoang, L. Lefferts, K. Seshan, *ChemSusChem* **2013**, *6*, 1651–1658.
[6] C. B. Rasrendra, M. Windt, Y. Wang, S. Adisasmito, I. G. B. N. Makertihartha, E. R. H. van Eck, D. Meier, H. J. Heeres, *J. Anal. Appl. Pyrolysis* **2013**, *104*, 299–307.
[7] E. Bartels, Über Die Bildung von Huminstoffen Aus Ketosen Durch Einwirkung Konzentrierter Halogenwasserstoffsäuren, PhD Thesis, Hamburg University, **1966**.
[8] S. K. R. Patil, C. R. F. Lund, *Energy Fuels* **2011**, *25*, 4745–4755.
[9] S. K. R. Patil, J. Heltzel, C. R. F. Lund, *Energy Fuels* **2012**, *26*, 5281–5293.
[10] I. V. Sumerskii, S. M. Krutov, M. Y. Zarubin, *Russ. J. Appl. Chem.* **2010**, *83*, 320–327.
[11] N. Baccile, G. Laurent, F. Babonneau, F. Fayon, M. M. Titirici, M. Antonietti, *J. Phys. Chem. C* **2009**, *113*, 9644–9654.
[12] M. Sevilla, A. B. Fuertes, *Chem. Eur. J.* **2009**, *15*, 4195–4203.
[13] R. L. Johnson, J. M. Anderson, B. H. Shanks, X. Fang, M. Hong, K. Schmidt-Rohr, *J. Magn. Reson.* **2013**, *234*, 112–124.
[14] J. M. Anderson, R. L. Johnson, K. Schmidt-Rohr, B. H. Shanks, *Carbon* **2014**, *74*, 333–345.
[15] T. M. C. Hoang, E. R. H. van Eck, W. P. Bula, J. G. E. Gardeniers, L. Lefferts, K. Seshan, *Green Chem.* **2014**, DOI 10.1039/C4GC01324G.
[16] G. C. A. Luijkx, F. van Rantwijk, H. van Bekkum, *Carbohydr. Res.* **1993**, *242*, 131–139.
[17] M. Gomes, A. Gandini, *J. Polym. Sci. A Polym. Chem.* **2011**, *49*, 3759–3768.
[18] W. Hübner, H. H. Mantsch, *Biophys. J.* **1991**, *59*, 1261–1272.
[19] C. Burket, R. Rajagopalan, a Marencic, K. Dronvajjala, H. Foley, *Carbon* **2006**, *44*, 2957–2963.
[20] W. Kolodziejski, J. Klinowski, *Chem. Rev.* **2002**, *102*, 613–628.
[21] D. Hobuß, S. Laschat, A. Baro, *Synlett* **2005**, 123–124.
[22] T. Okuyama, T. Fueno, *Bull. Chem. Soc. Jpn.* **1974**, *47*, 1263–1266.
[23] I. Scholz, M. Huber, T. Manolikas, B. H. Meier, M. Ernst, *Chem. Phys. Lett.* **2008**, *460*, 278–283.
[24] M. Weingarth, P. Tekely, G. Bodenhausen, *Chem. Phys. Lett.* **2008**, *466*, 247–251.
[25] M. Hohwy, C. M. Rienstra, C. P. Jaroniec, R. G. Griffin, *J. Chem. Phys.* **1999**, *110*, 7983–7992.
[26] B. Fung, A. Khitrin, K. Ermolaev, *J. Magn. Reson.* **2000**, *142*, 97–101.

CHAPTER 5

Aqueous Phase Reforming of Solubilized Glucose-derived Humins over Supported Pt Catalysts

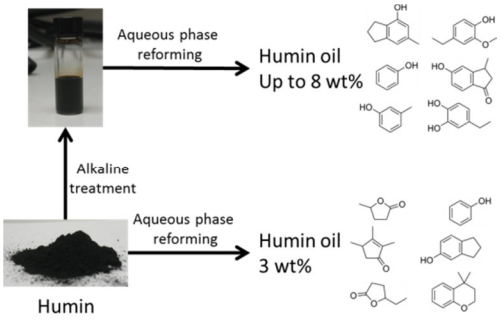

Abstract

The catalytic valorization of the humin by-products that are formed in biorefinery operations during acid-catalyzed conversion of sugar-containing feeds to value-added chemicals or fuel components, would make such biorefineries more economically viable. Here, we report the first study of the aqueous phase reforming (APR) of humin by-products to produce aromatic monomers and hydrogen using different Pt-based heterogeneous catalysts. Glucose-derived humins were solubilized by alkaline treatment prior to the APR reaction and subsequently subjected to APR at 225-250 °C at pH 9-11 for 20 h in a batch autoclave. Catalyst performance, arranged by gas and oil yields, increased in the order Pt/Al_2O_3 < Pt/TiO_2 < $Pt\text{-}Re/ZrO_2$. H_2, CO_2 and CH_4 were identified as the main components of the gas phase and up to 8 wt% of humin-oil was obtained. GCxGC-MS analysis showed the humin-oil to mainly contain phenolics and aromatic ketones with aliphatic carboxylic acids and paraffins being identified as minor products. When insoluble humins, *i.e.* without prior alkaline pretreatment, were used directly in an APR reaction under otherwise identical conditions, only 3 wt% of oil was formed, while gas yields were comparable to those observed for the alkali-treated humins. In this case, the oil contained more furanone-like structures and less phenolics. The products formed for both types of humin correlate with the differences in molecular structure, with the alkaline pretreatment changing a furan-based structure into one that is more arene-based in nature.

5.1. Introduction

Depletion of fossil fuel resources and an increased greenhouse effect has driven the development of so-called biorefineries. In such operations, biomass is converted to fuels and chemicals via several thermochemical and/or catalytic processes, analogous to oil refineries.[1] While ideally the entire biomass intake is converted to valuable end-products, current biorefining technologies have not yet reached such maturity. Indeed, no efficient conversion routes exist yet for all of the primary components of (lignocellulosic) biomass, nor for some of the by-products formed during the valorization processes. This loss of carbon in the form of waste limits the economic viability of biorefineries. As a consequence, waste generation should be avoided and processes that can valorize waste streams should be developed. As most biorefinery schemes focus on conversion of the carbohydrate fraction of lignocellulosic biomass to fuels and chemicals, lignin is of course the prime example of a primary component that is not yet valorized to its full potential, being currently simply burned for its energy value. Here the difficulty lies with the recalcitrant, highly heterogeneous, complex nature of lignin, while the potential of this component is directly related to this complex structure being very aromatic in nature and thus an interesting bio-based source of benzene derivatives.[2]

The carbohydrate valorization processes themselves can also produce waste, in particular in the form of a second recalcitrant, highly heterogeneous polymeric by-product called humins. For example, acid-catalyzed conversion processes of carbohydrates to furfural (FF), hydroxymethylfurfural (HMF) or to levulinic acid (LA) are affected by uncontrolled cross-polymerization reactions between sugars, dehydration intermediates, FF/HMF and to a more limited extent LA, which unavoidably lead to the formation of humins.[3–5] These carbonaceous, structurally complex by-products can cause losses of up to 30 wt% of the sugar feed and the formation of this solid material poses considerable challenges in terms of reactor engineering.[3] Humin formation should therefore either be limited or outlets for this by-product need to be formed, for instance by direct application in materials, as exemplified by the recent successful implementation of humins in furfuryl alcohol resins,[6] or by depolymerization and further processing to chemicals and fuel components. First attempts for such humin valorization efforts have recently been reported and include gasification for the production of syngas[7] and pyrolysis.[8] In the latter approach part of the humin is converted into a (complex) humin-oil, with volatiles such as furfural and 2,5-dimethylfuran and small amounts of phenol and benzofuran being detected in these first attempts.[8]

The possibilities for humin valorization by depolymerization are still largely unexplored, though, and given some of the similarities that this waste stream shares with lignin, it is of interest to explore whether any of the lignin depolymerization strategies can be translated to humins. Indeed, many different approaches for lignin valorization, being reductive, oxidative and/or redox-neutral in nature, are currently being studied.[2,9,10] In one such example, our group has, for instance, studied the production of aromatic

monomers and hydrogen from different lignins by a hydrothermal treatment process called Aqueous Phase Reforming (APR)[11] and, in a later variation, Liquid Phase Reforming which makes use of water:ethanol systems.[12] Lignin APR, yielded (limited amounts of) lignin-oil, containing several aromatic monomers including phenols, anisoles and catechols, depending on the structure of the lignin. These aromatic monomers were formed by cleavage of some of the linkages present in lignin, with ether bonds such as the so-called β-O-4 linkage being readily cleaved, while more recalcitrant linkages involving stronger C-C bonds were not.[11]

APR was originally developed by Dumesic and coworkers[13] and is now a well-studied reaction, in particular for the production of hydrogen from sugars and alcohols. Indeed, the (sugar) alcohols sorbitol, xylitol, and glycerol have been extensively studied,[13,14] with the structural similarities between the latter and the aliphatic parts of lignin being the original inspiration for transferring this APR approach from sugar derivatives to lignin. In general, high hydrogen yields in APR require catalysts that promote C-C bond cleavage over C-O bond cleavage, as well as the required, subsequent water-gas shift reaction (WGS). C-O bond cleavage followed by hydrogenation should be avoided in order to suppress the formation of alkanes.[13] The influence of reaction parameters such as catalyst and composition of the reaction mixture on reforming activity have been extensively reviewed.[14] It was shown that Pt and Pd combine high reforming activity with high hydrogen selectivity. Ru and Rh, on the other hand, improve the selectivity towards alkanes by catalyzing the Fischer-Tropsch reaction.[14] Furthermore, several bimetallic and alloyed catalysts were developed, with a Sn-promoted Raney Ni catalyst showing excellent activity, for instance.[15] The use of a Pt-Re alloy improved the stability of the supported metal particles, but the ReOx species present on the surface also increased the acidity of the catalyst. As a result, C-O bond cleavage was found to be enhanced leading to a higher activity and increased alkane selectivity. C-C bond cleavage was by some authors reported to increase as well.[16–18]

In addition to the choice of (bi)metal, the choice of support evidently also strongly influences catalyst performance in APR. γ-Alumina is often used, but has been shown to be only limitedly stable in water due to dissolution and its hydration to boehmite.[19,20] This phase transformation leads to a decrease in surface acidity and area. The same study also indicated sintering of the metal particles during hydrothermal treatment of Pt/Al_2O_3.[20] Several more water-stable catalysts were tested and it was found that acidic catalysts increase the selectivity towards alkanes while neutral and basic supports favor reactions that lead to the production of hydrogen. For example, the hydroxyl groups in TiO_2 are believed to improve the WGS reaction leading to H_2 but also catalyze C-O bond cleavage.[21] APR selectivities furthermore strongly depend on the pH of the reaction mixture.[14] Addition of KOH during the APR of glycerol, for instance, improved conversion and hydrogen selectivity by suppressing acid-catalyzed hydration reactions.[18] Similarly, the addition of NaOH had a positive effect on the APR of ethylene

glycol over Ni supported on carbon nanofibers resulting in increased hydrogen selectivity and catalyst stability.[22]

APR strategies comparable to those applied for (sugar) alcohols and lignin could also assist the valorization of humins. The complex, furan-rich structure (Chapter 2) of humins will pose additional catalytic challenges, though, compared to the simple (sugar) alcohols. The catalytic valorization of humins is furthermore hampered by their typical insolubility, in particular when heterogeneous catalysts are used. It was found, however, that the solubility of the humins can be improved by an alkaline pretreatment method as described in Chapter 3. This alkaline treatment is accompanied by strong changes in the molecular structure leading to an arene-rich structure functionalized with carboxylic acid groups (Chapter 3 and 4). These alkali-treated humins are soluble in alkaline water of pH > 7 and could thus be subjected to a typical APR treatment, similar to those described for lignin. The molecular structure of humins differs from lignin, though, in that C-C bonds rather than C-O bonds form the main linkages in both humins and alkali-treated humins (Chapter 2-4).[23–25] Suitable catalysts should therefore be able to cleave the (non-oxygenated) C-C bonds in the humin structure to allow for the production of aromatic monomers by APR. Here, we describe a first study of the APR of solubilized humins over a heterogeneous catalyst. Catalysts tested include a commercial 5% Pt/Al_2O_3 for benchmarking, a more water-stable catalyst 5% Pt/TiO_2 and a Pt-Re/ZrO_2 (1% Pt) catalyst to assess the effect of alloying. APR activity was assessed by the formation of gases during reforming as well as changes in the molecular weight. Residual humins were analyzed by IR, while the humin-oil was isolated by extraction and monomers therein characterized by GCxGC-MS.

5.2. Results and Discussion

5.2.1. Aqueous Phase Reforming of Humins

Glucose-derived humins, prepared under standardized conditions (see Chapter 2), were solubilized by the alkaline pretreatment described in Chapter 3. The reaction mixture was acidified with 6 M H_2SO_4 and the precipitated humins were isolated and washed with excess water. The obtained, alkali-soluble humins were redissolved in water after which the pH was adjusted to 9 with 1 M NaOH. These solubilized humins had an average molecular weight of 3000 g/mol and a carbon content of 20 g/L as determined by alkaline Gel Permeation Chromatography (GPC) (sodium-polystyrene sulfonates standard) and Total Organic Carbon analysis (TOC), respectively. Note that these values differ somewhat from those reported for the alkali-treated humins in Chapter 3, since 1) the alkaline pretreatment was done at a higher humin concentration, 2) any acid-soluble compounds are lost in the precipitation step and 3) the humins are redissolved in a different volume of water.

In a typical APR reaction, 20 g of humin solution (containing 0.55 g humin) with an initial pH of 9.2 and 0.1 g catalyst were stirred in a batch autoclave under argon for 20 h at 225 °C at autogenous pressure. After reaction, the reaction mixture was analyzed following the flow chart depicted in Figure 5.9. As gas formation was limited compared to the APR of sugar alcohols, a closed rather than semi-batch system was used to determine the extent of gas formation and gas phase composition. The total amount of gas formed is reported as the increase in pressure during the APR reaction. The gas phase was analyzed using GC-TCD and gas composition is reported as the relative amounts of H_2, CO_2 and CH_4. The liquid phase was analyzed to determine changes in pH and molecular weight. Any remaining humins were regenerated from solution to determine changes in their molecular structure and the oil yield was determined after extraction with $CHCl_3$.

At standard APR conditions (225 °C, 29 bar) for 20 h over a commercial Pt/Al_2O_3 only 4 bar of a mixture of H_2, CO_2 and CH_4 was formed during the reaction, which is only twice as much as observed in the blank reaction with dissolved humin but without catalyst (Table 5.1, Run 1 and 2). This shows that the reforming activity is limited at this fairly low temperature. The pH of the reaction mixture decreased from 9 to 8.3 during the blank reaction. With the catalyst a stronger decrease to pH 7.1 was observed, which could be caused by dissolution of formed CO_2 or by the formation of organic acids.

The amount of solids isolated by filtration of the liquid phase of the blank reaction, *i.e.* the char formed during reaction, was so little that their weight could not be determined. After APR at 225 °C, only 71 wt% of the original catalyst intake was recovered as solids. The loss of weight of the recovered spent catalyst, which should also contain any char formed, indicates degradation of the alumina during the reaction, which is known to increase at alkaline conditions.[26] In contrast to the result reported by Sievers *et al.*[20] for the Pt/Al_2O_3 subjected to hydrothermal treatment at standard APR conditions, the XRD patterns of the spent catalysts after APR did not show the typical signals from boehmite, which are expected around 2θ = 16.8, 32.9, 44.9, 57.5 and 57.9° (Figure 5.2). A similar behavior was previously reported for the liquid phase processing of organosolv lignin over Pt/Al_2O_3 in water:ethanol mixtures. Here, it was suggested that adsorption of lignin to the catalyst prevents the formation of boehmite.[27] A similar mechanism could take place in case of the APR of solubilized humins, but this should be studied in further detail. A remarkably sharp peak was observed in the XRD pattern of the spent catalyst around 2θ = 20° but could not be assigned. Further analysis of the isolated solids by thermogravimetric analysis (TGA) pointed at the formation of char giving a weight loss of 36% (Figure 5.3).

The filtered liquid phases, depicted in Figure 5.1, show no visual changes after the blank reaction or APR over Pt/Al_2O_3 at 225 °C, *i.e.* no change in color was observed. The liquid phase was analyzed by alkaline GPC and compared to the solution of humins before reaction. Note that the weight-average molecular weights (Mw) and polydispersities (PD) obtained by GPC provide us with relative rather than absolute changes, as the molecular weight of the parent humin is unknown due to its insolubility and proper standards for

humins are not available. A decrease in signal intensity was observed by GPC after reaction. As UV-detection (280 nm) was used for the GPC measurements, the drop in concentration of UV-absorbing species could, for example, be due to hydrogenation or precipitation of humins. In the chromatogram, a clear shift of the maximum compared to the original solubilized humins can still be observed though, and the extent of depolymerization, expressed as a decrease in Mw and PD, is similar after the blank reaction and reaction over Pt/Al_2O_3 at 225 °C. This, combined with the limited formation of solids, shows that the changes in Mw and PD observed under these conditions are indeed mainly the result of a thermal depolymerization reaction and is not caused by precipitation of the solid. Based on the results described in Chapter 3, in which a plateau in Mw is reached after alkaline hydrothermal for 16 h at 240 °C, it is a bit unexpected that further depolymerization was observed under the fairly similar, yet less basic APR conditions. This could be explained by the increased concentration of humins used during the alkaline pretreatment for APR leading to a less depolymerized humin. Residual humins could be recovered by acidification of the liquid phase, with 59 wt% and 41 wt% of the humins being regenerated for the blank reaction and APR over Pt/Al_2O_3, respectively. The remaining filtrate was extracted by $CHCl_3$ to give only 1 wt% and 2 wt% of humin-oil after the blank and APR reactions at 225 °C, respectively. Two factors contribute to the incomplete mass balance. First, the weight of the formed gases could not be determined. Second, several acid-soluble, non-extractable compounds might be present in aqueous phase and a minimal amount of solids might remain in the reactor, sticking to the stirrer and vessel.

The low hydrogen and monomers yields obtained by APR of the solubilized humins indicate that C-C bond cleavage activity is limited at 225 °C. The reaction temperature was therefore increased to 250 °C, now resulting in a pressure increase of 7 bar in the reaction vessel (Table 5.1, Run 3). The increased temperature led to a decreased H_2 yield, which is in line with trends reported for the APR of several sugars and alcohols at different temperatures.[13] The recovered solids accounted for 90 wt% of the original weight intake of catalyst, which points at increased char formation compared to the reaction at 225 °C. This was, however, not supported by TGA as a weight loss of 35% was observed (Figure 5.3). The GPC data show a further decrease in intensity and Mw upon increasing the reaction temperature to 250 °C, however this could be related to the increased char formation or increased hydrogenation of the humins, of which the latter is in line with the changes in the gas phase composition. (Table 5.1, Figure 5.4). A very small peak around at a retention time of 23.6 min is observed in the GPC chromatogram (Figure 5.4 insert). This peak is attributed to the presence of low molecular weight fragments with a Mw similar to the flow marker phenol. After acidification, 49 wt% of the humins was recovered and an oil yield of 4 wt% was obtained.

The low gas and oil yields obtained with Pt/Al_2O_3 could be related to the poor stability of Al_2O_3 in water due to dissolution of the alumina. A TiO_2-supported Pt catalyst

was therefore also tested, this support is known to be stable under hydrothermal conditions. A strong increase in gas yield was observed, with 12 bar of additional pressure being generated with a higher hydrogen yield compared to Pt/Al_2O_3 (Run 4). Upon filtration a large amount of char (at least 30 wt% of the humin intake) was isolated together with the catalyst and the reaction mixture had a light brown color. Surprisingly, GPC analysis did not indicate further reduction of Mw compared to the reaction over Pt/Al_2O_3 at 250 °C. This could be caused by the fact that the large molecules have a larger contribution to the calculated weight average molecular weight. If large humin molecules are cleaved or precipitate from solution the Mw will decrease rapidly and leads to a similar Mw value compared to the other reactions. After acidification, only a small amount of humins (12 wt%) was recovered and the oil yield was 5 wt%. These results point at an increased reforming reactivity by the use of a water stable support, even though monomer yields were not increased.

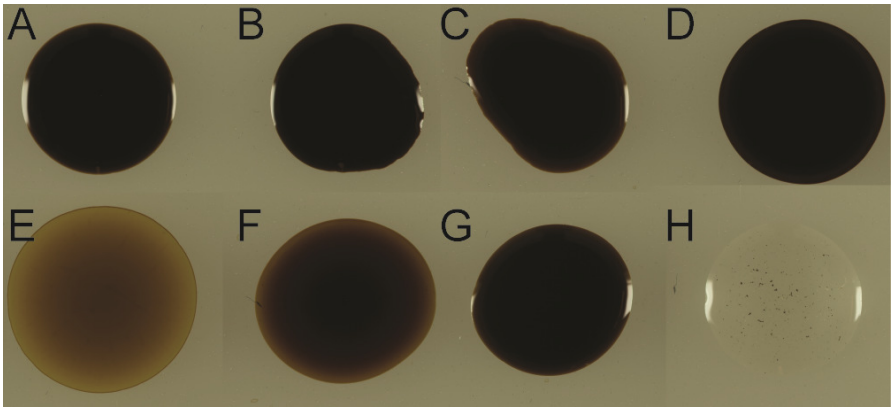

Figure 5.1. Droplets of solubilized humins (A.) and reaction mixtures after APR of solubilized humins: B. APR blank reaction at 225 °C, C. APR over Pt/Al_2O_3 at 225 °C, D. APR over Pt/Al_2O_3 at 250 °C, E. APR over Pt/TiO_2 at 250 °C, F. APR over Pt-Re/ZrO_2 at 250 °C, G. APR over Pt/TiO_2 at 250 °C pH 11 and H. APR of solid humin over Pt/TiO_2.

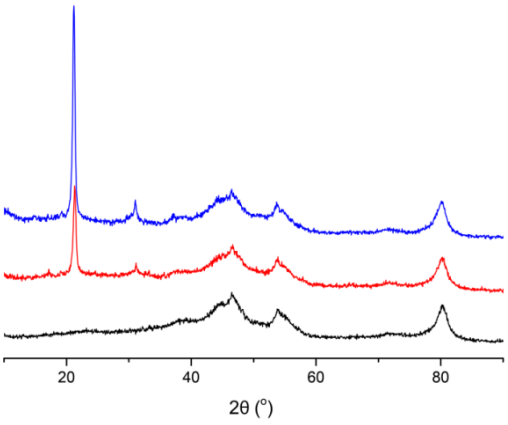

Figure 5.2. XRD patterns of Pt/Al_2O_3 (black) and the spent catalyst after APR of solubilized humins at 225 °C (red) and 250 °C (blue).

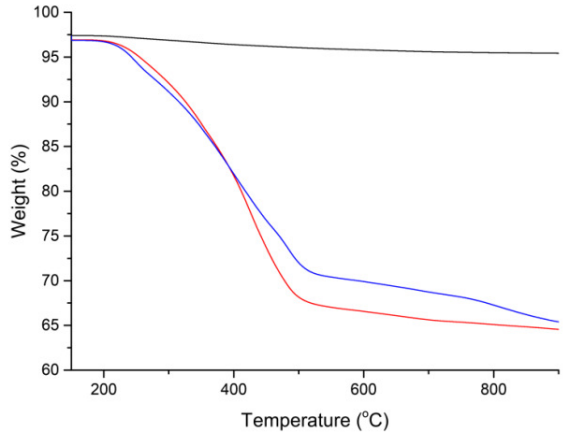

Figure 5.3. TGA of the fresh Pt/Al_2O_3 and the spent catalyst after APR of solubilized humins at 225 °C (red) and 250 °C (blue).

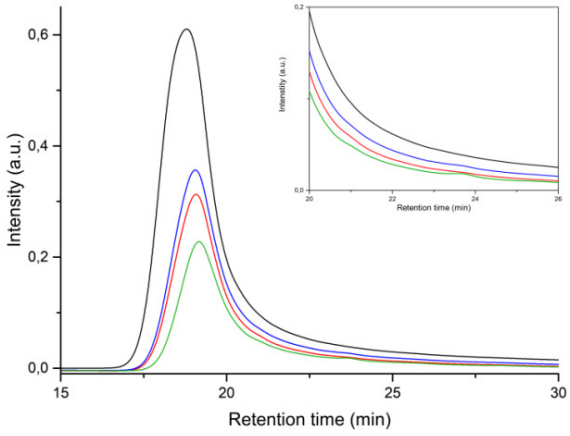

Figure 5.4. GPC chromatograms of solubilized humins (black), blank reaction (red), reaction over Pt/Al_2O_3 at 225 °C (blue) and 250 °C (green). The inset shows the small peak around 23.6 min pointing at the formation of monomers.

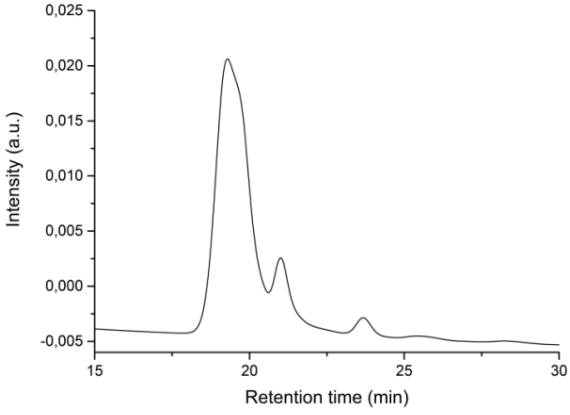

Figure 5.5. GPC chromatogram of the liquid phase after APR of solid humins over Pt/TiO_2.

Table 5.1. Reaction conditions, changes in pH, gas formation, gas phase composition, liquid phase analysis and recovered fractions after the APR of humins.

		Conditions [a]							Gas composition [b]			Liquid phase				Yield		
Run	Catalyst	T	pH	pH	Δ pH	P t_0	P t_{end}	ΔP	H_2	CH_4	CO_2	Mw [c]	Mw [d]	DP [c]	DP [d]	Solids [e]	Precipitate [f]	Humin-oil [g]
		°C	before	after		(bar)	(bar)	(bar)	(%)	(%)	(%)	g/mol	(%)		(%)	(wt%)	(wt%)	(wt%)
1	-	225	9.2	8.3	0.7	30	32.4	2.4	100	0	0	1850	62	4.4	81	-	59	1
2	Pt/Al_2O_3	225	9.2	7.1	1.9	30	34.8	4.8	49	26	25	1890	64	4.6	85	71	41	2
3	Pt/Al_2O_3	250	9.2	7.1	1.9	40.6	47.3	6.7	42	25	33	1429	48	3.9	73	90	49	4
4	Pt/TiO_2	250	9.2	7.5	1.5	41.1	53.1	12	55	23	22	1512	51	4.0	74	255 [h]	12	5
5	$Pt\text{-}Re/ZrO_2$	250	9.2	7.6	1.4	41.1	54.9	13.8	52	27	21	1560	50	4.3	77	66	50	8
6	Pt/TiO_2	250	11.0	8.6	2.4	41.0	47.3	6.3	56	38	16	1618	52	4.4	79	45	58	2
7	Pt/TiO_2 Solid humin	250	9.4	4.0	5.4	41.2	53.1	11.9	52	24	25	1132	-	1.4	-	72 [i]	-	3

[a] 20 h in a closed batch reactor. [b] Relative composition of the gas mixture collected over time. [c] Sodium-polystyrene sulfonates were used for calibration of the molecular weight. [d] Relative to the dissolved humins before reaction. [e] Solid isolated after the reaction, determined as wt% of added catalyst. [f] Precipitated humins after acidification with H_2SO_4, determined as wt% per 100 g dissolved humin based on TOC. [g] Oil extracted with $CHCl_3$, determined as wt% per 100 g dissolved humin based on TOC. [h] Extensive char formation was observed. [i] wt% of catalyst and solid humin intake.

The reaction with Pt/TiO_2 was also run at a pH of 11.0 instead of 9.2, to assess the effect of the drop in pH that was observed in all APR reactions (ΔpH 1.4-1.9). This drop might be caused by the formation of organic acids or by the dissolution of formed CO_2 in the aqueous phase and might decrease the solubility of the humins. The reaction run at pH 11 actually led to a lower gas yield of 6 bar with a relatively high yield of CH_4 and low yield of CO_2 (Run 6). The pH after reaction was 8.6, which is a larger drop than seen for the reactions run at lower pH. Although less char formation was observed compared to the reaction over Pt/TiO_2 at pH 9, an oil yield of only 2 wt% was found.

The $Pt\text{-}Re/ZrO_2$ catalyst gave the highest gas yield at 250 °C (14 bar, Run 5), producing a reaction mixture of lighter color. It should be noted that the Pt loading of this catalyst was only 1% compared to 5% for the Pt/Al_2O_3 and Pt/TiO_2 catalysts. For this reaction the Mw after APR is again similar to those found after APR at 250 °C over Pt/Al_2O_3 and Pt/TiO_2. After acidification, 58 wt% of the humins was regenerated and the highest oil yield of 8 wt% was obtained.

Taken together, the APR of solubilized humins over supported Pt/Al_2O_3 shows that actual depolymerization of the humins is mainly a thermal effect at 225 °C. When the reaction temperature is increased higher gas and oil yields are obtained, with a related increase in CO_2 yield. The oil yields are still limited, though, and more complete valorization of the humins would require a larger increase in temperature. The catalyst support was varied to further optimize the reaction and Pt/TiO_2 gave better gas yields than Pt/Al_2O_3, albeit with concomitant extensive char formation. The Pt-Re alloy on ZrO_2 showed the highest catalytic activity, which could be related to the increased C-C and C-O bond cleavage reported for this type of catalysts. When these results are compared to APR of lignin, comparable oil yields are obtained. Furthermore, much smaller amounts of solids are formed from the solubilized humins, with the Pt/TiO_2 run at pH 9.2 being the exception.[11]

For comparison, the APR reaction was also performed with untreated, solid humin over Pt/TiO_2 at 250 °C. Here, a high gas yield of 14 bar was obtained, which is comparable to the yield obtained with solubilized humins (Run 7). The reaction mixture was clear and almost colorless with 72 wt% the solid humins and catalyst intake found at the bottom of the autoclave which points at some reactivity of the untreated, insoluble humins. The GPC chromatogram indicates the presence of some oligomers and low molecular weight products in the liquid phase (Figure 5.5). The amount of precipitate upon acidification of the liquid phase was negligible; this was not unexpected as the pH of the reaction mixture was already as low as 4 and the amount of oligomers in the solution was fairly low. Extraction of the liquid phase yielded 3 wt% oil. The gas and oil yields after APR of solid humins over Pt/TiO_2 are very similar to those obtained after APR of solubilized humins at the same conditions.

5.2.2. Changes in the Molecular Structure of Humins after APR

ATR-IR spectra of the regenerated humins after APR over Pt/Al_2O_3 were recorded and compared to alkali-treated humins in Figure 5.6; the assignment of the spectrum of alkali-soluble humins can be found in Chapter 3. The first thing to notice is that the molecular structure of the humins hardly changes during the blank reaction, meaning that except for those bonds that are cleaved to give the observed reduction in Mw, not much else changes in the molecular structure. The C=O content of the humins decreased upon APR over Pt/Al_2O_3 observed as a decreased intensity of the peak at 1700 cm^{-1} which is related to the formation of CO and CO_2. Some residual Na_2SO_4 formed during acidification was observed at 1030 cm^{-1}. No further changes were observed for the humins after the APR over Pt/TiO_2 and $Pt\text{-}Re/ZrO_2$.

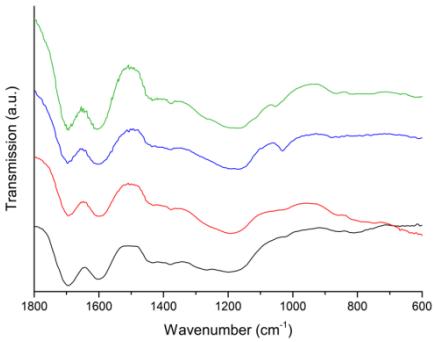

Figure 5.6. ATR-IR spectra of alkali-treated humins (black) compared to regenerated humins after the blank reaction (red), and APR over Pt/Al_2O_3 at 225 °C (blue) and 250 °C (green).

The ATR-IR spectrum of the humins after APR over Pt/TiO_2 without alkaline pretreatment was compared to the spectrum of the original, insoluble humins (Figure 5.7). Complete assignment of the IR spectra of glucose-derived humin can be found in Chapter 2. A decrease in C=O groups was observed as a decrease of the peak at 1700 cm^{-1}, which is in line with the formation of CO or CO_2. Disappearance of the peaks at 1510 and 1020 cm^{-1} points at a decrease in furan content possibly as a result of the formation of arene rings, indicated by the stronger signal at 1600 cm^{-1}. Weaker signals in the C-O stretch region (1400-1000 cm^{-1}) might point at cleavage of C-O bonds.

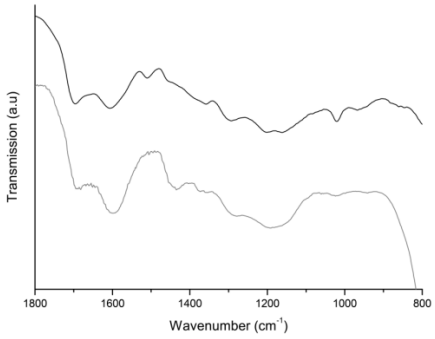

Figure 5.7. ATR-IR spectra of the original, insoluble glucose-derived humins (black) and glucose-derived humins after APR over Pt/TiO_2 (grey) without alkaline pretreatment.

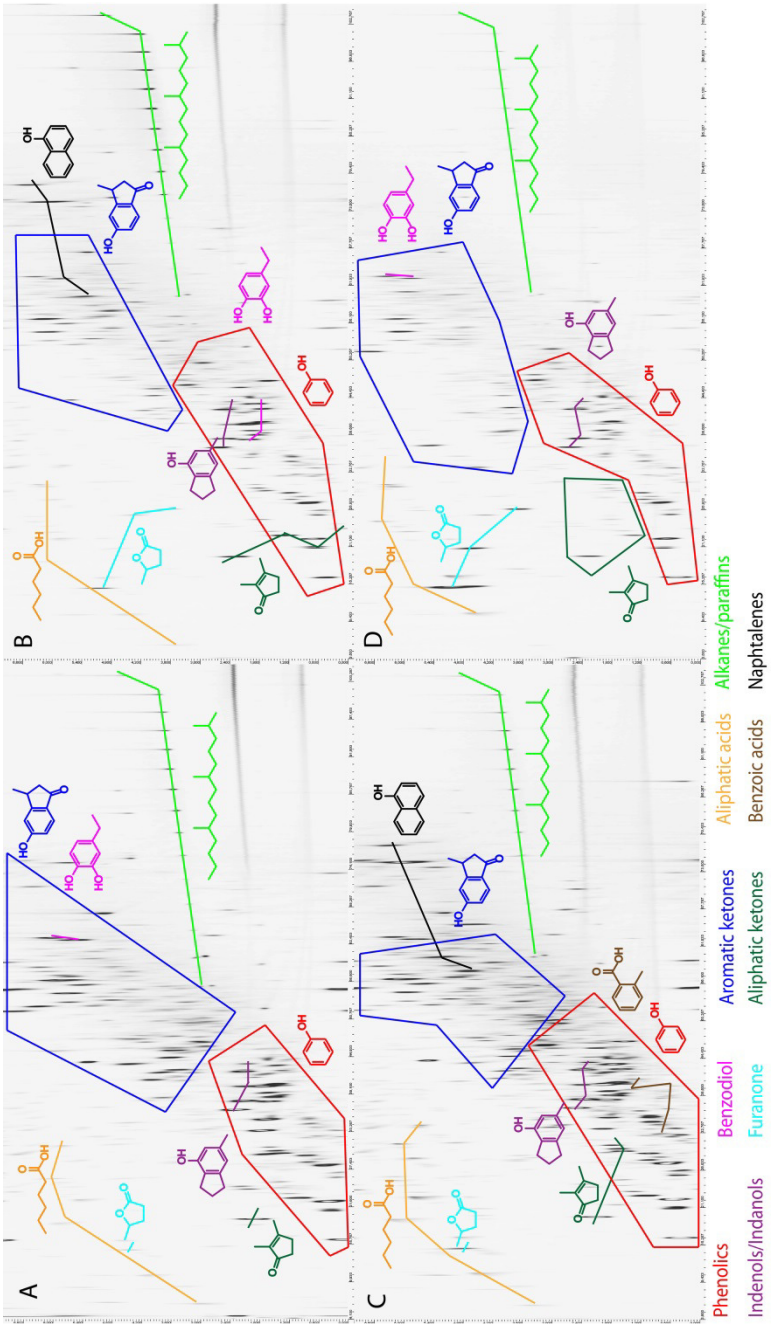

Figure 5.8. GCxGC-MS chromatograms of humin-oil after APR of solubilized humins over Pt/Al_2O_3 (A) Pt/TiO_2 (B) and $Pt\text{-}Re/ZrO_2$ (C). D. GCxGC-MS chromatogram of humin-oil after APR of untreated humins over Pt/TiO_2. The structures depicted are typical examples of the highlighted groups.

5.2.3. Composition of the Oil Fraction; Formation of Low Molecular Weight Products

GC-MS analysis of the humin-oil fractions obtained after APR of solubilized humins, revealed a complex mixture of mainly phenols and ketones, with similar patterns being observed for all catalysts. In order to improve the separation of these compounds the oil was further analyzed by GCxGC-MS, which allows for the identification of groups of similar compounds. A broad range of compounds was identified in the oil fraction obtained by APR of dissolved humins over Pt/Al_2O_3 at 225 °C (Figure 5.8A). The main products are phenols, benzodiols, indenols, indanols, and (aromatic) ketones, which is not surprising considering the arene-rich structure of alkaline-treated humins (Chapters 3 and 4). Furthermore, small organic acids and some benzoic acid were observed which could explain the decrease in pH after APR of the humins. It should be noted that the concentration of acids might be underestimated as these polar compounds would probably stay in the water phase during extraction with $CHCl_3$. Furthermore, furanone was observed reflecting the part of the furanic nature of the parent humins that is retained upon alkaline treatment. Upon APR over Pt/TiO_2 the alkane yield was slightly increased (Figure 5.8B). Also some naphthalenes were detected supporting the further aromatization of humins under hydrothermal conditions. The chromatogram of the oil derived from the $Pt\text{-}Re/ZrO_2$ run showed the largest amounts of phenolics (Figure 5.8C).

When the humins were directly subjected to APR, without alkaline pretreatment, the yield of phenols and polycyclic aromatic structures was lower. At the same time some furanic compounds and benzofurans were detected and the main products were furanones, which again provide some support for the furanic nature of the humins (Figure 5.8D). Previously, humin pyrolysis studies at 300-600 °C were reported to yield phenolic and (benzo)furanic compounds, with yields of volatiles of up to 30 wt% being obtained at the most elevated temperatures.[8] This is an indication that higher reaction temperatures are required to break down the humin structure more efficiently.

5.3. Conclusions

Humins are recalcitrant biomass-derived materials, which should be valorized to increase the viability of lignocellulosic biorefineries. Here, the first example of the conversion of alkali-soluble humins over a heterogeneous catalyst to a humin-oil was presented. Low APR activity was observed at 225 °C over Pt/Al_2O_3 as only small amounts of monomers were formed and some H_2, CH_4 and CO_2 were detected. Gas and monomer yields were increased after APR at 250 °C and catalyst activity was reported to increase in the following order: $Pt/Al_2O_3 < Pt/TiO_2 < Pt\text{-}Re/ZrO_2$. The obtained humin-oil consisted of a complex mixture of phenolics, cyclic and aromatic ketones. APR of untreated humins yielded more furan-derived compounds, supporting the furanic nature of the humins molecular structure, as reported in Chapter 2. The catalytic conversion of humins to aromatics and hydrogen by APR is limited by the reaction temperature and, relatedly, the

extent of C-C bond cleavage. Further efforts and choice of catalysts should be aimed at improved C-C bond activation and/or cleavage, for instance by using Ru or Rh or alloys of these metals with Re.

5.4. Experimental Section

Humins were prepared as described in Chapter 2. Alkaline pretreatment was performed in a Teflon-lined unstirred autoclave vessel which was filled with 5 g glucose-derived humin and 80 mL 2 M NaOH and was placed in an oven at 240 °C for 3 h. The humins were precipitated from the solution by acidification with 6 M H_2SO_4 to pH 1, isolated by filtration and washed with 6 L water. 100 mL water was added to redissolve the humin and the pH was adjusted to 9 or 11 with 1 M NaOH.

5% Pt/Al_2O_3 was obtained from Acros organics. The 5% Pt/TiO_2 catalyst was prepared by incipient wetness impregnation. TiO_2 (Degussa, P25) was dried under vacuum and impregnated with an aqueous solution of $H_2PtCl_6{\cdot}6H_2O$ (Sigma Aldrich, ACS reagent ≥37.50% Pt basis) to obtain a loading of 5%. Calcination was performed at 400 °C and reduction in 2:1 H_2:N_2 at 300 °C.

1% Pt-Re/ZrO_2 (Pt:Re 2:1 molar ratio) was prepared using ZrO_2 (Daiichi Kikenso RC-100, Degussa) that was calcined at 400 °C for 4 h under air before use. $H_2PtCl_6{\cdot}6H_2O$ (Sigma Aldrich, ACS reagent ≥37.50% Pt basis) and NH_4ReO_4 (Sigma Aldrich, ≥ 99%). Aqueous solutions of H_2PtCl_6 (0.05388 g $H_2PtCl_6{\cdot}6H_2O$ in 5 mL water) and NH_4ReO_4 (0.01396 g in 1 mL water) were sequentially added to a mixture of ZrO_2 (2.00 g) and water (14 mL) with continuous stirring. The mixture was stirred at room temperature overnight, evaporated to dryness and dried under vacuum at 50 °C overnight. The sample was calcined with O_2 (30 mL min^{-1}) at 400 °C for 2 h, than reduced with H_2 (30 mL min^{-1}) at 400 °C for 2 h to give the Pt-Re/ZrO_2 catalyst.

Catalytic reactions were performed in a 40 mL batch autoclave (Parr) equipped with a thermocouple, pressure transducer and gauge and magnetic driver. In a typical reaction the autoclave was loaded with 20 g dissolved humin (containing 0.55 g humin) and 0.1 g catalyst. For the APR of solid humins the reactor was loaded with 0.5 g humin, 0.1 g catalyst and 20 mL water and the pH was adjusted to 9 with 1 M NaOH. The reactor was flushed with argon and filled with 30 (225 °C) or 40 (250 °C) bar argon and this pressure was maintained during heating using a back-pressure regulator (BPR). When the desired temperature was reached, the autoclave was closed in order to monitor gas formation during the 20 h reaction. After reaction the composition of the gas phase was measured by a dual channel micro-GC coupled to a thermal conductivity device (TCD). A flow chart for characterization of the reaction products is found in Figure 5.9.

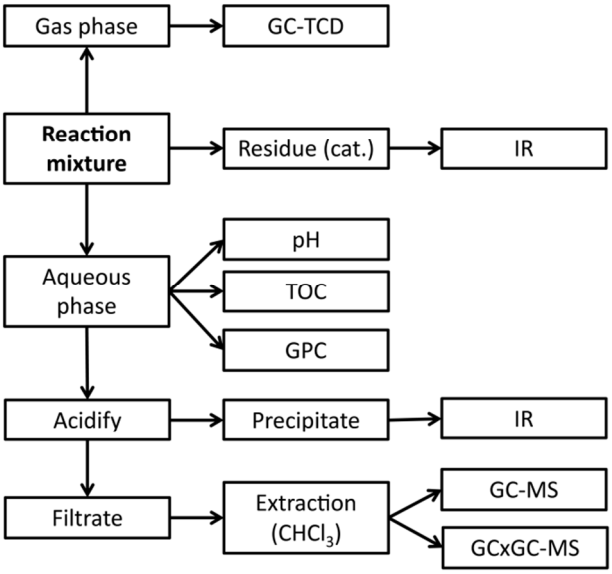

Figure 5.9. Flow chart for the characterization of humin APR products.

The liquid phase was filtered to remove the catalyst and any solids formed. Alkaline SEC performed on a Waters Alliance system equipped with a manually packed column (7.8 mm x 30 cm) with ethylene glycolmethacrylate copolymer TSK gel Toyo-pearl HW-55F according to the work of Gosselink *et al*.[28] Sodium-polystyrene sulfonates (Mw range 891 to 976000 Da) were used for calibration of the molar mass distribution. GPC measurements were performed at 40 °C with 0.5 M NaOH eluent at a flow rate of 1 mL min^{-1} and UV-detection at 280 nm.

Dissolved Organic Carbon (DOC) in water was determined on a Shimadzu TOC-5050A by Geolab at Utrecht University. In a combustion tube with oxidation catalyst at 680 °C the sample is oxidized to CO_2. The CO_2 is measured in a non-dispersive infrared gas analyzer. The total carbon content (TC) is measured, then inorganic carbon content (IC). DOC is the difference between TC and IC. All samples were diluted 500 time before analysis and the carbon content of the reaction mixture was compared to the carbon content of the dissolved humin. DOC was also used to calculate the amount of precipitated humins and oil yield in wt%. Based on elemental analysis data from Chapter 3 it was assumed that the solubilized humins had a carbon content of ~70 wt%.

The liquid phase was acidified by 6 M H_2SO_4 to precipitate residual humins, which were isolated by filtration and dried in air. The aqueous fraction was extracted by $CHCl_3$ (Merck, analytical grade). The extract was dried over $MgSO_4$ and the solvent was evaporated to obtain the humin-oil. The percentage of recovered humins and humin-oil was based on the concentration of humins in the starting solution, which was determined by DOC.

IR spectra of the humins were recorded using a Bruker Tensor 37 equipped with a MIRacle accessory with diamond ATR crystal. For each spectrum 32 scans were averaged. XRD patterns were recorded on a Bruker-AXS D2 Phaser powder X-ray diffractometer using Co-Kα with λ = 1.79026 Å. Measurements were carried out between 5−100° 2θ using a step size of 0.05° 2θ. TGA was performed with a Perkin−Elmer Pyris 1 apparatus. For analysis 15-20 mg of sample was dried at 150 °C for 2 h and heated with a ramp of 5 °C min^{-1} to 900 °C in an oxygen flow of 10 mL min^{-1}.

The humin-oil was analyzed by GCxGC-MS using a GCMS-QP2010 Ultra with electron ionization from Shimadzu. The 1st dimension column was a VF-5MS (30 m, 0.25 mm, 0.25 µm (length, ID, film)) and a VF-17ms (1 m, 0.15 mm, 0.15 µm) column was used for the 2nd dimension. Modulation was done by a ZX1 Thermal modulator (LN2) (Zoex). The temperature program started with an isothermal step at 40°C for 5 min, next the temperature was increased to 280 °C by 2.5 °C min^{-1}, which was followed by an isothermal step at 280°C for 5 min. A hot jet (375 ms) was pulsed every 7000 ms. Data analysis was performed using Comprehensive GC software; GC Image (Zoex) and Nist mass spectral library 2011 for GCMS (Nist 11 & Nist 11s). Groups of compounds are determined by MS and were slightly shifted between spectra due to different temperatures in the modulator.

5.5. Acknowledgements

Karst Lenzen and dr. Bo Feng from Utrecht University are acknowledged for the preparation of the Pt/TiO_2 and $Pt\text{-}Re/ZrO_2$ catalysts, respectively. Pascal Wijten and dr. Marleen Kerssens from Utrecht University are thanked for performing the GCxGC-MS measurements and taking photographs of the samples, respectively. Jacinta van der Putten and dr. Richard Gosselink from Wageningen University are thanked for performing the GPC measurements.

5.6. References

[1] J. J. Bozell, *Clean* **2008**, *36*, 641–647.
[2] J. Zakzeski, P. C. A. Bruijnincx, A. L. Jongerius, B. M. Weckhuysen, *Chem. Rev.* **2010**, *110*, 3552–3599.
[3] D. J. Hayes, J. Ross, M. H. B. Hayes, S. W. Fitzpatrick, in *Biorefineries - Industrial Processes and Products* (Eds.: B. Kamm, P.R. Gruber, M. Kamm), Wiley, **2006**, 139–164.
[4] B. Girisuta, L. P. B. M. Janssen, H. J. Heeres, *Chem. Eng. Res. Des.* **2006**, *84*, 339–349.
[5] J. Horvat, B. Klaić, B. Metelko, V. Šunjić, *Tetrahedron Lett.* **1985**, *26*, 2111–2114.
[6] J. M. Pin, N. Guigo, A. Mija, L. Vincent, N. Sbirrazzuoli, J. C. van der Waal, E. de Jong, *ACS Sustainable Chem. Eng.* **2014**, *2*, 2182–2190.
[7] T. M. C. Hoang, L. Lefferts, K. Seshan, *ChemSusChem* **2013**, *6*, 1651–1658.
[8] C. B. Rasrendra, M. Windt, Y. Wang, S. Adisasmito, I. G. B. N. Makertihartha, E. R. H. van Eck, D. Meier, H. J. Heeres, *J. Anal. Appl. Pyrolysis* **2013**, *104*, 299–307.
[9] A. J. Ragauskas, G. T. Beckham, M. J. Biddy, R. Chandra, F. Chen, M. F. Davis, B. H. Davison, R. Z. Dixon, P. Gilna, M. Keller, P. Langan, A. K. Naskar, J. N. Saddler, T. J. Tschaplinski, G. A. Tuskan, C. E. Wyman, *Science* **2014**, *344*, 1246843–1–10.
[10] S. Kang, X. Li, J. Fan, J. Chang, *Renew. Sustain. Energy Rev.* **2013**, *27*, 546–558.
[11] J. Zakzeski, B. M. Weckhuysen, *ChemSusChem* **2011**, *4*, 369–378.
[12] J. Zakzeski, A. L. Jongerius, P. C. A. Bruijnincx, B. M. Weckhuysen, *ChemSusChem* **2012**, *5*, 1602–1609.
[13] R. Cortright, R. Davda, J. Dumesic, *Nature* **2002**, *418*, 964–967.

[14] R. R. Davda, J. W. Shabaker, G. W. Huber, R. D. Cortright, J. A. Dumesic, *Appl. Catal. B Environ.* **2005**, *56*, 171–186.
[15] G. W. Huber, J. W. Shabaker, J. A. Dumesic, *Science* **2003**, *300*, 2075–2057.
[16] A. Ciftci, D. A. J. M. Ligthart, A. O. Sen, A. J. F. van Hoof, H. Friedrich, E. J. M. Hensen, *J. Catal.* **2014**, *311*, 88–101.
[17] A. Ciftci, D. A. J. M. Ligthart, E. J. M. Hensen, *Green Chem.* **2014**, *16*, 853–863.
[18] D. L. King, L. Zhang, G. Xia, A. M. Karim, D. J. Heldebrant, X. Wang, T. Peterson, Y. Wang, *Appl. Catal. B Environ.* **2010**, *99*, 206–213.
[19] N. Luo, X. Fu, F. Cao, T. Xiao, P. P. Edwards, *Fuel* **2008**, *87*, 3483–3489.
[20] R. M. Ravenelle, J. R. Copeland, W. Kim, J. C. Crittenden, C. Sievers, *ACS Catal.* **2011**, *1*, 552–561.
[21] A. Ciftci, S. Eren, D. A. J. M. Ligthart, E. J. M. Hensen, *ChemCatChem* **2014**, *6*, 1260–2169.
[22] T. van Haasterecht, C. C. I. Ludding, K. P. de Jong, J. H. Bitter, *J. Catal.* **2014**, *319*, 27–35.
[23] S. K. R. Patil, C. R. F. Lund, *Energy Fuels* **2011**, *25*, 4745–4755.
[24] S. K. R. Patil, J. Heltzel, C. R. F. Lund, *Energy Fuels* **2012**, *26*, 5281–5293.
[25] I. V. Sumerskii, S. M. Krutov, M. Y. Zarubin, *Russ. J. Appl. Chem.* **2010**, *83*, 320–327.
[26] X. Carrier, E. Marceau, J. F. Lambert, M. Che, *J. Colloid Interface Sci.* **2007**, *308*, 429–437.
[27] A. L. Jongerius, J. R. Copeland, G. S. Foo, J. P. Hofmann, P. C. A. Bruijnincx, C. Sievers, B. M. Weckhuysen, *ACS Catal.* **2013**, *3*, 464–473.
[28] R. J. A. Gosselink, J. E. G. van Dam, E. L. Scott, E. de Jong, J. P. M. Sanders, J. Li, G. Gellerstedt, *Holzforschung* **2010**, *64*, 193–200.

CHAPTER 6

Unexpected Benefits of Using Real Feeds in Biomass Conversion: High Hydroxymethylfurfural Selectivity and low Humin Formation in the Acid-catalyzed Dehydration of Sugar Beet-derived Thick Juice

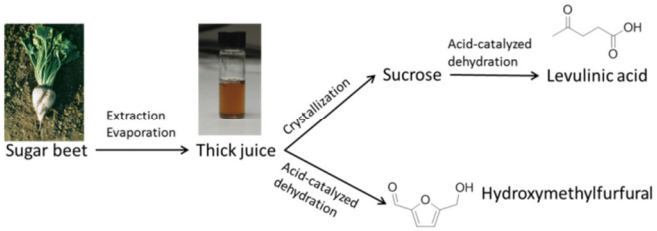

Abstract

Sucrose-containing refinery liquors, such as thick juice, can be used as feedstock for the production of hydroxymethylfurfural (HMF) and levulinic acid (LA). Remarkably, under the same processing conditions (0.01 M H_2SO_4 and 0.5 M sucrose at 180 °C for 6 h) the acid-catalyzed conversion of thick juice exclusively yielded HMF (23 mol%) as monomeric product rather than LA, which was obtained almost selectively from pure sucrose. Furthermore, about 50 wt% less humin was formed compared to reactions with pure sucrose at similar conditions. A selectivity switch was furthermore observed at increased acid concentrations, with LA being obtained as the main product from the thick juice. This remarkable effect can be explained in terms of the buffer function of carbonates present in the thick juice, as the acid-catalyzed dehydration of pure sucrose with added $CaCO_3$ also at least partially prevented rehydration of HMF to LA. The humins obtained from thick juice reactions also differ from the pure sugar-derived humins, with ^{13}C solid-state NMR spectra indicating a more conjugated molecular structure of thick juice-derived humins. Furthermore, the elemental analysis data shows that the amino acid impurities present in thick juice are incorporated in the humin structure. ATR-IR and ^{13}C solid-state NMR finally show that the thick juice humins formed at higher acid concentration to be more similar to the humins from pure sugars, showing that the buffer function of the carbonates in thick juice also influences the concentrations of intermediates involved in humin formation. The results thus show that thick juice is an interesting feed for the selective production of HMF at moderate conditions without the addition of organic solvents, heavy metal salts or ionic liquids.

Based on: I. van Zandvoort, E. J. B. Sirks, E. R. H. van Eck, H. J. Heeres, P. C. A. Bruijnincx, B. M. Weckhuysen, "Unexpected Benefits of Using Real Feeds in Biomass Conversion: High Hydroxymethylfurfural Selectivity and low Humin Formation in the Acid-catalyzed Dehydration of Sugar Beet-derived Thick Juice." *manuscript in preparation.*

6.1. Introduction

Hydroxymethylfurfural (HMF) and levulinic acid (LA) are important bio-based platform chemicals and can be produced from various kinds of simple carbohydrates as well as polysaccharides, including but not limited to fructose, glucose, sucrose, starch, cellulose, and whole lignocellulosic biomass.[1–4] While most attention has been devoted to the conversion of glucose, fructose or cellulose to HMF or LA,[5,6] sucrose, a disaccharide of fructose and glucose, would also be an attractive carbohydrate source, as it is produced in large volumes from sugar beet or cane of which 1.8 billion and 0.2 billion tons are harvested per year, respectively (2012).[7] It should be noted in this respect, that several governmental decisions have been made to stimulate the production of bio-based fuels and chemicals. For example, the American Department of Energy has set a goal that in 2030, 20% of transportation fuels and 25% of chemicals used in the USA should be derived from biomass.[8] The European Commission in turn has targeted that by 2020 10% of the used fuel should be bio-based.[9] This, together with further policy changes has urged sugar beet producers and refiners to look at alternative outlets, with strategies for the co-production of bio-based chemicals and fuels in a sugar beet refinery being of great interest. Recently, the EU has, for instance, decided to reduce the economic support for the production of refined sugar, making cultivation of sugar beets and sugar refining less viable. At the same time EU energy subsidies are available for sugar producers who use sucrose for the production of bio-ethanol.[10] Coproduction of bio-based chemicals from sucrose would also provide high value outlets for the sugar industry.

In a typical sugar beet refinery, the beets are washed, cut and the sucrose is subsequently extracted with water. This crude extract is purified by precipitation of inorganic substances and proteins by addition of $Ca(OH)_2$ and CO_2. Most of the impurities present are then included in the $CaCO_3$ precipitate that is formed, giving so-called *thin juice*, which is in turn concentrated by water evaporation to obtain a feed called *thick juice*. For sugar production, sucrose is then isolated by a crystallization process, which is initiated by addition of pulverized sugar crystals to the thick juice. In the last purification step the sugar crystals are centrifuged off to remove the remaining syrup that is known as molasses.[10]

It should be stressed that even after the carbonate purification step, various organic impurities, *e.g.* proteins, and minerals from the sugar beet will still be present in the sugar juice. In addition, the chemical composition of the juice is further complicated by the presence of other compounds, such as organic acids, phenols and polymeric products, which are formed during processing of the raw sucrose, such as the heating step to concentrate thin juice.[11–15] Of these various classes of impurities, the most important organic contaminants that are formed during the processing of sugar beets are melanoidins (formed by reactions between sugars and amino acids), alkaline hexose degradation products and caramels (formed by thermal degradation of the sugars).[11,12]

The production of bio-based chemicals could form a highly attractive and integral part of a sugar refinery when any available surplus of sucrose-containing feed can be converted to value added chemicals, such as HMF and LA. Although, the reported impurities are expected to pose a challenge with regards to (chemo-) catalytic valorization of these sugar beet-derived feeds, the use of thick juice as feedstock instead of pure sucrose would be more efficient since the last purification steps can then be avoided, thus improving the economics of the process. Notably, it has been previously shown that bio-ethanol[16,17] and bio-hydrogen[18] can be produced from thick juice by fermentation, with an economic assessment even showing that ethanol production from thick juice is the most viable way of co-producing bio-ethanol in a sugar refinery.[10] To our best knowledge, chemocatalytic routes for the valorization of thick juice to key renewable platform molecules, such as HMF or LA or to other bio-based chemicals or fuels, have not yet been reported. Indeed, the majority of the reported studies on the production of LA and HMF from carbohydrates make use of (analytically) pure sugar feeds.[4–6,19]

It is important to realize in this respect that results obtained for the conversion of pure sugars or polysaccharides can often not be directly translated to real feeds, as the impurities often strongly influence the conversion or product distribution. Indeed, this issue is not limited to sugar conversion, but (catalytic) processes that involve real biomass feeds are often hampered by impurities. It has been shown, for instance, that much less hydrogen is produced from crude glycerol than from pharma-grade glycerol during aqueous phase reforming.[20,21] In this case, the fatty acid salts are the impurities that deactivate the catalyst used, which results in a drop in reforming activity.[21] Another example can be found in biomass-to-liquids processes where biomass is gasified to syngas for subsequent Fischer-Tropsch synthesis of alkanes. To prevent catalyst deactivation the bio-syngas should in this case first be purified from oxygen- and nitrogen-containing compounds and organic impurities.[22] Sugar hydrogenolysis was also reported to be strongly dependent on the purity of the feed, with amino acid-derived compounds present in the complete biomass causing inhibition of the catalyst.[23] The effect of added reactants during the conversion of complete biomass was demonstrated by the one-pot conversion of giant reed to γ-valerolactone (GVL). High LA yields were obtained, however, subsequent hydrogenation to GVL was inhibited by poisoning of the catalyst by HCl that was used for the conversion of sugars to LA. This was prevented by neutralization of the reaction mixture prior to hydrogenation.[24]

The extensive literature on the production of HMF and LA from several carbohydrate sources, including sucrose, has been recently reviewed by Heeres and de Vries *et al.,*[5] Shanks *et al.*[19] and Rackemann *et al.*.[6] Sucrose conversion requires an acid to first hydrolyze the glycosidic bond between the sugar monomers to give fructose and glucose. The fructose monomer can then be dehydrated directly to HMF, while formation of HMF from the glucose monomer is thought to require isomerization to fructose first, a reaction that can be base or Lewis acid catalyzed.[25–27] It was shown for pure sucrose that

hydrolysis to the constituent sugars is faster than subsequent fructose dehydration at 160 °C in 0.1 wt% acid.[28] The HMF formed under these conditions was mainly derived from the fructose unit, with glucose conversion being low.[29] In general, selective HMF production from sugars comes with two considerable challenges. First, HMF is easily consumed in a consecutive rehydration reaction at elevated temperatures leading to the formation of LA and formic acid.[5,6,30] Second, condensation reactions of HMF with several of the sugar dehydration intermediates lead to the formation of heterogeneous, carbon-rich by-products called humins.[30–32] Humin formation not only considerably reduces the efficiency of a process, with a significant fraction of the carbon being lost to this route, it also poses a significant challenge from an engineering point of view, as the solids will foul the reactor. Fairly little is actually known about the mechanism of formation and the complex molecular structure of these humins and the influence of impurities from biomass on humin formation has not been reported before.[33,34] Previously, we proposed a furan-rich molecular structure for humins derived from glucose, fructose and glucose/fructose mixtures (see Chapter 2) based on a combination of ATR-IR, solid-state NMR and pyrolysis-GC-MS data; pure sucrose was not included as feed in this study.

The acid-catalyzed formation of LA from sucrose in water was first reported by Mulder in 1840.[35] No LA yields were reported since the main focus was actually on the formation of humin-like materials.[35] LA production from sucrose has since been studied under varying process conditions, in aqueous, organic or biphasic solutions and with different homogeneous and heterogeneous (Brønsted and Lewis) acidic catalysts.[6] The most prominent examples of LA production from sucrose are summarized in Table 6.1. Most examples are concerned with mineral acid-catalyzed conversion, with acid concentrations of 3.5-10 wt% at temperatures between 100 and 230 °C giving the best results; residence times vary as well, depending on temperature and acid concentration used.[6,36–39] One of the first systematic methods for LA synthesis from sucrose was developed in 1929 and yielded 22 mol% LA after 24 h at 100 °C in 7.4% aqueous HCl.[38] Thomas *et al.* extensively studied the effect of temperature, acid concentration and residence time to make the production of LA more economical and found that higher reaction temperatures increase the LA yield, while longer residence times lead to higher yields at lower reaction temperatures. An optimum in acid concentration was found at 6.5% (w/v), higher concentrations did not further increase the LA yield.[36] Acid strength correlated well with efficiency, with yields varying in the order HBr > HCl > H_2SO_4.[37] The use of several acidic resins was reported as well. While these catalysts seemed to have a lower activity than the mineral acids, catalyst regeneration is more efficient compared to the homogeneous acids.[40–42]

Selected examples of HMF formation from sucrose are also listed in Table 6.1. Only few examples have been reported of HMF production from aqueous solutions of sucrose. Low acid concentrations (0.001 M) and short reaction times are required when homogeneous acids are used as catalyst.[43] The fructose component of sucrose was

converted with high selectivity to HMF over niobic acid, albeit at low sucrose conversion.[44] As discussed above, the low selectivity to HMF in water is caused by acid-catalyzed polymerization to humins and/or rehydration to LA. Alternative approaches have sought to improve the HMF yields, for instance by using polar, aprotic organic solvents such as DMSO, DMF,[45] DMA,[46] and NMP[47] to suppress HMF degradation or by constant extraction of the HMF formed in a biphasic reaction system.[5]

DMSO is thought to increase the yield of HMF by stabilizing the furanose form of hexoses and thereby increases the reactivity of the sugar.[48] The use of MIBK or *n*-butanol as an extraction solvent was very successful to minimize humin formation and rehydration to LA.[48–51] Ionic liquids were studied as solvent and catalyst for the production of HMF from sucrose, showing very efficient conversion of the fructose component, but only 3% of the glucose formed was converted.[52] Several combinations of ionic liquids and catalysts were tested that improve conversion of the glucose unit.[53–58] It was also shown that Lewis-acidic zeolites can accelerate the isomerization of glucose to fructose, thereby improving the HMF yield.[59] Note that while the use of high boiling solvents or ionic liquids for the dehydration of sucrose can increase the HMF yield, isolation of HMF from these solvents is cumbersome; this requires extensive extractions and is more energy consuming and less well studied than isolation of HMF from aqueous solutions.[5]

Table 6.1. Selected examples of the production of LA and HMF from sucrose.

Ref	[Sucrose] (wt%)	Time	Catalyst(s)	Catalyst loading	Solvent[g]	Temperature (°C)	HMF yield[a] (mol%)	LA yield[a] (mol%)
Reactions in water								
[38]	29	24 h	HCl	2 M	water	100		21-22
[36]	30	1	HCl	2 M	water	162		41
[37]	5	16 h	H_2SO_4 HCl HBr	1 M 3 M 1 M	water	125		42[e] 60 70
[40]	33	41 h	Amberlite IR-120	70 wt%	water	100		16
[41]	17	9 h 24 h	Dowex MSC - 1H	62.5 wt%	water	100		23 24
[39]	31	60 min	HCl	3.84 M	water	98		50[e]
[42]	18	8 h 40 h	H_2SO_4 Nafion NR50	1.8 M 44 wt%	water	140		40-50[e] 35[e]
[60]	25	2.5 h	oxalic acid	0.03 M	water	145 for 15 min, then 125	27	
[43]	2	32 s	- H_2SO_4	- 0.001 M	water	250 (345 bar)	15 25	
[44]	12.7	4 h	niobium phosphate	1.4-3.4 wt%[f]	water	100	14	

Ref	[Sucrose] (wt%)	Time	Catalyst(s)	Catalyst loading	Solvent[g]	Temperature (°C)	HMF yield[a] (mol%)	LA yield[a] (mol%)
Reactions in organic (co-)solvents								
[61]	19	30 min[b]	pyridine H_3PO_4 5:3 (molar ratio)	11 mol% 6.5 mol%	water: dioxane 1:1	200-229	44	
[45]	3	3 h	Mg-Al hydrotalcite + Amberlyst-15 1:1 (wt)	200 wt%	DMF	120	54	
[47]	10	3 h	$FeCl_3$ + NH_4Br	19 mol% 35 mol%	NMP	90	40	
[46]	10	1 h	$CrCl_3$ + NH_4Br	9.5 mol% + 55 mol%	DMA	100	87	
Reactions in ionic liquids								
[52]	20	30 min	-	-	[HMIm]Cl	90	50	
[53]	17	3 h	$SnCl_4$	10 mol%	[EMmin]BF_4	100	65	
[54]	100	1 h	$CrCl_2$	10 mol%	CholineCl	100	62	
[55]	5	10 min	$CrCl_3$	20 mol%	[BMIm]Cl	100	76	
[56]	5	30 min	$GeCl_4$	10 mol%	[BMIm]Cl	120	55	
[57]	10	10 h	H_3BO_3	50 mol%	[EMIm] Cl	120	66	
[58]	10	30 min	$IrCl_3$ $AuCl_3$·HCl	7 mol%	[BMIm]Cl [BMIm]Cl	100 100	37 36	
[59]	10	50 min	H-β (Si/Al=25)	6 wt%	[BMIm]Cl	150	68	
Reactions in a biphasic solvent system[c]								
[62]	10	10 min	H_2SO_4	0.05 M	water:*n*-BuOH 1:1	150	30	
[49]		12 h	SPC-108	Fixed bed	water:MIBK	78	41	
[50]	10	30 min 60 min	H-mordenite (Si/Al =11)	3 wt%	water: MIBK 35:175	165	20 28	
[48]	10	5 min	HCl	0.1 M	MIBK:2-BuOH7:3 and water: DMSO 4:6[d]	170	25	
		4.5 h	-	-	DCM and water: DMSO 3:7[d]	140	25	
[63]	120 g/L ILs	4 h	$CrCl_3$	0.04 M	[BMIm] Cl : MIBK 3:7 (v/v)	100	100	
[64]	10	1 h	Al-TUD-1	7 wt%	H_2O:toluene 0.3:0.7	170	17	
[51]	23	3 min	TiO_2	fixed bed	H_2O:*n*-BuOH 3:1	180	16	

[a] Yield based on total monosaccharide concentration. [b] Reaction time excluding 32 min preheating. [c] Catalyst loading based on aqueous phase. [d] Organic phase: water 2:1. [e] Not clear whether yields are based on sucrose or monosaccharide concentration.

[f] Reaction volume not specified (assumed 50 mL). [g] DMA dimethylacetylamide, DMF dimethylformamide, DCM dichloromethane, MIBK methyl isobutyl ketone, BuOH butanol, DMSO dimethylsulfoxide, for ionic liquids: Im imidazolium, M methyl, E ethyl, B butyl, H hexyl.

Here, we report on the use of thick juice as an unpurified, industrial sucrose feed for the production of HMF or LA. The influence of process parameters on the production of these platform molecules was studied and the results compared to the yields obtained from pure sugars (*i.e.*, sucrose, fructose and glucose). In addition, the formation of humins from the thick juice feed was monitored, their elemental composition determined and the molecular structure studied with ATR-IR and 2D PASS ^{13}C solid-state NMR spectroscopy. The results show that thick juice behaves remarkably different from pure sucrose, by production of HMF with high selectivity and low humin formation and thereby providing a rare example of a catalytic biomass conversion process in which the use of a real, impure feedstock actually improves the selectivity. Thick juice can thus serve as an interesting feedstock for the selective production of HMF from sucrose under mild conditions in water.

6.2. Results and Discussion

6.2.1. Production of HMF and LA from Thick Juice

Thick juice had a sucrose concentration of 70 wt% and contained several inorganic impurities, including Ca. Standard conditions for the acid-catalyzed conversion of thick juice involved reactions run at 180 °C in 0.01 M H_2SO_4, and with an actual sucrose concentration of 0.5 M. All reaction conditions and yields can be found in Table 6.2. HPLC analysis of the products was complicated by the hydrolysis of sucrose to its sugar monomers on the acidic column. It is also known, however, that sucrose is rapidly hydrolyzed under the chosen reaction conditions,[28,65] and complete inversion of sucrose was therefore assumed for the sugar dehydration reactions. In addition, all reactions were run at the same monomer concentration, which allows for a fair comparison between sucrose and the individual and combined monosaccharides. The acid-catalyzed conversion of pure sucrose yielded 26 mol% LA, 1 mol% HMF and 21 wt% humins after 6 h under the standard conditions; while no fructose could be detected, a 22 mol% glucose yield was observed after reaction. As noted in the introduction, it is well-known that glucose is indeed less readily converted to HMF and LA. Reactions with either pure glucose or fructose gave conversions of 48 mol% and 100 mol%, respectively, again showing that fructose dehydration is faster than glucose dehydration.[25–27] Virtually no HMF was formed with the pure sugars, as any HMF formed was rapidly further converted to LA, with LA yields of 15 mol% and 39 mol% being obtained for glucose and fructose, respectively. A 1:1 mixture of glucose and fructose gave sugar conversions and LA yields that were very similar to the results found for the acid-catalyzed dehydration of pure sucrose, confirming its rapid inversion under the applied conditions (Table 6.2, Run 2-5).[60]

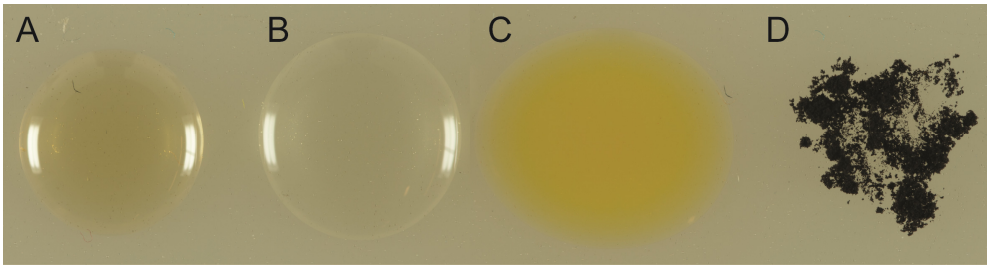

Figure 6.1. Droplets of thick juice (A), the reaction mixture before (B) and after acid-catalyzed dehydration and filtration (C) of thick juice and a sample of thick-juice humins (D).

The acid-catalyzed conversion of thick juice (Figure 6.1) gave rather different results (Table 6.2, Run 1). Indeed, under otherwise identical reaction conditions, *i.e.* same temperature, reaction time, added amount of sulfuric acid and sugar conversion level, HMF (23 mol%) was formed exclusively rather than the LA that was selectively formed in the dehydration of pure sucrose. Equally remarkable, thick juice yielded only half the amount of humins (~10 wt%) compared to the reactions with pure sucrose or a fructose/glucose mixture (~20 wt%) (Table 6.2 Run 1-5). However, the lower mass balance after the dehydration of thick juice could indicate the formation of more soluble humin precursors.

Sucrose concentration (0.25-1 M; *i.e*. 12-48 % (w/v) solutions of thick juice in water), reaction temperature (160-220 °C) and acid concentration (0.005-0.1 M) were varied to obtain the highest sugar conversions and product yields from thick juice at a fixed 6 h of reaction time (Table 6.2). While lowering the sugar concentration to 0.25 M did not influence sugar conversion or HMF yield, an increase in sugar concentration to 1 M led to a decrease in HMF yield (18 mol%) and increased humin formation (27 wt%) (Table 6.2, Run 6 and 7). The lowest reaction temperature of 160 °C resulted in low sugar conversions, but still a considerable HMF yield of 19 mol% was found. The reactions at higher temperatures of 200 and 220 °C did show (almost) complete glucose conversion, at 200 °C an HMF yield of 23 mol% and LA yield of 4 mol% were found, but also an increased humin formation was observed, and hardly any HMF was produced at the highest temperature (Table 6.2, Run 12-15). The amount of added acid was also found to have a strong influence on selectivity. A low acid concentration (0.005 M H_2SO_4) yielded more humins than the 0.01 M acid added under the standard conditions. This is in line with the Design of Experiment study presented in Chapter 2 that showed a decrease in humin formation at high acid concentrations. Importantly, at higher acid concentrations selectivity shifted towards LA formation, with a concomitant increase in humin yields. The reaction carried out in 0.1 M H_2SO_4 yielded the highest amount of LA (40 mol%) with 22 wt% of humin formed (Table 6.2, Run 8-11).

The acid-catalyzed conversions of thick juice (Table 6.2, Run 1, 16-18, Figure 6.2A) and pure sucrose (Table 6.2, Run 2, 22-24, Figure 6.2B) were monitored in time under

standard reaction conditions (180 °C, 0.01 M H_2SO_4). The results again show that fructose is converted faster than glucose and that the HMF yield goes through a maximum of 23-24 mol% after 4-6 h of reaction time. After a reaction time of 16 h only small amounts of HMF and LA are found in solution, indicating that most of the HMF that is initially formed is lost to humin formation rather than to rehydration to LA. The HMF yield in the acid-catalyzed dehydration of pure sucrose under otherwise identical conditions peaked at only 10 mol% after 4 h and rapidly falls to zero at longer reaction times. After 4 h, LA is already the major product, ultimately being obtained in 34% yield after 16 h. The build-up in concentration of HMF in the case of thick juice and of LA from pure sucrose, is ultimately reflected in the amount of humins formed. Indeed, as expected, higher HMF levels led to the formation of a larger amount of humins (Figure 6.2, Table 6.2).

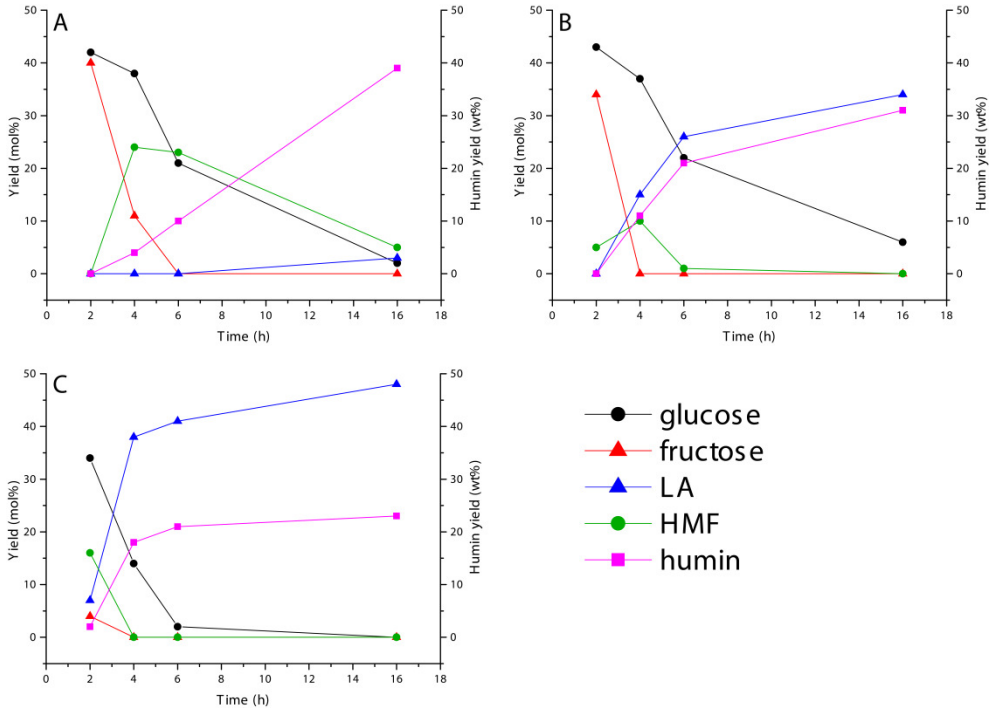

Figure 6.2. Products formed in time during the acid-catalyzed dehydration of thick juice (A) and sucrose (B) under standard conditions (0.5 M sucrose, 0.01 M H_2SO_4 and 180 °C) and (C) dehydration of thick juice with increased acid concentration: glucose (grey circles), fructose (grey triangles), HMF (black circles), LA (black triangles) and humins (black squares).

Table 6.2. Reaction conditions, yields, mass balance, and particle size of the humins for the acid-catalyzed dehydration of pure sugars and thick juice.

	Conditions					Yield [a]						Mass balance [b]
Run #	Feedstock	[sugar] (M)	[H_2SO_4] (M)	T (°C)	t (h)	Glucose (mol%)	Fructose (mol%)	FA (mol%)	LA (mol%)	HMF (mol%)	Humins (wt%)	(wt%)
	Variation of feedstock											
1	thick juice	0.5	0.01	180	6	21	0	0	0	23	10	56
2	sucrose	0.5	0.01	180	6	22	0	27	26	1	21	73
3	glucose	1	0.01	180	6	48	-	16	15	0	10	73
4	fructose	1	0.01	180	6	-	0	42	39	0	31	71
5	glucose/ fructose 1:1	0.5	0.01	180	6	22	0	30	29	1	20	72
	Variation of sugar concentration											
6	thick juice	0.25	0.01	180	6	27	0	0	0	24	10	64
7	thick juice	1	0.01	180	6	12	1	4	0	18	27	60
	Variation of acid concentration											
8	thick juice	0.5	0.005	180	6	24	0	3	0	24	15	68
9	thick juice	0.5	0.02	180	6	21	0	0	1	16	16	56
10	thick juice	0.5	0.05	180	6	17	0	26	25	2	22	69
11	thick juice	0.5	0.1	180	6	3	0	41	41	0	21	67

Run	Feedstock	Conditions				Yield [a]						Mass balance [b]
#		[sugar] (M)	[H_2SO_4] (M)	T (°C)	t (h)	Glucose (mol%)	Fructose (mol%)	FA (mol%)	LA (mol%)	HMF (mol%)	Humins (wt%)	(wt%)
		Variation of reaction temperature										
12	thick juice	0.5	0.01	160	6	35	13	0	0	19	4	74
13	thick juice	0.5	0.01	200	6	2	0	11	4	23	31	64
14	thick juice	0.5	0.01	220	6	0	0	0	4	2	41	46
		Variation of reaction time										
15	thick juice	0.5	0.01	180	2	42	40	0	0	0	0	45
16	thick juice	0.5	0.01	180	4	38	11	0	0	24	4	81
17	thick juice	0.5	0.01	180	16	1	0	6	3	5	39	50
18	thick juice	0.5	0.1	180	2	34	4	6	7	16	2	67
19	thick juice	0.5	0.1	180	4	14	0	39	38	1	18	73
20	thick juice	0.5	0.1	180	16	0	0	42	48	0	23	73
21	sucrose	0.5	0.01	180	2	43	34	0	0	5	0	53
22	sucrose	0.5	0.01	180	4	37	0	15	15	10	11	76
23	sucrose	0.5	0.01	180	16	6	0	36	34	0	31	74

[a] Complete inversion of sucrose is assumed. Yields are based on monosaccharide concentration. [b] Mass balance is calculated as the sum of all water soluble products (wt%), the amount of humins formed (wt%) and water formed during the reaction.

The time-profile of LA production from thick juice at high acid concentration (180 °C, 0.1 M H_2SO_4) was also determined and showed a more rapid depletion of the sugars and an increase in the rate of HMF rehydration to LA (Table 6.2, Run 11, 19-21 and Figure 6.2C). A considerable amount of HMF was present in the early stage of the reaction, but rapidly disappeared after 2 h at this higher acid concentration. After a reaction of 16 h most of the sugars were converted to give an LA yield of 48 mol% and a humin yield of 23 wt%. These results are in agreement with several kinetic models, which state that while both rehydration of HMF and humin formation are known to be acid-catalyzed, the influence of acid concentration on the rate of LA formation is more pronounced.[34,66,67]

The large differences in product distribution observed after reactions with pure sucrose and thick juice could be caused by a difference in the (initial) pH of the reaction mixtures, as the thick juice reaction mixture was found to have a pH of 3.5 after addition of 0.01 M H_2SO_4 while a pH 1.8 was measured for the pure sucrose solution. Taking this into account, reactions were also run at the same pH of 3.5, with the pH of the sucrose solution having been adjusted to 3.5 with a 1 M NaOH solution. As can be clearly seen from Figure 6.3, large differences in product distribution were again observed for these reactions run at similar initial pH, with LA still being the main product obtained from pure sucrose, in stark contrast with the exclusive formation of HMF from thick juice. Note that product yields are not directly comparable to the results in Table 6.2; a different oven was used, resulting in a somewhat higher actual temperature, as indicated by the higher sugar conversion and humin yield.

The high HMF yields obtained from thick juice at standard conditions can also be caused by the many impurities present in thick juice. As discussed in the introduction, it is well know that Lewis acids catalyze the formation of HMF, for instance; the amount of metals, such as Zn, Fe and Al, is below 0.0002 wt% in the juice used, however, and their effect therefore seems negligible. On the other hand, the buffer capacity of thick juice,[15] as a result of the presence of residual amino acids or organic acids, such as lactic acid and acetic acid, or inorganic compounds, such as phosphates and sulfates, could also play a role.[14] All these compounds are, again, only present in small amounts though. Carbonates, introduced to the juice in its purification process, are actually present in considerable amounts and can form a carbonate/bicarbonate buffer when dissolved. Indeed, it has been shown that the molasses fraction, which is a full part of the thick juice, does contain a considerable amount of carbonates.[68] The buffer function of thick juice is in fact illustrated by the difference in pH after a reaction under standard conditions, with pHs of 2.6 and 1.6 measured for thick juice and sucrose, respectively. That the carbonate/bicarbonate buffer might also play an important role in the observed selectivity difference is emphasized by a reaction with pure sucrose and added $CaCO_3$. When the pH is of the sucrose solution was increased to 3.5 with $CaCO_3$ instead of NaOH, a strong increase in HMF yield was noted accompanied by a similarly strong drop in LA yield. This indicates that carbonates in thick juice indeed aid in the stabilization of HMF and prevent

rehydration to LA. The fact that LA is predominantly formed from thick juice at higher acid concentrations shows that the buffer capacity is exceeded under these conditions (both thick juice and pure sucrose reaction mixtures have a starting pH of 1 when 0.1 M acid is added).

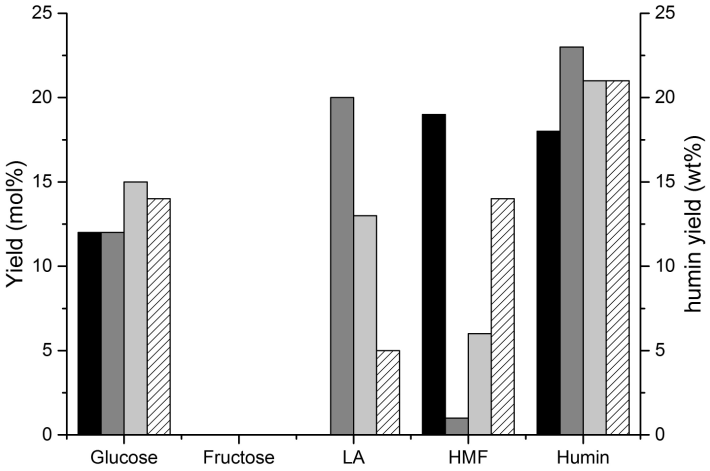

Figure 6.3. Comparison of dehydration products formed from thick juice at pH 3.5 (black), pure sucrose at pH 1.8 (dark grey), pure sucrose at pH 3.5 adjusted with a 1 M NaOH solution (light grey) and pure sucrose at pH 3.5 adjusted with $CaCO_3$ (shaded). All reactions were performed with 0.01 M H_2SO_4 at 180 °C for 6 h.

6.2.2. Characterization of Thick Juice Humins

6.2.2.1. Morphology

SEM images of the solid humins formed in during the acid-catalyzed dehydration of thick juice, sucrose, glucose and fructose showed the expected spherical humin morphology (Figure 6.4, Table 6.3).[33,34,67] Humin particle sizes are bigger than those reported in Chapter 2, with the difference being attributed to the use of a non-stirred autoclave in this study. In the non-stirred reactor, less nucleation occurs and, as a result, the humins particles can grow larger, as was also reported for HTC.[34,67] The thick juice and sucrose-derived humins both showed a broad, bimodal particle size distribution, with sucrose humins being slightly more agglomerated. Compared to humins from disaccharides, glucose-derived humins showed strong agglomeration and a narrower, mono-modal particle size distribution. The same particle size and size distribution is observed for fructose-derived humins, however, these particles were less agglomerated than glucose-derived humins.

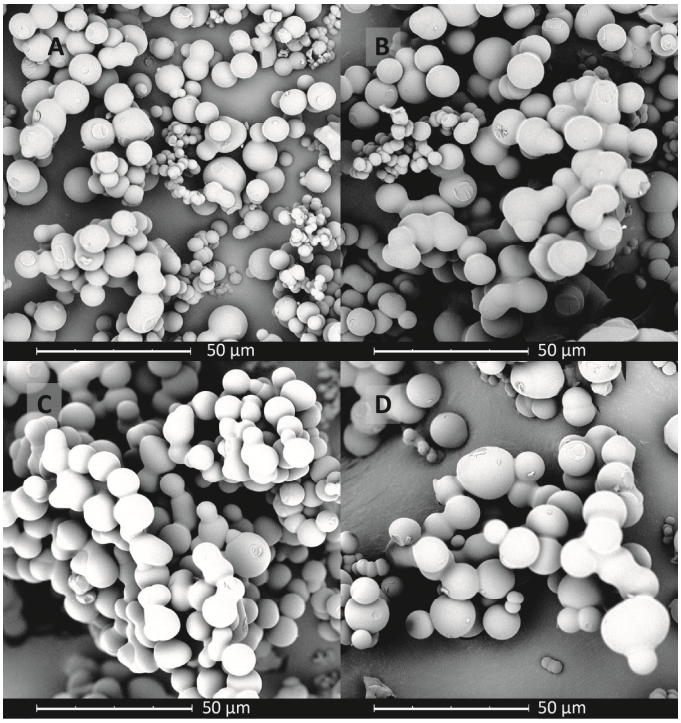

Figure 6.4. SEM images of humins from thick juice (A), sucrose (B), glucose (C), and fructose (D).

Table 6.3. Humins particle size after acid-catalyzed dehydration of different sugar feeds.[a]

Run #	Feedstock	[sugar] (M)	Particle size (µm)
1	thick juice	0.5	3-4, 7-11[b]
2	sucrose	0.5	3-4, 8-13
3	glucose	1	10-12
4	fructose	1	10-12
5	glucose/ fructose 1:1	0.5	10-12

[a] Conditions: 0.01 M H_2SO_4, 180 °C, 6 h. [b] bimodal distribution observed

6.2.2.2. Elemental Composition

Elemental analysis of the humins from thick juice showed that nitrogen is incorporated into their structure (Table 6.4). Residues of proteins present in the feed are thought to be the nitrogen source and could be included via Maillard reactions between sugars and amino acids or peptides.[13,69] Notably, the nitrogen content of the thick juice humins is higher than found in the original thick juice, which indicates that amino acids or peptides are preferentially included in the humin structure.[70,71] Humins formed at short reaction

times (Table 6.4, Run 1, 17, 19) furthermore show higher nitrogen contents than humins obtained after 16 h of reaction (Run 18 and 21). This indicates that Maillard reactions between sugars and amino acids take place at an early stage of humin formation.

Table 6.4. Elemental composition of the humins formed during the acid-catalyzed dehydration of pure sucrose and thick juice.

Conditions[a]				Elemental composition					
Run #	Feedstock	[H_2SO_4] (M)	t (h)	C (wt%)	H (wt%)	N (wt%)	O (wt%)	H/C	O/C
1	thick juice	0.01	6	62.29	4.32	0.61	32.79	0.83	0.39
2	sucrose	0.01	6	63.85	3.76	<0.01	32.38	0.71	0.38
15 [c]	thick juice	0.01	2	-	-	-	-	-	-
16	thick juice	0.01	4	60.97	4.26	1.10	33.68	0.84	0.41
17	thick juice	0.01	16	63.88	4.11	0.38	31.64	0.77	0.37
18	thick juice	0.1	2	60.99	3.87	0.50	34.65	0.76	0.43
20	thick juice	0.1	16	63.54	4.04	0.39	32.04	0.76	0.38

[a] 0.5 M sugar, 0.01 M H_2SO_4, 180 °C. [b] Calculated by difference [c] Not enough humins isolated for further analysis.

6.2.2.3. Molecular Structure: IR, Solid-state NMR and Pyrolysis-GC-MS

The ATR-IR spectra of the thick juice humin and the humins derived from pure sugars are compared in Figure 6.5 (for a detailed assignment see Chapter 2). The vibrations seen at 1510, 1020, 792 and 755 cm^{-1} again clearly point at the presence of furanic rings in the humin samples. While generally quite similar, the ratio between the peaks at 1700 and 1605 cm^{-1}, previously assigned to C=O and C=C, respectively, is different for the thick juice humins, indicating a different ratio of these functional groups. The peaks in C-O stretch region (1400-1000 cm^{-1}) are furthermore less intense for the thick juice humins. This points at the presence of less oxygen groups or broadening of the signals due to the presence of C-O groups in different chemical environments.

A comparison of ATR-IR spectra of humins from thick juice formed at different acid concentrations and reaction times provide some indications to the evolution of the humin structure (Figure 6.6). Low acidity and/or shorter reaction times result in stronger signals attributable to furanic rings (1514, 1020, 967, 793 and 766 cm^{-1}) and oxygen-containing functional groups (C=O at 1671 cm^{-1} and C-O at 1300-1000 cm^{-1}), for instance. This suggests that humins are further dehydrated during the reaction resulting in a lower oxygen content and further aromatization of the polymer. Such further dehydration is supported by the decrease in O/C and H/C ratios of the humin samples with increasing acid concentration, reaction time and reaction temperature (Table 6.4). At higher acid concentration and a reaction time longer than 4 h, the humins are more similar to humins derived from pure sugars. This is further evidenced by the ratio between the peaks at 1700 and 1605 cm^{-1}. This is related with the higher LA yields at these conditions, which

again shows that HMF is stabilized in thick juice at standard conditions, most likely as a result of the carbonates buffer.

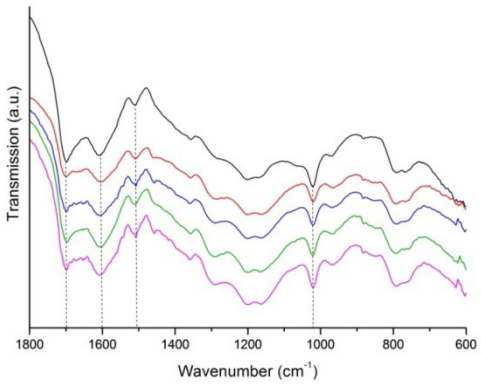

Figure 6.5. ATR-IR spectra of humins from thick juice (black), sucrose (red), fructose:glucose 1:1 (blue), glucose (green) and fructose (magenta) produced at standard conditions of 1 M monosaccharide or 0.5 M sucrose, 0.01 M H_2SO_4, 6 h at 180 °C.

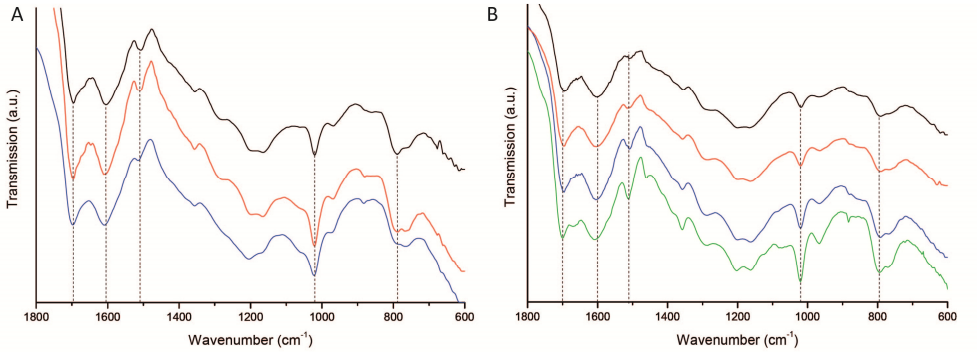

Figure 6.6. ATR-IR spectra of humins from thick juice prepared at different H_2SO_4 concentrations: 0.01 M (A) and 0.1 M (B). Reaction times were varied 16 h (black), 6 h (red), 4 h (blue) and 2 h (green) at a reaction temperature of 180 °C.

^{13}C solid-state NMR spectra of the humins from glucose, sucrose and thick juice were recorded using a 2D Phase Adjusted Spinning Sidebands (2D PASS) sequence (Figure 6.7), for which the peak assignment can be found in Table 6.5.[72,73] This method allows for the separation of spinning sidebands that are caused by anisotropic groups from the center bands in a second dimension. Summation of the projections of these sidebands and the center band gives a spectrum identical to one obtained by a CP MAS measurement. Shearing of the data leads to a sideband-free spectrum of high resolution, yet obtained at low MAS speeds without losing information about the anisotropic groups. We have previously reported the 2D PASS ^{13}C solid-state NMR spectra of humins from different sugar feeds (Chapter 2).

The 2D PASS ^{13}C solid-state NMR spectra show that sucrose-derived humins are very similar to humins prepared from a 1:1 glucose:fructose mixture. The ^{13}C NMR

spectrum of thick juice humins prepared under standard conditions showed some clear differences from the spectra of humins from pure sugars, indicating changes in the molecular structure. While similar in pattern, a higher intensity is seen for the aliphatic region (δ = 0-50 ppm), which is in line with the elemental composition of the humins. In the region δ = 60-100 ppm, representing alcohols and ethers, some intensity with features at δ = 73, 78 and 88 ppm are observed. Literature data shows that these signals can be attributed to secondary alcohols in sugar residues,[74–76] which indicates that more sugar (derivatives) are incorporated in the thick juice humins. Large differences between the spectra are readily apparent in the C=C region (δ = 100-160 ppm). The typical pattern expected for furanic structures was observed, as described in more detail in Chapter 2 and 4; compared to the pure sugar-derived humin spectra, the signal from linked furanic C_α is sharper, though, for humins from thick juice, which points at the formation of larger furanic network. Another important difference is the increase in intensity around δ = 130 ppm, which indicates a more conjugated structure of the humins, which could be caused by increased crosslinking within the humin structure,[77] formation of arene structures[78,79] or formation of pyrrole-like structures by inclusion of nitrogen containing molecules.[80,81] The latter seems unlikely since less than 1 wt% N was detected by elemental analysis. The peak at δ = 175 ppm, which are attributed to acids/esters, is much sharper for thick juice humins. Signals from ketones and aldehydes are observed at δ = 205 ppm and have a similar intensity for all humins.

Table 6.5. Peak assignment of the ^{13}C solid-state NMR spectra of humins.

δ (ppm)	Functional group	Chemical formula
14	Methyl	CH_3
29	Primary aliphatic C	CH_2
42	Secondary/tertiary saturated C	CH/C
60-100	Ether, alcohol, amines	C-OH, C-O-C, CH-NH
112	C_β-furan free	O-C=<u>C</u>H-C
122	C_β-furan linked	O-C=<u>C</u>-C
129	Conjugated aromatic C Conjugated N containing aromatic system	C-C=C-C=C C=C-NH-C=C, C=N-C
142	C_α furan free	C=<u>C</u>H-O
151	C_α furan linked	C=<u>C</u>-O
175	Acid, ester	COOH, COOC
205	Ketone, aldehyde	C=O

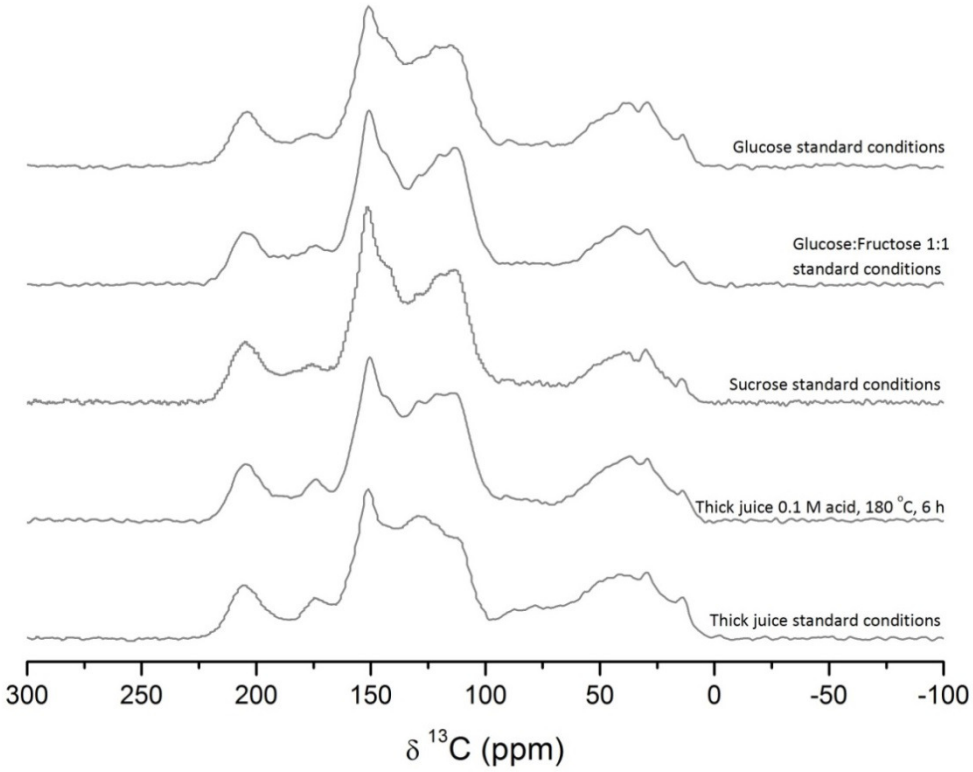

Figure 6.7. Sheared sum projections of the 2D PASS ^{13}C solid-state NMR spectra of humins from (top to bottom) glucose, glucose:fructose 1:1, sucrose and thick juice humins. Standard conditions are 180 °C, 0.01 M H_2SO_4 and 0.5 M sucrose for 6h.

The ^{13}C solid-state NMR spectrum of humins from thick juice prepared with an increased acid concentration (0.1 M) is more similar to the spectrum of humins from pure sucrose, which is in line with the IR data and expected from the catalytic data. The strong differences that were observed between the NMR spectra of humins from thick juice prepared at standard conditions and with a high acid concentration can be explained by the presence of different concentrations of intermediates leading to humin formation as a result of the HMF stabilization.

The pyrolysis-GC-MS data of humins from thick juice and sucrose (Figure 6.8) proved to be very similar, showing several peaks from furanic substances and some phenol and benzene-derived compounds, further supporting the furanic nature of humins. However, the pyrolysis-GC-MS chromatogram of humins from thick juice showed weaker signals from substituted furanics, *i.e.* 2-methylfuran and 2-acetylfuran. At the same time, some stronger signals from phenolics and other arene structures were observed (Figure 6.8), which again point at a more conjugated or arene-containing structure.

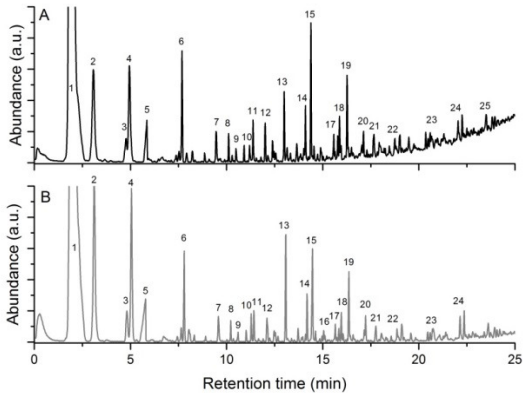

1. CO_2
2. acetone
3. 3-buten-2-one
4. 2-methylfuran
5. acetic acid
6. 2,5-dimethylfuran
7. toluene
8. 2-ethyl-5-methylfuran
9. 2,3,5-trimethylfuran
10. furfural
11. 2-cyclopenten-1-one
12. 1,2-dimethylbenzene
13. 2-acetylfuran
14. 5-methylfuran
15. phenol
16. benzofuran
17. 2-acetyl-5-methylfuran
2-methylphenol
18. 3-methylphenol
19. 2-methylbenzofuran
20. 2,3-dimethylphenol
21. 2-ethylphenol
22. azulene
23. 2-methylnaphthalene
24. 2-methyl-1,4-benzene dicarboxaldehyde
25. 2,5-dimethyl-1,4-benzene dicarboxaldehyde

Figure 6.8. Pyrolysis-GC-MS of humins from and thick juice (A) and sucrose (B).

Taken together, the humin characterization data indicate that the buffering function of thick juice influences the concentration of intermediates that are involved in humin formation and as a result changes details of the humin molecular structure. For example, Lund *et al.*[33] suggested that the molecular structure of humins strongly depends on the concentrations of HMF and 2,5-dioxo-6-hydroxy-hexanal (DHH), which is formed by rehydration of HMF on the 2,3-position and is believed to react with HMF via aldol condensations leading to the formation of humins.[30,33,34] When thick juice is used as a feed, the rehydration of HMF is blocked and DHH cannot be formed. Humins are, however, still formed via reactions of HMF with sugar dehydration products and reactions between the HMF rings, as described in Chapter 2. When the acid concentration is increased the buffer function is exceeded and the reaction pathways to LA and DHH are available leading to rehydration of HMF and a molecular structure that is more similar to that of humins derived from pure sugars.

6.3. Conclusions

The use of real biorefinery thick juice as feed for catalytic sugar valorization was shown to come with unexpected advantages. Indeed, the data reported show that thick juice is a promising feed for the production of HMF from raw sucrose in good yields up to 24 mol%, at moderate conditions and without the alternative solvents, heavy metal ions or ionic liquids that are typically required in literature. At modest acid concentration, acid-catalyzed conversion of thick juice gives a high selectivity of HMF without rehydration to LA and slow humin formation, while pure sucrose yields LA and two times more (insoluble) humins under the same reaction conditions. This is remarkable especially because impurities in crude biomass-derived feeds often make valorization to chemicals more challenging. The buffer capacity of thick juice, which can be attributed to the carbonates added to thick juice as part of the industrial purification protocol, seems to be key in the stabilization of HMF under reaction conditions, thus preventing rehydration to LA. At

higher acid concentrations, this buffer capacity is indeed exceeded, resulting in a selectivity switch to LA rather than HMF formation.

The buffer function of thick juice furthermore limits the formation of solid humins and influences the concentration of different intermediates involved in humin formation. As a result, the molecular structure of the thick juice humins is more conjugated, as shown by ^{13}C solid-state NMR. Humins derived from thick juice formed at a higher acid content were found to be more similar to the humins derived from pure sugars. This is consistent with the proposed importance of the buffer function of thick juice. IR spectra and elemental composition of humins from thick juice prepared at different conditions indicate further dehydration of the humins at more severe processing conditions. Elemental analysis also shows that incorporation of nitrogen containing compounds occurs at an early stage of humin formation.

The exclusive formation of HMF and low humin yield makes thick juice a promising raw feed for the production of HMF form sucrose. Co-production of HMF can be implemented in sugar refineries to convert a surplus of thick juice to valuable compounds. Our results furthermore show the importance of pH of the reaction mixture during the acid-catalyzed dehydration of sugars to bulk-chemicals. When the influence of buffers on the selectivity towards HMF, LA and humins is investigated, sugar conversion processes could be further optimized.

6.4. Experimental Section

Thick juice (65-70 °Bx, 65-70 wt% sucrose) was provided by Cosun. The light brown color and characteristic smell of this industrial sample already indicated that organic impurities are present in the thick juice, either ones that have been carried over by extraction from the sugar beet or impurities formed during the water-evaporation process.[11,13] The thick juice sample had a sucrose content of 70 wt% as determined by HPLC, with no other compounds being detected in the chromatogram in significant amounts. The HSQC NMR spectrum of thick juice in D_2O also did not show any organic contaminations at concentration levels detectable by NMR. The IR spectrum of freeze dried thick juice was identical to the IR spectrum of pure sucrose. These results show that that the level of impurities in the thick juice is very low. Elemental analysis indicated that the sample contains a small amount of nitrogen (0.2 wt% of freeze-dried thick juice), probably derived from the protein fraction of the sugar beet.[11,13,14]

In a typical experiment, 100 mL of an aqueous solution of 0.01 M H_2SO_4 and 0.5 M sucrose (corresponding to 24.4 g thick juice) was heated in an unstirred Teflon-lined autoclave vessel at 180 °C for 6 h while being rotated. The experiment was repeated with 1 M glucose, 1 M fructose or a combination of 0.5 M of each sugar. For the process parameter screening experiments, sucrose concentration (0.25 - 1 M), acid concentration (0.005 - 0.1 M), reaction time (2 - 16 h) and reaction temperature (160 - 220 °C) were altered. For the dehydration of pure sucrose at pH 3.5 the pH was adjusted to with a 1 M

NaOH solution or $CaCO_3$. Any humins formed were isolated by filtration and purified according to a previously developed protocol, *i.e.* washed with 2 L water, dried at RT, submitted to a Soxhlet extraction with water for 24 h, and finally dried in an oven at 120 °C for 24 h. This method was based on the humin preparation procedure described in Chapter 2. All reactions reported in Table 6.2 and Figure 6.2 were performed in the same oven. For the data presented in Figure 6.3 a new oven with a higher actual temperature was used.

Table 6.6. Impurities in thick juice and molasses.

Impurities in thick juice reported by the manufacturer		Concentrations reported for molasses[68]a	
Compound	**Concentration (wt%)**	**Compound**	**Concentration (wt%)**
Zn	<0.0002	Na_2CO_3	4.39
Al	<0.0002	K_2CO_3	1.22
Mn	<0.0002	$MgCO_3$	1.07
Fe	<0.0002	$CaCO_3$	15.46
K	0.6-0.8	CaO	3.23
Na	0.1		
Malic acid	0.02-0.1		
Lactic acid	0.2 - 0.5		
Acetic acid	0.1		
Pyrrilidone carbonic acid	0.2		
Citric acid	0.02-01		

[a] In dry substance of molasses. Concentrations of impurities reported for molasses are assumed to be about 10 times higher than in thick juice.

The liquid phase was analyzed with a Shimadzu HPLC system equipped with a Bio-Rad Aminex HPX-87H column and a differential refractometer. Samples were analyzed with 5 mM H_2SO_4 as eluent, a flow rate of 0.55 mL/min at 60 ˚C and the detector temperature set to 40 °C. Sucrose cannot be detected with this HPLC system, as it is rapidly inverted under these conditions. Injection of pure sucrose sample gave a chromatogram with peaks from glucose and fructose in a 1:1 ratio. It was assumed that sucrose is completely inverted during the sugar dehydration reaction.

Elemental analysis of the humins was carried out using an automated Euro EA3000 CHNS. Oxygen content was calculated by difference. SEM images were taken using a Phenom G2 (Fei company). Samples were coated with 4 nm Pt with 10 % Pd. ATR-IR spectra were recorded on a Bruker Tensor 37 IR spectrometer using a MIRacle accessory with a diamond ATR crystal. For each spectrum, 32 scans with a resolution of 4 cm^{-1} were averaged.

The ^{13}C solid-state NMR spectra were recorded at Radboud University Nijmegen. The spectra were measured on a 300 MHz solid-state NMR spectrometer using a 7.5 mm double resonant chemagnetics APEX probe, tuned at 75.45 MHz for carbon. The spectra

were obtained using ramped CPMAS at an rf-field of 55 kHz for carbon and 51 kHz for protons. Proton decoupling during acquisition was accomplished with a Spinal-64 sequence at an rf-field of 55 kHz, optimized to a pulse width and phase of 9 µs and 7°, respectively. MAS speeds were 4 kHz. After cross polarization a 2D PASS sequence was used to separate the spinning sidebands, employing cogwheel phase cycling.[82] Spectra were normalized over the integral.

Analytical programmed temperature vaporization (PTV) GC-MS of humins was conducted with a HP 5890 GC Series II system equipped with a 5972 MS detector, and the PTV was controlled by an Optic 2 device. Typically 1 mg of sample was used. The pyrolysis temperature program started at 40 °C followed by heating to 600 °C at a rate of 16 °C min^{-1}, and finally held at 600 °C for 0.5 min. After pyrolysis, the products were transferred into a capillary column (Agilent Technologies VF-5ms, 30 x 0.25 x 1.0) by a GC injector (split 50:1). Helium was used as the carrier gas at a flow rate of 1 mL min^{-1}. The following GC temperature program was applied: starting temperature of 40 °C for 5 min followed by heating at a rate of 10 °C min^{-1} to a final temperature of 250 °C. The MS detector was operated in the electron ionization mode (70 eV) with an interface temperature 280 °C. A scan range of m/z 35-400 was applied. Pyrolysis products were identified by comparison with mass spectra of authentic compounds and masses.

6.5. Acknowledgements

Suiker Unie and Dr. ir. Adeline Ranoux from Cosun Food Technology Center are kindly acknowledged for providing a refinery thick juice sample and their contributions to the Chapter. Bart Sirks is thanked for performing dehydration reactions. Prof. dr. ir. Erik Heeres, Léon Rohrbach and ir. Henk van de Bovenkamp from University of Groningen are acknowledged for the elemental analysis and pyrolysis-GC-MS measurements. Dr. Ernst van Eck from Radboud University Nijmegen is thanked for recording the ^{13}C solid-state NMR spectra.

6.6. References

[1] J. P. Lange, E. van der Heide, J. van Buijtenen, R. Price, *ChemSusChem* **2012**, *5*, 150–166.

[2] J. P. Lange, R. Price, P. M. Ayoub, J. Louis, L. Petrus, L. Clarke, H. Gosselink, *Angew. Chem. Int. Ed.* **2010**, *49*, 4479–4483.

[3] A. J. Ragauskas, C. K. Williams, B. H. Davison, G. Britovsek, J. Cairney, C. A. Eckert, W. J. Frederick Jr, J. P. Hallett, D. J. Leak, C. L. Liotta, J. R. Mielenz, R. Murphy, R. Templer, T. Tschaplinski, *Science* **2006**, *311*, 484–489.

[4] S. P. Teong, G. Yi, Y. Zhang, *Green Chem.* **2014**, *16*, 2015–2026.

[5] R. J. van Putten, J. C. van der Waal, E. de Jong, C. B. Rasrendra, H. J. Heeres, J. G. De Vries, *Chem. Rev.* **2013**, *113*, 1499–1597.

[6] D. W. Rackemann, W. O. S. Doherty, *Biofuels, Bioproducts and Biorefining* **2011**, *5*, 198–214.

[7] "Food and Agriculture Organization of the United Nations," can be found under http://faostat3.fao.org/faostat-gateway/go/to/download/Q/QC/E, **2014**.

[8] R. D. Perlack, L. L. Wright, A. F. Turhollow, R. L. Graham, B. J. Stokes, D. C. Erbach, Biomass as Feedstock for a Bioenergy and Bioproducts Industry: The Technical Feasibility of a Billion-Ton Annual Supply, **2005**.

[9] "EU strategy for biofuels," can be found under http://europa.eu/legislation_summaries/energy/renewable_energy/l28175_en.htm
[10] D. Krajnc, P. Glavič, *Chem. Eng. Res. Des.* **2009**, *87*, 1217–1231.
[11] M. Coca, M. T. Garcia, G. Gonzalez, M. Pena, J. A. Garcia, *Food Chem.* **2004**, *86*, 421–433.
[12] M. A. Godshall, M. A. Clarke, C. D. Dooley, R. S. Blanco, *J. Sugar Beet Res.* **1991**, *28*, 155–165.
[13] D. Baunsgaard, C. A. Andersson, A. Arndal, L. Munck, *Food Chem.* **2000**, *70*, 113–121.
[14] J. B. Stark, A. E. Goodban, H. S. Owens, *Ind. Eng. Chem.* **1950**, *43*, 603–605.
[15] H. W. S. Owens, J. B. Stark, A. E. Goodban, H. G. Walker, H. G. Walker Jr, *Agric. Food Chem.* **1955**, *3*, 350–353.
[16] S. Popov, J. Dodic, J. Rankovic, S. Dodić, J. Dodić, J. Ranković, Z. Zavargo, R. Jevtić Mučibabić, *Biomass and Bioenergy* **2009**, *33*, 822–827.
[17] R. Razmovski, V. Vučurović, *Fuel* **2012**, *92*, 1–8.
[18] D. Foglia, W. Wukovits, A. Friedl, M. Ljunggren, G. Zacchi, K. Urbaniec, M. Markowski, *Chem. Eng. Trans.* **2010**, *21*, 1153–1158.
[19] T. Wang, M. W. Nolte, B. H. Shanks, *Green Chem.* **2014**, *16*, 548–572.
[20] K. Lehnert, P. Claus, *Catal. Commun.* **2008**, *9*, 2543–2546.
[21] D. A. Boga, Aqueous Phase Reforming of Renewable Polyols for Production of Hydrogen Using Platinum Catalysts, PhD Thesis, Utrecht University, **2013**.
[22] J. Hu, F. Yu, Y. Lu, *Catalysts* **2012**, *2*, 303–326.
[23] D. C. Elliott, K. L. Peterson, D. S. Muzatko, E. V Alderson, T. R. Hart, G. G. Neuenschwander, *Appl. Biochem. Biotechnol.* **2004**, *113-116*, 807–285.
[24] A. M. Raspolli Galletti, C. Antonetti, E. Ribechini, M. P. Colombini, N. Nassi o Di Nasso, E. Bonari, *Appl. Energy* **2013**, *102*, 157–162.
[25] M. S. Feather, J. F. Harris, *Carbohydr. Res.* **1970**, *15*, 304–309.
[26] D. W. Harris, M. S. Feather, *Carbohydr. Res.* **1973**, *30*, 359–365.
[27] D. W. Harris, M. S. Feather, *J. Org. Chem.* **1974**, *39*, 724–725.
[28] S. Bower, R. Wickramasinghe, N. J. Nagle, D. J. Schell, *Bioresour. Technol.* **2008**, *99*, 7354–7362.
[29] C. Perez Locas, V. a Yaylayan, *J. Agric. Food Chem.* **2008**, *56*, 6717–6723.
[30] J. Horvat, B. Klaić, B. Metelko, V. Šunjić, *Tetrahedron Lett.* **1985**, *26*, 2111–2114.
[31] D. J. Hayes, J. Ross, M. H. B. Hayes, S. W. Fitzpatrick, in *Biorefineries - Industrial Processes and Products* (Eds.: B. Kamm, P.R. Gruber, M. Kamm), Wiley, **2006**, pp. 139–164.
[32] G. R. Akien, L. Qi, I. T. Horváth, *Chem. Commun.* **2012**, *48*, 5850–5852.
[33] S. K. R. Patil, J. Heltzel, C. R. F. Lund, *Energy Fuels* **2012**, *26*, 5281–5293.
[34] S. K. R. Patil, C. R. F. Lund, *Energy Fuels* **2011**, *25*, 4745–4755.
[35] Mulder, *J. Pract. Chemie* **1840**, *21*, 203–240.
[36] R. Thomas, H. Schuette, *J. Am. Chem. Soc.* **1931**, *53*, 2324–2328.
[37] Wiggins, *Adv. Carbohydr. Chem.* **1949**, *4*, 293–336.
[38] B. F. McKenzie, *Org. Synth.* **1929**, *9*, 50.
[39] V. E. Tarabanko, M. Y. M. Chernyak, S. V. Aralova, B. N. Kuznetsov, *React. Kinet. Catal. Lett.* **2002**, *75*, 117–126.
[40] B. C. Redmon, *US Patent 2,738,367*, **1956**.
[41] R. A. Schraufnagel, H. F. Rase, *Ind. Eng. Chem. Prod. Res. Dev.* **1975**, *14*, 40–44.
[42] H. Mehdi, V. Fábos, R. Tuba, A. Bodor, L. T. Mika, I. T. Horváth, *Top. Catal.* **2008**, *48*, 49–54.
[43] M. J. Antal, W. S. L. Mok, G. N. Richards, *Carbohydr. Res.* **1990**, *199*, 91–109.
[44] C. Carlini, M. Giuttari, A. Maria Raspolli Galletti, G. Sbrana, T. Armaroli, G. Busca, *Appl. Catal. A Gen.* **1999**, *183*, 295–302.
[45] A. Takagaki, M. Ohara, S. Nishimura, K. Ebitani, *Chem. Commun.* **2009**, 6276–6278.
[46] C. Wang, L. Fu, X. Tong, Q. Yang, W. Zhang, *Carbohydr. Res.* **2012**, *347*, 182–185.
[47] X. Tong, M. Li, N. Yan, Y. Ma, P. J. Dyson, Y. Li, *Catal. Today* **2011**, *175*, 524–527.
[48] J. N. Chheda, Y. Román-Leshkov, J. A. Dumesic, *Green Chem.* **2007**, *9*, 342–350.
[49] L. Rigal, A. Gaset, *Biomass* **1983**, *3*, 151–163.
[50] C. Moreau, R. Durand, C. Pourcheron, S. Razigade, *Ind. Crops Prod.* **1994**, *3*, 85–90.
[51] C. V. Mcneff, D. T. Nowlan, L. C. McNeff, B. Yan, R. L. Fedie, *Appl. Catal. A Gen.* **2010**, *384*, 65–69.
[52] C. Moreau, A. Finiels, L. Vanoye, *J. Mol. Catal. A Chem.* **2006**, *253*, 165–169.
[53] S. Hu, Z. Zhang, J. Song, Y. Zhou, B. Han, *Green Chem.* **2009**, *11*, 1746–1749.
[54] F. Ilgen, D. Ott, D. Kralisch, C. Reil, A. Palmberger, B. König, *Green Chem.* **2009**, *11*, 1948–1954.
[55] X. Qi, M. Watanabe, T. M. Aida, R. L. Smith, *ChemSusChem* **2010**, *3*, 1071–1077.
[56] Z. Zhang, Q. Wang, H. Xie, W. Liu, Z. K. Zhao, *ChemSusChem* **2011**, *4*, 131–138.

[57] T. Ståhlberg, S. Rodriguez-Rodriguez, P. Fristrup, A. Riisager, *Chemistry* **2011**, *17*, 1456–1464.
[58] Z. Wei, Y. Li, D. Thushara, Y. Liu, Q. Ren, *J. Taiwan Inst. Chem. Eng.* **2011**, *42*, 363–370.
[59] L. Hu, Z. Wu, J. Xu, Y. Sun, L. Lin, S. Liu, *Chem. Eng. J.* **2014**, *244*, 137–144.
[60] W. N. Haworth, W. G. M. Jones, *J. Chem. Soc.* **1944**, 667–670.
[61] M. L. Mednick, *J. Org. Chem.* **1962**, *27*, 398–403.
[62] Q. P. Peniston, *US 2,750,394*, **1956**.
[63] S. Lima, P. Neves, M. M. Antunes, M. Pillinger, N. Ignatyev, A. A. Valente, *Appl. Catal. A Gen.* **2009**, *363*, 93–99.
[64] S. Lima, M. M. Antunes, A. Fernandes, M. Pillinger, M. F. Ribeiro, A. A. Valente, *Molecules* **2010**, *15*, 3863–3877.
[65] P. Leininger, M. Kilpatrick, *J. Am. Chem. Soc.* **1938**, *1268*, 2891–2899.
[66] B. Girisuta, L. P. B. M. Janssen, H. J. Heeres, *Chem. Eng. Res. Des.* **2006**, *84*, 339–349.
[67] B. Girisuta, L. P. B. M. Janssen, H. J. Heeres, *Green Chem.* **2006**, *8*, 701–709.
[68] H. Olbrich, *The Molasses*, Biotechnologie-Kempe GmbH, Berlin, **1963**.
[69] A. E. Goodban, J. B. Stark, H. S. Owens, *Agric. Food Chem.* **1953**, *1*, 261–264.
[70] H. D. Belitz, W. Grosch, P. Schieberle, *Food Chemistry*, Springer-Verlag, Berlin Heidelberg, **2009**.
[71] R. Tressl, G. T. Wondrak, L. A. Garbe, R.-P. Krüger, D. Rewicki, *J. Agric. Food Chem.* **1998**, *46*, 1765–1776.
[72] F. G. Vogt, J. M. Gibson, D. J. Aurentz, K. T. Mueller, A. J. Benesi, *J. Magn. Reson.* **2000**, *143*, 153–160.
[73] O. N. Antzutkin, S. C. Shekar, M. H. Levitt, *J. Magn. Reson.* **1995**, *115*, 7–19.
[74] C. Sievers, T. Marzialetti, T. J. C. Hoskins, M. B. Valenzuela Olarte, P. K. Agrawal, C. W. Jones, M. B. V. Olarte, *Bioresour. Technol.* **2009**, *100*, 4758–4765.
[75] N. Baccile, G. Laurent, F. Babonneau, F. Fayon, M. M. Titirici, M. Antonietti, *J. Phys. Chem. C* **2009**, *113*, 9644–9654.
[76] P. E. Pfeffer, K. B. Hicks, M. H. Frey, S. J. Opella, W. L. Earl, *J. Carbohydr. Chem.* **1984**, *3*, 197–217.
[77] M. M. Titirici, M. Antonietti, N. Baccile, *Green Chem.* **2008**, *10*, 1204–1212.
[78] C. Falco, F. Perez Caballero, F. Babonneau, C. Gervais, G. Laurent, M. M. Titirici, N. Baccile, *Langmuir* **2011**, *27*, 14460–14471.
[79] C. Burket, R. Rajagopalan, a Marencic, K. Dronvajjala, H. Foley, *Carbon* **2006**, *44*, 2957–2963.
[80] N. Baccile, G. Laurent, C. Coelho, F. Babonneau, L. Zhao, M.-M. Titirici, *J. Phys. Chem. C* **2011**, *115*, 8976–8982.
[81] R. L. Johnson, J. M. Anderson, B. H. Shanks, X. Fang, M. Hong, K. Schmidt-Rohr, *J. Magn. Reson.* **2013**, *234*, 112–124.
[82] N. Ivchenko, C. E. Hughes, M. H. Levitt, *J. Magn. Reson.* **2003**, *164*, 286–293.

Summary and Concluding Remarks

Summary

The depletion of fossil fuels at a time of increasing energy demands is driving the development of alternative resources for the production of fuels and bulk chemicals. Of the alternative resources that are explored, biomass is the only renewable source of carbon currently available that can be feasibly converted to fuels and chemicals on a large scale. The many efforts aimed at efficient biomass conversion processes have led to the development of so-called biorefineries. While the first-generation of biorefineries makes use of readily processed, edible biomass, the use of the lignocellulosic parts of biomass is preferred for the production of chemicals and fuels, in order to avoid any competition with food or feed production. Such lignocellulosic biomass now constitutes the feedstock for the second-generation biorefineries that are coming online. Lignocellulosic biomass consist of two carbohydrate components, cellulose and hemicellulose, and lignin. In the biorefinery, these primary components are converted to so-called platform molecules *via* an integrated set of processes. The carbohydrate polymers can, for instance, be hydrolyzed to individual sugar monomers under acidic hydrothermal conditions. These, in turn can be dehydrated to form the platform molecules hydroxymethylfurfural (HMF) and furfural (FF) from C_6- and C_5-sugars, respectively. Finally, HMF can again be easily rehydrated to form the platform molecule levulinic acid (LA). These sugar-derived bulk chemicals can be used for the production of a whole range of bio-based materials, fuels and fine chemicals.

An important issue in the acid-catalyzed processing of carbohydrates and their derivatives is the unavoidable formation of large amounts of carbonaceous, insoluble by-products called humins. These humins are thought to be formed by cross-polymerization reactions between HMF, sugars and several sugar-dehydration intermediates, leading to loss of the carbohydrate feed and limiting the economic feasibility of the biorefinery. To get to more competitive biorefinery processes, the formation of humins should either be avoided or any humins formed should be valorized, *i.e.* by catalytic conversion to valuable chemicals. These two approaches would require insight in the humin formation mechanism and molecular structure, both of which are not yet unequivocally established. In addition, if catalytic valorization of this recalcitrant feed is targeted, the general insolubility of the humins should be addressed, as this limits the substrate-catalyst interaction and thus hampers conversion over a (heterogeneous) catalyst.

The work described in this PhD thesis aims to gain improved understanding of the (mechanism of) formation and the molecular structure of humins formed in acidic, hydrothermal sugar conversion processes. This knowledge can aid in controlling the extent

of humin formation and contribute to the development of (catalytic) routes for valorization of humins to chemicals or fuel components. First, the formation and molecular structure of the humins was studied as a function of feed and process parameters. Second, an alkaline pretreatment method was developed for the reactive solubilization of humins. These alkali-treated humin were again fully characterized and subsequently converted to chemicals and hydrogen by Aqueous Phase Reforming (APR) over supported Pt-containing catalysts. In addition, a sucrose-containing liquor from an industrial sugar-refinery was tested as a raw feed for the selective production of HMF at moderate aqueous conditions and the influence of such a real feed on the formed platform molecules and humins was assessed.

In **Chapter 2** a multiple-parameter and multiple-technique study of the formation, molecular structure and morphology of humins is presented. Pure sugars, D-glucose, D-fructose and D-xylose and mixtures thereof were subjected to acid-catalyzed dehydration at 180 °C, in 0.01 M H_2SO_4 for 6 h. Analysis of the liquid phase after reaction showed LA to be the main product from C_6-sugars while C_5-sugars yielded FF. Humin formation was the highest for fructose, which is thought to be the result of the high concentrations of HMF that are rapidly formed from this sugar, with HMF being a direct precursor to humins. Remarkably, humin yields from xylose were only slightly higher than from glucose, despite the accumulation of FF (rather than LA) in the reaction mixture. This indicates that FF has a lower propensity than HMF to form organic acids and humins. Further analysis of the liquid phase by Gel Permeation Chromatography (GPC) and elemental analysis after drying, pointed at the presence of water-soluble humin precursors in the liquid phase.

The effect of reaction intermediates on humin formation was tested by the addition of HMF or 1,2,4-trihydroxybenzene (TB) to a D-glucose feed. HMF addition (1:0.2 sugar:HMF molar ratio) did not change the yield of liquid phase products or humin much. In contrast, TB addition (1:0.2 and 1:0.01 sugar:TB molar ratio) led to a considerable increase in humin formation and related decrease in LA yield, indicating that this molecule acts as a cross-linker in humin formation. Notably, the incorporation of TB furthermore shows that humin formation also involves reactions other than the pure aldol condensation mechanism that was suggested by Lund *et al*.[1,2]

The influence of reaction parameters on the formation of humins from glucose was studied using Design of Experiment. The reaction temperature (113-247 °C), sugar concentration (0.66-2.34 M) and acid concentration (0-0.13 M) were varied at a constant reaction time of 6 h. The model obtained from the experimental data showed that humin formation is strongly influenced by reaction temperature and to a lesser extent by acid concentration, but statistically hardly depends on sugar concentration. It was also found that high temperatures and low acid concentrations lead to high humin production. These conditions are opposite to those that will lead to high yields in levulinic acid.

SEM indicates that the humin by-products have a spherical morphology, which strongly depends on feedstock. C_6-sugars formed interconnected particles with, for example, a size of 3-5 µm for glucose-derived humins (Figure 7.1). On the contrary, isolated particles of roughly the same size were formed from xylose. Surprisingly, much smaller, isolated particles were found when a high concentration of TB was added to the feed. Based on the elemental composition of the humins, a van Krevelen plot could be constructed that indicated that humin formation occurs via a net dehydration pathway. The chemical composition and chemical structure of humins was studied by ATR-IR, ^{13}C solid-state NMR and pyrolysis-GC-MS. These data showed that humins consist of a furan-rich polymer network containing alcohol, acid, ketone and aldehyde functional groups. The NMR data also points at the presence of aliphatic linkers (Figure 7.2). The molecular structure was found to strongly depend on the type of feedstock with xylose-derived humins, for example, having a more conjugated molecular structure than humins from C_6-sugars. The free 5-position of furfural thus gives rise to more direct linking between furan rings, leading to less aliphatic linkages and a more condensed network of furans moieties. Based on this information a model for the molecular structures of glucose and xylose-derived humins was proposed.

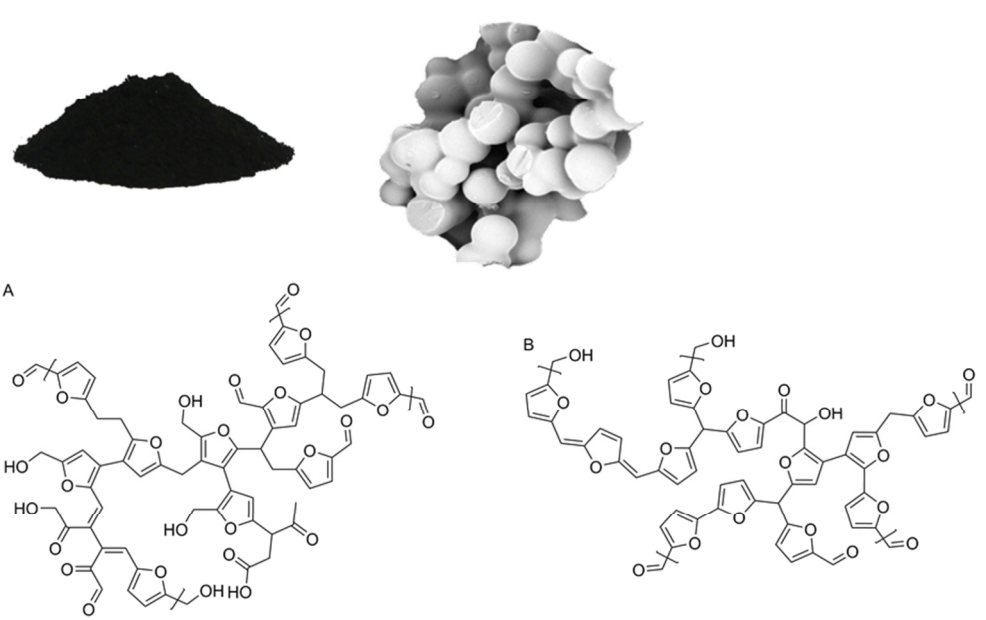

Figure 7.1.Top: humines and the morphology of glucose-derived humins. Bottom: the molecular structures of A. Glucose-derived humins and B. Xylose-derived humins as described in Chapter 2.

In **Chapter 3** an alkaline pretreatment method is reported that allows for the general insolubility of the humins prepared according to the method described in Chapter 2 to be overcome. Typical conditions for the reactive solubilization of glucose-derived

humin are 200 °C in 0.5 M NaOH for 3.5 h. These alkali-treated humins subsequently remain soluble down to a pH of about 7. GPC analysis allowed for relative changes in the molecular weight of the humins to be determined upon treatment at different conditions. Higher temperatures and prolonged reaction times led to a gradual decrease in the weight-average molecular weight of the solubilized humin, until different plateaus were reached depending on process conditions. Fructose- and xylose-derived humins were found to be more recalcitrant and complete dissolution required raising the temperature to 240 °C. This was rather unexpected for the fructose-derived humins given their structural similarity to the glucose-derived humins, while it was not for the more cross-linked xylose-derived humins. Alkaline pretreatment proved to be an effective method for the reactive solubilization of humin by-products allowing the first liquid-phase analysis on biomass-derived humins.

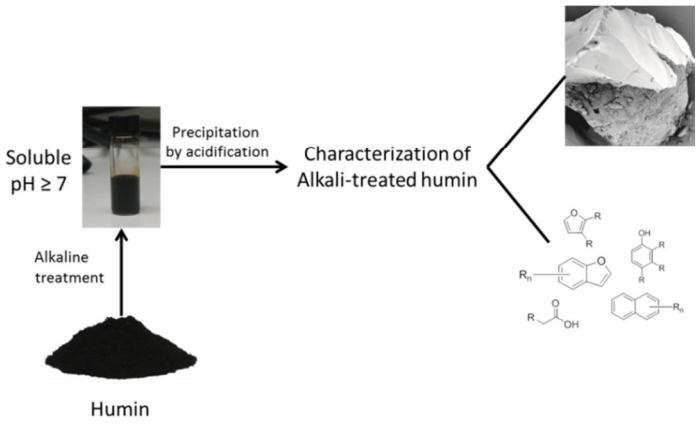

Figure 7.2. Alkaline treatment of humins with the morphology and chemical structures indentified in alkali-treated humins as described in Chapter 3.

Before further characterization, humins were precipitated from the solution by acidification, isolated, washed and dried. As expected, SEM images showed that the spherical morphology of humins is lost after alkaline treatment. The changes in elemental composition upon alkaline treatment pointed at further aromatization of the humins via dehydration and loss of CO. Characterization of the molecular structure of alkali-treated humins by ATR-IR, ^{13}C solid-state NMR and pyrolysis-GC-MS confirmed this aromatization and suggested at a more (polycyclic) aromatic structure, which might be the result of combined Diels-Alder and dehydration reactions (Figure 7.2). Furan-ring opening reactions might account for the changes seen in the aliphatic parts of the structure. Oxygen-containing functional groups also change upon alkaline treatment as the amount of ketone groups decreased, while the carboxylic acid content increased. The latter could be explained by the increased solubility of the alkali-treated humins. The reduction in molecular weight could finally be attributed to cleavage of the C-O-C bonds of which small amounts are thought to be present in the parent humin.

In **Chapter 4** the molecular structures of the (alkali-treated) humins studied in Chapter 2 and 3 are further investigated by advanced solid-state NMR techniques. A combination of complementary 1D and 2D solid-state NMR spectra of ^{13}C-labeled humins provided further insight into the molecular structure of these highly complex and structurally heterogeneous materials and allowed for refinement of the molecular structures proposed in Chapters 2 and 3.

For the untreated humins, the 1D direct excitation (DE) ^{13}C solid-state NMR spectrum showed a typical pattern for oxygen-containing aromatic rings, *i.e.* furans or phenols. The 1D ^{13}C spectrum obtained by cross polarization (CP), showing mainly protonated carbons, provided complementary information. Comparison of the DE and CP spectra confirmed that the observed signals from carbonyl functional groups are caused by ketones and gave additional insight in the substitution pattern of the aromatic rings; most C_α's are non-protonated and thus substituted, while most C_β's are protonated. These results were confirmed by a ^{1}H-^{13}C heteronuclear correlation (HETCOR) spectrum recorded with a short contact time. When a longer contact time was employed, long-range correlations between C_α's and aliphatic protons were observed as well, which indicates that C_α's are substituted with aliphatic groups and points at the presence of furanics rather than phenolic rings. C-C correlations were studied by Double Quantum Single Quantum (DQSQ) experiments after CP and DE that confirmed the furanic nature of the humins. In addition, different linkages could be identified, of which C_α-$C_{aliphatic}$ and C_α-C_α are the most abundant, C_β-C_β cross-links and C_β-$C_{aliphatic}$ cross-links being detected in minor amounts. The C-C correlations between the aliphatic carbons furthermore indicated that the linkers are not simply methylene groups, but rather are short chains. The spectrum finally showed that some LA, formed during acid-catalyzed conversion of sugars, was incorporated in the molecular structure through covalent bonds (Figure 7.3A).

The ^{13}C-labeled humins were subjected to alkaline treatment as described in Chapter 3. The 1D DE ^{13}C NMR spectrum of the alkali-treated humins gave a first indication of the formation of an arene-rich structure. Due to the small amount of protonated carbons present in the structure, the CP DQSQ spectrum provided little structural information about the aromatic region, though. The (low intensity) C_α-C_β correlations seen in the DE DQSQ spectrum indicate the presence of (benzo)furanic rings or phenolics. These two could, however, not be distinguished as the typical signals of such groups were overlapped by the strong signals from the arene rings that formed during alkaline treatment. In addition, a large increase in carboxylic acids was observed, which confirmed the results described in Chapter 3. Correlations between the aromatic and aliphatic carbons were not observed, meaning that the aliphatic and aromatic carbons are located far from each other, while C=O functional groups are located on the aliphatic carbon atoms. This data confirmed that upon alkaline pretreatment an arene-rich structure is formed at the expense of the furan content. Taken together, these observations allowed a molecular structure to be proposed for alkali-treated humins (Figure 7.3B).

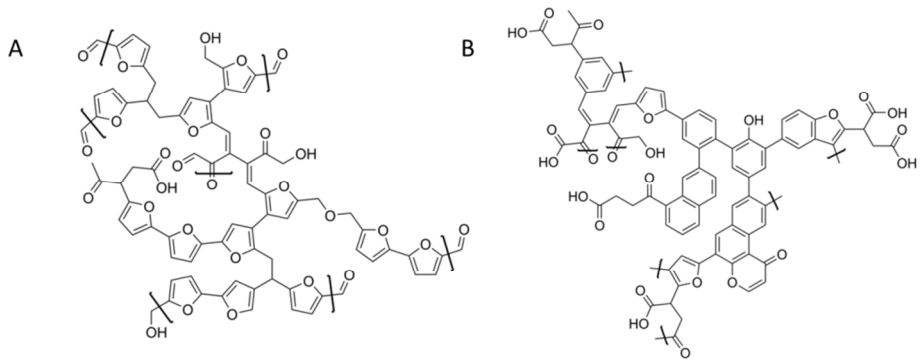

Figure 7.3. Proposed chemical structures of A. humins and B. alkali-treated humins based on an extensive NMR study of ^{13}C-labeled glucose-derived humins as described in Chapter 4.

The humins described in the previous chapters were submitted to a catalytic valorization step in **Chapter 5**. Here, the first example of the APR of humin by-products aimed at the production of aromatic monomers and hydrogen using different Pt-based heterogeneous catalysts is presented. Glucose-derived humins were first solubilized by the alkaline treatment that is described in Chapter 3. The APR reactions were performed at 225-250 °C and pH 9-11 for 20 h in a batch autoclave. Low APR activity was observed at 225 °C over Pt/Al_2O_3 as only small amounts of humin-oil were formed and some H_2, CH_4 and CO_2 was detected. As a similar reduction in Mw was seen for the blank reaction, run without a catalyst, humin depolymerization is considered to be mainly a thermal process at this temperature. After APR at 250 °C, increased gas and oil yields up to 7 bar and 4 wt% were found, respectively. Upon APR a decrease in the pH of the reaction mixture was observed, which might be the result of the formation of organic acids or CO_2.

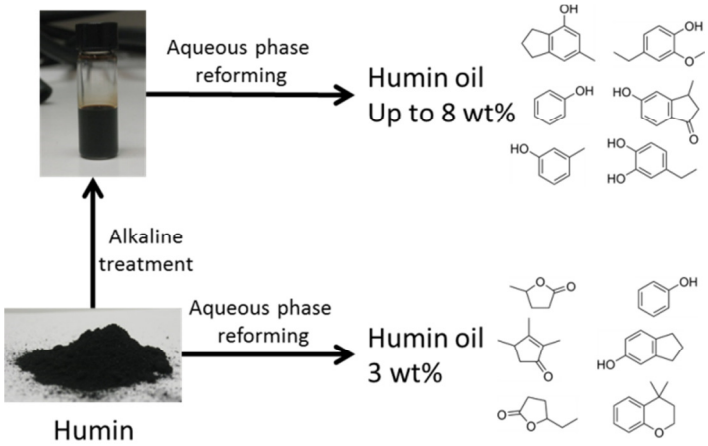

Figure 7.4. Compounds detected in humin oil after APR of glucose-derived humins with and without alkaline pretreatment as described in Chapter 5.

With the more water-stable Pt/TiO_2 catalyst more gas was formed, yet at the expense of more extensive coke formation. This reaction was repeated at pH 11 to evaluate the effect of the drop in pH that was typically seen for the humin APR reactions. Although less coke formation was observed, gas production dropped by half for the reaction run at high pH. The use of the bimetallic catalyst $Pt\text{-}Re/ZrO_2$ resulted in increased yields of 14 bar gas and 8 wt% of humin-oil. GCxGC-MS analysis showed the humin-oils to mainly contain phenolics and ketones with aliphatic carboxylic acids and paraffins being identified as minor products. When solid humins, *i.e.* without being subjected to alkaline pretreatment prior to APR, were directly used in an APR reaction over Pt/TiO_2 under otherwise identical conditions, 3 wt% of oil was formed, while gas yields were comparable to that of the alkali-treated humin. The GCxGC-MS detected more furan-derived compounds after APR of these untreated humins, which supports the furanic nature of the humins molecular structure. The products formed from both types of humin correlate with the differences in molecular structure, with the alkaline pretreatment changing a more furan-based one into one that is more arene-based in nature (Figure 7.4). The data demonstrated that humin-oils can be produced, yet conditions of higher severity are required to improve the yields. Indeed, reaction temperature and the extent of C-C bond cleavage are considered key factors for catalytic conversion of humins to chemicals and fuel components.

In **Chapter 6** thick juice, a sucrose-containing liquor, was used to study the acid-catalyzed conversion of real, biorefinery-derived sugar feeds for the production of HMF and LA. Remarkably, the acid-catalyzed conversion of thick juice with 0.5 M sucrose and 0.01 M H_2SO_4 at 180 °C for 6 h exclusively yielded HMF as liquid phase product. In stark contrast, LA was obtained almost selectively from pure sucrose under the same processing conditions. Furthermore, about 50 wt% less insoluble humins were formed from thick juice compared to reactions with pure sucrose. A maximum in HMF yield was observed at 4-6 h reaction time in the thick juice reaction. The build-up of HMF was, however, accompanied by an increased humin yield at increased reaction times (up to 16 h) and temperature (up to 220 °C). Furthermore, a selectivity switch was observed at increased acid concentrations of 0.1 M, with LA instead of HMF now being obtained as the main product from the thick juice. This selectivity switch can be explained in terms of the buffer function of the thick juice. This buffer capacity is (in part) the result of the carbonates that have formed in the thick juice during the sugar beet purification process by addition of $Ca(OH)_2$ and CO_2. During this process, most of the inorganic impurities and amino acids are included in the precipitating $CaCO_3$ and can thus be separated out. The importance of the carbonate buffer was exemplified by the observation that $CaCO_3$ added to a pure sucrose dehydration reaction indeed partially prevented rehydration of HMF to LA.

The buffer function of thick juice furthermore limited the formation of solid humins and influenced the concentration of different intermediates involved in humin

formation. This was reflected in the molecular structure of the thick juice humins, which is shown to be more conjugated by ^{13}C solid-state NMR. In line with the key role the carbonate buffer plays in thick juice, the humins derived from a reaction run at a higher acid content that exceeded the buffer function were found to be more similar to the humins obtained from pure sugars. In addition, the ATR-IR spectra and elemental composition of humins from thick juice prepared at different conditions indicate further dehydration of the humins at more severe processing conditions. Elemental analysis also proved that incorporation of nitrogen-containing compounds occurred at an early stage of humin formation. It can be concluded that thick juice is a promising feed for the production of HMF in good yields, at moderate conditions and without the need for the alternative solvents, heavy metal ions or ionic liquids that are typically required in literature.

Concluding Remarks

This PhD thesis describes the first steps towards catalytic valorization of humin by-products formed during the acid-catalyzed dehydration of carbohydrates. The obtained insight in the molecular structure, chemical properties, solubilization and reactivity contributes to better understanding of the humins and their formation mechanism. This is valuable knowledge for the optimization of biorefinery operations and will aid further valorization of the humin by-product. Based on the presented data some general conclusions, recommendations and future perspectives are presented.

Humins are complex, recalcitrant, sugar-derived polymers of which the chemical properties and molecular structure strongly depend on feed and processing conditions (**Chapter 2, 4 and 6**). Characterization of the material is challenging due to its limited solubility and heterogeneous structure. Furthermore, the chemical and physical properties of the material change easily when heated making it the difficult to handle and precluding the use of analytical methods using high energy excitation sources, such as (UV-)Raman. Humins can be studied by elemental analysis, IR, solid-state NMR and pyrolysis-GC-MS. In addition, 2D solid-state NMR of ^{13}C-enriched humins has shown to be an effective tool for structure elucidation and allowed us to distinguish between phenol, furan and polycyclic aromatic systems (**Chapter 4**). These studies could be extended by selectively studying interactions between non-protonated carbon atoms giving more insight in cross-links in the molecular structure of the humins and formation of arene structures during the alkaline pretreatment of humins.[3] Preparation of humins from differently labeled ^{13}C or ^{2}D glucose (or fructose) can contribute to better understanding of the mechanisms of humin formation and identification of specific linkages in its molecular structure.[4,5]

As reported in **Chapter 2**, humin formation can be limited by careful selection of the process parameters; a high LA yield and low humin yield were obtained at low reaction temperatures and high acid concentrations. This often involves prevention of solid humin formation by controlling the solubility and size of the water-soluble,

oligomeric humin precursors. This can, for example, be done by using different solvents or biphasic systems. Humin formation and oligomer formation can, however, not be completely excluded as sugar dehydration, HMF rehydration and humin formation are all acid-catalyzed reactions. It was furthermore shown that humins are formed *via* a complex network of reactions involving several reaction intermediates that is still poorly understood. Regarding the furan-rich nature of the humins, HMF seems to play a key role in humin formation. In addition, a limited amount of LA can be chemically bonded to the structure (**Chapter 4**).

As humin formation, be it insoluble or not, cannot be completely avoided, humin valorization strategies to chemicals or fuels need to be developed to obtain efficient biorefinery processes. Humin valorization over (heterogeneous) catalysts is, however, hampered by the humins' low solubility and high recalcitrance. The solubility of the humins can be increased by reactive solubilization in 0.5 M NaOH at 240 °C, but this method strongly changes the molecular structure (**Chapter 3 and 4**). Elemental analysis, IR and (1D and 2D) solid-state NMR spectroscopy are shown to be very useful tools to identify changes in the molecular structure of the humins. The observed aromatization of the humins upon alkaline treatment could lower their reactivity, but better substrate-catalyst interactions are expected when the humins are in solution. There are several alternative options to improve the catalyst-substrate interaction without reactive solubilization of the humins, including the use of metal nanoparticles or impregnation of the humins with a catalyst. These strategies will, however, complicate catalyst regeneration.

The APR experiments have shown that aromatics and limited amounts of hydrogen can be produced from humins with and without alkaline pretreatment (**Chapter 5**). The temperature at which these reaction were run was found to be a limiting factor for further depolymerization of the humins, however. In particular, given the molecular structures presented in **Chapter 2-4**, catalytic valorization of humins requires more C-C bond cleavage, a requirement that should be taken into account when choosing a catalyst. In order to obtain complete valorization of the humins, residues after catalysis could be gasified to produce hydrogen for hydrotreatment of the humins.

Given the high recalcitrance and limited solubility of the humins, selective, catalytic conversion to chemicals might not be the most efficient route for their valorization and, due to their complex molecular structure, a humin-oil that requires further upgrading will be obtained. Alternatively, thermochemical routes might be more suitable for the conversion of humins to a broader scale of products. These routes include (catalytic) pyrolysis[6] and gasification,[7,8] which are recently reported in literature. The potential of the latter route is limited by the humins' low hydrogen content, though. The first experimental studies on the pyrolysis of humins, on the other hand, already yielded 30% of volatiles.[6] In addition, humins could be applied as functional material[9] or as active carbon materials.[10] The latter was suggested for hydrothermal carbons (HTC),

which are used for the adsorption metal ions and organic contaminants from waste water streams[11–13] or as support for carbon-based catalysts.[14] In addition nitrogen-containing HTC are reported to have interesting energy storage properties.[15] Here, the nitrogen-containing humins from thick juice or other amino acid-containing feeds could find application. Another option that is studied is the use of humins as a soil additive to contribute to soil improvement and carbon sequestration.[16–18]

In current biorefinery processes humins are regarded as waste and burned for the production of energy.[19] Regardless of the efforts aimed at the prevention or reduction of humin formation, one can expect that biorefinery processes will produce a certain amount of humins, at least on the short to mid-term. Consequently, humins should be regarded as a recalcitrant fraction of biomass that requires valorization to valuable products. In this sense, the analogy can be made with efforts made for the structural characterization and (catalytic) valorization of lignin. Lignin is a complex, aromatic biopolymer that was extensively characterized to obtain insight in its biosynthesis and molecular structure, especially with regard to the distribution of different linkages. For lignin, insights in the molecular structure has spurred the development of pretreatments methods, depolymerization procedures, catalytic reactions and (chemo)thermal processes for its valorization.[20–22] In comparison, humin valorization is still in its infancy, with only few characterization[1,2,23] and valorization[6–9] efforts having been reported so far. It can nevertheless be expected that the increasing interest in the replacement of fossil fuel will increase these efforts and will eventually lead to the development of efficient processes for the valorization of humins.

References

[1] S. K. R. Patil, C. R. F. Lund, *Energy Fuels* **2011**, 25, 4745–4755.
[2] S. K. R. Patil, J. Heltzel, C. R. F. Lund, *Energy Fuels* **2012**, 26, 5281–5293.
[3] R. L. Johnson, J. M. Anderson, B. H. Shanks, X. Fang, M. Hong, K. Schmidt-Rohr, *J. Magn. Reson.* **2013**, 234, 112–124.
[4] N. Baccile, G. Laurent, F. Babonneau, F. Fayon, M. M. Titirici, M. Antonietti, *J. Phys. Chem. C* **2009**, 113, 9644–9654.
[5] G. R. Akien, L. Qi, I. T. Horváth, *Chem. Commun.* **2012**, 48, 5850–5852.
[6] C. B. Rasrendra, M. Windt, Y. Wang, S. Adisasmito, I. G. B. N. Makertihartha, E. R. H. van Eck, D. Meier, H. J. Heeres, *J. Anal. Appl. Pyrolysis* **2013**, 104, 299–307.
[7] T. M. C. Hoang, L. Lefferts, K. Seshan, *ChemSusChem* **2013**, 6, 1651–1658.
[8] T. M. C. Hoang, E. R. H. van Eck, W. P. Bula, J. G. E. Gardeniers, L. Lefferts, K. Seshan, *Green Chem.* **2014**, DOI 10.1039/C4GC01324G.
[9] J. M. Pin, N. Guigo, A. Mija, L. Vincent, N. Sbirrazzuoli, J. C. van der Waal, E. de Jong, *ACS Sustainable Chem. Eng*. **2014**, 2, 2182–2190.
[10] R. Azargohar, A. K. Dalai, *Appl. Biochem. Biotechnol*. **2006**, 131, 762–73.
[11] P. Regmi, J. L. Garcia Moscoso, S. Kumar, X. Cao, J. Mao, G. Schafran, *J. Environ. Manag.* **2012**, 109, 61–69.
[12] S. Kumar, V. A. Loganathan, R. B. Gupta, M. O. Barnett, *J. Environ. Manag.* **2011**, 92, 2504–2512.
[13] Z. Liu, F.-S. Zhang, *Desalination* **2011**, 267, 101–106.
[14] K. Nakajima, M. Hara, *ACS Catal*. **2012**, 2, 1296–1304.
[15] N. Baccile, G. Laurent, C. Coelho, F. Babonneau, L. Zhao, M. M. Titirici, *J. Phys. Chem. C* **2011**, 115, 8976–8982

[16] M. M. Titirici, R. J. White, C. Falco, M. Sevilla, *Energy Environ. Sci*. **2012**, 5, 6796–6822.
[17] C. J. Ennis, A. G. Evans, M. Islam, T. K. Ralebitso-Senior, E. Senior, *Crit. Rev. Environ. Sci. Technol.* **2012**, 42, 2311–2364.
[18] A. Gajić, H. J. Koch, B. Märländer, *Zuckerindustrie* **2011,** 136, 791–799.
[19] D. J. Hayes, J. Ross, M. H. B. Hayes, S. W. Fitzpatrick, in *Biorefineries* - Industrial Processes and Products (Eds.: B. Kamm, P.R. Gruber, M. Kamm), Wiley, **2006**, 139–164.
[20] J. Zakzeski, P. C. A. Bruijnincx, A. L. Jongerius, B. M. Weckhuysen, *Chem. Rev.* **2010**, 110, 3552–3599.
[21] A. J. Ragauskas, G. T. Beckham, M. J. Biddy, R. Chandra, F. Chen, M. F. Davis, B. H. Davison, R. Z. Dixon, P. Gilna, M. Keller, P. Langan, A. K. Naskar, J. N. Saddler, T. J. Tschaplinski, G. A. Tuskan, C. E. Wyman, *Science* **2014**, 344, 1246843–1–10.
[22] H. Wang, M. Tucker, Y. Ji, *J. Appl. Chem.* **2013**, 2013, 1–9.
[23] I. V. Sumerskii, S. M. Krutov, M. Y. Zarubin, *Russ. J. Appl. Chem*. **2010**, 83, 320–327.

Samenvatting en Slotbeschouwing

Samenvatting

De combinatie van een tekort aan fossiele brandstoffen en een toenemende vraag naar energie stimuleert in belangrijke mate de ontwikkeling van alternatieve bronnen voor de productie van chemicaliën en brandstoffen. Biomassa is de enige hernieuwbare bron van koolstof, die momenteel beschikbaar is als duurzaam alternatief voor de productie van chemicaliën en brandstoffen. De zoektocht naar efficiënte processen voor de omzetting van biomassa heeft geleid tot de ontwikkeling van zogenaamde bioraffinaderijen. De eerste-generatie bioraffinaderijen maken gebruik van die delen van de plant die weliswaar chemisch makkelijk om te zetten zijn, maar ook als voedsel kunnen dienen. Om deze competitie met de voedselvoorziening te voorkomen, moet men meer en meer gebruik gaan maken van de onverteerbare delen van de plant. Deze onverteerbare delen bestaan voornamelijk uit lignocellulose, een combinatie van de componenten cellulose, hemicellulose en lignine, en vormen de grondstof voor tweede-generatie bioraffinaderijen. Een mogelijke route voor de productie van bulkchemicaliën uit deze lignocellulose is de zuur-gekatalyseerde dehydratatie van de (hemi)cellulose. Deze suikerpolymeren worden dan eerst gehydrolyseerd tot individuele suikermoleculen; glucose (C_6) uit cellulose en een mengsel van C_5- en C_6-suikers uit hemicellulose. De C_6- en C_5- suikers kunnen vervolgens worden gedehydrateerd tot, respectievelijk, hydroxymethylfurfural (HMF) en furfural (FF). HMF kan onder zure condities ook nog gemakkelijk worden gerehydrateerd tot levulinezuur (LA) en mierenzuur. Deze chemische bouwstenen kunnen dan verder worden toegepast voor de productie van allerlei polymeren, brandstoffen en chemicaliën.

Een groot nadeel van deze zuur-gekatalyseerde suikeromzettingen is dat HMF en FF polymerisatiereacties kunnen aangaan met verschillende tussenproducten van de dehydratatiereactie, wat leidt tot de vorming van zogenaamde humines. De vorming van deze koolstofrijke, onoplosbare bijproducten beperkt de opbrengst van het proces en daarmee de economische haalbaarheid van een bioraffinaderij. Om dit te verbeteren kan men de vorming van humine proberen te voorkomen of de humines zelf proberen om te zetten naar waardevolle chemicaliën, bijvoorbeeld met behulp van een katalysator. Voor beide strategieën is echter inzicht nodig in de vorming en de moleculaire structuur van de humines. Echter, een eenduidig structuurvoorstel voor humines is nog niet beschikbaar in de literatuur. De optie om de humines om te zetten met een (heterogene) katalysator wordt verder nog bemoeilijkt door de onoplosbaarheid van het materiaal. Dit bemoeilijkt de interactie tussen substraat en een (heterogene) katalysator en kan de activiteit beperken.

Het werk dat beschreven wordt in dit proefschrift heeft als doel de vorming, chemische eigenschappen en structuur van humines beter te begrijpen. Deze kennis kan bijdragen aan het beperken van huminevorming en aan de valorisatie van humines naar chemicaliën. Om het laatste te bereiken worden de belangrijkste obstakels aangepakt: ten eerste is meer inzicht gekregen in de chemische structuur van humines. Ten tweede is de oplosbaarheid van humines verbeterd door een alkalische voorbehandeling, waarna de humines met behulp van een heterogene Pt katalysator omgezet konden worden naar kleine hoeveelheden chemicaliën en waterstof. Ten slotte is ook aangetoond dat ruwe suikerstroop met een hoog sucrosegehalte, diksap, een grondstof met potentie is voor de productie van HMF met een hoge selectiviteit onder milde condities.

Hoofdstuk 2 beschrijft de karakterisering van humines uit verschillende suikers met behulp van verschillende analytische en spectroscopische technieken. Op deze manier is inzicht verkregen in de vorming, morfologie en moleculaire structuur van de humines. Glucose, fructose en xylose en mengsels van deze suikers werden zes uur verhit tot 180 °C in een waterige oplossing in aanwezigheid van 0.01 M H_2SO_4. Uit analyse van de vloeistoffase bleek dat voornamelijk LA werd gevormd uit C_6-suikers, terwijl FF het belangrijkste product uit C_5-suikers is. De hoogste humineopbrengst werd verkregen na dehydratatie van fructose. Dit komt mogelijk doordat HMF, een belangrijke precursor voor humines, snel gevormd wordt uit deze suiker. Dat de humineopbrengst uit xylose slechts enkele procenten hoger dan uit glucose was, is opmerkelijk omdat tijdens de dehydratatie van xylose een hoge concentratie FF (i.p.v. LA) opgebouwd wordt. Blijkbaar polymeriseert FF minder snel tot humines en vormt het minder snel organische zuren dan HMF. Analyse van de vloeistoffase na reactie met GelPermeatieChromatografie (GPC) en elementanalyse (na drogen) liet zien dat er ook wateroplosbare oligomeren aanwezig zijn, die gezien kunnen worden als voorlopers van de onoplosbare humines.

De invloed van eventuele tussenproducten op huminevorming werd getest door het toevoegen van HMF of 1,2,4-trihydroxybenzeen (TB) tijdens de dehydratatie van glucose. Het toevoegen van HMF (molverhouding suiker:HMF 1:0,2) veranderde weinig aan de producten of gevormde humines. De huminevorming nam daarentegen toe terwijl de LA-opbrengst afnam wanneer TB (molverhouding suiker:TB 1:0,2 en 1:0,01) werd toegevoegd aan de reactie. Dit molecuul speelt mogelijk een rol als *crosslinker* in de structuur van humines. Dit experiment laat verder zien dat humines niet alleen worden gevormd door aldolcondensaties, zoals Lund *et al.* hebben voorgesteld,[1,2] maar dat ook andere reactiepaden bijdragen aan de polymerisatie en huminevorming.

Met behulp van de methode *Design of Experiment* (DoE) is de invloed van zuurconcentratie (0-0,13 M), suikerconcentratie (0,66-0.2,34 M) en reactietemperatuur (113-247 °C) op de vorming van humine uit glucose bestudeerd. Deze data toont aan dat huminevorming het sterkst afhankelijk is van de zuurconcentratie, gevolgd door de reactietemperatuur. De suikerconcentratie heeft statistisch gezien echter geen invloed op

de huminevorming. De data laat ook zien dat de reactiecondities die leiden tot vorming van veel humines tegengesteld zijn aan de condities die leiden tot de vorming van LA.

Elektronenmicroscopie heeft laten zien dat humines een bolvormige morfologie hebben die sterk afhangt van de reactiecondities en suikers. Zo bestaan de humines gevormd uit glucose bijvoorbeeld uit onderling verbonden deeltjes met een diameter van 3-5 µm (Figuur 7.1). Uit xylose worden juist geïsoleerde bolletjes gevormd. Het was opmerkelijk dat bij een hoge concentratie toegevoegd TB kleinere, geïsoleerde deeltjes gevormd worden. Op basis van elementanalyse aan de humines is een van Krevelen plot geconstrueerd die aangeeft dat humines via dehydratiereacties worden gevormd. Een combinatie van IR, ^{13}C vaste stof NMR en pyrolyse-GC-MS verschafte meer inzicht in de molecuulstructuur van de humines. Deze data heeft aangetoond dat humines furaanrijke polymeren zijn met alcoholen, carbonzuren, aldehydes en ketonen als functionele groepen. De NMR spectra duiden ook op de aanwezigheid van alifatische ketens tussen de furaanringen. Verder bleek de molecuulstructuur sterk afhankelijk van de gebruikte uitgangsstof. Uit de NMR spectra bleek bijvoorbeeld dat humines uit xylose een meer geconjugeerde structuur hebben, wat te verklaren valt aan de hand van de niet-gesubstitueerde 5-positie van FF. Deze vrije positie maakt het mogelijk om furaanringen direct aan elkaar te verbinden en leidt tot een meer gecondenseerde structuur. Op basis van deze informatie is een voorstel gedaan voor de chemische structuur voor humines uit zowel C_6- als C_5-suikers (Figuur 7.1).

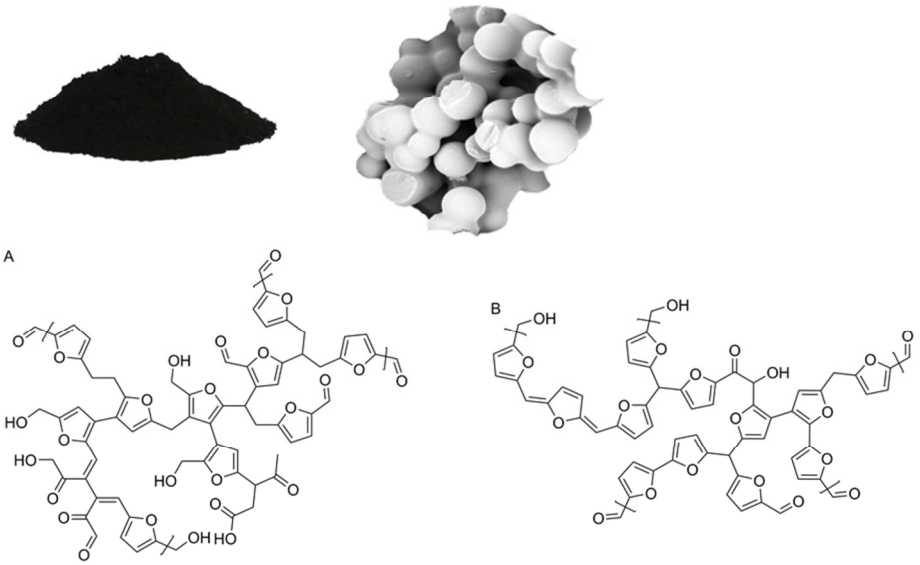

Figuur 7.1. Boven: humine en de morfologie van glucosehumine. Onder: de molecuulstructuren voor A. Glucosehumine en B. Xylosehumine zoals beschreven in Hoofdstuk 2.

In **Hoofdstuk 3** is een alkalische voorbehandeling ontwikkeld om de oplosbaarheid van de humines uit Hoofdstuk 2, te verbeteren. Glucosehumines kunnen worden opgelost met behulp van reactie bij 200 °C in 0.5 M NaOH voor 3,5 uur. Na de alkalische behandeling blijven de humines in oplossing tot pH ≥ 7. GPC metingen toonden de relatieve verandering in het molecuulgewicht na alkalische behandeling onder verschillende condities. Een hogere reactietemperatuur en langere reactietijden leidden tot lagere molecuulgewichten, terwijl een verhoogde baseconcentratie weinig effect had. Humines uit fructose en xylose bleken recalcitranter te zijn en waren pas compleet opgelost na reactie bij een hogere temperatuur van 240 °C. Voor de fructosehumines kwam dit als een verrassing, omdat deze een structuur hebben die vergelijkbaar is met de glucosehumines. Voor de xylosehumines valt de hogere recalcitrantie te verklaren aan de hand van de meer geconjugeerde structuur. Het is gebleken dat de alkalisch behandeling van humines een efficiënte methode is om de humines volledig op te lossen, al gaat dit gepaard met een verandering in chemische structuur.

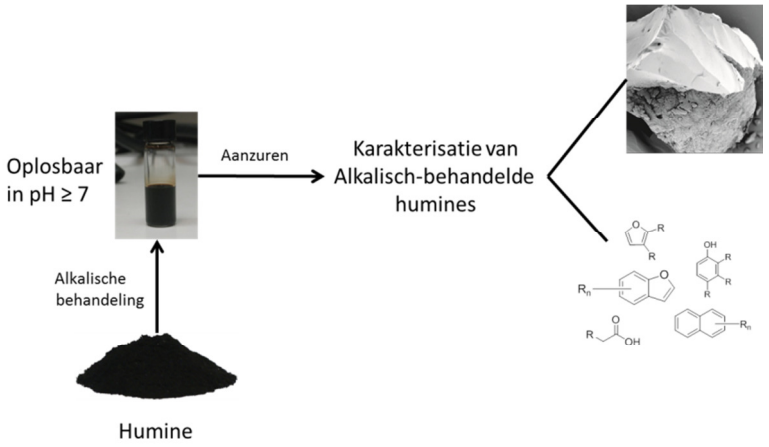

Figuur 7.2. De alkalische behandeling van humines en de morfologie en structuren die aanwezig zijn in de teruggewonnen humines zoals beschreven in Hoofdstuk 3.

Voor verdere karakterisering werden de alkalisch behandelde humines neergeslagen door de oplossing aan te zuren. Vervolgens zijn de humines geïsoleerd, gewassen en gedroogd. Elektronenmicroscopiemetingen lieten zien dat de bolvormige morfologie van de humines volledig verloren is gegaan (Figuur 7.2). Aan de hand van de elementsamenstelling van de behandelde humines is een van Krevelenplot geconstrueerd. Uit deze plot bleek dat de humines aromatischer van structuur worden door dehydratatiereacties en verlies van CO tijdens de alkalische behandeling. Analyse van de behandelde humines met behulp van IR, ^{13}C vaste stof NMR en pyrolyse-GC-MS liet zien dat de humines inderdaad een meer (polycyclische) aromatische structuur hebben gekregen (Figuur 7.2). Deze structuurverandering is mogelijk het gevolg van een

combinatie van Diels-Alder en dehydratiereacties. De veranderingen die ook werden gezien in het alifatische deel van de structuur kunnen het gevolg zijn van het openen van de furaanring. De alkalische behandeling resulteerde verder in een afname in ketonen en een toename in carbonzuren. Dit laatste kan de verbeterde oplosbaarheid van de humines in basische oplosmiddelen deels verklaren. De afname in het molecuulgewicht van de humines kan deels verklaard worden aan de hand van het breken van C-O-C bindingen waarvan kleine hoeveelheden in de originele humines aanwezig zijn.

In **Hoofdstuk 4** wordt moleculaire structuur van de (alkalisch-behandelde) humines die beschreven is in Hoofdstuk 2 en 3 verder onderzocht met behulp van vaste stof NMR technieken. Een combinatie van complementaire 1D en 2D ^{13}C vaste stof NMR spectra van de ^{13}C-verrijkte humines heeft nieuwe inzichten gegeven in de moleculaire structuur van deze complexe, heterogene materialen en heeft geleid tot een verfijning van de molecuulstructuur die eerder was voorgesteld.

Voor de onbehandelde humines gaf het 1D ^{13}C NMR spectrum, na directe excitatie van de ^{13}C (DE), een patroon dat kenmerkend is voor aromatische ringen met zuurstofgroepen, ofwel gesubstitueerde furanen en fenolen. Wanneer de C-atomen worden aangeslagen via crosspolarisatie (CP) worden voornamelijk de geprotoneerde C-atomen in het spectrum weergeven. De DE en CP 1D ^{13}C NMR spectra zijn vergeleken wat er op duidde dat de signalen van carbonylgroepen toegeschreven kunnen worden aan ketonen. Verder bleek hieruit dat de C_α's niet geprotoneerd en dus gesubstitueerd zijn terwijl de C_β's wel geprotoneerd zijn. Deze observaties werden bevestigd met een ^{1}H-^{13}C correlatie (HETCOR) spectrum met een korte contacttijd. Wanneer een langere contacttijd werd toegepast, werden er correlaties tussen C_α's en alifatische protonen waargenomen wat erop wijst dat de C_α's verbonden zijn met de alifatische groepen. Dit duidt ook op de aanwezigheid van furaanringen i.p.v. fenolen. De C-C correlaties zijn verder bestudeerd aan de hand van Double-Quantum Single-Quantum (DQSQ) NMR spectroscopie waarmee de furaanrijke-structuur van de humines werd bevestigd. Verder konden verschillende verbindingen tussen de furaanring geïdentificeerd worden waarvan C_α-C_α en C_α-$C_{alifatisch}$ het meest voorkomen. In mindere mate zijn ook C_β-C_β crosslinks en C_β-$C_{alifatisch}$ gedetecteerd (Figuur 7.3A).

^{13}C-gelabelde humines zijn ook behandeld met alkali, zoals beschreven in **Hoofdstuk** 3. Het 1D DE ^{13}C spectrum liet al zien dat tijdens de alkalische behandeling een meer areenrijke structuur gevormd wordt. Het 1D CP ^{13}C spectrum bevatte echter weinig structuurinformatie in het aromatische gebied door de beperkte hoeveelheid protonen in de alkalisch-behandelde humines. De C-C correlaties werden verder bestudeerd met DE DQSQ waarin nog steeds C_α-C_β correlaties werden gedetecteerd maar door de overlappende signalen van de areenringen kon het onderscheid tussen fenol, furaan en benzofuraan nu niet worden gemaakt. De toename in de hoeveelheid carbonzuren die

was waargenomen voor de humines beschreven in Hoofdstuk 3 kon inderdaad worden bevestigd. Correlaties tussen de aromatische en alifatische groepen werden niet gezien, wat betekent dat deze groepen ver van elkaar liggen. De C=O groepen daarentegen bleken verbonden te zijn met de alifatische groepen. Deze data bewijst dat tijdens de alkalische behandeling van humines een areenrijke structuur wordt gevormd ten koste van de furaanringen. Op basis hiervan kon een voorstel voor de molecuulstructuur voor de humines na alkalische behandeling worden gemaakt (Figuur 7.3B).

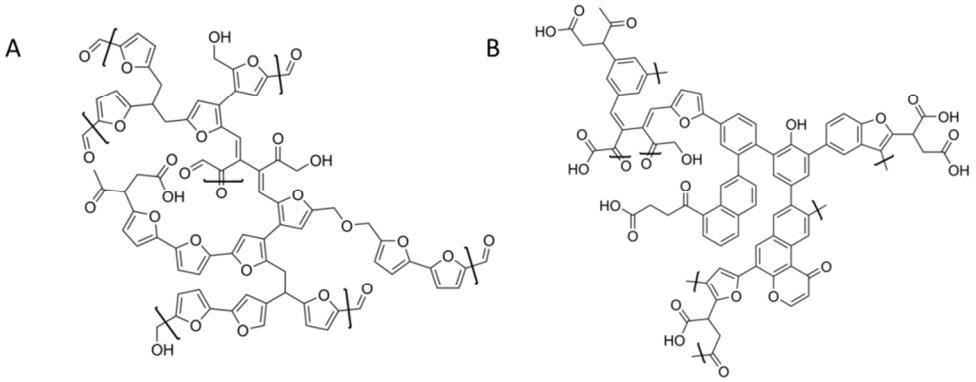

Figuur 7.3. Moleculaire structuur van A. Glucosehumine en B. Alkalisch behandelde glucosehumines op basis van verschillende NMR spectra van ^{13}C-verrijkte glucosehumines zoals beschreven in Hoofdstuk 4.

De katalytische omzetting van de humines wordt beschreven in **Hoofdstuk 5.** In dit hoofdstuk wordt het eerste voorbeeld gepresenteerd van de omzetting van humines naar aromaten en waterstof in de waterfase met behulp van gedragen Pt-katalysatoren, dit proces wordt ook wel *Aqueous Phase Reforming* (APR) genoemd. Glucosehumines werden eerst behandeld met base, zoals beschreven in Hoofdstuk 3. De APR reacties zijn vervolgens uitgevoerd bij 225-250 °C en pH 9-11 in een batchautoclaaf gedurende 20 uur. De lage APR activiteit van de Pt/Al_2O_3 bleek uit de beperkte hoeveelheid olie en gassen (H_2, CH_4 en CO_2) die waren gevormd. De afname in molecuulgewicht was vergelijkbaar met de blanco reactie (zonder katalysator), wat erop duidt dat de depolymerisatie voornamelijk een thermisch effect is bij deze temperatuur. Na een APR reactie bij 250 °C waren de gas- en olieopbrengst toegenomen tot, respectievelijk, zeven bar en vier gewichtsprocent. De afname in de pH van het reactiemengsel die werd gemeten wordt waarschijnlijk veroorzaakt door de vorming van organische zuren of CO_2.

Het gebruik van Pt/TiO_2, een katalysator die stabieler is in water dan Pt/Al_2O_3, leidde tot meer gasopbrengst maar ook tot meer asvorming. Een reactie met deze katalysator bij pH 11, met als doel het effect van de pH afname te bestuderen, leidde tot de vorming van minder as maar ook tot halvering van de gasproductie. Het effect van het gebruik van een legering is getest met $Pt\text{-}Re/ZrO_2$ als katalysator wat leidde tot een

hoge gasopbrengst van 14 bar en een olieopbrengst van 8 gewichtsprocent. GCxGC-MS analyse aan de olie toonde aan dat deze voornamelijk fenolen en ketonen bevat, verder waren carbonzuren en paraffines in kleinere hoeveelheden gevormd. Ter vergelijking zijn de humines ook direct, d.w.z. zonder alkalische voorbehandeling, omgezet met Pt/TiO_2. Dit gaf een vergelijkbare gasopbrengst als de alkalisch-behandelde humines terwijl de olieopbrengst iets af nam. Met behulp van GCxGC-MS werden voornamelijk furaanafgeleide producten gedetecteerd wat de voorgestelde furaanrijke structuur van humines verder ondersteunt. De producten die gevormd worden uit beide humines zijn te relateren aan verschillen in de molecuulstructuur (Figuur 7.4). Tijdens de alkalische behandeling verandert de furaanrijke structuur immers in een meer areenrijke structuur. Deze experimenten tonen duidelijk aan dat de reactietemperatuur en het breken van voldoende C-C bindingen bepalende factoren zijn voor de katalytische omzetting van humines naar chemicaliën en brandstoffen.

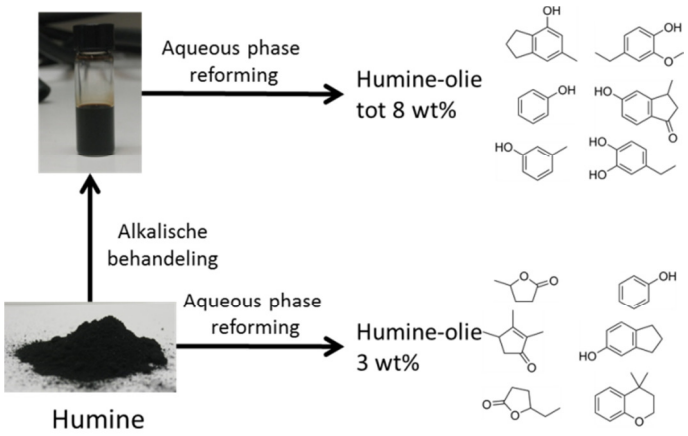

Figuur 7.4. Samenstelling van de humine-olie die gevormd wordt tijdens de APR reactie op humines en alkalische behandelde humines zoals beschreven in Hoofdstuk 5.

In **Hoofdstuk 6** is diksap, een industrieel tussenproduct uit de suikerraffinage met een hoog sucrosegehalte, gebruikt als grondstof voor de zuur-gekatalyseerde vorming van LA en HMF. Dit is een voorbeeld van hoe ruwe suikerstromen gebruikt kunnen worden voor de productie van bulkchemicaliën. De dehydratatie van pure sucrose met 0,5 M sucrose en 0,01 M H_2SO_4 bij 180 °C voor 6 uur gaf LA als hoofdproduct. Het was zeer opmerkelijk dat uit diksap, onder dezelfde condities, HMF selectief gevormd wordt. Verder werd er een 50% lagere humineopbrengst gevonden in vergelijking met pure sucrose. De maximale HMF-opbrengst uit diksap werd gevonden na een reactietijd van 4-6 uur. De opbouw van HMF in de waterfase leidt uiteindelijk tot een zeer hoge humineopbrengst bij langere reactietijden (16 uur) of hogere reactietempaturen (220 °C). Het verhogen van de zuurconcentratie veranderde de selectiviteit van de reactie en

resulteerde in de vorming van LA als belangrijkste product uit diksap. Deze selectiviteitsverandering kan uitgelegd worden aan de hand van de bufferfunctie van het diksap, die deels veroorzaakt wordt door de aanwezigheid van carbonaten. Deze carbonaten worden gevormd tijdens een zuiveringsstap in de raffinage van suikerbieten waarbij $Ca(OH)_2$ en CO_2 worden toegevoegd. Het doel van deze zuiveringsstap is dat de aminozuren en anorganische onzuiverheden worden neerslagen met het zo gevormde $CaCO_3$. Dat de buffercapaciteit van $CaCO_3$ ook daadwerkelijk een belangrijke rol speelt in de reacties met diksap, werd aangetoond met een dehydratatiereactie van pure sucrose waar $CaCO_3$ aan was toegevoegd. Hierbij werd inderdaad meer HMF en minder LA gevormd.

De bufferfunctie van diksap beperkt de vorming van humines, maar beïnvloedt ook de concentratie van verschillende tussenproducten die leiden tot huminevorming. Dit leidt tot een meer geconjugeerde structuur voor de humines uit diksap, zoals aangetoond met ^{13}C vaste stof NMR. Wanneer de humines worden gevormd bij een zuurconcentratie die de bufferfunctie van het diksap overschrijdt, is het NMR spectrum meer vergelijkbaar met dat van de humines uit pure suikers. Dit klopt met de rol die de carbonaatbuffer heeft tijdens de dehydratie van diksap. Bovendien is met behulp van elementanalyse en IR spectra aangetoond dat de humines verder gedehydrateerd worden bij meer extreme reactiecondities. Elementanalyse toonde ook aan dat de humines uit diksap stikstof bevatten dat afkomstig is van aminozuurresten uit de suikerbiet en dat incorporatie van deze aminozuurresten plaats vindt in een vroeg stadium van de huminevorming. Deze resultaten tonen aan dat diksap een grondstof met potentie is voor de productie van zuivere HMF, zonder dat het nodig is om metalen, organische oplosmiddelen of ionische vloeistoffen te gebruiken, zoals vaak beschreven wordt in de literatuur.

Slotbeschouwing

Dit proefschrift beschrijft de eerste stappen naar de katalytische valorisatie van de humines die gevormd worden tijdens de zuurgekatalyseerde dehydratatie van suikers. De verkregen inzichten in de molecuulstructuur, chemische eigenschappen, oplosbaarheid en reactiviteit van de humine dragen bij aan beter begrip van humines en hoe deze gevormd worden. Dit is belangrijke kennis om bioraffinaderijen efficiënter te maken en de verdere valorisatie van deze bijproducten mogelijk te maken. Op basis van de gepresenteerde resultaten kunnen een aantal algemene conclusies, aanbevelingen en vooruitzichten worden gegeven.

Humines zijn complexe, recalcitrante polymeren die uit suikers gevormd worden en waarvan de chemische eigenschappen en molecuulstructuur sterk afhangen van de grondstof en reactiecondities (**Hoofdstuk 2, 4, en 6**). Het materiaal is moeilijk te karakteriseren door de beperkte oplosbaarheid en heterogene structuur. Verder verandert dit materiaal gemakkelijk wanneer het wordt verwarmd waardoor het lastig te hanteren is. Dit sluit ook verschillende analysemethodes uit die gebruik maken van een

hoge excitatie-energie, zoals (UV) Raman. 2D vaste stof NMR van ^{13}C-gelabelde humines bleek een effectieve methode te zijn voor structuuropheldering en geeft de mogelijkheid om onderscheid te maken tussen fenolen, furanen en polycyclische aromaten. Deze studie kan worden uitgebreid door de correlaties tussen niet-geprotoneerde C-atomen selectief te bestuderen, wat meer inzicht kan geven in de vorming van areenstructuren tijdens de alkalische behandeling van humines.[3] Verder kunnen humines uit glucose of fructose met ^{13}C en D^2 labels of verschillende posities bijdragen aan nieuwe inzichten in de vorming van humines en specifieke verbindingen in de molecuulstructuur.[4,5]

Zoals beschreven in **Hoofdstuk 2** kan huminevorming worden beperkt door de reactiecondities zorgvuldig te kiezen; zo geeft een combinatie van hoge concentratie zuur en lage temperatuur bijvoorbeeld hoge LA opbrengsten en een lage humineopbrengst. Het beperken van de humine opbrengst richt zich meestal op het beïnvloeden van de lengte en oplosbaarheid van de oligomere voorlopers van humines. Dit kan bereikt worden met behulp van bijvoorbeeld organische oplosmiddelen of een tweefasensysteem. De vorming van humines of oligomeren kan echter niet volledig worden voorkomen omdat suikerdehydratatie, HMF rehydratie als huminevorming allen zuurgekatalyseerde reacties zijn. Het is verder aangetoond dat humines gevormd worden via een complex netwerk van reacties waarbij veel tussenproducten betrokken zijn en waar we nog steeds weinig inzicht in hebben. De furaanrijke structuur van de humines wijst er op dat HMF een belangrijke rol speelt in de vorming van humines. Verder is aangetoond dat kleine hoeveelheden LA voorkomen in de structuur via chemische bindingen (**Hoofdstuk 4**).

Omdat huminevorming momenteel niet vermeden kan worden is de omzetting van deze bijproducten naar chemicaliën of brandstoffen wenselijk. De valorisatie van humines met behulp van een (heterogene) katalysator wordt echter bemoeilijkt door de beperkte oplosbaarheid en recalcitrantie van het materiaal. Zoals aangetoond kan de oplosbaarheid van het materiaal verbeterd worden door een reactie in 0,5 M NaOH bij 240 °C. Deze methode leidt echter tot sterke veranderingen in de molecuulstructuur (**Hoofdstuk 3 en 4)**. De vorming van een meer aromatische structuur van de humines na alkalische behandeling zal de reactiviteit verder verlagen, maar vergroot tegelijkertijd de mogelijkheid tot interactie tussen het substraat en de katalysator. Er zijn alternatieven om deze interacties te vergroten, bijvoorbeeld door het gebruik van metallische nanodeeltjes of door de humines te impregneren met het actieve metaal. Deze methodes maken hergebruik van de katalysator echter wel moeilijk.

Met de APR reacties is aangetoond dat een beperkte hoeveelheid aromaten en waterstof geproduceerd kan worden uit humine. Uit deze experimenten bleek ook dat de reactietemperatuur een beperkende factor is voor de katalytische omzetting van humines. Wanneer men kijkt naar de molecuulstructuur van de humines, zowel voor als na alkalische behandeling (**Hoofdstuk 2-4**), is het breken van C-C bindingen een belangrijke

eis wanneer een katalysator gekozen wordt. Het residu dat overblijft na de reactie kan vergast worden om waterstof, wat mogelijk nodig is tijdens de katalyse, te verkrijgen.

Gezien de recalcitrante aard en beperkte oplosbaarheid van de humines is de selectieve, katalytische valorisatie van dit materiaal naar specifieke chemicaliën waarschijnlijk niet de meest efficiënte optie. Ook zal er door de complexe structuur van humines altijd een complexe humine-olie gevormd worden die verder omgezet moet worden naar zuivere componenten. Thermochemische methodes zijn mogelijk ook geschikt voor de conversie van humines naar een breed scala aan producten. (katalytische) pyrolyse[6] en vergassen,[7,8] zijn voorbeelden hiervan en beide methoden zijn recent voor het eerst toegepast op humines. Vergassen lijkt een minder interessante optie vanwege de beperkte hoeveelheid waterstof in de humines. Tijdens verkennende studies naar de pyrolyse van humines werd daarentegen 30% van de humines omgezet vluchtige componenten. Een andere mogelijkheid is om humines te gebruiken in functionele materialen[9] of als actieve kool.[10] Deze laatste toepassing biedt mogelijkheden voor de adsorptie van metaal ionen en organische componenten uit afvalwaterstromen, zoals ook is laten zien met materialen die verkregen zijn via de hydrothermische behandeling van suikers.[11–13] Een andere optie is het functionaliseren van de humines om (dragers voor) katalysatoren te verkrijgen.[14] Verder is er aangetoond dat functionele materialen uit suikers die ook stikstof bevatten interessante eigenschappen hebben voor de opslag van energie. Deze toepassing kan interessant zijn voor de humines gevormd uit diksap of andere suikerstropen met resten van aminozuren. Ten slotte wordt de toepassing van humines als bodemverbeteraar bestudeerd, deze methode draagt ook bij aan de opslag van koolstof (*carbon sequestration*).[16–19]

In de huidige bioraffinaderijen worden humines gezien als afval en verbrand voor warmteproductie. Om een volledig efficiënte bioraffinaderij te verkrijgen moet de vorming van humines worden voorkomen. Een zekere hoeveelheid humines zal echter altijd gevormd worden, omdat zowel suiker dehydratatie, HMF rehydratatie en huminevorming zuurgekatalyseerde reacties zijn. Daarom moeten de gevormde humines gezien worden als een recalcitrante fractie van de biomassa die omgezet moet worden naar meer waardevolle producten. In dit opzicht kan een analogie met ontwikkelingen op het gebied van de karakterisatie en valorisatie van lignine gemaakt worden. Lignine is ook een complex, aromatisch biopolymeer dat uitvoerig geanalyseerd is om inzicht te krijgen in de biosynthese en molecuulstructuur. Dit inzicht heeft de ontwikkeling van voorbehandelingsmethoden, depolymerisatiereacties, katalytische reacties en (chemo-)thermische processen voor de valorisatie van lignine sterk versneld.[20–22] In vergelijking hiermee staat de kennis met betrekking van humines nog in de kinderschoenen en slechts enkele voorbeelden van de karakterisatie[1,2,23] en valorisatie[6–9] van humines zijn tot nu toe gerapporteerd.

Referenties

[1] S. K. R. Patil, C. R. F. Lund, *Energy Fuels* **2011**, 25, 4745–4755.
[2] S. K. R. Patil, J. Heltzel, C. R. F. Lund, *Energy Fuels* **2012**, 26, 5281–5293.
[3] R. L. Johnson, J. M. Anderson, B. H. Shanks, X. Fang, M. Hong, K. Schmidt-Rohr, *J. Magn. Reson.* **2013**, 234, 112–124.
[4] N. Baccile, G. Laurent, F. Babonneau, F. Fayon, M. M. Titirici, M. Antonietti, *J. Phys. Chem. C* **2009**, 113, 9644–9654.
[5] G. R. Akien, L. Qi, I. T. Horváth, *Chem. Commun.* **2012**, 48, 5850–5852.
[6] C. B. Rasrendra, M. Windt, Y. Wang, S. Adisasmito, I. G. B. N. Makertihartha, E. R. H. van Eck, D. Meier, H. J. Heeres, *J. Anal. Appl. Pyrolysis* **2013**, 104, 299–307.
[7] T. M. C. Hoang, L. Lefferts, K. Seshan, *ChemSusChem* **2013**, 6, 1651–1658.
[8] T. M. C. Hoang, E. R. H. van Eck, W. P. Bula, J. G. E. Gardeniers, L. Lefferts, K. Seshan, *Green Chem.* **2014**, DOI 10.1039/C4GC01324G.
[9] J. M. Pin, N. Guigo, A. Mija, L. Vincent, N. Sbirrazzuoli, J. C. van der Waal, E. de Jong, *ACS Sustainable Chem. Eng*. **2014**, 2, 2182–2190.
[10] R. Azargohar, A. K. Dalai, *Appl. Biochem. Biotechnol*. **2006**, 131, 762–73.
[11] P. Regmi, J. L. Garcia Moscoso, S. Kumar, X. Cao, J. Mao, G. Schafran, *J. Environ. Manag.* **2012**, 109, 61–69.
[12] S. Kumar, V. A. Loganathan, R. B. Gupta, M. O. Barnett, *J. Environ. Manag.* **2011**, 92, 2504–2512.
[13] Z. Liu, F.-S. Zhang, *Desalination* **2011**, 267, 101–106.
[14] K. Nakajima, M. Hara, *ACS Catal*. **2012**, 2, 1296–1304.
[15] N. Baccile, G. Laurent, C. Coelho, F. Babonneau, L. Zhao, M. M. Titirici, *J. Phys. Chem. C* **2011**, 115, 8976–8982
[16] M. M. Titirici, R. J. White, C. Falco, M. Sevilla, *Energy Environ. Sci*. **2012**, 5, 6796–6822.
[17] C. J. Ennis, A. G. Evans, M. Islam, T. K. Ralebitso-Senior, E. Senior, *Crit. Rev. Environ. Sci. Technol.* **2012**, 42, 2311–2364.
[18] A. Gajić, H. J. Koch, B. Märländer, *Zuckerindustrie* **2011,** 136, 791–799.
[19] D. J. Hayes, J. Ross, M. H. B. Hayes, S. W. Fitzpatrick, in *Biorefineries* - Industrial Processes and Products (Eds.: B. Kamm, P.R. Gruber, M. Kamm), Wiley, **2006**, 139–164.
[20] J. Zakzeski, P. C. A. Bruijnincx, A. L. Jongerius, B. M. Weckhuysen, *Chem. Rev.* **2010**, 110, 3552–3599.
[21] A. J. Ragauskas, G. T. Beckham, M. J. Biddy, R. Chandra, F. Chen, M. F. Davis, B. H. Davison, R. Z. Dixon, P. Gilna, M. Keller, P. Langan, A. K. Naskar, J. N. Saddler, T. J. Tschaplinski, G. A. Tuskan, C. E. Wyman, *Science* **2014**, 344, 1246843–1–10.
[22] H. Wang, M. Tucker, Y. Ji, *J. Appl. Chem.* **2013**, 2013, 1–9.
[23] I. V. Sumerskii, S. M. Krutov, M. Y. Zarubin, *Russ. J. Appl. Chem*. **2010**, 83, 320–327.

LIST OF ABBREVIATIONS

2D PASS	two-dimensional phase adjusted spinning sideband
APR	aqueous phase reforming
ATR	attenuated total reflection
BPR	back pressure regulator
BuOH	butanol
CP	cross polarization
DE	direct excitation
CSA	chemical shift anisotropy
DHH	2,5-dioxo-6-hydroxy-hexanal
DMA	dimethylacetamide
DCM	dichloromethane
DMF	dimethylformamide
DMSO	dimethylsulfoxide
DOC	dissolved organic carbon
DoE	design of experiment
DOE	US department of energy
DQSQ	double quantum single quantum
EXPANSE	exchange with protonated and non-protonated spectral editing
FA	formic acid
FF	furfural
FT	Fourier transform
GC	gas chromatography
GPC	gel permeation chromatography
HMF	hydroxymethylfurfural
HETCOR	heteronuclear correlation
HTC	hydrothermal carbon
IC	inorganic carbon
IR	infrared spectroscopy
LA	levulinic acid
MAS	magic angle spinning
MIBK	methyl isobutyl ketone
NMP	*n*-methyl-2-pyrrolidone
NMR	nuclear magnetic resonance
MS	mass spectrometry
rf	radio frequency
RID	refractive index detector
SEM	scanning electron microscopy
TB	1,2,4-trihydroxybenzene
TC	total carbon
TCD	thermal conductivity detector
TGA	thermogravimetric analysis
TOSS	total suppression of spinning sidebands
UV	ultra violet
WGS	water-gas shift
XRD	X-ray diffraction

This thesis is based on:

I. van Zandvoort, Y. Wang, C. B. Rasrendra, E. R. H. van Eck, P. C. A. Bruijnincx, H. J. Heeres, B. M. Weckhuysen, "Formation, Molecular Structure, and Morphology of Humins in Biomass Conversion: Influence of Feedstock and Processing Conditions" *ChemSusChem* **2013**, 6, 1745-1758.

I. van Zandvoort, E. R. H. van Eck, P. de Peinder, P. C. A. Bruijnincx, H. J. Heeres, B. M. Weckhuysen "Full, Reactive Solubilization of Humin By-products by Alkaline Treatment and Characterization of the Alkali-treated Humins Formed" *ACS Sustainable Chem. Eng., accepted.*

I. van Zandvoort, E. Koers, P. C. A. Bruijnincx, M. Baldus, B. M. Weckhuysen, "Structural Characterization of ^{13}C-Enriched Humins and Alkali-treated ^{13}C Humins by 2D Solid-state NMR" *submitted for publication.*

I. van Zandvoort, E. J. B. Sirks, E. R. H. van Eck, P. C. A. Bruijnincx, B. M. Weckhuysen, "Unexpected Benefits of Using Real Feeds in Biomass Conversion: High Hydroxymethylfurfural Selectivity and low Humin Formation in the Acid-catalyzed Dehydration of Sugar Beet-derived Thick Juice" *manuscript in preparation.*

Other publications:

J. Beckers, R. Drost, I. van Zandvoort, P. F. Collignon, G. Rothenberg, "Selective Hydrogen Oxidation in the Presence of C_3 Hydrocarbons using Perovskite Oxygen Reservoirs" *ChemPhysChem* **2008**, 9, 1062-1068.

Oral presentations

I. van Zandvoort, Y. Wang, C. B. Rasrendra, E .R. H. van Eck, P. C. A. Bruijnincx, H. J. Heeres, B. M. Weckhuysen, "Towards the Catalytic Conversion of Humin By-products" XIth European Congress on Catalysis, Lyon, France, 3 September 2013.

I. van Zandvoort, Y. Wang, C. B. Rasrendra, E. R. H. van Eck, P. C. A. Bruijnincx, H. J. Heeres, B. M. Weckhuysen, "Towards the Catalytic Conversion of Humin By-products" The Netherlands' Catalysis and Chemistry Conference, Noordwijkerhout, the Netherlands, 12 March 2013.

I. van Zandvoort, Y. Wang, C. B. Rasrendra, E. R. H. van Eck, P. C. A. Bruijnincx, H. J. Heeres, B. M. Weckhuysen, "Towards Catalytic Valorization of Humin By-products Formed during Biomass Processing: Molecular Structure and Chemical Properties" CAT4BIO: International Conference on Advances in Catalysis for Biomass Valorization, Thessaloniki, Greece, 10 July 2012.

I. van Zandvoort, Y. Wang, C. B. Rasrendra, E. R. H. van Eck, P. C. A. Bruijnincx, H. J. Heeres, B. M. Weckhuysen, "Catalytic Routes for the Valorization of Humin By-products formed during Biomass Processing: Molecular Structure and Chemical Properties" The Netherlands' Catalysis and Chemistry Conference, Noordwijkerhout, the Netherlands, 7 March 2012.

Poster presentations

I. van Zandvoort, Y. Wang, C. B. Rasrendra, E. R. H. van Eck, P. C. A. Bruijnincx, H. J. Heeres, B. M. Weckhuysen, "Towards the Catalytic Conversion of Humin By-products" XIth European Congress on Catalysis, Lyon, France, 3 September 2013.

I. van Zandvoort, Y. Wang, C. B. Rasrendra, E. R. H. van Eck, P. C. A. Bruijnincx, H. J. Heeres, B. M. Weckhuysen, "Catalytic Valorization of Humin By-products formed during Biomass Processing: Molecular Structure and Chemical Properties" International Congress on Catalysis, Munich, Germany, 1-6 July 2012.

DANKWOORD

Tijdens mijn promotieonderzoek heb ik veel slimme mensen ontmoet, leuke reizen gemaakt en nieuwe dingen geleerd. In dit, waarschijnlijk meest gelezen, deel van mijn proefschrift zou ik graag iedereen willen bedanken die mij de afgelopen jaren heeft geholpen, gemotiveerd, gesteund of geëntertaind.

Ten eerste wil ik mijn promotor Prof. dr. ir. Bert Weckhuysen noemen. Beste Bert, bedankt dat je mij de mogelijkheid hebt gegeven om mijn promotieonderzoek onder jouw begeleiding uit te voeren. Na mijn sollicitatie moest ik misschien wat langer nadenken maar ik weet zeker dat ik de juiste keuze heb gemaakt. Ik ben je extra dankbaar voor het mogelijk maken van de lange herstelperiode na mijn hersenschudding.

Op mijn eerste dag aan de Universiteit Utrecht kwam ik er achter dat ik ook een copromotor en dagelijks begeleider zou hebben: Dr. Pieter Bruijnincx. Beste Pieter, ik heb erg veel van jou geleerd. Bedankt dat ik altijd bij kon aankloppen (of binnenvallen) voor vragen, discussies, motivatie en advies.

Ik heb veel samengewerkt met mensen van buiten de Universiteit Utrecht. I would like to thank the CatchBio user committee for the suggestions and fruitful discussions. Ed de Jong en Jan Kees van der Waal, jullie wil ik graag extra bedanken voor jullie input en de mogelijkheid om mijn industriële carrière bij Avantium te starten. Peter de Peinder (Vibspec), fantastisch hoe jij altijd hebt geholpen met het interpreteren van IR spectra. Jammer dat humine te sterk fluoresceert om Raman te kunnen meten. Adeline Ranoux (Cosun) en Erik van Hellemond (Suiker Unie), bedankt voor de discussie en input rond de dehydratatie van sucrose in diksap zoals beschreven in Hoofdstuk 6. Two other universities were involved in the humin valorization project: Professor Erik Heeres and Yuehu Wang from University of Groningen and Professor Seshan, Professor Leon Lefferts and Chau Hoang from Twente University, thank you for the nice discussions and your input.

Ernst van Eck van de Radboud Universiteit Nijmegen, ik wil jou graag bedanken voor het opnemen en uitwerken van de mooie 2D PASS NMR spectra voor de Hoofdstukken 2, 3 en 6. Several analyses and the preparation of humins were performed at Professor Erik Heeres' group in Groningen. CB, Wang and Henk thanks for preparing the humin samples and your help in the lab. Erik, Arjan, Henk, Léon en Jan Henk, jullie bedankt voor het regelen en/of uitvoeren van de GCxGC-MS, elementanalyse, Pyrolyse-GC-MS en GPC metingen.

Ook binnen de Universiteit Utrecht heb ik verschillende laboratoria gezien. Professor Marc Baldus en Eline Koers hebben de vaste stof NMR spectra van de ^{13}C-gelabelde humines uit Hoofdstuk 4 mogelijk gemaakt. De verschillende kleurtjes waren voor jullie even wennen maar we hebben een mooie slag gemaakt in het ophelderen van de structuur van humine. In hetzelfde gebouw heeft Hans Wienk ook verschillende pogingen gedaan om vloeistof NMR te meten aan mijn alkalisch-behandelde humines. Hans, ben je nu echt te oud voor Lowlands? Professor Bert Klein Gebbink en Johann Jastrzebski, hartelijk dank voor het gebruik van jullie NMR spectrometers, zuurkasten en hoogvacuümsysteem. Mies van Steenbergen, bedankt voor de vrolijke (Lady Gaga) noten in de ochtend en je hulp met vriesdrogers en vacuümovens.

Natuurlijk draait de groep Anorganische Chemie en Katalyse niet zonder technische en secretariële ondersteuning. Ik wil daarom Iris, Inez, Dymph en Monique heel erg bedanken voor hun inspanningen. Vooral Dymph en Monique, ik vond het geweldig hoe jullie mij hebben geholpen tijdens respectievelijk de laatste fase van mijn promotie en mijn re-integratie. Ad^{E}, dankjewel dat ik nooit lang zonder autoclaaf heb gezeten. Ad^{M}, dankzij jou was de veiligheid in orde en ik vond het erg leuk om deel uit te maken van het BHV team. Fouad, jij houdt de IR en Raman apparatuur werkend en de chemicaliënkasten vol. Pascal, bedankt voor het uitvoeren van de GCxGC-MS metingen en de uurtjes data-analyse achter jouw computer. Vincent, Rien, Marjan, Herrick en Oscar jullie ook bedankt voor de prettige samenwerking. Hans en Chris, bedankt voor het beantwoorden van alle vragen over de 'Senseo SEM' ofwel Phenom. Marleen, dankjewel voor het maken van de foto's van de huminesamples. Jammer dat het 'humines in plakjesproject' met Peter M., Fouad en Peter de P. niet meer in het proefschrift is gekomen.

My colleagues from the Biomass group Annelie, Dilek, Peter H., Andrei, Wenhao, Joe Z., Carlo, Joe S., Robin, Fiona, Peng Fei, Kichii, Michal, Fang, Sophie, Jan Philipp, Sankar, Sandra and Sang-Ho. And of course the dark-side of the lab: Tomas, Rob, Anne-Mette, Selvedin, Daniel and (sometimes) Stefan. Thanks for the discussions and good atmosphere in the lab (keep the Friday afternoon music!). Sandra, good luck continuing the humin project.

Verder heb ik verschillende studenten begeleid tijdens mijn promotie. Daan Lugard begon toen ik zelf amper een half jaar met mijn onderzoek bezig was. Het onderzoek naar het maken of afbreken van modelverbindingen voor humines is doorgezet door René Manchester en Gerben Roebersen. Gerben, jij hebt echt de eerste katalytische omzetting van humines uitgevoerd. Karst Lenzen heeft hier nog hard aan verder gewerkt. Helaas is het toch erg lastig gebleken om de humines af te breken zoals beschreven in Hoofdstuk 5. Sanne van Leeuwen, dankjewel voor je literatuurstudie. Je ziet er misschien weinig van terug in mijn thesis maar het is zeker van pas gekomen voor de selectie van katalysatoren.

Bart Sirks, jouw werk met het diksap (Joe S. and Dimitrije thanks for all the jokes...) vormde de basis voor Hoofdstuk 6.

Natuurlijk moest er ook af en toe practicum gegeven worden. Ik heb dit altijd met veel plezier gedaan wil vooral Paul Peijzel en Vera Kaats bedanken voor de trainingen, hulp en gezelligheid. Jan en Ko heel erg bedankt voor het treffen van alle voorbereidingen en technische ondersteuning.

In het Wentgebouw heb ik mijn kantoor gedeeld met Tamara, Annelie en Peter H. Bedankt voor de gezelligheid en sorry voor de herrie die Annelie en ik af en toe veroorzaakten. It was even more *gezellig* in the open office in the David de Wied building where I could distract Annelie, Bart, Hirsa, Luis, Piter, Upakul, Dilek, Peter N., Davide, Jinbao, Peter H., Sam, Ramon, Nazila, Zafer, Rogier, Peter B., Wang, Jeroen, Robin and Frank from their work. In office 4.88 I got a bit more focused thanks to Elena. Marleen, Elena, Tao (thanks for the chocolates), Marianna, Thomas, Manuel and Monique and Emke, thanks for the nice time. After moving to the new building we got a lot closer with the Organic Chemistry group. Peter S., Eric, Ties, Emma, Manuel, Suresh, Bas and Henk thanks for all the chats, drinks and help.

I would like to thank Remco, Daan, Stefan, Harry, Peter de P., Zea, Vlien, Frits, Annelie, Rob, Ruben, Annemarie, Manuel, Peter S., Fouad, Robin (and Remi), Peter M., Inge, Piter, Bert and Pieter for making CatchBio meetings, courses and conferences a social occasion.

During my time at Inorganic Chemistry and Catalysis I enjoyed many borrels, BBQs, lunches, coffees, cakes, dinners and chats! Upakul, Luis, Clare, Joe S., Fouad, Daniel, Carlo, Peter M., Zafer, Roy, Annelie, Rob, Davide, Inge, Tamara, Joe Z., Lucian, Hirsa, Javi and Sandra, Christoph, Wenhao, JX, Sam, Ramon, Elena, Fiona, Dimitrije, Zoran, Marleen, Korneel, Thomas, Rafael, Jesper, Arjan, Piter, Evelien, Hendrik, Qingyun, Dilek, Jovana, Inés, Peter B., Jinbao, Tomas, Joris, Jeroen, Mustafa, Gang, Arjen, Lisette, Marjolein, Katinka, Harry, Petra, Krijn, Rogier, Herrick, Rien, Marjan, Robin, Frank, Matti, Monica, René, Pascal, Peter N., Jelle, Boyang, Fang, Sandra, Nazila, Sophie, Manuel, Sang-Ho, Jamal, Tao, Ara, Ana, Gareth and ……. (Please, insert your name if I forgot to mention you), thanks!

Special thanks for the awesome nights out and all the times I could crash somewhere. Some people even managed to bear my voice during karaoke nights. Wenhao, when will we hear the wolf's cry? Thomas en Maren, de reisjes naar Aachen en Oktoberfest, maar ook voor jullie bruiloft waren fantastisch. Roy, bedankt voor het organiseren van de reisjes naar Winterberg. Upakul, Sankar and Sonu, Clare and Rob, the Indian dinners were amazing.

Everyone, thanks for all the phone calls, visits, messages, food, cookies, tea, flowers *etc.* I got when I was ill. It really made me feel better. ☺

After or before work I tried to do some sports. Jesper, Clare, Joe S. and Daniel thanks for motivating me to go to the gym and let me show off doing sit-ups. Upakul and Wenhao, thanks for teaching me the joys of basketball. Annelie, Peter M. and Clare thanks, for climbing safely. Cycling team, I'll see you in spring! Peter M., Elena, Joe S., Upakul, Mara, Wenhao and Zafer, thanks for all the fun we had with Rufus.

Annelie, goeie tip om naar Utrecht te komen. Ik vond het erg gezellig met jou in het kantoor, lab en daarbuiten. Je komt toch wel weer terug?
Zafer, thanks for all the nice chats, coffees and dinners and say hi to your mum! Upakul, you have to say hi to your mum as well! I love all the nonsense and serious things.
Clare, thanks for the crop tops, parties, concussion survival kit, cat hair, sports, food, cakes and proper tea.
Marleen, na studiegenoot, vriendin, collega en koppelaar, denk ik dat we niet meer van elkaar afkomen op een positieve manier. Veel geluk met Hans en 'Spartel'.

Riet, jouw adviezen hebben mij geholpen om door te zetten met werken en geduld te hebben met herstellen.

Kirsten, sorry dat je straks echt drie kwartier mijn scheikundegepraat moet aanhoren, maar ik leg het straks nog wel een keer uit...

Papa en mama, ik kan jullie niet genoeg bedanken voor alle liefde en steun maar ook voor jullie advies en vriendschap. Ik vind het heel fijn dat jullie altijd interesse in mijn werk hebben getoond.

Peter, dankjewel dat jij er altijd voor mij bent, het is namelijk zo gezellig met jou. Als we straks allebei doctor zijn kan ik misschien wat beter stilzitten.

Ilona

Ilona van Zandvoort was born the 3rd of August 1986 in Velsen, the Netherlands. After finishing secondary school she started her chemistry studies at the University of Amsterdam in 2004. She finished her BSc in Chemistry in 2007 with a specialization in organic chemistry and spectroscopy with a Bachelor thesis titled "Looking into Film Formation; Fluorescence Studies on Water-borne Organic Coatings" under the supervision of prof. Fred Brouwer. She obtained her MSc in Chemistry with a specialization in analytical chemistry with a main focus on spectroscopy in 2009 at the University of Amsterdam. Her MSc thesis was titled "Binding of Antihistamines to Human Serum Albumin studied by means of Complementary Spectroscopic Techniques." and was supervised by dr. Gert van der Zwan and prof. Cees Gooijer at VU University Amsterdam. In the same year she started as a PhD student at Utrecht University under supervision of prof. Bert Weckhuysen and dr. Pieter Bruijnincx. Her research, as described in this thesis, was funded by CatchBio. Ilona is currently working as a junior scientist at Avantium.